Robust chaos in piecewise-linear maps

A thesis submitted

in partial fulfillment for the award of the degree of

Doctor of Philosophy

by

Indranil Ghosh

School of Mathematical and Computational Sciences

Massey University

Palmerston North, New Zealand

December 2023

To my father, in loving memory.

Acknowledgements

This thesis would not have reached its final form without the tremendous support and inspiration from some special people throughout this Ph.D. journey. I would love to take this opportunity to express my appreciation to each of them.

First and foremost, I would extend my sincere gratitude to my main supervisor, Dr. David J.W. Simpson for his guidance and assistance. He entrusted me with this Ph.D. position and supported my living expenses with a prestigious scholarship. I would love to thank him for letting me work in this relevant and rich field of switched dynamical systems and also funding my research visits/conferences: UoA, SIAM AN22, SIAM DS23, Dynamical Systems in NZ 2022, NZMS 2022/2023, NZMASP 2023, NZMRI 2023, NSW ANZIAM meeting 2023, and so on. I would forever be indebted to him for his guidance, comments and suggestions.

Secondly, I would love to thank my co-supervisor, Dist. Prof. Robert I. McLachlan for his advice and support, especially guiding me towards the right path in terms of some research questions. He has also showered me with invaluable career advice and advice related to life in general.

Next, I want to thank my colleagues and friends with whom I have collaborated and learnt from. The list is long and I wanted to mention a few who have left a mark in my research journey: Dr. Hammed Olawale Fatoyinbo, Dr. Sishu Shankar Muni, Dr. Sarath Babu, and Prof. Costas Efthimiou.

Now, it would be my pleasure to mention my family members (mostly overseas) whom I owe a lot. To my late father Asit Kumar Ghosh, who passed away due to COVID-19 in 2022, a year into my Ph.D. I miss him every second, but I am sure he is proud of me and is well aware of the progress I have made. To my mother Panchali Ghosh, who has been my rock my entire life and has been there for me through thick and thin. To my elder brother Avranil Ghosh, who has guided and supported me especially through our hard times and without whom I would have reached a breaking point. I also want to thank my partner Wang Fangshu, who herself being a Ph.D. student in Applied Lingusitics (Massey University), knows how challenging a Ph.D. journey could be from time to time and has provided me with a great deal of emotional support.

I would also love to thank the administrative staff from the School of Mathematical and

Computational Sciences, Massey University who have supported me with all the admin procedures starting from my confirmation until the submission of my thesis.

Last but not least, I want to acknowledge the Marsden Fund contract MAU1809 managed by Royal Society Te Apārangi, that supported my Ph.D. work.

Indranil Ghosh

Abstract

Piecewise-linear maps describe the dynamical behaviour of a wide variety of physical systems that switch between different modes of evolution, such as optimal control systems, mechanical systems with contact events, and social and economics systems involving decisions or constraints. This thesis focuses on a canonical form for two-dimensional continuous piecewise-linear maps, known as the border-collision normal form. Recent work showed that where the normal form is orientation-preserving it can exhibit chaotic dynamics that is robust in the sense that it occurs throughout an open region of four-dimensional parameter space. In this thesis we first use renormalisation to partition this region by the number of connected components of the chaotic attractor, revealing previously undescribed bifurcation structure in a succinct way. Next, we prove that in part of this region the attractor satisfies Devaney's definition of chaos, strengthening existing results. Here we also show that the one-dimensional stable manifold of a fixed point densely fills a two-dimensional area of phase space, and identify a heteroclinic bifurcation, not described previously, at which the attractor undergoes a crisis and may be destroyed. We then generalise the results to the orientation-reversing and non-invertible parameter regimes of the normal form by developing new ways of constructing trapping regions and invariant expanding cones that establish the existence of chaotic attractors. Bifurcations of the attractor are explored numerically by using Eckstein's greatest common divisor algorithm and comparing the results to those generated through renormalisation. Finally we extend the study to higher dimensional maps by constructing a novel trapping region for the N-dimensional border-collision normal form.

Contents

List of Figures

List of Tables

Chapter 1

Introduction

Dynamical systems refer to behaviour evolving in time. *Dynamics* refers to the fact that the system either settles to a steady-state, keeps repeating in cycles, or exhibits more complicated behaviour, and is something *dynamicists* analyze and study. Dynamical systems as a subject emerged in the mid-1600s with the development of differential equations by Isaac Newton in regards to his discoveries of laws of motion and universal gravitation [133]. In this way the dynamics of natural phenomena can be studied in terms of mathematical models. In applied mathematics and natural sciences, the term *mathematical model* represents a description of a system (an ensemble of interacting elements that act according to a prescribed set of rules) using mathematical concepts. Usually, mathematical models [136] can be realised in many forms like dynamical systems, statistical models, or game theoretic models. Notable examples include mathematical models describing the motion of planets, the swinging of a pendulum, fluid flow, and population growth, to name a few.

Many dynamical systems are described with *ordinary differential equations*, where time is a continuous variable, given by

$$\frac{dX}{dt} = f(X, t), \tag{1.1}$$

or *difference equations*, where time is a discrete variable, given by

$$X_t = f(X_{t-1}, t). \tag{1.2}$$

Difference equations are sometimes referred to as *iterated maps* or simply *maps* if the variable t does not exist on the right side of (1.2). Maps arise as Poincaré maps of ordinary differential equations. For any point x on a cross section S, we follow the solution to the ordinary differential equations around to its next intersection with S, $P(x)$, giving us the

Poincaré map P. Other representations of dynamical systems include *partial differential equations*, *delay differential equations*, and *cellular automata*, which are not within the scope of this thesis.

In the above equations the variables X and X_t are the state variables of the systems and can be either a scalar or a vector quantity. The function f represents the rule according to which the systems evolve over time. The model formulation (1.1) assumes that the rate of change of X is determined by the value of X, and the value of t. Also for (1.2) the value of X at the current time step is determined by its value at the previous time step, and the value of t.

In the following discussion we assume for simplicity that the equations (1.1) and (1.2) define unique solutions (forwards in time, and given a suitable initial point). To determine the behaviour of solutions to (1.1) or (1.2) it is helpful to work in *phase space*, which is the space of all possible values of X. In this space solutions are curves, for (1.1), or sets of points, for (1.2), parameterised by t. Each is called an *orbit* or a *trajectory*, and the representation of these orbits in the phase space is called the *phase portrait* of the dynamical system. An orbit can be *periodic* when the solution of the dynamical system repeats over time. We also see a *limit cycle* which is a periodic orbit that is isolated from other periodic orbits. But when analysing a mathematical model the researcher should always keep the famous quote by statistician George Box in mind: "*All models are wrong, but some are useful*". For example, a pendulum may be modelled by

$$m\frac{d^2\theta}{dt^2} + k\sin(\theta) = 0, \tag{1.3}$$

where m is the mass, $\sqrt{\frac{k}{m}}$ is the natural frequency of motion, and $\theta(t)$ is the angle of displacement. This model disregards friction and displacements outside the plane so is an approximation to reality but allows us to understand the behaviour of pendulums quantatively.

One is often interested in the long term behaviour. The behaviour can be constant, periodic or more "complicated", meaning that the solution is an irregular function of time. For the differential equation (1.1) a *zero* of f where $\frac{dX}{dt} = 0$ is called an *equilibrium*, whereas for the map (1.2) a solution to $f(X) = X$ is called a *fixed point*. Equilibria and fixed points are the simplest kinds of *invariant sets*, defined precisely in Chapter 2.

The notion of *stability* is also defined precisely in Chapter 2 but we outline it here. A fixed point is *stable* if for any initial condition close to the fixed point, the orbit remains in the vicinity of the fixed point. If it is not stable it is *unstable*, meaning there exists an

initial condition close to the fixed point from which the orbit will diverge away from the vicinity of the fixed point. More generally an invariant set is an *attractor* if all nearby orbits converges to it and it satisfies an indivisibility property.

Even when (1.1) and (1.2) have a unique attractor, the value of X at large and intermediate values of t can be highly sensitive to the initial condition, making long term prediction of the system behaviour impossible, even though the systems are deterministic in nature. This behaviour in general is described as *chaos*. The high sensitivity to initial conditions is popularly known as the *butterfly effect*. This term emerges from the Edward Lorenz paper: *Predictability: Does the Flap of a Butterfly's Wings in Brazil set off a Tornado in Texas?* [91]. Chaotic dynamics has applications in fields including sociology, computer science, ecology, economics, physics, biology, and more. One application of particular significance to this thesis is in the field of cryptography, where the encryption algorithms use the initial conditions of different chaotic maps as their keys [16]. The chaos provides an effective and efficient way to scramble a message in a way that seems random but is deterministic so can be deciphered given knowledge of the chaotic map. A type of bio-inspired computing, known as DNA computing, exploits chaos theory for image encryption purposes and has several applications in the computational sciences [9]. Another application area of chaos theory is population dynamics which exhibits a wide array of chaotic behaviours [42, 90], useful in predicting how a population evolves within an ecosystem over time. In economics and finance, chaos theory can be applied to improve models [21,77,84], given the fact that economic and financial systems are often highly stochastic in nature. Quantum physicists often try studying the dynamics of chaotic classical systems in terms of quantum theory and mechanics giving rise to the field of *quantum chaos* [17, 65]. Chaos theory has also been extensively applied to correctly describe the dynamics of planetary motions [100].

A dynamical system usually depends on a set of parameters and the qualitative structure of the system can change under the variation of one or more parameters. Examples of qualitative changes include the creation and destruction of fixed points or a change in their stability. These abrupt qualitative changes are referred as *bifurcations* and the parameters at which they occur are called *bifurcation points*. The number of distinct parameters that must be varied for a bifurcation to occur generically is the *codimension* of the bifurcation. One of the simplest codimension-one bifurcations is the *saddle node bifurcation* where two fixed points move towards each other, collide and mutually annihilate. All types of bifurcations can broadly be placed into one of the following two groups:

1. *Local bifurcation*: A bifurcation is local if the change in dynamics occurs in an

arbitrarily small part of phase space.

2. *Global bifurcation*: A bifurcation is global if it is not local.

In many mathematical models, such as the above pendulum model, the equations of motion are smooth. This thesis concerns models for which the equations of motion are piecewise-smooth (PWS) [35]. A PWS map on a phase space $\mathcal{S} \in \mathbb{R}^N$ is a map of the form

$$\mathbf{x}_{i+1} = f_J(\mathbf{x}_i), \quad \mathbf{x}_i \in \mathcal{S}_J, \tag{1.4}$$

where $\mathcal{S}_J$ are regions that partition $\mathcal{S}$. Also each f_J is a *smooth function*, i.e., it has continuous derivatives up to some order in $\mathcal{S}_J$. PWS equations apply to physical systems with switches, impacts, and other abrupt events. These kinds of systems are pervasive in nature, ranging from diverse engineering applications [8] to gene switching [45] and cryptography [79]. Maps of the form (1.4) arise as Poincaré maps of PWS differential equations, with specific applications including systems from mechanics with friction [8,18,20], power electronics [12, 76, 144], and ecology [6, 31, 111]. For example, objects in contact switch between being stuck due to static friction and sliding across one another, giving rise to PWS equations of motion. In ecology, PWS models describe population dynamics with selective switching between alternative habitats or diets. PWS maps have also been used to model a wide variety of discrete-time phenomena in economics [23, 70, 86]. A significant example is the Hicksian trade cycle model. Hicks used a piecewise-linear model of a trade cycle to popularise the idea that endogeneous fluctuations could be coupled in a nonlinear phenomenon with a growth process, see [50, 114]. Other application areas of PWS systems include neurodynamics [29, 118] (adding non-smoothness to the model helps mimic the dynamics of individual neuron spikes associated with the corresponding bursts) and game theory [107]. Also, from a theoretical perspective, PWS systems can exhibit complicated dynamics yet are relatively amenable to an exact analysis. For this reason, they provide a useful tool for us to explore complex aspects of dynamical systems, such as chaos.

This thesis revolves around a piecewise-linear family of maps for which phase space is separated into two regions by a linear *switching manifold*. The family will be defined later but here we motivate it by considering an arbitrary PWS map on $\mathbb{R}^N$. Under parameter variation an invariant set of the map can collide with a switching manifold. This type of bifurcation is unique to PWS systems and termed a *discontinuity induced bifurcation*. The simplest kind of such bifurcation is a *border-collision bifurcation* (BCB) which occurs when a fixed point collides with a switching manifold [35, 126]. This is a local bifurcation and our focus is on understanding what dynamics is created in the bifurcation, which, as

will be explained shortly, leads us to the piecewise-linear maps that will be studied. Note that the term BCB was coined by Nusse and Yorke in 1992 in their pioneering paper [102], but BCBs were considered much earlier e.g. [22, 47, 48] and termed C-bifurcations in the Russian literature. Experimental demonstrations of BCBs can be found in both circuit systems [11, 74] and mechanical systems [106].

Next we describe three ways by which BCBs arise in Poincaré maps. First, let us consider a PWS ODE or a hybrid system (i.e. a combination of ODEs and maps), and let us suppose that under parameter variation a limit cycle collides tangentially (grazes) a switching manifold. This is called a *grazing bifurcation* or a *sliding bifurcation* if sliding motion is involved (*sliding motion* refers to a novel type of evolution constrained to a switching manifold) [49,126,138]. Poincaré maps associated with grazing and sliding bifurcations are PWS. Different sorts of grazing and sliding bifurcations give different degrees of severity in the nonsmoothness of the map, e.g. many give a square-root singularity. Of the various sorts, the so-called grazing-sliding bifurcation gives a continuous map that is asymptotically piecewise-linear and hence relevent to the map studied in this thesis. One application of grazing-sliding bifurcation has been reported in an application in power system electronics [26]. In another study, it was reported that sliding bifurcations play a vital role in understanding the dynamics of dry friction oscillators [39]. Other applications where grazing-sliding bifurcations have been identified include relay control systems [30, 37].

Many PWS ODE models have several switching manifolds that intersect or have a corner. For example, simple mathematical models of DC/DC power converters include two switching manifolds, one for periodic switching events and the other for where the current is brought to pause. These manifolds intersect and form a corner [34, 144], and when a periodic orbit collides with the corner the resulting PWS Poincaré map is continuous and asymptotically piecewise-linear so provides a second scenario where our BCBs arise. This is because at a corner collision there is no smooth component of the switching manifold that is tangent to the periodic orbit and so no square-root term arises [25, 36, 126].

Third, hybrid dynamical systems, when subjected to a time delay in the switch, have solutions with corners occurring at points beyond the switching manifolds [123]. Except under parameter variation as a codimension-one bifurcation, termed an *event collision*, these corners can occur on switching manifolds when the time delay is non-zero [124]. Poincaré maps for event collisions are also continuous and asymptotically PWL.

Now consider a continuous, asymptotically piecewise-linear map

$$\mathbf{x}_{i+1} = \begin{cases} f_L(\mathbf{x}_i), & s(\mathbf{x}_i) \leq 0, \\ f_R(\mathbf{x}_i), & s(\mathbf{x}_i) \geq 0, \end{cases} \tag{1.5}$$

where s is a smooth function defining the switching manifold and f_L and f_R represent the functional components of (1.4) for pieces of the map either side of the switching manifold. Let us suppose a BCB occurs at $\mathbf{x} = 0$ when a parameter $\mu = 0$. We apply a coordinate transformation to (1.5) and Taylor expand f_L and f_R to first order by assuming f_L and f_R are C^1 to get the form

$$\mathbf{x}_{i+1} = f(\mathbf{x}_i; \mu, \nu) = \begin{cases} A_L(\nu)\mathbf{x}_i + b(\nu)\mu + o(\|\mathbf{x}_i\|, \mu), & e_1^{\mathsf{T}}\mathbf{x}_i \leq 0, \\ A_R(\nu)\mathbf{x}_i + b(\nu)\mu + o(\|\mathbf{x}_i\|, \mu), & e_1^{\mathsf{T}}\mathbf{x}_i \geq 0, \end{cases} \tag{1.6}$$

where ν represents other parameters of the map, $o(\|x_i\|, \mu)$ contains the higher order nonlinear terms. Because $\mathbf{x}$ and μ are small, the linear terms dominate f_J, with $J = L, R$. Then, by dropping the nonlinear terms the following piecewise-linear approximation can be obtained:

$$\mathbf{x}_{i+1} = f(\mathbf{x}_i; \mu, \nu) = \begin{cases} A_L(\nu)\mathbf{x}_i + b(\nu)\mu, & e_1^{\mathsf{T}}\mathbf{x}_i \leq 0, \\ A_R(\nu)\mathbf{x}_i + b(\nu)\mu, & e_1^{\mathsf{T}}\mathbf{x}_i \geq 0. \end{cases} \tag{1.7}$$

Note that by the assumed continuity of the map A_L and A_R differ only in their first column. A second coordinate change can be employed to transform A_L and A_R to *companion matrices* C_L and C_R respectively, and b to the vector e_1. This is always possible unless (1.7) has a degeneracy (non-observable) as explained in Chapter 2. This form is now a normal or canonical form, given by

$$x_{i+1} = \begin{cases} C_L\mathbf{x}_i + e_1\mu, & e_1^{\mathsf{T}}\mathbf{x}_i \leq 0, \\ C_R\mathbf{x}_i + e_1\mu, & e_1^{\mathsf{T}}\mathbf{x}_i \geq 0, \end{cases} \tag{1.8}$$

where the companion matrices are

$$C_J = \left[-M_J \middle| \frac{I}{0 \ldots 0} \right], \tag{1.9}$$

where, $M_J \in \mathbb{R}^N$, and I is the $(N-1) \times (N-1)$ identity matrix. This form is called

the *border-collision normal form* and includes (up to a change of variables) almost all continuous, piecewise-linear maps with two pieces, and does so with a minimal number of parameters [102, 129]. In the two-dimensional case, which is very central to this thesis, we can write the companion matrices as

$$C_J = \begin{bmatrix} \tau_J & 1 \\ -\delta_J & 0 \end{bmatrix}, \tag{1.10}$$

where τ_J is the trace of C_J and δ_J is the determinant of C_J. The dynamics of the border-collision normal form can be very rich even in only two dimensions, see [10, 54, 125].

Banerjee, Yorke, and Grebogi in their pioneering paper [14] identified an open parameter region $\Phi_{\mathrm{BYG}} \subset \mathbb{R}^4$ (to be defined below) throughout which the two-dimensional border-collision normal form has a chaotic attractor [58]. This is an example of *robust chaos* in the sense that it occurs throughout an open region of parameter space [143]. Robust chaos does not occur for generic families of smooth one-dimensional maps as these have dense windows of periodicity [139], but is typical for systems with sufficiently many dimensions [60, 61], a well-known example being the Lorenz system [64, 137]. One can impose further requirements on the robustness, such as that the attractor varies continuously with respect to Hausdorff distance [57] or with respect to its invariant measure [5]. Robust chaos is a desirable phenomenon in practical applications that exploit chaos. For example, in chaos-based cryptography [79], robust chaos is favoured as periodic windows in the key space can be taken over by an attacker to break the encryption [4]. Robust chaos can be useful to devices that have advantageous functional characteristics when operated in a chaotic regime, for example, power converters [28], optical resonators [89], and energy harvesters [82].

The motivating goal of this thesis is to study the bifurcation structure within Φ_{BYG} and beyond to show how the family of maps they considered naturally subdivides through *renormalisation* [93, 122]. Renormalisation was the key mathematical tool used in the 1970's to explain the period-doubling route to chaos by analysing the dynamics of families of unimodal maps. Renormalisation involves showing that, for some member of a family of maps, a higher iterate or induced map is conjugate to different member of the same family. It has also been used in understanding the bifurcation structure of skew-tent maps [72] and, particularly relevant to our studies, has been applied to a two-parameter family of two-dimensional, piecewise-linear maps by Pumariño *et al.* [112].

By applying renormalisation to Φ_{BYG} we are able to explain features of the dynamics described previously by other researchers in a more concise manner, and reveal and ex-

plain dynamics not reported previously. We further show how the robustness extends more broadly to orientation-reversing and non-invertible cases via explicit constructions of trapping regions and invariant expanding cones and how the renormalisation can be extended as well. An extension of these methods to higher dimensions appears promising and this will be touched upon. It is hoped that this thesis will be useful to future researchers because it unfolds many mysteries in the robust chaos parameter region in terms of the topology of the attractor. The fact that any non-degenerate, continuous, piecewise linear map can be transformed to the normal form under some coordinate transformation, emphasises the fact that the results can be applied to all kinds of applications.

The thesis is organised as follows: In Chapter 2 we review the relevant topics and the background material in a more mathematically precise manner than given above. In Chapter 3 we study the region Φ_{BYG}, where the map is invertible, orientation-preserving, and dissipative (for the most part). We apply renormalisation to partition this region by the number of connected components of the chaotic attractor. This reveals previously undescribed bifurcation structure in a succinct way. Next, in Chapter 4 we further strengthen the existence of robust chaos by identifying a subregion where the attractor satisfies Devaney's definition of chaos. We further show that the stable manifold of a saddle fixed point, despite being a one-dimensional object, densely fills an open region containing the attractor. We also identify a heteroclinic bifurcation (where the unstable manifold of a saddle fixed point and the stable manifold of a period-3 solution form an intersection), not described previously, at which the attractor undergoes a crisis and may be destroyed. This can also be interpreted as a homoclinic bifurcation where the stable and the unstable manifolds of the period-three solution also form an intersection.

In Chapter 5 we construct a trapping region in phase space and an invariant expanding cone in tangent space, showing that the normal form exhibits a chaotic attractor throughout an open region of parameter space, this time generalising the construction to include the non-invertible and orientation-reversing cases. The resulting parameter region is again open so the chaos is robust within this family of maps. The boundaries of the parameter region are where the construction fails in some way: three of these boundaries correspond to bifurcations where the chaotic attractor is destroyed. In Chapter 6, we further extend the application of renormalisation to the non-invertible and orientation-reversing cases. In Chapter 7 we begin to generalise the constructions to the N-dimensional border-collision normal form, but a completion of this task remains for future work. Finally in Chapter 8 we provide conclusions and direct the reader to future directions. Note that the content in each of Chapters 3–6 has been published (or hopefully will be published) as a regular journal

article, as shown in Table 1.1.

Chapter	Paper title	Status
3	I. Ghosh and D.J.W. Simpson, "Renormalisation of the two-dimensional border-collision normal form" in *Int. J. Bifurcation Chaos, 32(12):2250181, 2022.*	Published
4	I. Ghosh and D.J.W. Simpson, "Robust Devaney chaos in the two-dimensional border-collision normal form." in *Chaos, 32:043120, 2022*.	Published
5	I. Ghosh, R.I. McLachlan, and D.J.W. Simpson, "Robust chaos in orientation-reversing and non-invertible two-dimensional piecewise-linear maps." Submitted to: *J. Nonlinear Sci.*	Under Review
6	I. Ghosh, R.I. McLachlan, and D.J.W. Simpson, "The bifurcation structure within robust chaos for two-dimensional piecewise-linear maps." in *Commun. Nonlinear Sci. Numer. Simul., 134, 2024*	Published

Table 1.1: A list of manuscripts complementing this thesis.

Chapter 2

Background

This chapter provides background on theoretical aspects of discrete-time dynamical systems, i.e., maps. For more details the interested reader is encouraged to look in Abraham *et al.* (1997) [1], Galor (2007) [51], Sandefur (1990) [119], etc. We first reintroduce what a map is, but in a more technical form. Then we go on to introducing all the background of this thesis, for example, stability, stable and unstable manifolds, attractors, Lyapunov exponents, chaos, renormalisation, and the border collision normal form.

2.1 Maps

For any set χ in $\mathbb{R}^N$ and any continuous function $f : \chi \to \chi$, i.e, from χ to itself, a *map* is given by

$$\mathbf{x} \mapsto f(\mathbf{x}), \tag{2.1}$$

where χ is the *phase space* of the map. The map f defines evolution of the dynamical system by composition with itself. Given, $\mathbf{x}_0 \in \chi$, let $\mathbf{x}_1 = f(\mathbf{x}_0)$. Then,

$$\mathbf{x}_2 = f(\mathbf{x}_1) = f(f(\mathbf{x}_0)) = f^2(\mathbf{x}_0).$$

For all natural numbers $n \in \mathbf{N}$, we have,

$$\mathbf{x}_n = f(\mathbf{x}_{n-1}) = f(f(\mathbf{x}_{n-2})) = \underbrace{f(f(\ldots f(f(\mathbf{x}_0))\ldots))}_{n \text{ times}} = f^n(\mathbf{x}_0),$$

for the composition of f with itself n times. The point $f^n(\mathbf{x})$ is the n^{th} *iterate* of x under f.

2.2 Fixed points, invariant sets, and stability

This section focuses on fixed points and how their stability can be understood in terms of the eigenvalues of the Jacobian matrix of the fixed point.

Definition 2.1. A *fixed point* of (2.1) is a point $\mathbf{x}^* \in \chi$ for which $f(\mathbf{x}^*) = \mathbf{x}^*$.

We write $B_\epsilon(\mathbf{x})$ for the ball of radius $\epsilon > 0$ centred at a point $\mathbf{x} \in \mathbb{R}^N$.

Definition 2.2. A fixed point $\mathbf{x}^*$ of (2.1) is *Lyapunov stable* if for all $\epsilon > 0$, there exists $\delta > 0$, such that $f^n(\mathbf{x}) \in B_\epsilon(\mathbf{x}^*)$ for all $\mathbf{x} \in B_\delta(\mathbf{x}^*)$ and all $n \geq 0$.

Definition 2.3. A fixed point $\mathbf{x}^*$ of (2.1) is *asymptotically stable* if it is Lyapunov stable and there exists $\delta > 0$ such that $f^n(\mathbf{x}) \to \mathbf{x}^*$ as $n \to \infty$ for all $\mathbf{x} \in B_\delta(\mathbf{x}^*)$.

Note that *unstable* means not Lyapunov stable. Now we are going to examine stability in the simplest case that the invariant set is a fixed point. The above definition can be discussed in terms of approximation of the map (2.1) near the fixed point $\mathbf{x}^*$ from the affine approximation

$$\mathcal{A}(\mathbf{x}) = Df(\mathbf{x}^*)(\mathbf{x} - \mathbf{x}^*) + \mathbf{x}^*,$$

which assumes f is C^1 at $\mathbf{x}^*$. Here, Df denotes the $N \times N$ Jacobian matrix of first derivatives. Now notice that if $Df(\mathbf{x}^*)v = \lambda v$, where $v \in \mathbb{R}^N$ and $\lambda \in \mathbb{R}$, then we have

$$\mathcal{A}^m(\mathbf{x}^* + v) = \mathbf{x}^* + \lambda^m v,$$

for all $m \geq 0$. Here λ is an eigenvalue of $\mathcal{A}$ and v is a corresponding N dimensional eigenvector. If $\lambda > 0$, the forward orbit of any point on the line through $\mathbf{x}^*$ with direction v will remain on one side of the fixed point, while if $\lambda < 0$, the forward orbit hops back-and-forth over the fixed point. Also, at least for the affine approximation $\mathcal{A}$, the forward orbit of $\mathbf{x}^* + v$ will converge to the fixed point $\mathbf{x}^*$ if $|\lambda| < 1$ and will diverge away from $\mathbf{x}^*$ if $|\lambda| > 1$.

For a complex eigenvalue $\lambda \in \mathbb{C}$, f is invariant on the two-dimensional subspace spanned by the real and imaginary parts of an eigenvector $v \in \mathbb{C}^N$. On this subspace the forward orbits converge to the fixed point if $|\lambda| < 1$ and diverge if $|\lambda| > 1$.

For any point (close to $\mathbf{x}^*$), the action of f can be decomposed into a sum involving a set of N linearly independent eigenvectors of $Df(\mathbf{x}^*)$, assuming such a set exists. If all

the eigenvalues of $Df(\mathbf{x}^*)$ have modulus less than 1, then $\mathbf{x}^*$ is *asymptotically stable*. If at least one of the eigenvalues of the Jacobian matrix has modulus greater than 1, then $\mathbf{x}^*$ is *unstable*. Formally these results are a direct outcome of the Hartman-Grobman theorem [66] given below. Before we state the theorem we need the following definitions. Note that the eigenvalues of $Df(\mathbf{x}^*)$ are also referred to as the *stability multipliers* of $\mathbf{x}^*$.

Definition 2.4. A fixed point $\mathbf{x}^*$ is said to be *hyperbolic* if it has no stability multipliers with modulus equal to 1.

Definition 2.5. A function $h : \mathbb{U} \to \mathbb{U}$, with $\mathbb{U} \subset \mathbb{R}^N$, is a *homeomorphism* if it is continuous, one-to-one, onto and there exists an inverse h^{-1} which is also continuous.

Theorem 2.1 (Hartman-Grobman Theorem)**.** *Let the map f be C^1 and the fixed point $\mathbf{x}^*$ be hyperbolic. Then there exists a neighbourhood of $\mathbf{x}^*$ within which f is conjugate to $\mathcal{A}(\mathbf{x})$.*

Definition 2.6. For a hyperbolic fixed point $\mathbf{x}^*$, if all stability multipliers of $\mathbf{x}^*$ have modulus less than 1 then $\mathbf{x}^*$ is *attracting*, if all the stability multipliers have modulus greater than 1 then $\mathbf{x}^*$ is *repelling*, otherwise it is a *saddle*.

The eigenvalues of $Df(\mathbf{x}^*)$ for a two-dimensional map can be determined from its trace and determinant, which we denote $\tau = \mathrm{trace}(Df(\mathbf{x}^*))$ and $\delta = \det(Df(\mathbf{x}^*))$ respectively. The eigenvalues λ are the solutions of the characteristic equation given by

$$\lambda^2 - \tau\lambda + \delta = 0. \tag{2.2}$$

Solving $|\lambda| = 1$ produces three cases:

- $\lambda = 1$, where $\delta = \tau - 1$,
- $\lambda = -1$, where $\delta = -\tau - 1$, and
- $\lambda = e^{i\phi}$ for some $\phi \in (0, \pi)$, where $\delta = 1$ and $\tau \in (-2, 2)$.

The fixed point $\mathbf{x}^*$ is attracting in the (τ, δ)-plane bounded by the lines $\delta = \tau - 1$, $\delta = -\tau - 1$ and $\delta = 1$. We get saddle fixed points in two cases:

- $\delta > -\tau - 1$ and $\delta < \tau - 1$, and
- $\delta > \tau - 1$ and $\delta < -\tau - 1$.

Elsewhere it is repelling, see Fig. 2.1.

A fixed point can be generalised to an invariant set.

Definition 2.7. A set $\Gamma \subset \chi$ is *invariant* under f, if $f(\Gamma) = \Gamma$.

2.3 Periodic solutions

This section shows how the above elementary theory for fixed points extends easily to periodic solutions.

Definition 2.8. For any $\mathbf{x} \in \chi$, if there exists a positive integer p such that $f^p(\mathbf{x}) = \mathbf{x}$, then $\mathbf{x}$ is called a *periodic point* of the map f.

Definition 2.9. An orbit of the map f given by $\{\mathbf{x}, f(\mathbf{x}), f^2(\mathbf{x}), \ldots, f^{p-1}(\mathbf{x})\}$ is said to be a *periodic solution* of period $p \geq 2$, if

$$f^j(\mathbf{x}) \neq \mathbf{x},$$

for all $j < p$ and

$$f^p(\mathbf{x}) = \mathbf{x}.$$

The periodic point $\mathbf{x}$ in Definition 2.8 is a fixed point of f^p. In this way the stability of fixed points and their classification as attracting, saddles, or repelling can be extended to periodic solutions. The Jacobian matrix of f^p at $\mathbf{x}$ is a product of the Jacobian matrices

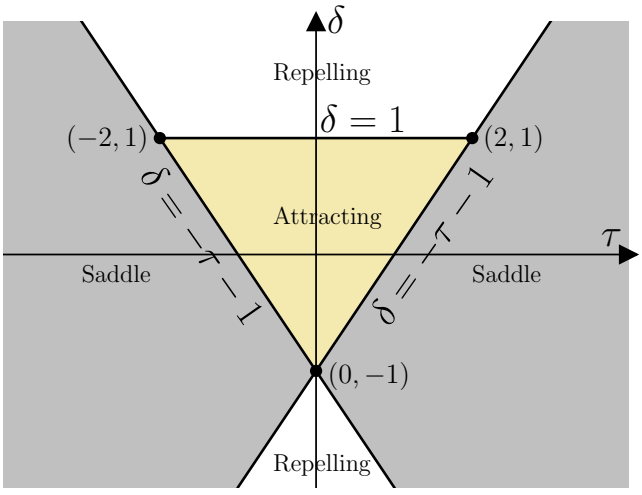

Figure 2.1: The stability of a fixed point of two-dimensional C^1 map f in terms of τ and δ calculated at the fixed point.

evaluated at each point of the periodic solution, specifically

$$Df^p(\mathbf{x}) = Df(f^{p-1}(\mathbf{x}))\dots Df(f(\mathbf{x}))Df(\mathbf{x}). \tag{2.3}$$

In fact each point $f^k(x)$ in the periodic solution of Definition 2.9 is a fixed point of f^p. The corresponding Jacobian matrix $Df^p(f^k(\mathbf{x}))$ is a product of the p matrices on the right-hand side of (2.3) but arranged under different cyclic permutation. Importantly the eigenvalues are the same for all cyclic permutations thus these eigenvalues are an inherent property of the periodic solution; they are the stability multipliers of the solution.

2.4 Attractors

In this section we start by defining a forward invariant set and a trapping region followed by the definition of attracting set in terms of a trapping region. We also define topological attractors and Milnor attractors.

Note we write $\mathrm{int}(\chi)$ for the interior of the set χ.

Definition 2.10. A set $\Omega \subset \chi$ is

1. *forward invariant* if $f(\Omega) \subset \Omega$, and
2. is a *trapping region* if it is non-empty, compact, and $f(\Omega) \subset \mathrm{int}(\Omega)$.

For a forward invariant set $\Omega \subset \chi$, the restriction of f to Ω is a map on Ω. This is denoted by $f|_\Omega$. All the theories developed for maps naturally apply to the restrictions of maps to forward invariant sets. Furthermore, the iteration $f^{i+1}(\Omega) \subset f^i(\Omega)$ for all $i \geq 0$ (which follows from 1), means the sets $f^i(\Omega)$ form a nested sequence.

Definition 2.11. An invariant set $\Lambda \subset \chi$ is said to be an *attracting set* of f if it has a trapping region Ω such that

$$\Lambda = \bigcap_{i\geq 0}^{\infty} f^i(\Omega). \tag{2.4}$$

Definition 2.12. An attracting set containing a dense orbit is said to be a *topological attractor*.

The above definition ensures that attractors do not contain smaller attracting sets [63].

Definition 2.13. The set of all points whose forward orbits converge to an invariant set Λ is called the *basin of attraction* $B(\Lambda)$ of Λ.

Theorem 2.2. *Let $\Lambda \subset \chi$ be an attracting set of a continuous map $f : \chi \to \chi$. Then Λ is non-empty, compact, and invariant.*

For a proof of the above theorem, refer to [43]. Next, we define *Milnor attractors* [98] in the following way:

Definition 2.14. An invariant set $\Lambda \subset \chi$ is said to be a *Milnor attractor* if

1. the basin of attraction $B(\Lambda)$ has positive Lebesgue measure, and
2. for any closed, invariant, proper subset $\Lambda' \subset \Lambda$, $B(\Lambda) \setminus B(\Lambda')$ also has positive Lebesgue measure.

The basin of attraction has positive measure ensures that the orbits of some random initial conditions converge to the attractor and hence is the structure that we will actually observe. The second condition guarantees that every part of the attractor plays an important role. This points towards the fact that a Milnor attractor is not always a topological attractor, because its basin of attraction does not need to contain a neighbourhood of the attractor. The Feigenbaum attractor [98] corresponds to the limit point of the period-doubling cascade in the logistic family of maps and is a nice example of a Milnor attractor that is not a topological attractor.

2.5 Stable and unstable manifolds

In this section we first define what an invertible and a non-invertible map is, before delving into stable and unstable manifolds. These manifolds, being the simplest global invariant manifolds, play quite a substantial role in defining the global dynamics of the map.

Definition 2.15. A map $f : \chi \to \chi$ is *invertible* if it is one-to-one and onto. Otherwise, the map is non-invertible.

If f is invertible, a backward orbit can be generated by iterating the points under f^{-1}. This brings us to the definition of a *preimage*.

Definition 2.16. A *preimage* of a point $\mathbf{x} \in \chi$ is a point $\mathbf{z} \in \chi$ for which $f(\mathbf{z}) = \mathbf{x}$.

The map f could be locally invertible, even though it is non-invertible. From the *inverse function theorem* it could be said that if f is C^1 and $Df(\mathbf{x})$ is invertible at $\mathbf{x} \in \mathrm{int}(\chi)$, then there exists a neighbourhood $\mathcal{N} \subset \chi$ of $\mathbf{x}$ such that $f : \mathcal{N} \to f(\mathcal{N})$ is a diffeomorphism.

Definition 2.17. If $\det(Df(\mathbf{x})) > 0$ throughout $\mathcal{N}$ then f is *orientation-preserving* on $\mathcal{N}$, and if $\det(Df(\mathbf{x})) < 0$ throughout $\mathcal{N}$ then f is *orientation-reversing* on $\mathcal{N}$.

Definition 2.18. Let $\Lambda \subset \chi$ be an invariant set of f. The *stable manifold* of Λ is

$$W^s(\Lambda) = \{\mathbf{x} \in \chi |\ f^n(\mathbf{x}) \to \Lambda \text{ as } n \to \infty\}, \tag{2.5}$$

and the *unstable manifold* of Λ is

$$W^u(\Lambda) = \{\mathbf{x} \in \chi |\ \mathbf{x} \text{ has a sequence of preimages converging to } \Lambda\}. \tag{2.6}$$

If $W^s(\Lambda)$ and $W^u(\Lambda)$ intersect, their intersection gives *homoclinic orbits* that converge to Λ both as $n \to \infty$ and $n \to -\infty$. Orbits that belong to the stable manifold of one set and the unstable manifold of a different set are called *heteroclinic orbits*. A point on a homoclinic orbit is said to be a *homoclinic point* and a point on a heteroclinic orbit is said to be a *heteroclinic point*.

If a fixed point $\mathbf{x}^*$ of the map f is repelling, it is plausible that its stable manifold $W^s(\mathbf{x}^*)$ consists of more than just the point $\mathbf{x}^*$ when f is non-invertible. Moreover $\mathbf{x}^*$ can have a homoclinic orbit, and this can imply chaos under certain conditions, where $\mathbf{x}^*$ is termed a *snap-back repeller* [95, 96].

Next we define the stable and the unstable subspaces that explain how stable and unstable manifolds emanate from fixed points. These refer to generalised eigenvectors which are needed to accommodate Jacobian matrices that are non-diagonalisable, i.e. the geometric multiplicities of their eigenvalues are not all equal to the algebraic multiplicities. Recall, if λ is an eigenvalue of a matrix A with algebraic multiplicity k, any non-zero vector in the nullspace of $(\lambda I - A)^k$ is a generalised eigenvector corresponding to λ. Every $N \times N$ matrix A has a set of N linearly independent genearlised eigenvectors, see [104].

Definition 2.19. Let $A \in \mathbb{R}^{N \times N}$ and let $v_1, v_2, \ldots, v_N$ be a linearly independent set of generalised eigenvectors of A. We can write $v_k = u_k + iw_k$ and denote the corresponding eigenvalue as $\lambda_k \in \mathbb{C}$.

1. The *stable subspace* of A, given by E^s, is the span of all u_k and w_k for which $|\lambda_k| < 1$, and

2. the *unstable subspace* of A, given by E^u, is the span of all u_k and w_k for which $|\lambda_k| > 1$,

If f is linear, then W^s and W^u are the linear subspaces E^s and E^u respectively. Then, the number of stable and unstable eigenvalues give their dimensions respectively. For a hyperbolic fixed point $\mathbf{x}^*$ and $A = Df(\mathbf{x}^*)$ if f is nonlinear then $W^s(\mathbf{x}^*)$ emanates from $\mathbf{x}^*$ tangent to E^s. This works similarly for $W^u(\mathbf{x}^*)$.

2.6 Lyapunov exponents and chaos

The concept of chaos has been introduced in a qualitative way in Chapter 1. In this section we try to understand chaos in a more mathematical way, first in terms of maximum Lyapunov exponents and then providing a definition by Devaney. Various non-equivalent definitions of chaos have been also used in the literature, see [120].

The *Lyapunov exponent* measures the asymptotic rate of separation of infinitesimally close orbits of a dynamical system, i.e., the rate at which nearby orbits converge or diverge. This rate varies for different alignments of the initial separation vector. Oseledet's theorem [52] says that there exists a spectrum of Lyapunov exponents, equal to the number of dimensions of the dynamical system. Of these Lyapunov exponents, the largest one is said to be the *maximal Lyapunov exponent*. A positive maximal Lyapunov exponent refers to an exponential instability and is indicative of *chaos*.

Definition 2.20. According to Devaney [15,32], for an invariant set $\Lambda \subset \chi$, a map f is said to be *chaotic* if the following conditions are satisfied:

1. f is transitive, i.e, for any two open sets $\Lambda_1, \Lambda_2 \subset \chi$ with $\Lambda_1 \cap \Lambda \neq \varnothing$ and $\Lambda_2 \cap \Lambda \neq \varnothing$, there exists $n \geq 0$, such that $f^n(\Lambda_1) \cap \Lambda_2 \neq \varnothing$,

2. periodic points of f are dense in Λ, and

3. f displays sensitive dependence on initial conditions, i.e., there exists a positive real number δ such that for every point $x \in \Lambda$ and every neighbourhood $\mathcal{N}$ of this point x, there exists $y \in \mathcal{N}$ and $n \geq 0$ such that the distance between $f^n(x)$ and $f^n(y)$ is greater than δ.

Note that condition (3) is redundant, see [15].

2.7 Bifurcations

We have already defined what a *bifurcation* is in Chapter 1. The simplest types of bifurcations take place when the stability of a fixed point changes, or more generally the

dimension of its unstable manifold changes. The three generic ways this can happen are when an eigenvalue attains the value 1 (saddle-node bifurcation), -1 (period-doubling bifurcation), or $e^{\pm i\theta}$ for some $0 < \theta < \pi$ (Neimark-Sacker bifurcation) [83]. These are all codimension-one bifurcations.

At a saddle-node bifurcation two fixed points collide and annihilate. At a period-doubling bifurcation, on the other hand, under parameter variation a period-2 solution is created, whose stability matches that of the fixed point on the other side of the bifurcation. The bifurcation is termed a *subcritical bifurcation* when the period-2 solution coexists with the fixed point when $\lambda > -1$, and called a *supercritical bifurcation* when the period-2 solution coexists with the fixed point when $\lambda < -1$. Finally, at a Neimark-Sacker bifurcation, there exists a complex conjugate pair of eigenvalues $e^{\pm i\theta}$ with $0 < \theta < \pi$ for a fixed point. Under parameter variation, excepting some disallowed values of θ called *strong resonances* [83], an invariant circle is created at the bifurcation.

These bifurcations can also be recognised on the (τ, δ)-plane (see Fig. 2.1):

1. saddle-node bifurcations occur on the line $\delta = \tau - 1$,

2. period-doubling bifurcations occur on the line $\delta = -\tau - 1$, and

3. Neimark-Sacker bifurcations occur on the line $\delta = 1$ with $-2 < \tau < 2$.

2.8 Renormalisation

Renormalisation [122] was famously employed by Feigenbaum in the 1970's to prove that the bifurcation values in period-doubling cascades converge at a rate that is independent of the equations of motion. That is, this rate is a universal constant. Below we explain this and how we intend to apply renormalisation to families of piecewise-linear maps.

Let a one-parameter family of maps be denoted by f_μ where $\mu \in \mathbb{R}$ is the bifurcation parameter. Suppose this family has an infinite sequence $\{\mu_n\}$ of period-doubling bifurcations where, at each μ_n, a period-2^n solution emerges. Such a sequence is called a *period-doubling cascade* and these are a common mechanism by which chaotic dynamics is created under parameter variation. Such cascades occur over finite parameter ranges, meaning the sequence converges to some value μ_∞. Usually the convergence occurs monotonically and between any two consecutive bifurcations, μ_n and μ_{n+1}, there is a point where the period-2^n has a stability multiplier of 0.

Discovered by Feigenbaum in the 1970's, although in fact described earlier by Myrberg, see e.g. [101], the *Feigenbaum constant* F is a universal constant for period-doubling cascades. The constant F is the limiting value of $\frac{\mu_n-\mu_{n-1}}{\mu_{n+1}-\mu_n}$ and given by $F \approx 4.669$.

To briefly indicate where this number comes from, let $\mathfrak{U}$ denote the collection of all unimodal maps $f : [-1, 1] \to [-1, 1]$, that attain their maximum value at $x = 0$, and with $f(0) = 1$. Then, the *renormalisation operator* $\mathfrak{R} : \mathfrak{U} \to \mathfrak{U}$ is given by,

$$(\mathfrak{R}f)(\mathbf{x}) = -\frac{1}{a}f^2(-a\mathbf{x}), \tag{2.7}$$

provided, $a = -f(1)$, $b = f(a)$, $0 < a < b < 1$ and $f(b) < a$. Given some member f of $\mathfrak{U}$, $\mathfrak{R}$ generates another member that is conjugate to the second iterate f^2. We can think of $\mathfrak{R}$ as an infinite-dimensional map. It has a fixed point corresponding to a particular member of $\mathfrak{U}$ that relates to the limit μ_∞. It is known that this fixed point is hyperbolic and has exactly one positive (unstable) eigenvalue. This eigenvalue is Feigenbaum's constant F.

2.9 The border-collision normal form

Now the focus of this background chapter shifts from maps in general to piecewise-linear maps. Applications of piecewise-linear maps were discussed in Chapter 1. The piecewise-linear map that we focus on in this thesis is the *border-collision normal form*. As given earlier by (1.8), the N-dimensional border-collision normal form is

$$\mathbf{x}_{i+1} = \begin{cases} C_L\mathbf{x}_i + e_1\mu, & e_1^{\mathsf{T}}\mathbf{x}_i \leq 0, \\ C_R\mathbf{x}_i + e_1\mu, & e_1^{\mathsf{T}}\mathbf{x}_i \geq 0, \end{cases}$$

where C_L and C_R are companion matrices and e_1 is the first standard basis vector of $\mathbb{R}^N$.

Also recall from Chapter 1 we obtained the more general form

$$\mathbf{x}_{i+1} = f(\mathbf{x}_i; \mu, \nu) = \begin{cases} A_L(\nu)\mathbf{x}_i + b(\nu)\mu, & e_1^{\mathsf{T}}\mathbf{x}_i \leq 0, \\ A_R(\nu)\mathbf{x}_i + b(\nu)\mu, & e_1^{\mathsf{T}}\mathbf{x}_i \geq 0, \end{cases}$$

as (1.7) to describe the dynamics near a border-collision bifurcation. This form assumes the bifurcation happens at $\mathbf{x} = 0$ when $\mu = 0$. The matrices A_L and A_R and the vector b are arbitrary except A_L and A_R differ in only their first columns for the continuity of f. Except in special cases, the map (1.7) can be transformed to (1.8) via an affine change of

coordinates. Here we explain this precisely.

Let us write an arbitrary affine coordinate transformation as

$$\mathbf{x} \mapsto T\mathbf{x} + q\mu, \qquad \mu \mapsto a\mu, \tag{2.8}$$

where $T \in \mathbb{R}^{N\times N}$, $q \in \mathbb{R}^N$ and $a \in \mathbb{R}$. In order for (2.8) to be invertible and not disrupt the switching manifold we require

1. $e_1^{\mathsf{T}} T = e_1^{\mathsf{T}}$,
2. $e_1^{\mathsf{T}} q = 0$,
3. $\det(T) \neq 0$, and
4. $a \neq 0$.

Actually in condition (1) we only require $e_1^{\mathsf{T}} T = \kappa e_1^{\mathsf{T}}$ for some $\kappa > 0$ but if this is possible we can always impose $\kappa = 1$ by scaling.

The existence of such a transformation requires us to consider the fixed points of (1.7). If the matrices $I - A_L$ and $I - A_R$ are nonsingular, there are two possible fixed points given by

$$\mathbf{x}_J = (I - A_J)^{-1} b\mu, \tag{2.9}$$

for $J = L, R$. Each of these two fixed points is said to be *admissible* if it lies on the appropriate side of the switching manifold or on it. Otherwise it is said to be *virtual*. Let

$$\rho^{\mathsf{T}} = e_1^T \mathrm{adj}(I - A_J), \tag{2.10}$$

where $\mathrm{adj}(M)$ denotes the *adjugate* of a matrix M (for any square matrix M the adjugate exists and satisfies $\mathrm{adj}(M)M = M\mathrm{adj}(M) = \det(M)I$). By multiplying both sides of (2.9) by e_1^{T} on the left, we get

$$e_1^{\mathsf{T}} \mathbf{x}_J = \frac{\rho^{\mathsf{T}} b}{\det(I - A_J)} \mu. \tag{2.11}$$

As the parameter μ is varied from zero, both the fixed points move from the switching manifold if and only if $\rho^{\mathsf{T}} b \neq 0$, which is therefore a non-degeneracy condition for the BCB at $\mu = 0$, see [126].

The coordinate change that we aim to achieve is only possible if (1.7) satisfies an 'observability' condition [33]. The pair (A_L, e_1^{T}) is said to be *observable* if the matrix

$$\mathcal{O}_J = \begin{bmatrix} e_1^{\mathsf{T}} A_J^{N-1} & \dots & e_1^{\mathsf{T}} A_J & e_1^T \end{bmatrix}, \tag{2.12}$$

is invertible for $J = L$. This property refers to the linear map $\mathbf{x} \mapsto A_L\mathbf{x}$. For more detailed discussion see [126]. The following result shows that observability is exactly the condition we need in order to be able to transform the left piece of the general map (1.7) to the left piece of the normal form (1.8).

Lemma 2.1. *There exists an invertible matrix T with $e_1^{\mathsf{T}} T = e_1^{\mathsf{T}}$, such that TA_LT^{-1} is a companion matrix of the form C_J, if and only of $\mathcal{O}_L$ is non-singular.*

The next result shows that the same transformation applies to the right piece of (1.7). This is a consequence of the continuity of (1.7).

Lemma 2.2. *Suppose T is invertible with $e_1^{\mathsf{T}} T = e_1^{\mathsf{T}}$ and TA_LT^{-1} is a companion matrix. If A_R differs from A_L in only its first column then TA_RT^{-1} is also a companion matrix.*

These results lead us to the following theorem that provides explicit formulas for the components of the transformation (2.8). Again, see [126] for a more detailed discussion.

Theorem 2.3. *Suppose $\mathcal{O}_L$ is nonsingular. Let*

$$T = [A_L^{N-1}\mathcal{O}_L^{-1}e_1 | \dots | A_L\mathcal{O}_L^{-1}e_1 | \mathcal{O}_L^{-1}e_1]^{-1}, \tag{2.13}$$

$$q = (I - C)^{-1}(e_1\rho^{\mathsf{T}} - T)b, \tag{2.14}$$

$$a = \rho^{\mathsf{T}} b, \tag{2.15}$$

for any companion matrix C with $I - C$ non-singular. Then under the transformation (2.8)*, the map* (1.7) *transforms to* (1.8)*.*

The idea is that (1.7) approximates the dynamics of a general piecewise-smooth map for small values of $\mathbf{x}$ and μ (i.e. near the border-collision bifurcation). Since (1.7) is piecewise-linear, the magnitude of $\mu \neq 0$ can be scaled to unity, so, for purposes of understanding the dynamics of (1.7) with $\mu \neq 0$, it suffices to consider $\mu = 1$.

Next, we discuss the border-collision normal form in one dimension, followed by the normal form in two-dimensions.

2.9.1 The border-collision normal form in one-dimension

The border-collision normal form in one dimension consists of skew tent maps

$$x \mapsto \begin{cases} \tau_L x + 1, & x \leq 0, \\ \tau_R x + 1, & x \geq 0. \end{cases} \tag{2.16}$$

As we will see this corresponds to the two-dimensional border-collision normal form in the special case $\delta_L = \delta_R = 0$, and it is helpful to view the bifurcation structures described in later sections as extensions or perturbations from the structure that arises in one dimension. Here we focus on slopes $\tau_L > 1$ and $\tau_R < -1$. For any values of the parameters τ_L and τ_R for which (2.16) has an attractor, this attractor is unique. The attractor exists if a certain condition on the parameters τ_L and τ_R is satisfied, i.e., $\phi_0(\tau_L, \tau_R) > 0$ (ϕ_0 is defined below). However, proving the uniqueness of the attractor is a tedious task and has been reported by Ito *et al.* [72,73]. Fig. 2.2 shows typical examples of the attractor using $\tau_L > 1$ and $\tau_R < -1$ with which (2.16) is piecewise-expanding, so the attractor is chaotic in a strict sense by the results of Lasota and Yorke [85] and Li and Yorke [88]. In panel (a) the attractor is the interval $[\tau_R + 1, 1]$ whose endpoints are the first and second iterates of the switching value $x = 0$. In panel (b) the attractor is a disjoint union of four intervals whose endpoints are the first through eighth iterates of $x = 0$.

For all values of τ_L and τ_R the nature of the attractor is well understood [94, 103, 134]. Fig. 2.3 shows how the part of the (τ_L, τ_R)-plane that is relevent to us divides into regions according to the number of intervals that comprise the attractor. In the top-left region labelled LR the map has a stable period-two solution. This solution has one point in the left half-plane and one point in the right half-plane, so is termed an LR-cycle. This region is bounded by the curve $\alpha_0(\tau_L, \tau_R) = 0$, where

$$\alpha_0(\tau_L, \tau_R) = \tau_L \tau_R + 1, \tag{2.17}$$

which is where the LR-cycle loses stability by attaining a stability multiplier of -1. The boundary in the lower-right part of the figure is a homoclinic bifurcation where $x = 0$ maps in two iterations to the fixed point of (2.16) in $x < 0$. This occurs on the curve $\phi_0(\tau_L, \tau_R) = 0$, where

$$\phi_0(\tau_L, \tau_R) = \tau_L \tau_R + \tau_L - \tau_R. \tag{2.18}$$

As shown by Ito *et al.* [72, 73] the remaining boundaries can be identified through renormalisation as follows. Suppose there exists an interval neighbourhood I of $x = 0$ that maps into $x > 0$ then, on the second iteration, back into I. In this case the restriction of the second iterate of (2.16) to I is piecewise-linear with two pieces. The $x < 0$ piece corresponds to iterates with symbolic itinerary LR and has slope $\tau_L\tau_R < -1$, while the $x > 0$ piece corresponds to iterates with symbolic itinerary RR and has slope $\tau_R^2 > 1$, i.e., the interval always maps to the right piece of the map. Thus the second iterate of (2.16) on I is conjugate to (2.16) with τ_R^2 in place of τ_L and $\tau_L\tau_R$ in place of τ_R. This corresponds to the *substitution rule* $(L, R) \mapsto (RR, LR)$, and induces the *renormalisation operator*

$$g_0(\tau_L, \tau_R) = (\tau_R^2, \tau_L\tau_R). \tag{2.19}$$

By using the preimages of the homoclinic bifurcation boundary we define the sequence of regions

$$\mathcal{R}_n = \left\{(\tau_L, \tau_R) \,\middle|\, \tau_R < -1, \phi_0(g^n(\xi)) > 0, \phi_0\big(g^{n+1}(\xi)\big) \le 0, \alpha_0(\tau_L, \tau_R) < 0\right\}, \tag{2.20}$$

shown in Fig. 2.3. These are non-empty for all $n \ge 0$ and converge to $(\tau_L, \tau_R) = (1, -1)$ as $n \to \infty$. In $\mathcal{R}_0$ the attractor consists of one interval:

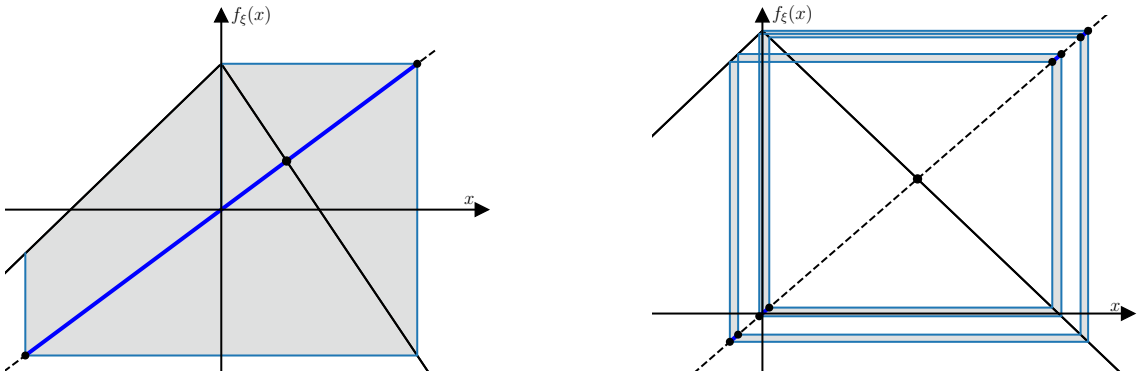

(a) $(\tau_L, \tau_R) = (1.3, -2)$. (b) $(\tau_L, \tau_R) = (1.1, -1.1)$.

Figure 2.2: Cobweb diagrams showing the attractor of the skew tent map (2.16) with two different combinations of the parameter values. In (a) the attractor is an interval; in (b) the attractor is the union of four disjoint intervals. The maps are also instances of the two-dimensional border-collision normal form (2.21) with $\xi = (1.3, 0, -2, 0)$ in panel (a) and $\xi = (1.1, 0, -1.1, 0)$ in panel (b).

Theorem 2.4. *For any* $(\tau_L, \tau_R) \in \mathcal{R}_0$ *with* $\tau_L \geq 1$*, the interval* $[\tau_R + 1, 1]$ *is the unique attractor.*

A simple proof of Theorem 2.4 can be found in the work by Veitch and Glendinning [140]. The condition $\tau_L \geq 1$ is needed because for some $0 < \tau_L < 1$ and $\tau_R < -1$ the attractor is periodic. This condition can be weakened but this is not needed for our purposes.

To characterise the attractor in the other regions $\mathcal{R}_n$ we first make the following observation that follows simply from the definitions of g and $\mathcal{R}_n$.

Proposition 2.1. *If* $(\tau_L, \tau_R) \in \mathcal{R}_n$ *with* $n \geq 1$*, then* $g_0(\tau_L, \tau_R) \in \mathcal{R}_{n-1}$.

Thus if $(\tau_L, \tau_R) \in \mathcal{R}_n$ then $g^n(\tau_L, \tau_R) \in \mathcal{R}_0$. Theorem 2.4 can be applied at this parameter point because any point below $\tau_R = -1$ maps under g to the right of $\tau_L = 1$. Moreover, the above conjugacy can be shown to hold under all n applications of g, see

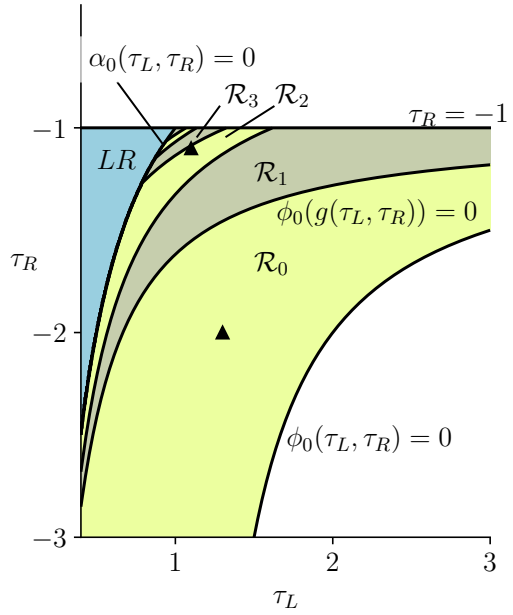

Figure 2.3: A two-parameter bifurcation diagram of the skew tent map family (2.16). In the part of $\mathcal{R}_0$ that is shown the attractor of (2.16) is an interval. In each $\mathcal{R}_n$ with $n \geq 1$ the attractor is comprised of 2^n disjoint intervals. Below $\phi_0(\tau_L, \tau_R) = 0$ the map has no attractor; above $\tau_R = -1$ it has a stable fixed point in $x > 0$; in the top-left region it has a stable LR-cycle (period-two solution). The triangles indicate the parameter values used in Fig. 2.2.

Ito *et al.* [72, 73], thus the 2^n-iterate of (2.16) has an interval attractor. The images of this interval under (2.16) give 2^n disjoint intervals and hence the following result.

Theorem 2.5. *If $(\tau_L, \tau_R) \in \mathcal{R}_n$ with $n \geq 1$, then* (2.16) *has a unique attractor comprised of 2^n disjoint intervals.*

2.9.2 The border-collision normal form in two dimensions

In two dimensions it is convenient to write $\mathbf{x} = (x, y) \in \mathbb{R}^2$. The normal form (1.8) can be written as

$$(x, y) \mapsto f_\xi(x, y) = \begin{cases} \begin{bmatrix} \tau_L x + y + 1 \\ -\delta_L x \end{bmatrix}, & x \leq 0, \\ \begin{bmatrix} \tau_R x + y + 1 \\ -\delta_R x \end{bmatrix}, & x \geq 0, \end{cases} \tag{2.21}$$

for the left and right pieces of (2.21), where

$$\xi = (\tau_L, \delta_L, \tau_R, \delta_R). \tag{2.22}$$

From here on we write

$$f_{L,\xi}(x, y) = \begin{bmatrix} \tau_L x + y + 1 \\ -\delta_L x \end{bmatrix}, \tag{2.23}$$

and

$$f_{R,\xi}(x, y) = \begin{bmatrix} \tau_R x + y + 1 \\ -\delta_R x \end{bmatrix}. \tag{2.24}$$

The family (2.21) was originally formulated by Nusse and Yorke [102] with an additional parameter μ that when varied through zero brings about a border-collision bifurcation [10]. The simplicity of (2.21) belies the incredible complexity of its dynamics; it can exhibit two-dimensional attractors [54, 56], large numbers of coexisting attractors [112, 125, 130], and Arnold tongues with a unique sausage-string geometry [128]. In the special case $\tau_L = -\tau_R$ and $\delta_L = \delta_R$, (2.21) reduces to the Lozi family [92].

At any point with $x \neq 0$ the derivative of (2.21) has determinant

$$\det\big((\mathrm{D}f_\xi)(x,y)\big) = \begin{cases} \delta_L, & x < 0, \\ \delta_R, & x > 0. \end{cases}$$

Consequently we have the following cases.

- If $\delta_L > 0$ and $\delta_R > 0$ then f_ξ is orientation-preserving. This is the most natural case to consider from an applied perspective because Poincaré maps derived from time-reversible flows on $\mathbb{R}^N$ are necessarily orientation-preserving [142].
- If $\delta_L < 0$ and $\delta_R < 0$ then f_ξ is orientation-reversing. This case was considered in the seminal work of Misiurewicz [99] for the Lozi map. Such maps can be embedded into higher dimensional orientation-preserving maps and in this way help us understand high-dimensional chaos in physical systems [78].
- If δ_L and δ_R have opposite signs then f_ξ is non-invertible with the left and right half-planes mapping onto either the top or the bottom half-plane. Such maps, except piecewise-smooth instead of piecewise-linear, apply to a wide range of power converters [13, 41, 144]. For instance, the boost converter described by Banerjee *et al.* [14] regulates output voltage via a switch that is activated whenever the current reaches a threshold value. This causes the flow (in phase space) to fold back over itself resulting in a stroboscopic map that is piecewise-smooth (due to the switch) and non-invertible (due to the folding) [27, 46].
- If one of δ_L and δ_R is zero then f_ξ is non-invertible with one half-plane mapping onto a line [80]. Such maps arise as leading-order approximations to grazing-sliding bifurcations in relay control systems [38] and mechanical systems with stick-slip friction [40, 135]. This is because trajectories of the differential equations become constrained to a codimension-one discontinuity surface causing the range of one piece of the Poincaré map to have one less dimension than the domain of the map [38]. This also occurs for the Hicksian trade cycle model of Puu *et al.* [114] and the influenza outbreak model of Roberts *et al*. [115].

Let

$$\Phi = \big\{\xi \in \mathbb{R}^4 \,\big|\, \tau_L > |\delta_L + 1|,\ \tau_R < -|\delta_R + 1|\big\} \tag{2.25}$$

denote the set of all ξ for which f_ξ has two saddle fixed points (Lemma 2.3). Banerjee *et al.* [14] considered $\xi \in \Phi$ in the orientation-preserving case and showed that on one side of

a homoclinic bifurcation the stable manifold of one fixed point has transverse intersections with the unstable manifolds of both fixed points and argued that this implies the existence of a chaotic attractor. Their conclusion was verified rigorously by Glendinning and Simpson [58] using the methodology of Misiurewicz [99]. First, a forward invariant region $\Omega \subset \mathbb{R}^2$ was identified by using one of the unstable manifolds, and this was perturbed into a *trapping region* that necessarily contains a topological attractor. Second, an *invariant expanding cone* $\Psi \subset T\mathbb{R}^2$ (see §5.4) was constructed by using eigenvectors of the two pieces of $\mathrm{D}f_\xi$. The existence of this object implies that nearby forward orbits diverge exponentially and that the attractor is chaotic in the sense of having a positive Lyapunov exponent. In general this approach works brilliantly for piecewise-linear maps because the invariance and expansion properties can be verified by simple, explicit computations. For more complicated constructions the verification is best done on a computer [59]. The construction is robust to nonlinear perturbations to the pieces of the map and has been used to show that chaos persists for intervals of parameter values beyond border-collision bifurcations [131]. Recently this approach has also been applied to piecewise-smooth maps with a square-root singularity that arise for mechanical systems with hard impacts [97]. Further techniques can reveal more properties of the attractor, such as sensitive dependence on initial conditions, continuity with respect to ξ [5, 81], and the presence of an SRB measure [55].

For any $\xi \in \Phi$ the map f_ξ has fixed points

$$X = \left(\frac{-1}{\tau_R - \delta_R - 1}, \frac{\delta_R}{\tau_R - \delta_R - 1} \right), \tag{2.26}$$

$$Y = \left(\frac{-1}{\tau_L - \delta_L - 1}, \frac{\delta_L}{\tau_L - \delta_L - 1} \right), \tag{2.27}$$

where X is in the right half-plane and Y is in the left half-plane, see Fig 2.4 for a typical phase portrait of (2.21) consisting of the fixed points X and Y along with an attractor Λ. The stability multipliers associated with X and Y are the eigenvalues of the Jacobian matrices

$$A_L = \begin{bmatrix} \tau_L & 1 \\ -\delta_L & 0 \end{bmatrix}, \qquad A_R = \begin{bmatrix} \tau_R & 1 \\ -\delta_R & 0 \end{bmatrix}. \tag{2.28}$$

Since $\xi \in \Phi$, A_L has eigenvalues $\lambda_L^s \in (-1, 1)$ and $\lambda_L^u > 1$, while A_R has eigenvalues $\lambda_R^s \in (-1, 1)$ and $\lambda_R^u < -1$. This implies X and Y are saddles. In fact, Φ is the set of all parameter combinations for which f_ξ has two saddle fixed points:

Lemma 2.3. *The map f_ξ has two saddle fixed points if and only if $\xi \in \Phi$.*

Proof. If $\delta_L = \tau_L - 1$ then f_L has no fixed points, while if $\delta_L \neq \tau_L - 1$ then f_L has the unique fixed point Y, given by (2.27). Similarly if $\delta_R = \tau_R - 1$ then f_R has no fixed points, while if $\delta_R \neq \tau_R - 1$ then f_R has the unique fixed point X, given by (2.26).

If $\xi \in \Phi$ then X and Y are saddle fixed points of f_ξ, as noted above. Conversely, suppose f_ξ has two saddle fixed points. By the above remarks, these must be X and Y. Since they are fixed points of f_ξ, Y is in the left half-plane, so $\tau_L > \delta_L + 1$ by (2.27), and X is in the right half-plane, so $\tau_R < \delta_R + 1$ by (2.26). Since they are saddles, also $\tau_L > -(\delta_L + 1)$ and $\tau_R < -(\delta_R + 1)$, hence $\xi \in \Phi$. □

Let P be one of the saddle fixed points X or Y. The stable manifold of P is defined as

$$W^s(P) = \left\{ z \in \mathbb{R}^2 \,\middle|\, f_\xi^n(z) \to P \text{ as } n \to \infty \right\}. \tag{2.29}$$

For all $\xi \in \Phi^{(1)}$ the map f_ξ is invertible so the unstable manifold of P is defined analogously as

$$W^u(P) = \left\{ z \in \mathbb{R}^2 \,\middle|\, f_\xi^{-n}(z) \to P \text{ as } n \to \infty \right\}. \tag{2.30}$$

Since P is a saddle, $W^s(P)$ and $W^u(P)$ are one-dimensional. As with smooth maps, from P they emanate tangent to the stable and unstable subspaces $E^s(P)$ and $E^u(P)$. These

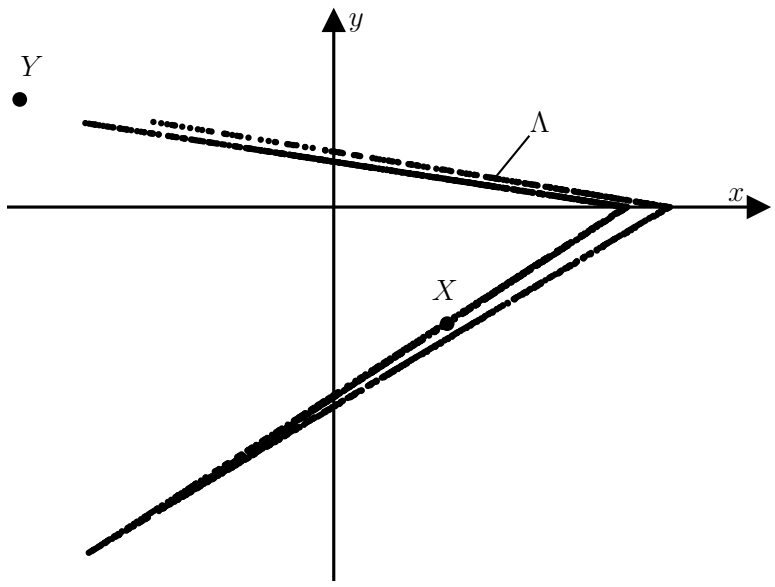

Figure 2.4: A typical phase portrait of f_ξ. We have shown the fixed points X and Y. The black dots show 2000 iterates of the forward orbit of the origin after transient dynamics has decayed.

subspaces are the lines through P with directions given by the eigenvectors of $\mathrm{D}f_\xi(P)$. But since f_ξ is piecewise-linear, $W^s(P)$ and $W^u(P)$ in fact *coincide* with $E^s(P)$ and $E^u(P)$ in a neighbourhood of P. Globally they have a piecewise-linear structure: $W^s(P)$ has kinks on the switching line $x = 0$ and on the backward orbits of these points; $W^u(P)$ has kinks on the image of switching line, $y = 0$, and on the forward orbits of these points.

In the next chapter, we consider the part of Φ for which the border-collision normal form is orientation-preserving and introduce a renormalisation operator that divides the parameter space according to the number of components of a chaotic attractor.

Chapter 3

Renormalisation of the two-dimensional border-collision normal form.

3.1 Introduction

The two-dimensional border-collision normal form introduced in Chapter 1 given by

$$f_{L,\xi}(x,y) = \begin{bmatrix} \tau_L x + y + 1 \\ -\delta_L x \end{bmatrix},$$

and

$$f_{R,\xi}(x,y) = \begin{bmatrix} \tau_R x + y + 1 \\ -\delta_R x \end{bmatrix},$$

with $(x,y) \in \mathbb{R}^2$ and $\xi \in \mathbb{R}^4$, has the border-collision bifurcation parameter (denoted by μ) scaled to 1. Banerjee *et al.* [14] identified an open parameter region $\Phi_{\mathrm{BYG}} \subset \mathbb{R}^4$ (defined below) throughout which f_ξ has a chaotic attractor, and this was shown formally by Glendinning and Simpson [58].

While it is known from the work of Glendinning and Simpson [58] that f_ξ has a chaotic attractor throughout Φ_{BYG}, the attractor undergoes bifurcations (more specifically, crises [62]) as the value of ξ is varied within Φ_{BYG}. The purpose of this chapter is to reveal the bifurcation structure within Φ_{BYG} and we achieve this via renormalisation. Renormalisation has also been applied to subfamilies of (2.21) by Pumariño *et al.* [112, 113] and Ou [108].

In this chapter, we apply renormalisation to (2.21) in the following way. On the preimage of the closed right half-plane, denoted Π_ξ, the second iterate of f_ξ is conjugate to

an alternate member of (2.21). That is, f_ξ^2 is conjugate to $f_{g(\xi)}$ for a certain function $g : \mathbb{R}^4 \to \mathbb{R}^4$. By repeatedly iterating a boundary of $\Phi_{\rm BYG}$ backwards under g, we are able to divide $\Phi_{\rm BYG}$ into regions $\mathcal{R}_n$, for $n = 0, 1, 2, \ldots$. We then show that throughout each $\mathcal{R}_n$ the map f_ξ has a chaotic Milnor attractor with 2^n connected components.

The analysis required to achieve these results is significantly more difficult than those of skew tent maps in §2.9.1 because the dimension of the renormalisation operator, $f_\xi \mapsto f_{g(\xi)}$, is four not two. It is necessary to characterise certain aspects of the *global* dynamics of the four-dimensional quadratic map g and show that the relevant dynamics of f_ξ occurs entirely within Π_ξ. While the novel calculations in this chapter are not mathematically technical, they were certainly challenging to derive.

Our main results are presented in §3.2, see Theorems 3.1–3.3. Sections 3.3–3.8 work toward proofs of these results. First §3.3 describes the phase space of (2.21), primarily saddle fixed points and their stable and unstable manifolds. Then in §3.4 we consider the second iterate f_ξ^2 on Π_ξ and construct a conjugacy to $f_{g(\xi)}$. In §3.5 we derive geometric properties of the boundaries of $\mathcal{R}_0$ and in §3.6 study the dynamics of g.

Chaos is proved in the sense of a positive Lyapunov exponent. This positivity is achieved for all points in the attractor, including points whose forward orbits intersect the switching line where f_ξ is not differentiable. This is achieved by using one-sided directional derivatives which are always well-defined in our setting, §3.7. A recursive application of the renormalisation is performed in §3.8.

3.2 Main results

In this section we motivate and define the parameter region $\Phi_{\rm BYG}$ and the renormalisation operator $f_\xi \mapsto f_{g(\xi)}$, then state the main results. First Theorem 3.1 clarifies the geometry of the regions $\mathcal{R}_n \subset \mathbb{R}^4$. Next Theorem 3.2 describes the dynamics of f_ξ in $\mathcal{R}_0$. Finally Theorem 3.3 describes the dynamics of f_ξ in $\mathcal{R}_n$ for any $n \geq 0$ and follows from a recursive application of the renormalisation to Theorem 3.2.

3.2.1 The parameter region $\Phi_{\rm BYG}$

For any $\xi \in \Phi^{(1)}$, where

$$\Phi^{(1)} = \big\{ \xi \in \mathbb{R}^4 \,\big|\, \tau_L > \delta_L + 1,\, \delta_L > 0,\, \tau_R < -(\delta_R + 1),\, \delta_R > 0 \big\}, \tag{3.1}$$

the fixed points X and Y have one-dimensional stable and unstable manifolds. Fig. 3.1 illustrates the stable (blue) and unstable (red) manifolds of Y. These intersect if and only if $\phi(\xi) \leq 0$, where

$$\phi(\xi) = \delta_R - (1+\tau_R)\delta_L + \frac{1}{2}\big((1+\tau_R)\tau_L - \tau_R - \delta_L - \delta_R\big)\left(\tau_L + \sqrt{\tau_L^2 - 4\delta_L}\right). \quad (3.2)$$

Equation (3.2) can be derived by directly calculating the first few linear segments of the stable and unstable manifolds of Y as they emanate from Y, see [58]. As a bifurcation, $\phi(\xi) = 0$ is a homoclinic corner [127] and is analogous to a 'first' homoclinic tangency for smooth maps [110]. Banerjee *et al.* [14] observed that an attractor is often destroyed here, so focussed their attention on the parameter region

$$\Phi_{\mathrm{BYG}} = \big\{\xi \in \Phi^{(1)} \,\big|\, \phi(\xi) > 0\big\}, \quad (3.3)$$

where the stable and unstable manifolds of Y do not intersect (except at Y itself). Indeed for all $\xi \in \Phi_{\mathrm{BYG}}$, f_ξ has a trapping region and therefore a topological attractor [55].

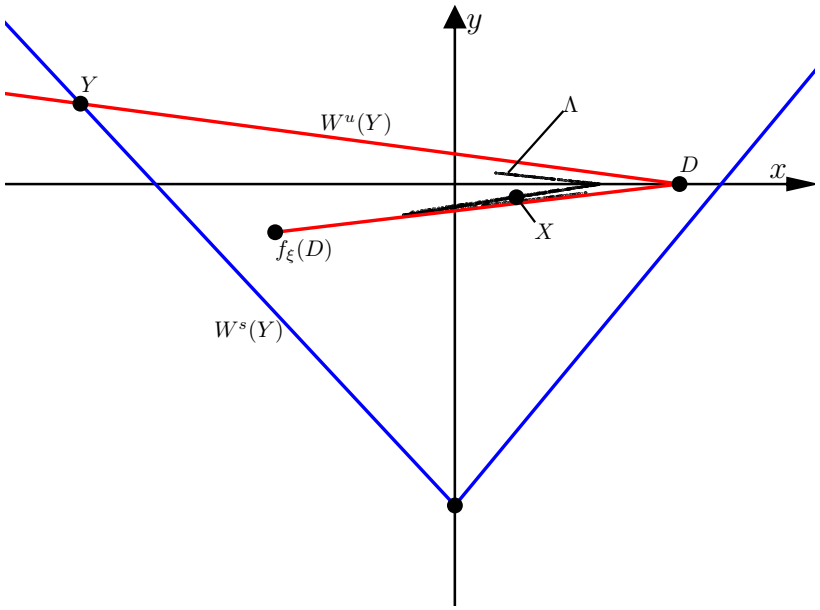

Figure 3.1: A sketch of the phase space of f_ξ (2.21) with $\xi \in \Phi_{\mathrm{BYG}}$. We have shown the fixed points X and Y and the initial parts of $W^s(Y)$ (blue) and $W^u(Y)$ (red) as they emanate from Y (these manifolds do not intersect when $\phi(\xi) > 0$). The small black dots show 1000 iterates of the forward orbit of the origin after transient dynamics has decayed.

3.2.2 The renormalisation operator

On $\mathbb{R}^2$ the second iterate f_ξ^2 is a continuous, piecewise-linear map with four pieces. But if we restrict our attention to the set

$$\Pi_\xi = \big\{ f_\xi^{-1}(x,y) \,\big|\, x \geq 0 \big\}, \tag{3.4}$$

then f_ξ^2 has only two pieces:

$$f_\xi^2(x,y) = \begin{cases} (f_{R,\xi} \circ f_{L,\xi})(x,y), & x \leq 0, \\ f_{R,\xi}^2(x,y), & x \geq 0. \end{cases} \tag{3.5}$$

As shown in Fig. 3.2, the boundary of Π_ξ intersects the switching line at $(x,y) = (0,-1)$ and has slope $-\tau_L < 0$ in $x < 0$ and slope $-\tau_R > 0$ in $x > 0$. For any $\xi \in \Phi^{(1)}$, the map (3.5) is affinely conjugate to the normal form (2.21) (see Proposition 3.3). This is because the switching line of (3.5) satisfies the non-degeneracy conditions mentioned in §2.9.

When the affine transformation to the normal form is applied, the matrix parts of the pieces of (3.5) undergo a similarity transform, thus their traces and determinants are not changed. The matrix part of the $x \leq 0$ piece of (3.5) is $A_R(\xi)A_L(\xi)$, which has trace $\tau_L\tau_R - \delta_L - \delta_R$ and determinant $\delta_L\delta_R$. The matrix part of the $x \geq 0$ piece of (3.5) is $A_R(\xi)^2$, which has trace $\tau_R^2 - 2\delta_R$ and determinant δ_R^2. Hence (3.5) can be transformed to $f_{g(\xi)}$ where

$$g(\xi) = \big(\tau_R^2 - 2\delta_R, \delta_R^2, \tau_L\tau_R - \delta_L - \delta_R, \delta_L\delta_R\big). \tag{3.6}$$

Notice we are transforming the left piece of (3.5) to the right piece of $f_{g(\xi)}$ and the right

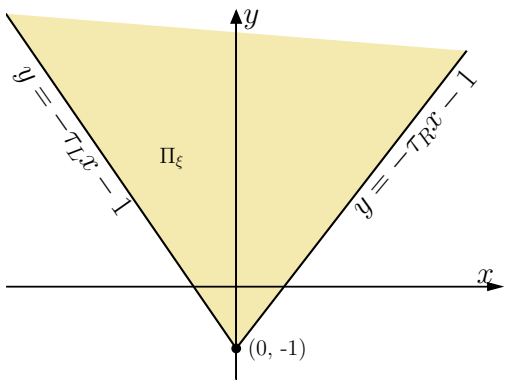

Figure 3.2: The preimage of the closed right half-plane (3.4).

piece of (3.5) to the left piece of $f_{g(\xi)}$. This ensures $g(\xi) \in \Phi^{(1)}$ (see Proposition 3.7) so our renormalisation operator $f_\xi \mapsto f_{g(\xi)}$ produces another member of the family (2.21) in $\Phi^{(1)}$. Also observe

$$\xi^* = (1, 0, -1, 0) \tag{3.7}$$

is a fixed point of g and lies on the boundary of $\Phi^{(1)}$.

3.2.3 Division of parameter space

For all $n \geq 0$ let

$$\zeta_n(\xi) = \phi\big(g^n(\xi)\big). \tag{3.8}$$

The surface $\zeta_n(\xi) = 0$ is an n^{th} preimage of $\phi(\xi) = 0$ under g. We now use these surfaces to form the regions

$$\mathcal{R}_n = \big\{\xi \in \Phi^{(1)} \,\big|\, \zeta_n(\xi) > 0, \zeta_{n+1}(\xi) \leq 0\big\}, \tag{3.9}$$

for all $n \geq 0$. The following result (proved in §3.6.2) gives properties of these regions.

Theorem 3.1. *The $\mathcal{R}_n$ are non-empty, mutually disjoint, and converge to $\{\xi^*\}$ as $n \to \infty$. Moreover,*

$$\Phi_{\text{BYG}} \subset \bigcup_{n=0}^{\infty} \mathcal{R}_n \,. \tag{3.10}$$

Being four-dimensional the $\mathcal{R}_n$ are inherently difficult to visualise. Fig. 3.3 shows two-dimensional cross-sections obtained by fixing the values of $\delta_L > 0$ and $\delta_R > 0$. For any such cross-section only finitely many $\mathcal{R}_n$ are visible because as $n \to \infty$ they converge to $\{\xi^*\}$ for which $\delta_L = \delta_R = 0$. Notice $\mathcal{R}_1$ contains some points that do not belong to Φ_{BYG}. For this reason the two sets in (3.10) are not equal.

3.2.4 A chaotic attractor with one connected component

The next result shows f_ξ has a chaotic, connected Milnor attractor for all $\xi \in \mathcal{R}_0$ when $\delta_R < 1$. This is proved in §3.7.3 and based on the results of [58]. The attractor is the closure of the unstable manifold of X,

$$\Lambda(\xi) = \text{cl}(W^u(X)). \tag{3.11}$$

Theorem 3.2. *For the map f_ξ with any $\xi \in \mathcal{R}_0$,*

1. *$\Lambda(\xi)$ is bounded, connected, and invariant,*

2. *every $z \in \Lambda(\xi)$ has a positive Lyapunov exponent, and*

3. *if $\delta_R < 1$ there exists forward invariant $\Delta \subset \mathbb{R}^2$ with non-empty interior such that*

$$\bigcap_{n=0}^{\infty} f_\xi^n(\Delta) = \Lambda(\xi). \tag{3.12}$$

Lyapunov exponents for (2.21) are clarified in §3.7. Stronger notions of chaos have been obtained on subsets of $\mathcal{R}_0$, see [55, 58]. While we have not been able to prove that $\Lambda(\xi)$ is a topological attractor, (3.12) shows it contains the ω-limit set of all points in Δ. The set Δ has positive Lebesgue measure, thus $\Lambda(\xi)$ is a Milnor attractor [98]. If Δ is a trapping region (i.e. it maps to its interior) then $\Lambda(\xi)$ is an attracting set by definition [117]. If Δ is the trapping region of [58] (there denoted Ω_{trap}) then (3.12) appears to be true for some but not all $\xi \in \mathcal{R}_0$. We expect the extra condition $\delta_R < 1$ is unnecessary but is included in Theorem 3.2 because our proof utilises an area-contraction argument.

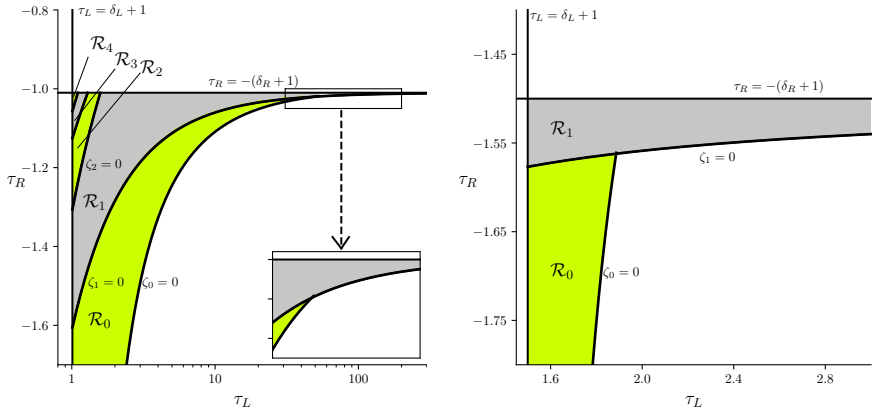

(a) $\delta_L = \delta_R = 0.01$ (b) $\delta_L = \delta_R = 0.5$

Figure 3.3: Two-dimensional cross-sections of the parameter regions $\mathcal{R}_n$. In panel (a) $\mathcal{R}_n$ is visible for all $n = 0, 1, \ldots, 4$; in panel (b) only $\mathcal{R}_0$ and $\mathcal{R}_1$ are visible. In both panels Φ_{BYG} is bounded by the vertical line $\tau_L = \delta_L + 1$, the horizontal line $\tau_R = -\delta_R - 1$, and the curve $\zeta_0 = 0$. See Fig. 3.5 for a one-parameter slice through panel (a) at $\tau_R = -1.12$.

3.2.5 A chaotic attractor with many connected components

For any $\xi \in \mathcal{R}_n$ we have $g^n(\xi) \in \mathcal{R}_0$ (see Lemma 3.8), while Theorem 3.2 describes the dynamics in $\mathcal{R}_0$. Thus by combining the renormalisation with Theorem 3.2 we are able to describe the dynamics of f_ξ with $\xi \in \mathcal{R}_n$.

In view of the way g is constructed, our renormalisation corresponds to the substitution rule

$$(L, R) \mapsto (RR, LR), \tag{3.13}$$

which is identical to that described in §2.9.1 for skew tent maps. Given a word $\mathcal{W}$ comprised of L's and R's of length k, let $\mathcal{F}(\mathcal{W})$ be the word of length $2k$ that results from applying (3.13) to every letter in $\mathcal{W}$. If an orbit of $f_{g(\xi)}$ has symbolic itinerary $\mathcal{W}$, the corresponding orbit of f_ξ has symbolic itinerary $\mathcal{F}(\mathcal{W})$.

The attractor of Theorem 3.2 is the closure of the unstable manifold of X. Consequently for $\xi \in \mathcal{R}_n$ the corresponding attractor is the closure of the unstable manifold of a periodic solution with symbolic itinerary $\mathcal{F}^n(R)$, see Table 3.1.

Theorem 3.3. *Let $n \geq 0$ and $\xi \in \mathcal{R}_n$. Then $g^n(\xi) \in \mathcal{R}_0$ and there exist mutually disjoint sets $S_0, S_1, \ldots, S_{2^n-1} \subset \mathbb{R}^2$ such that $f_\xi(S_i) = S_{(i+1) \bmod 2^n}$ and*

$$f_\xi^{2^n}\big|_{S_i} \text{ is affinely conjugate to } f_{g^n(\xi)}\big|_{\Lambda(g^n(\xi))} \tag{3.14}$$

for each $i \in \{0, 1, \ldots, 2^n - 1\}$. Moreover,

$$\bigcup_{i=0}^{2^n-1} S_i = \mathrm{cl}(W^u(\gamma_n)), \tag{3.15}$$

where γ_n is a saddle-type periodic solution of f_ξ with symbolic itinerary $\mathcal{F}^n(R)$.

Numerical explorations suggest that (3.15) is the unique attractor of (2.21) for any $\xi \in$

Table 3.1: The first few words in the sequence generated by repeatedly applying the symbolic substitution rule (3.13) to R.

n	$\mathcal{F}^n(R)$
0	R
1	LR
2	RRLR
3	LRLRRRLR
4	RRLRRRLRLRLRRRLR

$\mathcal{R}_n$. Theorem 3.3 tells us it has 2^n connected components and is the closure of the unstable manifold of a saddle-type period-2^n solution. Each component S_i is invariant under 2^n iterations of f_ξ. Equation (3.14) tells us that the dynamics of $f_\xi^{2^n}$ on S_i is equivalent (under an affine coordinate change) to that of $f_{g^n(\xi)}$ on $\Lambda(g^n(\xi))$. Since $g^n(\xi) \in \mathcal{R}_0$, the properties listed in Theorem 3.2 apply to $f_\xi^{2^n}$ on S_i. Thus (3.15) is a chaotic Milnor attractor of f_ξ.

As an example, consider f_ξ with

$$\xi_{\rm ex} = (1.15, 0.01, -1.12, 0.01) \in \mathcal{R}_2 \,. \tag{3.16}$$

Fig. 3.4-a shows 1000 points of the forward orbit of the origin after transient behaviour has decayed. As expected these points appear to converge to a chaotic attractor with four connected components. By Theorem 3.3 each component is affinely conjugate to $\Lambda(g^2(\xi))$ which is approximated in Fig. 3.4-b by again iterating the origin. The set $\Lambda(g^2(\xi))$ has a complicated branched structure but this is not visible in Fig. 3.4-b because the determinants are extremely small.

3.2.6 Consequences for one-parameter bifurcation diagrams

Fig. 3.5 shows a numerically computed one-parameter bifurcation diagram obtained by varying the value of τ_L from $\xi_{\rm ex}$. This corresponds to a horizontal slice through Fig. 3.3-a. Each time we cross some $\zeta_n = 0$, pairs of connected components coalesce. So as we cross $\zeta_2 = 0$ the number of connected components decreases from four to two, and after $\zeta_1 = 0$ the attractor has a single connected component. The attractor is destroyed at $\zeta_0 = 0$ past which typical forward orbits diverge.

Within $\Phi_{\rm BYG}$ other one-parameter bifurcation diagrams should have a similar structure. This is because, by the definition of the regions $\mathcal{R}_n$ and the fact they are mutually disjoint (Theorem 3.1), each $\mathcal{R}_n$ can only abut $\mathcal{R}_{n-1}$ (if $n \neq 0$) and $\mathcal{R}_{n+1}$ (except possibly at isolated points, but this doesn't appear to be the case, see Fig. 3.3). Thus as parameters are varied the number of connected components of the attractor is expected to only either halve or double.

3.3 The stable and unstable manifolds of the fixed points

In this section, we discuss the stable and unstable manifolds of the saddle fixed points X and Y. Here and throughout this chapter

$$0 < \lambda_L^s < 1 < \lambda_L^u \tag{3.17}$$

denote the eigenvalues of A_L, and

$$\lambda_R^u < -1 < \lambda_R^s < 0 \tag{3.18}$$

denote the eigenvalues of A_R. These are functions of ξ with $\xi \in \Phi^{(1)}$.

3.3.1 Stable and unstable manifolds of piecewise-linear maps

In the remainder of this section we reproduce the geometric constructions of [58] that will be needed below.

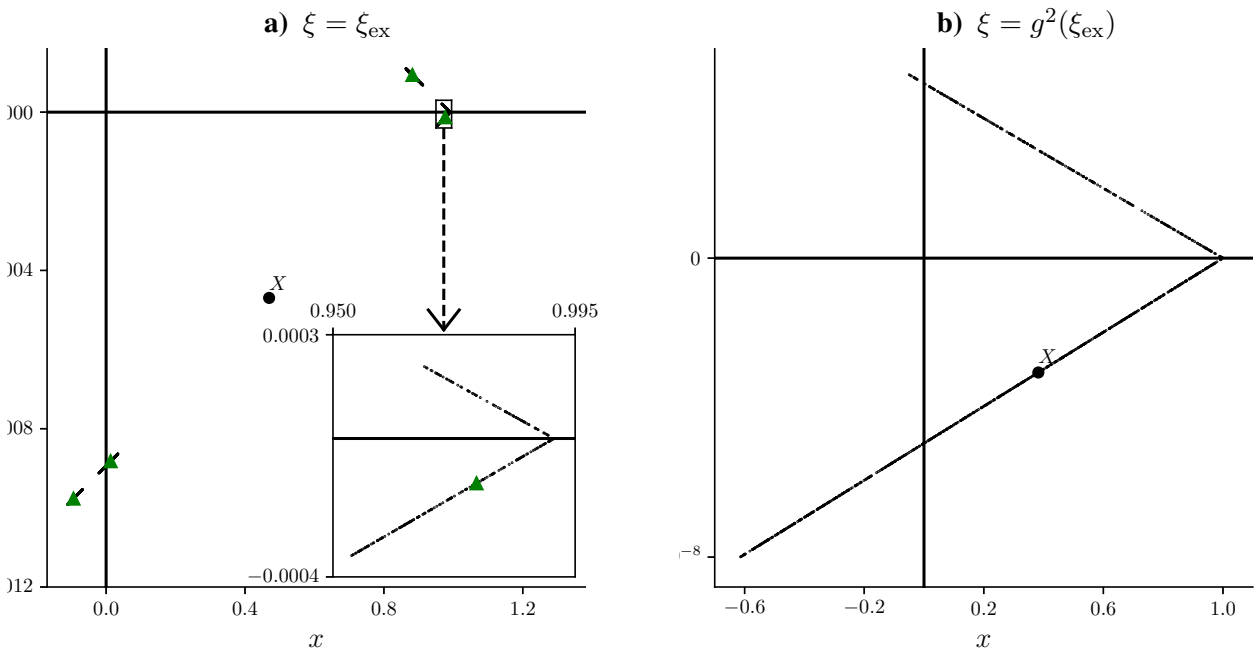

Figure 3.4: Numerically computed attractors of f_ξ with $\xi = \xi_{\text{ex}}$, (3.16), in panel (a), and $\xi = g^2(\xi_{\text{ex}})$ in panel (b). In panel (a) the four small triangles are the points of a periodic solution with symbolic itinerary $\mathcal{F}^2(R) = RRLR$.

3.3.2 The stable and unstable manifolds of Y

Since the eigenvalues of A_L are positive, $W^s(Y)$ and $W^u(Y)$ each have two dynamically independent branches. Let D denote the first kink of the right branch of $W^u(Y)$ as we follow it outwards from Y, see Fig. 3.6. Notice D is the intersection of $E^u(Y)$ with $y = 0$. Now let B denote the intersection of $E^u(Y)$ with the line through $f_\xi(D)$ and parallel to $E^s(Y)$. Then let $\Omega(\xi)$ be the closed compact triangle with vertices D, $f_\xi(D)$, and B.

The following result says $\Omega(\xi)$ is forward invariant under f_ξ. This was proved by direct calculations by Glendinning and Simpson [58]. The key observation is that $f_\xi(D)$ lies to the right of $E^s(Y)$ because $\phi(\xi) > 0$.

Proposition 3.1. *For any* $\xi \in \Phi_{\text{BYG}}$, $f_\xi(\Omega(\xi)) \subset \Omega(\xi)$.

The next result tells us that the attractor of Theorem 3.2 is contained in $\Omega(\xi)$.

Lemma 3.1. *For any* $\xi \in \Phi_{\text{BYG}}$, $\Lambda(\xi) \subset \Omega(\xi)$.

Proof. Since $\Omega(\xi)$ is forward invariant we only need to show $X \in \Omega(\xi)$. By direct calcu-

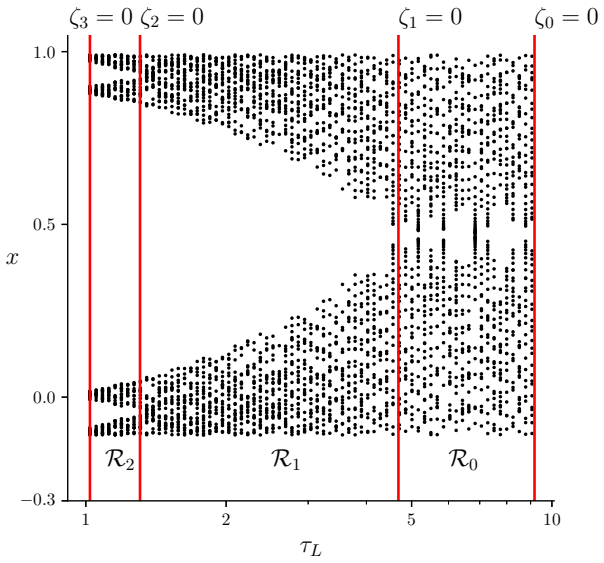

Figure 3.5: A bifurcation diagram of f_ξ with $\tau_R = -1.12$, $\delta_L = \delta_R = 0.01$, and using τ_L as the bifurcation parameter. A log-scale is used for τ_L as in Fig. 3.3-a. For many values of τ_L we are plotting several points of the forward orbit of the origin after transient dynamics has decayed. The bifurcations at which $\zeta_i = 0$ for $0 \leq i \leq 3$ are indicated. See Fig. 3.4-a for a phase portrait with $\tau_L = 1.15$.

lations we find that the line through D and $f_\xi(D)$ is $y = \ell(x)$ where

$$\ell(x) = \frac{\delta_R}{\lambda_L^s - \tau_R}\left(x - \frac{1}{1-\lambda_L^s}\right).$$

From (2.26) we obtain, after much simplification,

$$X_2 - \ell(X_1) = \frac{\delta_R\left(\lambda_L^{s^2} - \tau_R\lambda_L^s + \delta_R\right)}{(\delta_R + 1 - \tau_R)(\lambda_L^s - \tau_R)(1-\lambda_L^s)}.$$

In view of (3.1) and (3.17), each factor in this expression is positive, thus X lies above the line through D and $f_\xi(D)$. Also $X_1 > 0$ and $X_2 < 0$, thus $X \in \Omega(\xi)$ as required. □

3.3.3 The stable and unstable manifolds of X

Since the eigenvalues of A_R are negative, $W^s(X)$ and $W^u(X)$ each have one dynamically independent branch. Let T denote the intersection of $E^u(X)$ with $y = 0$ and let V denote the intersection of $E^s(X)$ with $x = 0$, see Fig. 3.7. It is easily shown that

$$T = \left(\frac{1}{1-\lambda_R^s}, 0\right). \tag{3.19}$$

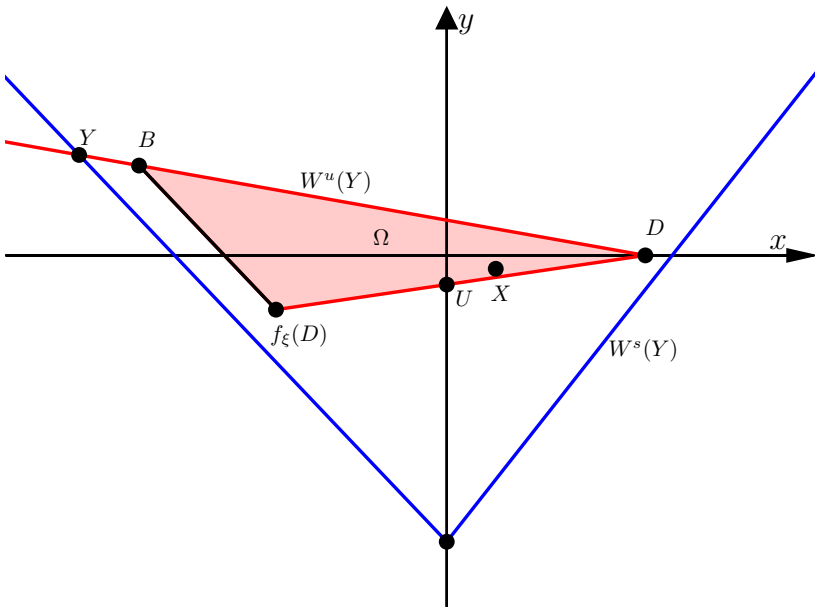

Figure 3.6: A sketch of the phase space of f_ξ with $\xi \in \Phi_{\text{BYG}}$. The triangle $\Omega(\xi)$ is shaded.

If $f_\xi^2(T)$ lies to the left of $E^s(X)$, as in Fig. 3.7-a, then $W^s(X)$ and $W^u(X)$ intersect transversely. If $f_\xi^2(T)$ lies to the right of $E^s(X)$, as in Fig. 3.7-b, then $W^s(X)$ and $W^u(X)$ have no intersection. The following result was obtained by Glendinning [55] by calculating $f_\xi^2(T)$ explicitly.

Proposition 3.2. *For any $\xi \in \Phi^{(1)}$, $f_\xi^2(T)$ lies to the left of $E^s(X)$ if and only if $\psi(\xi) > 0$, where*

$$\psi(\xi) = (\tau_L\tau_R - \delta_R)\lambda_R^u + \left(\frac{\delta_L}{\delta_R} + \delta_L - 1\right)\lambda_R^s - \tau_L(1+\delta_R) + \tau_R(1-\delta_L). \qquad (3.20)$$

As a bifurcation, $\psi(\xi) = 0$ is a homoclinic corner for the fixed point X. This is analogous to the surface $\phi(\xi) = 0$ for the fixed point Y as discussed in §3.2.1.

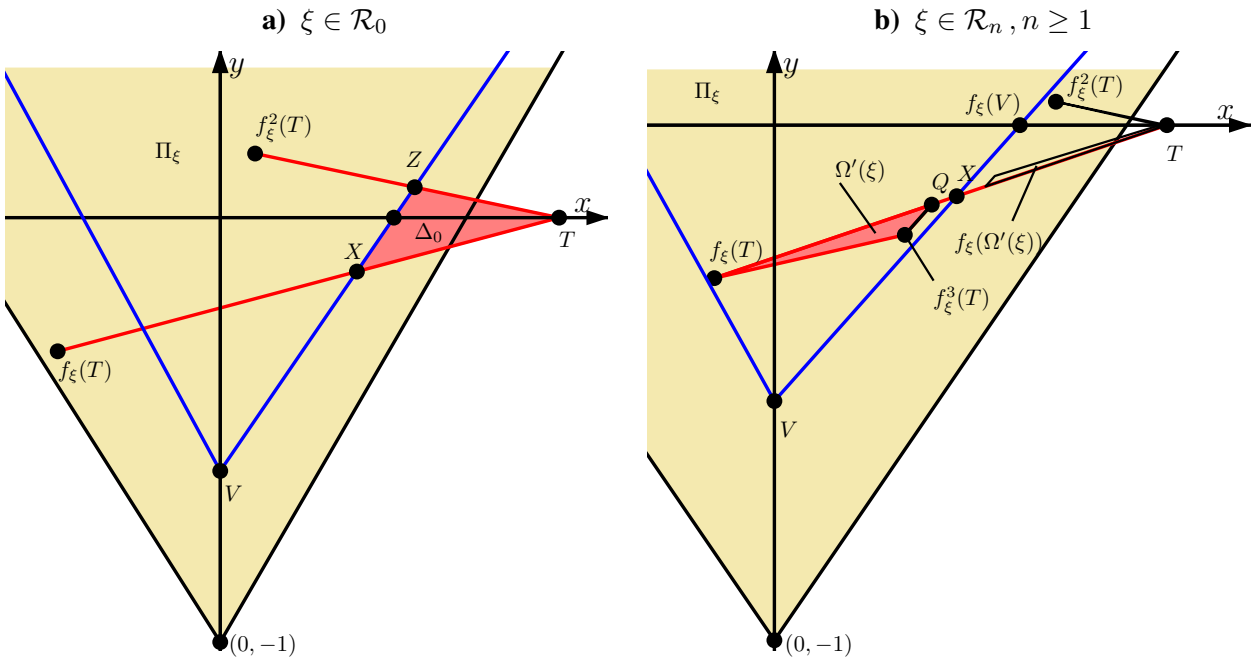

Figure 3.7: Sketches of phase space with $\xi \in \mathcal{R}_0$ in panel (a) and $\xi \in \mathcal{R}_n$ with $n \geq 1$ in panel (b). The set Δ_0 in panel (a) is introduced in §3.7.3. The set Ω' in panel (b) is introduced in §3.8.1.

3.4 The second iterate of f_ξ

As discussed in §3.2.2, on Π_ξ the second iterate of f_ξ is a continuous, piecewise-linear map with two pieces, (3.5). Next in §3.4.1 we provide the affine transformation that converts (3.5) to the normal form (2.21). Then in §3.4.2 we show that the bifurcation surface $\psi(\xi) = 0$ of the previous section is in fact identical to $\zeta_1(\xi) = \phi(g(\xi)) = 0$.

3.4.1 A transformation to the normal form

Any continuous, two-piece, piecewise-linear map on $\mathbb{R}^2$ can be transformed to (2.21) under an affine coordinate transformation, see §2.9.

The switching line of (3.5) satisfies this condition for any $\xi \in \Phi^{(1)}$. As clarified by Proposition 3.3, the required coordinate transformation is

$$h_\xi(x, y) = \frac{1}{\tau_R + \delta_R + 1} \begin{bmatrix} x \\ \delta_R x + \tau_R y - \delta_R \end{bmatrix}. \tag{3.21}$$

Proposition 3.3. *For any $\xi \in \Phi^{(1)}$,*

$$f_\xi^2 = h_\xi^{-1} \circ f_{g(\xi)} \circ h_\xi \,, \tag{3.22}$$

on Π_ξ.

Proof. By directly composing (2.21) and (3.21) we obtain

$$h_\xi \circ f_\xi^2 = \begin{cases} \dfrac{1}{\tau_R + \delta_R + 1} \begin{bmatrix} (\tau_R^2 - \delta_R)x + \tau_R y + \tau_R + 1 \\ -\delta_R^2 x \end{bmatrix}, & x \le 0, \\ \dfrac{1}{\tau_R + \delta_R + 1} \begin{bmatrix} (\tau_L \tau_R - \delta_L)x + \tau_R y + \tau_R + 1 \\ -\delta_L \delta_R x \end{bmatrix}, & x \ge 0, \end{cases}$$

and it is readily seen that $f_{g(\xi)} \circ h_\xi$ produces the same expression. □

Write $(\tilde{x}, \tilde{y}) = h_\xi(x, y)$. Notice that x and $\tilde{x}$ have opposite signs, i.e.

$$\operatorname{sgn}(x) = -\operatorname{sgn}(\tilde{x}). \tag{3.23}$$

This is because $\tau_R + \delta_R + 1 < 0$ by (3.1). Thus the left piece of $f_{g(\xi)}$ corresponds to the right piece of f_ξ^2 in (3.5), and this is consistent with how g was introduced in §3.2.2.

3.4.2 A reinterpretation of ψ

In §3.3.3 we saw that the fixed point X of f_ξ has a homoclinic corner when $\psi(\xi) = 0$. The same is true for f_ξ^2: its fixed point X has a homoclinic corner when $\psi(\xi) = 0$. Notice X is a fixed point of $f_{R,\xi}^2$, which is transformed under (3.22) to $f_{L,g(\xi)}$, which has the fixed point Y. Thus, while the stable and unstable manifolds of X lie in Π_ξ, they transform to the stable and unstable manifolds of Y for $f_{g(\xi)}$. The latter manifolds have a homoclinic corner when $\phi(g(\xi)) = 0$, which suggests that $\psi(\xi) = 0$ and $\phi(g(\xi)) = 0$ are the same surface. The following result tells us that this is indeed the case.

Lemma 3.2. *For any* $\xi \in \Phi^{(1)}$,

$$\phi(g(\xi)) = \tau_R \lambda_R^{u^2} \psi(\xi). \tag{3.24}$$

Proof. Equation (3.2) can be written as

$$\phi(\xi) = (1 + \tau_R)\lambda_L^{u^2} - (\tau_R + \delta_L + \delta_R)\lambda_L^u + \delta_R\,. \tag{3.25}$$

To evaluate $\phi(g(\xi))$, in (3.25) we replace δ_L with δ_R^2, δ_R with $\delta_L\delta_R$, and τ_R with $\tau_L\tau_R - \delta_L - \delta_R$, see (3.6). Also we replace λ_L^u with $\lambda_R^{u^2}$ because $\lambda_R^{u^2}$ is the unstable eigenvalue of A_R^2 (which has trace and determinant given by the first two components of (3.6)). It is a simple (though tedious) exercise to show that upon performing these substitutions and simplifying we obtain $\tau_R \lambda_R^{u^2} \psi(\xi)$. □

3.5 The geometry of the boundary of $\mathcal{R}_0$

The region $\mathcal{R}_0 \subset \mathbb{R}^4$ is bounded by $\zeta_0(\xi) = \phi(\xi) = 0$, $\zeta_1(\xi) = \phi(g(\xi)) = 0$, and the hyperplanes specified in (3.1). Since parameter space is four-dimensional these are difficult to visualise. We can benefit from the fact that the δ_L and δ_R components of g are decoupled from τ_L and τ_R. Thus two-dimensional slices

$$\Phi_{\text{slice}}(\delta_L, \delta_R) = \{(\tau_L, \tau_R) \,|\, \tau_L > \delta_L + 1, \tau_R < -\delta_R - 1\}, \tag{3.26}$$

defined by fixing the values of δ_L and δ_R, map to one another under g. In any such slice $\zeta_0(\xi) = 0$ and $\zeta_1(\xi) = 0$ are curves. In this section we show that for any values $0 < \delta_L < 1$ and $0 < \delta_R < 1$, these curves have the geometry shown in Fig. 3.8.

Observe $\zeta_0(\xi) = 0$ is the same as $\phi(\xi) = 0$, while, by Lemma 3.2, $\zeta_1(\xi) = 0$ is the same as $\psi(\xi) = 0$. However, we find the scaled function

$$\hat{\psi}(\xi) = \lambda_R^u \psi(\xi), \tag{3.27}$$

easier to work with than $\psi(\xi)$. By (3.24) the sign of $\hat{\psi}(\xi)$ is the same as that of $\zeta_1(\xi)$. From (3.20) we obtain

$$\hat{\psi}(\xi) = -\delta_L\Big(\lambda_R^{u^2} - 1\Big) + \lambda_R^u\Big(\lambda_R^{u^2} - 1\Big)\tau_L + (1 - \delta_R)\lambda_R^{u^2}\,. \tag{3.28}$$

The remainder of this section is organised as follows. First in §3.5.1 we study the curve $\phi(\xi) = 0$. We then derive analogous properties for $\hat{\psi}(\xi) = 0$ and obtain some additional bounds, §3.5.2. Lastly we show these curves intersect at a unique point in Φ_{slice}, §3.5.3.

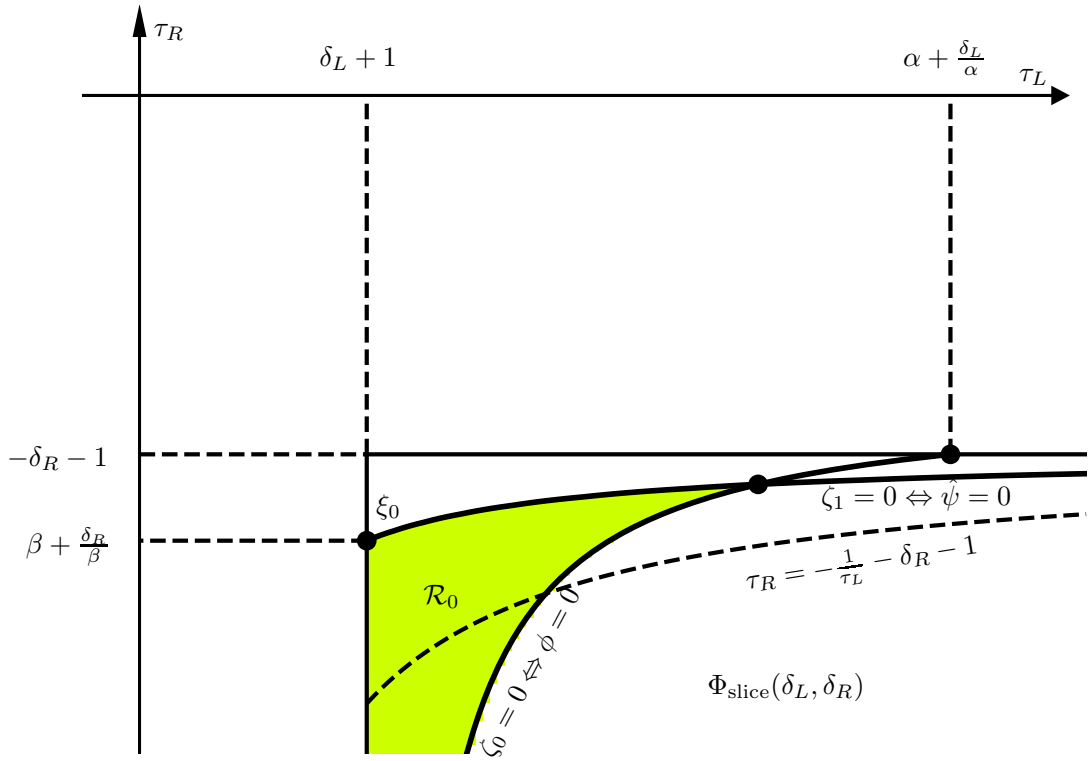

Figure 3.8: A sketch of $\zeta_0(\xi) = 0$ and $\zeta_1(\xi) = 0$ (equivalently $\phi(\xi) = 0$ and $\hat{\psi}(\xi) = 0$) in $\Phi_{\text{slice}}(\delta_L, \delta_R)$ with $0 < \delta_L < 1$ and $0 < \delta_R < 1$. The curve $\tau_R = -\frac{1}{\tau_L} - \delta_R - 1$ is shown dashed.

3.5.1 The curve $\phi(\xi) = 0$

We first show the curve $\phi(\xi) = 0$ does not exist in $\Phi_{\text{slice}}(\delta_L, \delta_R)$ if $\delta_L \geq 1$.

Lemma 3.3. *Let $\xi \in \Phi^{(1)}$. If $\delta_L \geq 1$ then $\phi(\xi) < 0$.*

Proof. We can rearrange (3.25) as

$$\phi(\xi) = (\tau_R + \delta_R + 1)\lambda_L^u(\lambda_L^u - 1) - \delta_R\Big(\lambda_L^{u^2} - 1\Big) + (1 - \delta_L)\lambda_L^u\,. \tag{3.29}$$

By inspection the first two terms in (3.29) are negative and if $\delta_L \geq 1$ then the last term is less than or equal to zero. □

The next result shows that $\phi(\xi) = 0$ appears roughly as in Fig. 3.8.

Proposition 3.4. *Let $0 < \delta_L < 1$ and $\delta_R > 0$. There exists a unique C^∞ function $G : (-\infty, -\delta_R - 1] \to (\delta_L + 1, \infty)$ such that*

$$\phi\big(G(\tau_R), \delta_L, \tau_R, \delta_R\big) = 0, \tag{3.30}$$

for all $\tau_R \in (-\infty, -\delta_R - 1]$. Moreover, G is strictly increasing, $G(\tau_R) \to \delta_L + 1$ as $\tau_R \to -\infty$, and $G(-\delta_R - 1) = \alpha + \frac{\delta_L}{\alpha}$ where $\alpha \in \mathbb{R}$ is the largest solution to

$$-\delta_R\alpha^2 + (1 - \delta_L)\alpha + \delta_R = 0\,. \tag{3.31}$$

Proof. First fix $\tau_R \leq -\delta_R - 1$. With $\tau_L = \delta_L + 1$ we have $\lambda_L^u = 1$ and so (3.25) simplifies to $\phi(\xi) = 1 - \delta_L > 0$. As $\tau_L \to \infty$ we have $\lambda_L^u \to \infty$ and so $\phi(\xi) \to -\infty$ (because the $\lambda_L^{u^2}$-coefficient in (3.25) is negative). Thus by the intermediate value theorem there exists $\tau_L = G(\tau_R) > \delta_L + 1$ satisfying (3.30).

To demonstrate the uniqueness of G we differentiate (3.25) to obtain

$$\frac{\partial\phi}{\partial\tau_L} = (2(1 + \tau_R)\lambda_L^u - (\tau_R + \delta_L + \delta_R))\frac{\partial\lambda_L^u}{\partial\tau_L}. \tag{3.32}$$

It is a simple exercise to show that $\frac{\partial\lambda_L^u}{\partial\tau_L} = \frac{\lambda_L^u}{\lambda_L^u - \lambda_L^s}$. Also if $\phi = 0$ then by (3.25) we can replace $(\tau_R + \delta_L + \delta_R)$ in (3.32) with $\frac{\delta_R}{\lambda_L^u} + (1 + \tau_R)\lambda_L^u$ to obtain

$$\left.\frac{\partial\phi}{\partial\tau_L}\right|_{\phi=0} = \left((1 + \tau_R)\lambda_L^u - \frac{\delta_R}{\lambda_L^u}\right)\frac{\lambda_L^u}{\lambda_L^u - \lambda_L^s}. \tag{3.33}$$

By inspection $\frac{\partial\phi}{\partial\tau_L}\big|_{\phi=0} < 0$. Thus G is unique (because if $\phi = 0$ for two distinct values of $\tau_L > \delta_L + 1$ then $\frac{\partial\phi}{\partial\tau_L} \geq 0$ at at least one of these values).

Since $\phi(\xi)$ is C^∞ the function G is C^∞ by the implicit function theorem. From (3.25) we obtain

$$\frac{\partial\phi}{\partial\tau_R} = \lambda_L^u(\lambda_L^u - 1), \tag{3.34}$$

which is evidently positive. Thus $\frac{dG}{d\tau_R} = -\frac{\frac{\partial\phi}{\partial\tau_L}}{\frac{\partial\phi}{\partial\tau_R}}\Big|_{\phi=0} > 0$, so G is strictly increasing.

Also $G(\tau_R) \to \delta_L + 1$ as $\tau_R \to -\infty$ because if we fix $\tau_L = \delta_L + 1 + \varepsilon$, then $\phi(\xi) \to -\infty$ as $\tau_R \to -\infty$ for any $\varepsilon > 0$. Finally, by substituting $\tau_R = -\delta_R - 1$ into (3.25) we obtain

$$\phi(\xi)\big|_{\tau_R = -\delta_R - 1} = -\delta_R\lambda_L^{u^2} + (1 - \delta_L)\lambda_L^u + \delta_R\,. \tag{3.35}$$

Since $\tau_L = \lambda_L^u + \frac{\delta_L}{\lambda_L^u}$ we have $G(-\delta_R - 1) = \alpha + \frac{\delta_L}{\alpha}$. □

3.5.2 The curve $\hat{\psi}(\xi) = 0$

The arguments presented here for $\hat{\psi}$ mirror those above for ϕ. We first show $\hat{\psi}(\xi) = 0$ does not exist in $\Phi_{\text{slice}}(\delta_L, \delta_R)$ if $\delta_R \geq 1$.

Lemma 3.4. *Let $\xi \in \Phi^{(1)}$. If $\delta_R \geq 1$ then $\hat{\psi}(\xi) < 0$.*

Proof. By inspection the first two terms in (3.28) are negative and if $\delta_R \geq 1$ then the last term is less than or equal to zero. □

We now show $\hat{\psi}(\xi) = 0$ appears roughly as in Fig. 3.8.

Proposition 3.5. *Let $\delta_L > 0$ and $0 < \delta_R < 1$. There exists a unique C^∞ function $H : [\delta_L + 1, \infty) \to (-\infty, -\delta_R - 1)$ such that*

$$\hat{\psi}\big(\tau_L, \delta_L, H(\tau_L), \delta_R\big) = 0, \tag{3.36}$$

for all $\tau_L \in [\delta_L + 1, \infty)$. Moreover, H is strictly increasing, $H(\tau_L) \to -\delta_R - 1$ as $\tau_L \to \infty$, and $H(\delta_L + 1) = \beta + \frac{\delta_R}{\beta}$ where $\beta \in \mathbb{R}$ is the smallest (most negative) solution to $p(\beta) = 0$ where

$$p(\beta) = (1 + \delta_L)\beta^3 + (1 - \delta_L - \delta_R)\beta^2 - (1 + \delta_L)\beta + \delta_L\,. \tag{3.37}$$

Proof. Fix $\tau_L \geq \delta_L + 1$. With $\tau_R = -\delta_R - 1$ we have $\lambda_R^u = -1$ and so (3.28) simplifies to $\hat{\psi}(\xi) = 1 - \delta_R > 0$. Also $\hat{\psi}(\xi) \to -\infty$ as $\tau_R \to -\infty$, thus, by the intermediate value theorem, there exists $\tau_R = H(\tau_L) < -\delta_R - 1$ satisfying (3.36).

From (3.28),

$$\frac{\partial \hat{\psi}}{\partial \tau_R} = \Big(3\tau_L \lambda_R^{u^2} + 2(1 - \delta_L - \delta_R)\lambda_R^u - \tau_L\Big)\frac{\lambda_R^u}{\lambda_R^u - \lambda_R^s},$$

and if $\hat{\psi}(\xi) = 0$ this can be simplified to

$$\left.\frac{\partial \hat{\psi}}{\partial \tau_R}\right|_{\hat{\psi}=0} = \left(\tau_L\Big(1 + \lambda_R^{u^2}\Big) - \frac{2\delta_L}{\lambda_R^u}\right)\frac{\lambda_R^u}{\lambda_R^u - \lambda_R^s}, \tag{3.38}$$

which is positive. Hence $H(\tau_L)$ satisfying (3.36) is unique for all $\tau_L \geq \delta_L + 1$. Moreover, H is C^∞ because $\hat{\psi}$ is C^∞. From (3.28),

$$\frac{\partial \hat{\psi}}{\partial \tau_L} = \lambda_R^u\Big(\lambda_R^{u^2} - 1\Big) < 0,$$

thus $\frac{dH}{d\tau_L} = -\frac{\frac{\partial \hat{\psi}}{\partial \tau_R}}{\frac{\partial \hat{\psi}}{\partial \tau_L}}\Big|_{\hat{\psi}=0} > 0$, i.e. H is strictly increasing.

We have $H(\tau_L) \to -\delta_R - 1$ as $\tau_L \to \infty$ because if $\tau_R = -\delta_R - 1 - \varepsilon$ then $\hat{\psi}(\xi) \to -\infty$ as $\tau_L \to \infty$ for any $\varepsilon > 0$. Finally, by substituting $\tau_L = \delta_L + 1$ into (3.28) we obtain $\hat{\psi}(\xi)\big|_{\tau_L = \delta_L + 1} = p(\lambda_R^u)$ and so $H(\delta_L + 1) = \beta + \frac{\delta_R}{\beta}$ as required. □

Next we obtain upper bounds on the values of β and $\beta + \frac{\delta_R}{\beta}$. These are the values of λ_R^u and τ_R for the point at which the curve $\hat{\psi}(\xi) = 0$ meets the boundary $\tau_L = \delta_L + 1$, see Fig. 3.8.

Lemma 3.5. *Let $\delta_L > 0$ and $0 < \delta_R < 1$. The value of β in Proposition 3.5 satisfies $\beta > -\frac{1+\sqrt{5}}{2}$ and $\beta + \frac{\delta_R}{\beta} > -2$.*

Proof. The function p can be rewritten as

$$p(\beta) = \delta_L(\beta - 1)^2(\beta + 1) - \delta_R\beta^2 + \beta\big(\beta^2 + \beta - 1\big). \tag{3.39}$$

The first two terms of (3.39) are negative, so since $p(\beta) = 0$ the last term of (3.39) must be positive. This requires $\beta > -\frac{1+\sqrt{5}}{2}$.

Also p can be rewritten as

$$p(\beta) = \left[(\beta+1)\left(1-\frac{1}{\beta}\right)\left(1+\delta_L-\frac{\delta_L}{\beta}\right)+(1-\delta_R)\right]\beta^2.$$

Thus $p(\beta)=0$ implies

$$-(\beta+1) = \frac{1-\delta_R}{\left(1-\frac{1}{\beta}\right)\left(1+\delta_L-\frac{\delta_L}{\beta}\right)}. \tag{3.40}$$

Since $\beta<0$ the denominator of (3.40) is greater than 1 and so $-(\beta+1)<1-\delta_R$. Thus $(\beta+1)^2<(1-\delta_R)^2$ which can be rearranged as $\beta^2+\delta_R<-2\beta-\delta_R(1-\delta_R)$. Since $0<\delta_R<1$ this can be reduced to $\beta+\frac{\delta_R}{\beta}>-2$. □

Lastly we show that the curve $\tau_R=-\frac{1}{\tau_L}-\delta_R-1$ lies below $\hat{\psi}(\xi)=0$, as in Fig. 3.8. This result is used later in the proof of Proposition 3.8.

Lemma 3.6. *Let $\delta_L>0$, $0<\delta_R<1$, and $\tau_L\geq\delta_L+1$. Then*

$$H(\tau_L) > -\frac{1}{\tau_L}-\delta_R-1. \tag{3.41}$$

Proof. By iterating (3.19) under $f_{R,\xi}$ and $f_{L,\xi}$ we obtain

$$f_\xi^2(T) = \left(\tau_L\left(\frac{\tau_R}{1-\lambda_R^s}+1\right)-\frac{\delta_R}{1-\lambda_R^s}+1, -\delta_L\left(\frac{\tau_R}{1-\lambda_R^s}+1\right)\right). \tag{3.42}$$

The second component of (3.42) is clearly positive with any $\tau_R<-\delta_R-1$. The first component of (3.42) can be rearranged as

$$f_\xi^2(T)_1 = \left(\tau_L-\frac{(\tau_R+\delta_R)\lambda_R^s-1}{\tau_R+\delta_R+1}\right)\left(\frac{\tau_R}{1-\lambda_R^s}+1\right). \tag{3.43}$$

If $\tau_L=\frac{-1}{\tau_R+\delta_R+1}$ (equivalently $\tau_R=-\frac{1}{\tau_L}-\delta_R-1$) then (3.43) simplifies to a quantity that is clearly negative. In this case $f_\xi^2(T)$ is located in the second quadrant of $\mathbb{R}^2$, so certainly it lies to the left of $E^s(X)$. Thus $\psi(\xi)>0$ by Proposition 3.2, so $\hat{\psi}(\xi)<0$.

We have shown $\tau_R=-\frac{1}{\tau_L}-\delta_R-1$ implies $\hat{\psi}(\xi)<0$. Therefore if $\hat{\psi}(\xi)=0$ (equivalently $\tau_R=H(\tau_L)$), then $\tau_R>-\frac{1}{\tau_L}-\delta_R-1$, as required. □

3.5.3 The curves $\phi(\xi) = 0$ and $\hat{\psi}(\xi) = 0$ intersect at a unique point

Proposition 3.6. *Fix* $0 < \delta_L < 1$ *and* $0 < \delta_R < 1$. *There exist unique* $\tau_L > \delta_L + 1$ *and* $\tau_R < -\delta_R - 1$ *such that* $\phi(\xi) = \hat{\psi}(\xi) = 0$.

Proof. By Propositions 3.4 and 3.5 the curves $\phi(\xi) = 0$ and $\hat{\psi}(\xi) = 0$ must intersect. To show this intersection is unique it suffices to show that at any point of intersection the slope $\frac{d\tau_R}{d\tau_L}$ of $\phi(\xi) = 0$ is greater than that of $\hat{\psi}(\xi) = 0$.

From the calculations performed in the proof of Proposition 3.4, the slope of $\phi(\xi) = 0$ is

$$\left(\frac{dG}{d\tau_R}\right)^{-1} = \frac{-(1+\tau_R)\lambda_L^u + \frac{\delta_R}{\lambda_L^u}}{(\lambda_L^u - 1)(\lambda_L^u - \lambda_L^s)}.$$

Consequently

$$\left(\frac{dG}{d\tau_R}\right)^{-1} > -\frac{\lambda_R^u + 1}{\lambda_L^u - 1}, \tag{3.44}$$

because $\tau_R < \lambda_R^u$, $\delta_R > 0$, and $\lambda_L^s > 0$. From the calculations performed in the proof of Proposition 3.5, the slope of $\hat{\psi}(\xi) = 0$ is

$$\frac{dH}{d\tau_L} = \frac{\left(\lambda_R^{u^2} - 1\right)(\lambda_R^u - \lambda_R^s)}{\tau_L\left(1 + \lambda_R^{u^2}\right) - \frac{2\delta_L}{\lambda_R^u}}.$$

Consequently

$$\frac{dH}{d\tau_L} < -\frac{\lambda_R^u\left(\lambda_R^{u^2} - 1\right)}{\lambda_L^u\left(\lambda_R^{u^2} + 1\right)}, \tag{3.45}$$

because $\tau_L > \lambda_L^u$, $\delta_L > 0$, and $\lambda_R^s < 0$.

Now suppose for a contradiction that $\left(\frac{dG}{d\tau_R}\right)^{-1} \leq \frac{dH}{d\tau_L}$ at a point where both $\phi(\xi) = 0$ and $\hat{\psi}(\xi) = 0$. By (3.44) and (3.45) this implies

$$-\frac{\lambda_R^u + 1}{\lambda_L^u - 1} < -\frac{\lambda_R^u\left(\lambda_R^{u^2} - 1\right)}{\lambda_L^u\left(\lambda_R^{u^2} + 1\right)},$$

which can be rearranged as

$$-\frac{(\lambda_R^u + 1)[\lambda_L^u(\lambda_R^u + 1) + \lambda_R^u(\lambda_R^u - 1)]}{\lambda_L^u(\lambda_L^u - 1)\left(\lambda_R^{u^2} + 1\right)} < 0.$$

For this to be true the term in square brackets must be negative, and this implies

$$\lambda_L^u(\tau_R + 1) < -2, \tag{3.46}$$

because $\tau_R < \lambda_R^u$ and $\lambda_R^u(\lambda_R^u - 1) > 2$. However, $\phi(\xi) = 0$, so by applying the quadratic formula to (3.25) we obtain

$$\tau_R + \delta_L + \delta_R - \sqrt{(\tau_R + \delta_L + \delta_R)^2 - 4(1 + \tau_R)\delta_R} = 2\lambda_L^u(\tau_R + 1).$$

Thus (3.46) implies

$$\tau_R + \delta_L + \delta_R - \sqrt{(\tau_R + \delta_L + \delta_R)^2 - 4(1 + \tau_R)\delta_R} < -4,$$

which can be rearranged as

$$\tau_R < \frac{-2\delta_L - 3\delta_R - 4}{2 + \delta_R}.$$

Since $\delta_L, \delta_R > 0$ this implies $\tau_R < -2$. But the curve $\hat{\psi}(\xi) = 0$ increases with τ_L, thus on $\hat{\psi}(\xi) = 0$ the value of τ_R is greater than its value at the boundary $\tau_L = \delta_L + 1$ where it equals $\beta + \frac{\delta_R}{\beta}$. So the bound $\beta + \frac{\delta_R}{\beta} > -2$ of Lemma 3.5 provides a contradiction. Therefore $\left(\frac{dG}{d\tau_R}\right)^{-1} > \frac{dH}{d\tau_L}$ at any point where $\phi(\xi) = 0$ and $\hat{\psi}(\xi) = 0$ intersect, hence the intersection point is unique. □

3.6 Dynamics of the renormalisation operator

In this section we study the dynamics of g on $\Phi^{(1)}$, where

$$\Phi^{(1)} = \left\{\xi \in \mathbb{R}^4 \,\middle|\, \tau_L > \delta_L + 1,\ \delta_L > 0,\ \tau_R < -(\delta_R + 1),\ \delta_R > 0\right\}.$$

We first show that any $\xi \in \Phi^{(1)}$ maps under g to another point in $\Phi^{(1)}$.

Proposition 3.7. *If $\xi \in \Phi^{(1)}$ then $g(\xi) \in \Phi^{(1)}$.*

Proof. Write $g(\xi) = \left(\tilde{\tau}_L, \tilde{\delta}_L, \tilde{\tau}_R, \tilde{\delta}_R\right)$. By (3.6) and the assumption $\xi \in \Phi^{(1)}$ we obtain

$$\begin{aligned}
\tilde{\tau}_L - \left(\tilde{\delta}_L + 1\right) &= \tau_R^2 - 2\delta_R - \left(\delta_R^2 + 1\right) = \tau_R^2 - (\delta_R + 1)^2 > 0, \\
\tilde{\delta}_L &= \delta_R^2 > 0, \\
\tilde{\tau}_R + \tilde{\delta}_R + 1 &= \tau_L\tau_R - \delta_L - \delta_R + \delta_L\delta_R + 1 \\
&< -(\delta_L + 1)(\delta_R + 1) - \delta_L - \delta_R + \delta_L\delta_R + 1 \\
&= -2(\delta_L + \delta_R) < 0, \\
\tilde{\delta}_R &= \delta_L\delta_R > 0,
\end{aligned}$$

which implies $g(\xi) \in \Phi^{(1)}$. □

Next in §3.6.1 we consider the subset of $\Phi^{(1)}$ for which $\hat{\psi}(\xi) < 0$. We show that any point in this subset maps under g to another point in this subset. This result is central to showing that the regions $\mathcal{R}_n$ are mutually disjoint and proving Theorem 3.1 in §3.6.2. Recall, the sign of $\hat{\psi}(\xi)$ is the same as that of $\zeta_1(\xi)$ by (3.27).

3.6.1 The subset of $\Phi^{(1)}$ for which $\hat{\psi}(\xi) < 0$

We first show that the point at which the curve $\hat{\psi}(\xi) = 0$ meets $\tau_L = \delta_L + 1$ maps under g to a point below the dashed curve of Fig. 3.8 in the corresponding slice $\Phi_{\text{slice}}(\tilde{\delta}_L, \tilde{\delta}_R)$.

Lemma 3.7. *Let $\delta_L > 0$ and $0 < \delta_R < 1$. Let $\xi_0 = (\delta_L + 1, \delta_L, \beta + \frac{\delta_R}{\beta}, \delta_R)$ where β is as given in Proposition 3.5. Write $g(\xi_0) = \left(\tilde{\tau}_L, \tilde{\delta}_L, \tilde{\tau}_R, \tilde{\delta}_R\right)$. Then*

$$\tilde{\tau}_R < -\frac{1}{\tilde{\tau}_L} - \tilde{\delta}_R - 1. \tag{3.47}$$

Proof. The inequality (3.47) is equivalent to

$$\tilde{\tau_L}\left(\tilde{\tau}_R + \tilde{\delta}_R + 1\right) + 1 < 0. \tag{3.48}$$

By (3.6) we have $\tilde{\tau}_L = \tau_R^2 - 2\delta_R$, $\tilde{\tau}_R = \tau_L\tau_R - \delta_L - \delta_R$, and $\tilde{\delta}_R = \delta_L\delta_R$; also $\tau_L = \delta_L + 1$. Upon substituting these into (3.48), after simplification the left-hand side of (3.48) becomes

$$\omega = (1+\delta_L)\tau_R^3 + (1-\delta_L)(1-\delta_R)\tau_R^2 - 2\delta_R(1+\delta_L)\tau_R - 2\delta_R(1-\delta_L)(1-\delta_R) + 1. \tag{3.49}$$

Thus it remains for us to show that $\omega < 0$.

Into (3.49) we substitute $\tau_R = \beta + \frac{\delta_R}{\beta}$ to obtain, after much rearranging,

$$\omega = p(\beta) + q(\beta) + \delta_L\delta_R\beta(\beta+2) + (1-\delta_L)(\beta+1) + \delta_R^2(1+\delta_L)\left(\beta + \frac{\delta_R}{\beta}\right)\frac{1}{\beta^2}, \quad (3.50)$$

where p is given by (3.37) and

$$q(\beta) = \big(\delta_L(2-\delta_R) + \delta_R\big)\beta + \delta_R^2(1-\delta_L)(1-\delta_R)\frac{1}{\beta^2}. \quad (3.51)$$

Since $\beta < -1$ we have

$$\begin{aligned} q(\beta) &< -\big(\delta_L(2-\delta_R) + \delta_R\big) + \delta_R^2(1-\delta_L)(1-\delta_R) \\ &< -\big(\delta_L(2-\delta_R) + \delta_R\big) + \delta_R^2(1-\delta_R) \\ &= -\delta_L(2-\delta_R) - \delta_R\big(\delta_R^2 - \delta_R + 1\big) \\ &< 0. \end{aligned}$$

Also $p(\beta) = 0$ and by inspection the last three terms of (3.50) are negative (because $\beta+1 < 0$ and $\beta + 2 > 0$ by Lemma 3.5). Therefore $\omega < 0$. □

We now use Lemma 3.7 to show that the subset of $\Phi^{(1)}$ for which $\hat{\psi}(\xi) < 0$ is forward invariant under g.

Proposition 3.8. *Let $\xi \in \Phi^{(1)}$. If $\hat{\psi}(\xi) \le 0$ then $\hat{\psi}(g(\xi)) < 0$.*

Proof. Write $g(\xi) = \left(\tilde{\tau}_L, \tilde{\delta}_L, \tilde{\tau}_R, \tilde{\delta}_R\right)$. Since $\xi \in \Phi^{(1)}$ we have $\delta_L, \delta_R > 0$.

First suppose $0 < \delta_R < 1$. If $\tilde{\delta}_R \ge 1$ then certainly $\hat{\psi}(g(\xi)) < 0$ by Lemma 3.4, so let us suppose $\tilde{\delta}_R < 1$. Since $\tilde{\delta}_L = \delta_R^2 < 1$, by Proposition 3.6 the curves $\phi = 0$ and $\hat{\psi} = 0$ intersect at a unique point in $\Phi_{\text{slice}}(\tilde{\delta}_L, \tilde{\delta}_R)$, call it $\tilde{\xi}_{\text{int}}$, see Fig. 3.9. With $\xi = \xi_0$ as in Lemma 3.7, the inequality (3.47) implies $\hat{\psi}(g(\xi_0)) < 0$ by Lemma 3.6. Also $\phi(g(\xi_0)) = 0$, because $\hat{\psi}(\xi_0) = 0$, thus $g(\xi_0)$ lies on $\phi = 0$ and below $\tilde{\xi}_{\text{int}}$, as in Fig. 3.9.

Now if $\hat{\psi}(\xi) \le 0$ and $\xi \ne \xi_0$, then $g(\xi)$ lies in the shaded region of Fig. 3.9. The curve $\hat{\psi} = 0$ does not enter this region because the intersection point $\tilde{\xi}_{\text{int}}$ is unique. Thus $g(\xi)$ lies below the curve $\hat{\psi} = 0$, that is $\hat{\psi}(g(\xi)) < 0$.

Second suppose $\delta_R \ge 1$. Then

$$\tilde{\tau}_R = \tau_L\tau_R - \delta_L - \delta_R < -(\delta_L+1)(\delta_R+1) - \delta_L - \delta_R < -3,$$

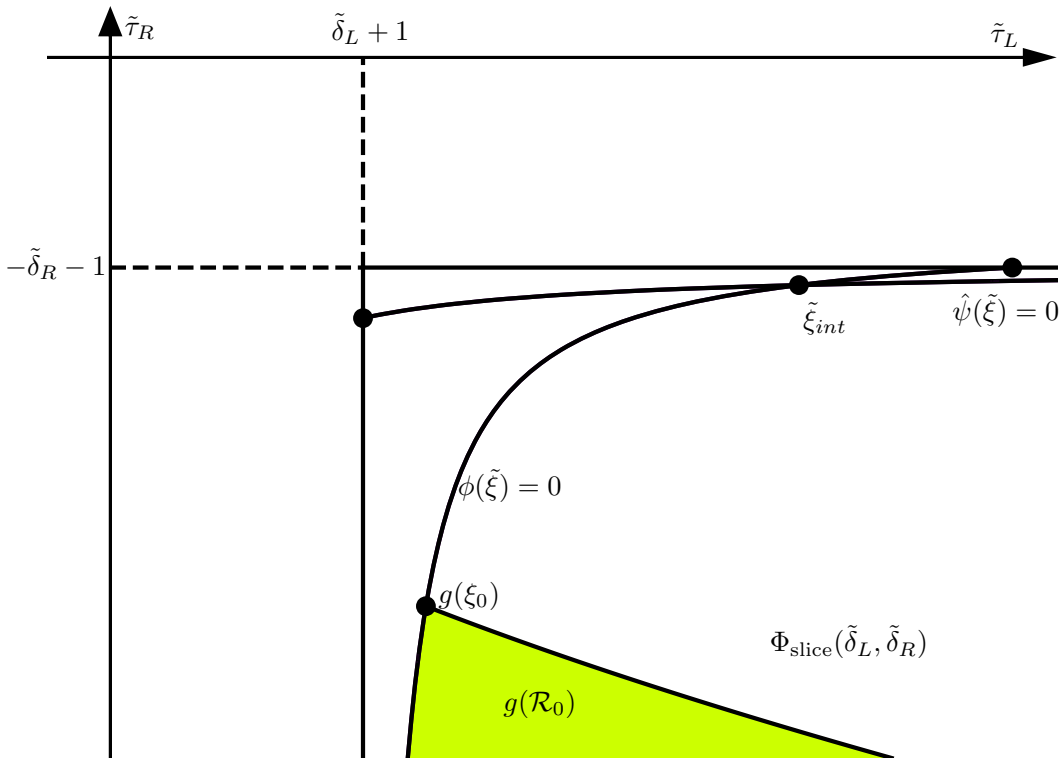

Figure 3.9: A sketch of $\phi(\tilde{\xi}) = 0$ and $\hat{\psi}(\tilde{\xi}) = 0$ where $\tilde{\xi} = g(\xi)$ with $0 < \tilde{\delta}_L < 1$ and $0 < \tilde{\delta}_R < 1$. The point $\tilde{\xi}_{\text{int}}$ is the unique intersection of $\phi(\tilde{\xi}) = 0$ and $\hat{\psi}(\tilde{\xi}) = 0$. The point ξ_0 is as in Lemma 3.7.

where we have used $\delta_L > 0$ and $\delta_R \geq 1$ to produce the last inequality. Thus $\tilde{\tau}_R < -2$ and so $g(\xi)$ lies below $\hat{\psi} = 0$ by Lemma 3.5. That is, $\hat{\psi}(g(\xi)) < 0$. □

3.6.2 Arguments leading to a proof of Theorem 3.1

Here we prove Theorem 3.1 after a sequence of lemmas.

Lemma 3.8. *Let $\xi \in \mathcal{R}_n$ for some $n \geq 1$. Then $g^i(\xi) \in \mathcal{R}_{n-i}$ for all $i = 1, 2, \ldots, n$.*

Proof. We have $\zeta_n(\xi) > 0$ and $\zeta_{n+1}(\xi) \leq 0$ by (3.9). Thus $\zeta_{n-i}(g^i(\xi)) > 0$ and $\zeta_{n-i+1}(g^i(\xi)) \leq 0$ by (3.8). Also $g^i(\xi) \in \Phi^{(1)}$ by Proposition 3.7. Thus $g^i(\xi) \in \mathcal{R}_{n-i}$ by (3.9). □

Lemma 3.9. *Let $\xi \in \Phi^{(1)}$ with $g(\xi) \in \mathcal{R}_{n-1}$ for some $n \geq 1$. Then $\xi \in \mathcal{R}_n$.*

Proof. We have $\zeta_{n-1}(g(\xi)) > 0$ and $\zeta_n(g(\xi)) \leq 0$ by (3.9). Thus $\zeta_n(\xi) > 0$ and $\zeta_{n+1}(\xi) \leq 0$ by (3.8). So $\xi \in \mathcal{R}_n$ because also $\xi \in \Phi^{(1)}$. □

Lemma 3.10. *Let $\xi \in \mathcal{R}_n$ for some $n \geq 1$. Then $\zeta_0(g(\xi)) > 0$.*

Proof. We have $\zeta_n(\xi) > 0$ by (3.9), thus $\zeta_1(g^{n-1}(\xi)) > 0$ by (3.8). Thus $\zeta_1(\xi) > 0$ by Proposition 3.8 (recall the sign of ζ_1 is the same as that of $\hat{\psi}$). That is, $\zeta_0(g(\xi)) > 0$. □

Lemma 3.11. *Let $\xi \in \Phi^{(1)}$ and write $g^i(\xi) = (\tau_{L,i}, \delta_{L,i}, \tau_{R,i}, \delta_{R,i})$ for each i. Then $\tau_{L,2} > \tau_L^2 \tau_R^2$ and $\tau_{R,2} < \tau_L \tau_R$.*

Proof. By (3.6),

$$\tau_{L,2} = \tau_{R,1}^2 - 2\delta_{R,1} = (\tau_L \tau_R - \delta_L - \delta_R)^2 - 2\delta_L \delta_R \,,$$

which can be rearranged as

$$\tau_{L,2} = (\tau_L \tau_R - \delta_L)^2 + (\tau_L \tau_R - \delta_R)^2 - \tau_L^2 \tau_R^2 \,.$$

Then from the bounds in (3.1) we obtain $\tau_{L,2} > \tau_L^2 \tau_R^2$. Also

$$\tau_{R,2} = \tau_{L,1}\tau_{R,1} - \delta_{L,1} - \delta_{R,1} < \tau_{L,1}\tau_{R,1} \,.$$

By substituting $\tau_{L,1} > 1$ and $\tau_{R,1} > \tau_L \tau_R$ we obtain $\tau_{R,2} < \tau_L \tau_R$. □

Proof of Theorem 3.1. Suppose for a contradiction that the $\mathcal{R}_n$ are *not* mutually disjoint. So there exists $\xi \in \mathcal{R}_m \cap \mathcal{R}_n$ for some $0 \leq m < n$. This implies $g^{n-1}(\xi) \in \mathcal{R}_1$ by Lemma 3.8, and so $\hat{\psi}(g^{n-1}(\xi)) > 0$ (the sign of ζ_1 is the same as that of $\hat{\psi}$). Also $g^m(\xi) \in \mathcal{R}_0$, so $\hat{\psi}(g^m(\xi)) \leq 0$. By Proposition 3.8, $\hat{\psi}(g^{m+i}(\xi)) \leq 0$ for all $i \geq 0$. In particular $\hat{\psi}(g^{n-1}(\xi)) \leq 0$, and this is a contradiction. Therefore the $\mathcal{R}_n$ are mutually disjoint.

Now choose any $\xi \in \Phi_{\mathrm{BYG}}$. To verify (3.10) we show there exists $n \geq 0$ such that $\xi \in \mathcal{R}_n$. Certainly this is true if $\hat{\psi}(\xi) \leq 0$, because in this case $\xi \in \mathcal{R}_0$, so let us assume $\hat{\psi}(\xi) > 0$. In view of Lemma 3.11, we consider the map $\tilde{g} : \mathbb{R}^2 \to \mathbb{R}^2$ defined by

$$\tilde{g}(\tau_L, \tau_R) = \big((\tau_L \tau_R)^2, \tau_L \tau_R\big).$$

For any $j \geq 1$ the j^{th}-iterate of $\tilde{g}$ is given explicitly by

$$\tilde{g}^j(\tau_L, \tau_R) = \Big((\tau_L \tau_R)^{2k_j}, (\tau_L \tau_R)^{k_j}\Big),$$

where $k_j = 3^{j-1}$. Then Lemma 3.11 implies $\tau_{R,2j} < (\tau_L \tau_R)^{k_j}$ (using the notation of Lemma 3.11) and so $\tau_{R,2j} \to -\infty$ as $j \to \infty$. Thus there exists $m \geq 0$ such that $\tau_{R,m} \leq$

-2. Then $\hat{\psi}(g^m(\xi)) < 0$ by Lemma 3.5. Now let $n \in \{1, 2, \ldots, m\}$ be the smallest integer for which $\hat{\psi}(g^n(\xi)) \leq 0$. Then $\hat{\psi}(g^{n-1}(\xi)) > 0$, so $\phi(g^n(\xi)) > 0$. That is, $g^n(\xi) \in \mathcal{R}_0$. Hence $\xi \in \mathcal{R}_n$, by n applications of Lemma 3.9. This completes our verification of (3.10).

To show that $\mathcal{R}_j$ is non-empty for all $j \geq 0$, first observe $\hat{\psi}(\xi^*) > 0$. Also $\mathcal{R}_0$ is certainly non-empty. So for any $j \geq 1$ we can choose $\xi \in \Phi_{\mathrm{BYG}}$ sufficiently close to ξ^* that $\hat{\psi}(g^i(\xi)) > 0$ for all $i = 0, 1, \ldots, j-1$. Again let $n \geq 1$ be the smallest integer for which $\hat{\psi}(g^n(\xi)) \leq 0$. Then $n \geq j$ and $g^n(\xi) \in \mathcal{R}_0$. Thus $g^{n-j}(\xi) \in \mathcal{R}_j$ (by again using Lemma 3.9), i.e. $\mathcal{R}_j$ is non-empty.

Finally, choose any $\varepsilon > 0$ and let $B_\varepsilon(\xi^*)$ be the open ball in $\mathbb{R}^4$ centred at ξ^* and with radius ε using the Euclidean norm. We now show there exists $m \geq 1$ such that $\mathcal{R}_n \subset B_\varepsilon(\xi^*)$ for all $n > m$. This will prove that $\mathcal{R}_n \to \{\xi^*\}$ as $n \to \infty$. Choose any $\xi \in \Phi^{(1)}$ with $\xi \notin B_\varepsilon(\xi^*)$. It is simple exercise to show that $|\tau_L \tau_R| \geq 1 + \frac{\varepsilon}{\sqrt{2}}$. Thus, as above, there exists $m \geq 0$ such that $\tau_{R,m} \leq -2$ and $\xi \in \mathcal{R}_n$ for some $n \leq m$. Hence for any $n > m$ the region $\mathcal{R}_n$ contains no points outside of $B_\varepsilon(\xi^*)$. That is $\mathcal{R}_n \subset B_\varepsilon(\xi^*)$ for all $n > m$ and therefore $\mathcal{R}_n \to \{\xi^*\}$ as $n \to \infty$. □

3.7 Positive Lyapunov exponents

For smooth maps Lyapunov exponents are usually defined in terms of the derivative of the map. The border-collision normal form f_ξ is not differentiable on $x = 0$, so instead we work with one-sided directional derivatives, §3.7.1. We then define Lyapunov exponents in terms of these derivatives, §3.7.2. This definition coincides with the familiar interpretation of Lyapunov exponents as the asymptotic rate of separation of nearby forward orbits [129]. Then in §3.7.3 we prove Theorem 3.2.

3.7.1 One-sided directional derivatives

Definition 3.1. The *one-sided directional derivative* of a function $F : \mathbb{R}^2 \to \mathbb{R}^2$ at $z \in \mathbb{R}^2$ in a direction $v \in \mathbb{R}^2$ is

$$\mathrm{D}_v^+ F(z) = \lim_{\delta \to 0^+} \frac{F(z + \delta v) - F(z)}{\delta}, \tag{3.52}$$

if this limit exists.

The following result tells us that one-sided directional derivatives of the n^{th} iterate of (2.21) exist everywhere and for all $n \geq 1$. This follows from the piecewise-linearity and

continuity of (2.21). For a proof see [129].

Lemma 3.12. *For any $\xi \in \mathbb{R}^4$, $z \in \mathbb{R}^2$, $v \in \mathbb{R}^2$, and $n \geq 1$, $\mathrm{D}_v^+ f_\xi^n(z)$ exists.*

3.7.2 Lyapunov exponents

In view of Lemma 3.12 we can use the following definition.

Definition 3.2. The *Lyapunov exponent* of f_ξ at $z \in \mathbb{R}^2$ in a direction $v \in \mathbb{R}^2$ is

$$\lambda(z, v) = \limsup_{n\to\infty} \frac{1}{n} \ln\big(\big\|\mathrm{D}_v^+ f_\xi^n(z)\big\|\big). \tag{3.53}$$

If the forward orbit of z does not intersect $x = 0$, then $\mathrm{D}f_\xi^n(z)$ (the Jacobian matrix of f_ξ^n at z) is well-defined for all $n \geq 1$. Moreover, $\mathrm{D}_v^+ f_\xi^n(z) = \mathrm{D}f_\xi^n(z)v$, so, in this case, (3.53) reduces to the usual expression given for smooth maps.

The following result is Theorem 2.1 of [58], except in the work only forward orbits that do not intersect $x = 0$ were considered. The generalisation to one-sided directional derivatives is elementary so we do not provide a proof. The proof in the work by Glendinning and Simpson [58] is achieved by constructing an invariant expanding cone for multiplying vectors v under the matrices A_L and A_R, and we will do this later in Chapter 5.

Proposition 3.9. *For any $\xi \in \Phi_{\mathrm{BYG}}$, $z \in \mathbb{R}^2$, and $v = (1, 0)$,*

$$\liminf_{n\to\infty} \frac{1}{n} \ln\big(\big\|\mathrm{D}_v^+ f_\xi^n(z)\big\|\big) > 0. \tag{3.54}$$

3.7.3 Arguments leading to a proof of Theorem 3.2

We are now ready to prove Theorem 3.2. Once we have constructed the set Δ, the equality (3.12) follows from the arguments given in the proof of Lemma 6.2 of [58]. We reproduce these arguments here for convenience.

Proof of Theorem 3.2. The set $\Lambda(\xi)$ is bounded because $X \in \Omega$ and Ω is bounded and forward invariant (Proposition 3.1). Also $\Lambda(\xi)$ is connected and invariant by the definition of an unstable manifold. With $v = (1, 0)$ and any $z \in \Lambda(\xi)$, the Lyapunov exponent $\lambda(z, v)$ is well-defined by Lemma 3.12. Moreover $\lambda(z, v) > 0$ by Proposition 3.9 and because the supremum limit is greater than or equal to the infimum limit.

It remains for us to prove part (iii). Here we assume $\delta_R < 1$; also $\delta_L < 1$ by Lemma 3.3. Since $\xi \in \mathcal{R}_0$ we have $\zeta_1(\xi) \leq 0$ and so $\psi(\xi) \geq 0$ by (3.24). Thus $f_\xi^2(T)$ lies on or to the left of $E^s(X)$ by Proposition 3.2. Let Z denote the intersection of $E^s(X)$ with $\overline{Tf_\xi^2(T)}$ (the line segment connecting T and $f_\xi^2(T)$). Notice $\overline{XT}$ and $\overline{TZ}$ are subsets of $W^u(X)$ while $\overline{ZX}$ is a subset of $W^s(X)$.

Let Δ_0 be the filled triangle with vertices X, T, and Z, see Fig. 3.7-a. Also let $\Delta = \bigcup_{n=0}^\infty f_\xi^n(\Delta_0)$. The set Δ is forward invariant, by definition, and has non-empty interior because it contains Δ_0. As in the work by Glendinning and Simpson [58], let $\tilde{\Delta} = \bigcap_{n=0}^\infty f_\xi^n(\Delta)$.

We now show $\Lambda(\xi) \subset \tilde{\Delta}$. Choose any $z \in \Lambda(\xi)$. Let $\{z_k\}$ be a sequence of points in $W^u(X)$ with $z_k \to z$ as $k \to \infty$. For each k, $f_\xi^{-n}(z_k) \to X$ as $n \to \infty$, thus there exists $n_k \geq 1$ such that $f_\xi^{-n_k}(z_k) \in \overline{XT}$. Thus $f_\xi^{-n_k}(z_k) \in \Delta_0$, so $z_k \in \Delta$. This is true for all k, thus $z \in \Delta$. But $z \in \Lambda(\xi)$ is arbitrary, thus $\Lambda(\xi) \subset \Delta$. Also $\Lambda(\xi)$ is forward invariant, thus $\Lambda(\xi) \subset \tilde{\Delta}$.

Finally we show $\tilde{\Delta} \subset \Lambda(\xi)$. The determinants δ_L and δ_R of the pieces of f_ξ are both less than 1, thus the area (Lebesgue measure) of $f_\xi^n(\Delta)$ converges to 0 as $n \to \infty$. Now choose any $z \in \tilde{\Delta}$. Then $z \in f_\xi^n(\Delta)$ for all $n \geq 0$ and so the distance of z to the boundary of $f_\xi^n(\Delta)$ converges to 0 as $n \to \infty$. The boundary of Δ_0 consists of $\overline{XZ}$, which lies in the part of $W^s(X)$ that converges linearly to X, and two line segments in $W^u(X)$. Consequently the boundary of $f_\xi^n(\Delta_0)$ is contained in $\overline{Xf_\xi^n(Z)} \cup W^u(X)$ for all $n \geq 0$. Thus the boundary of Δ is contained in $\overline{Zf_\xi(Z)} \cup W^u(X)$, so the boundary of $f_\xi^n(\Delta)$ is contained in $\overline{f_\xi^n(Z)f_\xi^{n+1}(Z)} \cup W^u(X)$ for all $n \geq 0$. But $\overline{f_\xi^n(Z)f_\xi^{n+1}(Z)}$ converges to X, hence the distance of z to $W^u(X)$ must be 0. Thus $z \in \Lambda(\xi)$. But $z \in \tilde{\Delta}$ is arbitrary, thus $\tilde{\Delta} \subset \Lambda(\xi)$. This completes our demonstration of (3.12). □

3.8 Implementing the renormalisation recursively

In this section we work towards a proof of Theorem 3.3. First in §3.8.1 we use the unstable manifold of X to construct a triangle $\Omega'(\xi)$ that maps to $\Omega(g(\xi))$ under the affine transformation h_ξ for converting f_ξ^2 to $f_{g(\xi)}$. In particular we show that $\Omega'(\xi)$ is a subset of both $\Omega(\xi)$ and Π_ξ and this allows us to implement the renormalisation recursively in §3.8.2.

3.8.1 Properties of the set mapping to $\Omega(g(\xi))$

Suppose $\xi \in \Phi^{(1)}$ with $\zeta_1(\xi) > 0$ (equivalently $\psi(\xi) < 0$). Then $f_\xi^2(T)$ lies to the right of $E^s(X)$ by Proposition 3.2. Thus $f_\xi^3(T)$ lies to the left of $E^s(X)$ (because $\lambda_R^u < 0$). Now let Q denote the intersection of $E^u(X)$ with the line through $f_\xi^3(T)$ and parallel to $E^s(X)$, see Fig. 3.7-b. Then let $\Omega'(\xi)$ be the filled triangle with vertices $f_\xi(T)$, $f_\xi^3(T)$, and Q.

Lemma 3.13. *Let $\xi \in \Phi^{(1)}$ with $\zeta_1(\xi) > 0$. Then*

1. $\Omega'(\xi) \subset \Pi_\xi$,
2. $\Omega'(\xi) \cap f_\xi(\Omega'(\xi)) = \varnothing$,
3. $f_\xi(\Omega'(\xi)) \subset \big\{(x,y) \in \mathbb{R}^2 \,\big|\, x > 0\big\}$,
4. $h_\xi(\Omega'(\xi)) = \Omega(g(\xi))$,
5. *and if $\zeta_0(\xi) > 0$ then $\Omega'(\xi) \subset \Omega(\xi)$.*

Proof. Let $\Xi_R = \big\{(x,y) \in \mathbb{R}^2 \,\big|\, x > 0\big\}$ denote the open right half-plane and let Ψ be the triangle with vertices X, $f_\xi(T)$, and V. We now prove parts (1)–(5) in order.

1. Observe $f_\xi(X) = X \in \Xi_R$, thus $X \in \Pi_\xi$ by (3.4). Similarly $f_\xi(V) \in \Xi_R$, thus $V \in \Pi_\xi$. Also $f_\xi^2(T) \in \Xi_R$, thus $f_\xi(T) \in \Pi_\xi$. That is, all vertices of Ψ belong to Π_ξ, thus $\Psi \subset \Pi_\xi$ because these sets are convex.

   From (3.19) and (3.42) we find that the slope of the line through T and $f_\xi^2(T)$ is $\frac{-\delta_L}{\tau_L - \lambda_R^s}$, which is negative, thus $f_\xi^2(T)$ lies to the left of T. Consequently $f_\xi^3(T)$ lies above $f_\xi(T)$. Also $f_\xi(T)$ lies above V because

   $$f_\xi(T)_2 - V_2 = \frac{1 - \delta_R}{(1 - \lambda_R^s)\Big(1 - \frac{1}{\lambda_R^u}\Big)} > 0.$$

   Therefore $f_\xi^3(T) \in \Psi$. Thus $\Omega'(\xi) \subset \Psi \subset \Pi_\xi$.

2. Observe $f_\xi(\Psi)$ is the quadrilateral with vertices X, $f_\xi(V)$, $f_\xi^2(T)$, and T. Thus Ψ and $f_\xi(\Psi)$ intersect only at X. But $\Omega'(\xi) \subset \Psi$ does not contain X, thus $\Omega'(\xi) \cap f_\xi(\Omega'(\xi)) = \varnothing$.

3. The left-most point of $f_\xi(\Psi)$ is $X \in \Xi_R$, thus $f_\xi(\Omega'(\xi)) \subset f_\xi(\Psi) \subset \Xi_R$.

4. For the map f_ξ^2, the fixed point X is a saddle with positive eigenvalues. Thus its unstable manifold has two dynamically independent branches. The branch that emanates to the left has its first and second kinks at $f_\xi(T)$ and $f_\xi^3(T)$. Let $\mathcal{B}$ denote this branch up to the second kink, that is $\mathcal{B}$ is the union of the line segments $\overline{X f_\xi(T)}$ and $\overline{f_\xi(T) f_\xi^3(T)}$.

   By the conjugacy relation (3.22), $h_\xi(\mathcal{B})$ is part of one branch of the unstable manifold of the analogous fixed point of $f_{g(\xi)}$. Since h_ξ flips points across the switching line (3.23), $h_\xi(\mathcal{B})$ is part of the unstable manifold of Y (for the map $f_{g(\xi)}$). This branch has its first and second kinks at D and $f_{g(\xi)}(D)$, thus $h_\xi(\mathcal{B})$ is the union of the line segments $\overline{YD}$ and $\overline{D f_{g(\xi)}(D)}$. By similar reasoning Q maps under h_ξ to the point B of $f_{g(\xi)}$. This verifies part (4).

5. The first components of T and D are $T_1 = \frac{1}{1-\lambda_R^s}$ and $D_1 = \frac{1}{1-\lambda_L^s}$. Observe $0 < T_1 < D_1$, thus T lies between $(0,0)$ and D. By iterating these under $f_{R,\xi}$ we have that $f_\xi(T)$ lies on the line segment connecting $(1,0)$ and $f_\xi(D)$.

   Now suppose $\zeta_0(\xi) > 0$. Then $f_\xi(T) \in \Omega(\xi)$ because $(1,0) \in \Omega(\xi)$, $f_\xi(D) \in \Omega(\xi)$, and $\Omega(\xi)$ is convex. Moreover, $f_\xi^3(T) \in \Omega(\xi)$ because $\Omega(\xi)$ is forward invariant (Proposition 3.1). Also $X \in \Omega(\xi)$ by Lemma 3.1. Thus the triangle with vertices $f_\xi(T)$, $f_\xi^3(T)$, and X is contained in $\Omega(\xi)$ (again by the convexity of $\Omega(\xi)$). This triangle contains $\Omega'(\xi)$, thus $\Omega'(\xi) \subset \Omega(\xi)$ as required.

□

3.8.2 Arguments leading to a proof of Theorem 3.3

Proof of Theorem 3.3. Let $I_n = \{0, 1, \ldots, 2^n - 1\}$. We use induction on n to prove Theorem 3.3 and show that

$$\text{if } \zeta_0(\xi) > 0 \text{ then } S_i \subset \Omega(\xi) \text{ for all } i \in I_n. \tag{3.55}$$

With $n = 0$ the statements in Theorem 3.3 are true trivially with $S_0 = \Lambda(\xi)$. Also (3.55) is true because $\zeta_0(\xi) > 0$ (since $\xi \in \mathcal{R}_0$) and $S_0 \subset \Omega(\xi)$ by Lemma 3.1.

Now suppose the result is true for some $n \geq 0$; it remains for us to verify the result for $n+1$. Choose any $\xi \in \mathcal{R}_{n+1}$. Then $g(\xi) \in \mathcal{R}_n$ by Lemma 3.8. By the induction hypothesis applied to the point $g(\xi)$, we have $g^{n+1}(\xi) \in \mathcal{R}_0$ and there exist mutually disjoint sets

$\tilde{S}_0, \tilde{S}_1, \ldots, \tilde{S}_{2^n-1} \subset \mathbb{R}^2$ with $f_{g(\xi)}\Big(\tilde{S}_i\Big) = \tilde{S}_{(i+1) \bmod 2^n}$ and

$$f_{g(\xi)}^{2^n}\big|_{\tilde{S}_i} \text{ is affinely conjugate to } f_{g^{n+1}(\xi)}\big|_{\Lambda(g^{n+1}(\xi))} \tag{3.56}$$

for all $i \in I_n$. Also $\zeta_0(g(\xi)) > 0$ by Lemma 3.10, thus by (3.55) the induction hypothesis also gives $\tilde{S}_i \subset \Omega(g(\xi))$ for all $i \in I_n$.

Let $S_{2i} = h_\xi^{-1}\Big(\tilde{S}_i\Big)$ for each $i \in I_n$ (these sets are mutually disjoint because h_ξ is a homeomorphism). Let $S_{2i+1} = f_\xi(S_{2i})$ for each $i \in I_n$ (these sets are mutually disjoint because f_ξ is a homeomorphism). For any $i, j \in I_n$ we have $S_{2i} \subset \Omega'(\xi)$ by Lemma 3.13(4) and $S_{2j+1} \cap \Omega'(\xi) = \varnothing$ by Lemma 3.13(2), so $S_{2i} \cap S_{2j+1} = \varnothing$. Therefore the sets $S_0, S_1, \ldots, S_{2^{n+1}-1}$ are mutually disjoint.

For each $i \in I_n$, $S_{2i} \subset \Pi_\xi$ by Lemma 3.13(1), so

$$f_\xi^2\big|_{S_{2i}} \text{ is affinely conjugate to } f_{g(\xi)}\big|_{\tilde{S}_i} \tag{3.57}$$

by Proposition 3.3. Also $f_\xi^2(S_{2i}) = S_{2i+2 \bmod 2^{n+1}}$, so $f_\xi(S_{2i+1}) = f_{R,\xi}(S_{2i+1}) = S_{2i+2 \bmod 2^{n+1}}$ using also Lemma 3.13(3). Thus

$$f_\xi^2\big|_{S_{2i+1}} \text{ is affinely conjugate to } f_\xi^2\big|_{S_{2i}}$$

using $f_{R,\xi}$ as the affine transformation. By further use of (3.22) we have that $f_\xi^{2^{n+1}}\big|_{S_{2i}}$ and $f_\xi^{2^{n+1}}\big|_{S_{2i+1}}$ are affinely conjugate to $f_{g(\xi)}^{2^n}\big|_{\tilde{S}_i}$, thus also to $f_{g^{n+1}(\xi)}\big|_{\Lambda(g^{n+1}(\xi))}$ by (3.56) (this verifies (3.14) for $n+1$).

The induction hypothesis also implies

$$\bigcup_{i=0}^{2^n-1} \tilde{S}_i = \mathrm{cl}(W^u(\gamma_n)), \tag{3.58}$$

where γ_n is a periodic solution of $f_{g(\xi)}$ with symbolic itinerary $\mathcal{F}^n(R)$. By (3.22), $h_\xi^{-1}(\gamma_n)$ is a periodic solution of f_ξ^2. Since h_ξ flips the left and right half-planes, see (3.23), the symbolic itinerary of $h_\xi^{-1}(\gamma_n)$ is obtained by swapping L and R's in $\mathcal{F}^n(R)$. Then $\gamma_{n+1} = h_\xi^{-1}(\gamma_n) \cup f_\xi\big(h_\xi^{-1}(\gamma_n)\big)$ is a periodic solution of f_ξ and since $f_\xi\big(h_\xi^{-1}(\gamma_n)\big)$ is contained in the right half-plane (Lemma 3.13(3)) its symbolic itinerary is obtained by further replacing each L with LR and each R with RR, hence γ_{n+1} has symbolic itinerary $\mathcal{F}^{n+1}(R)$. Also

by (3.57) and (3.58),

$$\bigcup_{i=0}^{2^{n+1}-1} S_i = \mathrm{cl}(W^u(\gamma_{n+1})),$$

which verifies (3.15) for $n+1$. Finally, if $\zeta_0(\xi) > 0$ then for all $i \in I_n$ we have $S_{2i} \subset \Omega(\xi)$ by Lemma 3.13(5) and $S_{2i+1} \subset \Omega(\xi)$ because $\Omega(\xi)$ is forward invariant verifying (3.55) for $n+1$. □

Chapter 4

Robust Devaney chaos in the two-dimensional border-collision normal form.

4.1 Introduction

In Chapter 3, we used renormalisation to partition a region slightly larger than Φ_{BYG} into subregions $\mathcal{R}_0, \mathcal{R}_1, \mathcal{R}_2, \ldots$. We showed that if $\xi \in \mathcal{R}_n$ for some $n \geq 0$, then f_ξ has a chaotic attractor with 2^n connected components. Here f_ξ is the border-collision normal form given by

$$f_{L,\xi}(x,y) = \begin{bmatrix} \tau_L x + y + 1 \\ -\delta_L x \end{bmatrix},$$

and

$$f_{R,\xi}(x,y) = \begin{bmatrix} \tau_R x + y + 1 \\ -\delta_R x \end{bmatrix},$$

with the set $\Sigma = \{(0,y)|y \in \mathbb{R}\}$ – the y-axis as the switching manifold of f_ξ. For any $\xi \in \mathbb{R}^4$, its image $f_\xi(\Sigma)$ is the x-axis. Fig. 4.1 shows the attractor for typical $\xi \in \mathcal{R}_0$ where it has one connected component and is the closure of the unstable manifold of a saddle fixed point X i.e., $\Lambda = \mathrm{cl}(W^u(X))$, see (3.11). We were further able to show that if $\xi \in \mathcal{R}_n$ for some $n \geq 1$, then $f_\xi^{2^n}$ is conjugate to f_η for some $\eta \in \mathcal{R}_0$. In this way, anything one can prove about the dynamics in $\mathcal{R}_0$ immediately extends to every $\mathcal{R}_n$ with $n \geq 1$. For this reason, it is helpful to better understand the dynamics in $\mathcal{R}_0$.

Already it is known that f_ξ has a chaotic attractor for all $\xi \in \mathcal{R}_0$, but only in the sense of a positive Lyapunov exponent. In this chapter we extend a result of Glendinning and

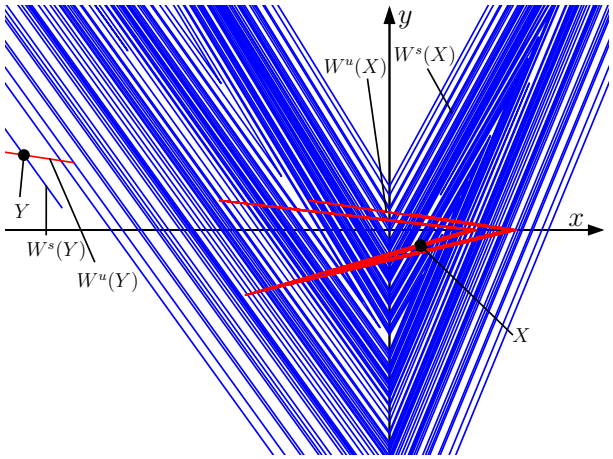

Figure 4.1: A phase portrait of (2.21) with $\xi = (1.5, 0.2, -2, 0.5)$ which corresponds a point in $\mathcal{R}_0$, see Fig. 4.2(a). There are two saddle fixed points, X and Y. The figure shows numerical computations of the stable (blue) and unstable (red) manifolds of X. The closure of the unstable manifold of X, denoted Λ, is a chaotic attractor; by Theorem 4.2 the map exhibits Devaney chaos on Λ. The stable manifold $W^s(X)$ can be 'grown' by iterating a certain line segment $\overline{f_\xi(V)f_\xi^{-1}(V)}$ backwards under f_ξ, see §4.3, and this figure shows this line segment and its subsequent eight preimages (forming the densely filled manifold illustrated in blue). By Theorem 4.1, $W^s(X)$ is dense in a region containing Λ.

Simpson [58] and show that throughout a relatively large subset of $\mathcal{R}_0$ the attractor satisfies Devaney's definition of chaos: transitivity, dense periodic orbits, and sensitive dependence on initial conditions [32], see §2.8. In view of the renormalisation, these properties also hold in the corresponding subsets of $\mathcal{R}_n$ with $n \geq 1$.

The key objects that we employ to verify Devaney chaos are *invariant expanding cones*. These allow us to obtain a lower bound for the rate at which line segments grow under iteration by either piece of f_ξ. Indeed such cones have been used to verify transitivity in other families of piecewise-linear maps [99, 121].

Below we also show that the stable manifold of X is dense in an open region containing the attractor. This is illustrated in Fig. 4.1 where we have numerically grown $W^s(X)$ outwards for eight iterations beyond its first kink with the switching manifold, $x = 0$. Already we can see the manifold is leaving only small gaps; by iterating further we have observed that the size of the gaps steadily reduces further. Thus $W^s(X)$ behaves like a two-dimensional object, when really it is one-dimensional. This is reminscent of a *blender* that for smooth invertible maps only occurs for maps that are at least three-dimensional [68]. Blenders are a central feature of hetero-dimensional cycles and useful for explaining the breakdown of uniform hyperbolicity [19].

The remainder of this chapter is organised as follows. The main results are presented in §4.2. Here we also show that the chaotic attractor can persist beyond $\Phi_{\rm BYG}$ and even outside $\mathcal{R}_1$. It appears that if the attractor is not destroyed at the curved boundary of $\Phi_{\rm BYG}$, then it is destroyed in a heteroclinic bifurcation where the unstable manifold of X develops an intersection with the stable manifold of a period-three solution.

In §4.3 we introduce essential features of the phase space of f_ξ, then in §4.4 identify invariant expanding cones on the tangent space of f_ξ. We put these together in §4.5 to prove statements about how line segments map under f_ξ. In §4.6 we establish related results for the inverse of f_ξ, then in §4.7 prove transitivity and the denseness of periodic solutions. Sensitive dependence follows immediately as it is a redundant aspect of Devaney's definition [15].

Throughout this chapter, whenever we define a point, for example P, the notation P_1 and P_2 denote the x and the y-components of P, until specified otherwise.

4.2 Main results

In this section we briefly discuss some of the concepts introduced in the last chapter before moving onto the main results.

4.2.1 A division of parameter space

The robust chaos parameter region of Banerjee, Yorke, and Grebogi [14] is the set

$$\Phi_{\rm BYG} = \{\xi \in \Phi \,|\, \phi(\xi) > 0\}, \tag{4.1}$$

where

$$\phi(\xi) = \delta_R - (\tau_R + \delta_L + \delta_R - (1+\tau_R)\lambda_L^u)\lambda_L^u. \tag{4.2}$$

Note that the above equation has a different notation than (3.2) because in (3.2) we had not introduced the eigenvalues yet. We introduced the renormalisation operator $g : \Phi \to \Phi$ in the last chapter defined by

$$g(\xi) = \big(\tau_R^2 - 2\delta_R, \delta_R^2, \tau_L\tau_R - \delta_L - \delta_R, \delta_L\delta_R\big),$$

For all $n \geq 0$, let

$$\mathcal{R}_n = \big\{\xi \in \Phi \,\big|\, \phi(g^n(\xi)) > 0,\ \phi\big(g^{n+1}(\xi)\big) \leq 0\big\}. \tag{4.3}$$

Sample two-dimensional slices of the sets $\mathcal{R}_n$ were shown in Fig. 3.3. Fig. 4.2 shows two more slices with some additional curves that will be important below.

We now state the main results. These are proved in later sections and involve the functions

$$J_1(\xi) = \frac{\lambda_L^u \lambda_R^{u^2}}{\lambda_L^u + |\lambda_R^u|}, \tag{4.4}$$

$$J_2(\xi) = \max\left\{\lambda_L^s, \frac{\sqrt{2}\lambda_L^s}{\lambda_L^s + 1}\right\} + \max\left\{|\lambda_R^s|, \frac{\sqrt{2}|\lambda_R^s|}{|\lambda_R^s| + 1}\right\}. \tag{4.5}$$

Since the eigenvalues λ_R^s and λ_R^u are negative we have used absolute values to make the signs of the various quantities readily apparent. The results here tell about the dynamics of f_ξ in $\mathcal{R}_0$ because $J_1(\xi) > 1$ implies $\xi \in \mathcal{R}_0$ for any $\xi \in \Phi_{\text{BYG}}$, see Lemma 4.7.

Theorem 4.1. *Let $\xi \in \Phi_{\text{BYG}}$ and suppose $J_1(\xi) > 1$ and $\lambda_L^s + |\lambda_R^s| < 1$. Then $W^s(X)$ is dense in a triangular region containing Λ.*

Theorem 4.2. *Let $\xi \in \Phi_{\text{BYG}}$ and suppose $J_1(\xi) > 1$ and $J_2(\xi) < 1$. Then f_ξ is chaotic in the sense of Devaney on Λ.*

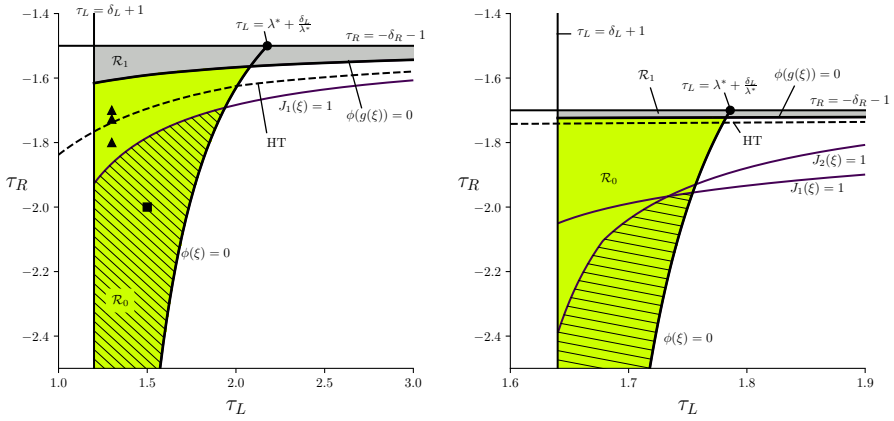

(a) $\delta_L = 0.2$, $\delta_R = 0.5$ (b) $\delta_L = 0.64$, $\delta_R = 0.7$

Figure 4.2: Two-dimensional slices of parameter space defined by fixing $\delta_L = 0.2$ and $\delta_R = 0.5$ in panel (a) and $\delta_L = 0.64$ and $\delta_R = 0.7$ in panel (b). The regions $\mathcal{R}_0$ and $\mathcal{R}_1$ are coloured yellow and grey respectively. The curved boundary $\phi(\xi) = 0$ intersects the horizontal boundary $\tau_R = -\delta_R - 1$ at $\tau_L = \lambda^* + \frac{\delta_L}{\lambda^*}$, where λ^* is the largest root of the quadratic $-\delta_R\lambda^2 + (1 - \delta_L)\lambda + \delta_R$, see Chapter 3 where this root was denoted α. The striped regions are where Theorems 4.1 and 4.2 apply. The dashed curves labelled HT are heteroclinic bifurcations discussed in §4.2.2. In panel (a) the black square indicates the parameter values of Fig. 4.1; the black triangles indicate the parameter values of Fig. 4.3.

Notice $J_2(\xi) < 1$ is a stronger condition than $\lambda_L^s + |\lambda_R^s| < 1$. The striped regions in Fig. 4.2 show where the conditions of Theorem 4.2 hold for the given fixed values of δ_L and δ_R. As mentioned above these are necessarily subsets of $\mathcal{R}_0$. In panel (a) the condition $J_2(\xi) < 1$ does not influence the boundary of the striped region because this condition is satisfied automatically when the values of δ_L and δ_R are sufficiently small. In panel (b) we have chosen values of δ_L and δ_R that highlight the nonsmoothness of the constraint $J_2(\xi) < 1$.

The conditions $J_1(\xi) > 1$ and $J_2(\xi) < 1$ arise quite naturally. First $J_1(\xi) > 1$ ensures the second iterate f_ξ^2 is expanding in some directions, whilst $J_2(\xi) < 1$ ensures the inverse f_ξ^{-1} is expanding in some other directions. Below we use these expansion properties to verify Devaney chaos. Nevertheless, numerical explorations suggest that these conditions are sub-optimal and that Λ in fact has Devaney chaos for all $\xi \in \mathcal{R}_0$. A proof of this remains for future work.

4.2.2 A heteroclinic bifurcation involving Λ

For the most part Λ appears to vary continuously as ξ is varied continuously within $\mathcal{R}_0$, but jumps in size when it develops intersections with the stable manifold of a period-three cycle. This is illustrated in Fig. 4.3. By decreasing the value of τ_R an intersection first occurs at $\tau_R \approx -1.727455$. This heteroclinic bifurcation is an example of a *crisis* [62]. It also clearly portrays the homoclinic bifurcation where the unstable manifold of the period-three cycle converges to the chaotic attractor.

Numerically we have computed curves in Fig. 4.2 (labelled HT) where the heteroclinic bifurcation occurs. This was a computationally intensive task because, unlike the simple corner intersections associated with $\phi(\xi) = 0$ for example that involve the first couple of linear pieces of $W^s(Y)$ and $W^u(Y)$ as they emanate outwards from Y, the corner intersections associated with the heteroclinic bifurcation involve the limiting outer-most part of $W^u(X)$ as is it grown outwards from X indefinitely. Curves of such bifurcations were considered by Osinga [105] where it was argued that other bifurcations may contribute to the crisis. It remains to be seen whether or not such bifurcations are present in our piecewise-linear setting.

The attractor Λ appears to persist to the right of $\phi(\xi) = 0$ in the narrow strip bounded above by $\phi(g(\xi)) = 0$ and bounded below by the heteroclinic bifurcation curve. From a point within this strip, if we cross $\phi(g(\xi)) = 0$ we enter $\mathcal{R}_1$ and Λ is replaced by an attractor with two connected components, while if we cross the heteroclinic bifurcation forward

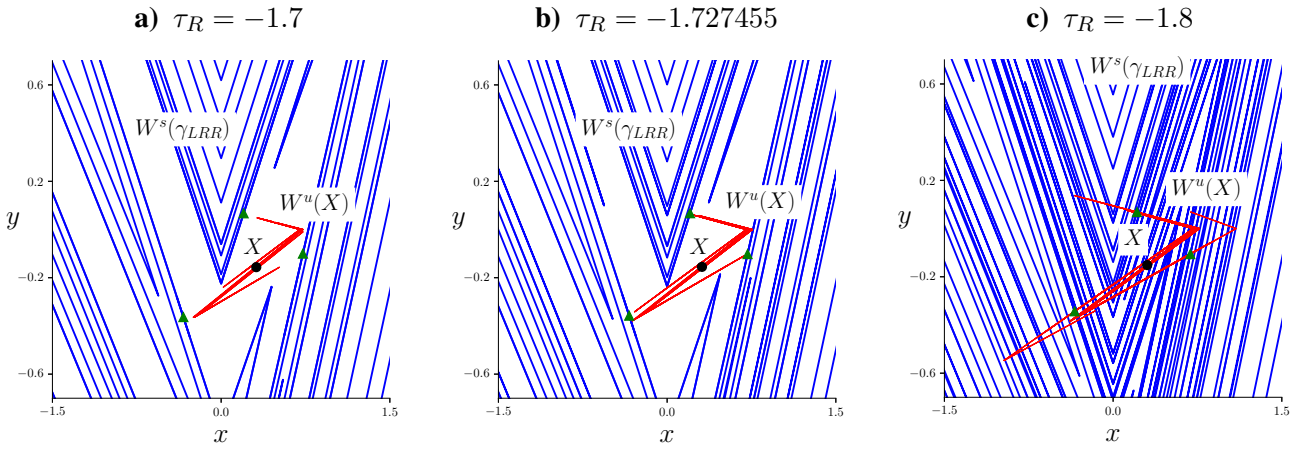

Figure 4.3: Phase portraits of (2.21) with $\delta_L = 0.2$, $\delta_R = 0.5$, $\tau_L = 1.3$, and three different values of τ_R as indicated. These parameter combinations are shown in Fig. 4.2. In each plot the three green triangles are the points of a saddle-type LRR-cycle, denoted γ_{LRR}. The stable manifold of the period-three cycle is denoted in blue, whereas the chaotic attractor is denoted by red. The black dot represents X.

orbits of points near X are able to diverge so $W^u(X)$ suddenly becomes unbounded and the attractor is destroyed. Numerical investigations suggest this occurs for any values of $\delta_L > 0$ and $\delta_R > 0$, that is, it is always the stable manifold of the LRR-cycle (period-three solution with symbolic itinerary LRR) that is responsible for the crisis.

4.3 The stable and unstable manifolds of the fixed points

Recall from Chapter 3 that first kink of the right branch of $W^u(Y)$, as we follow it outwards from Y, occurs at the point

$$D = \left(\frac{1}{1 - \lambda_L^s}, 0 \right), \tag{4.6}$$

see Fig. 4.4. For all $\xi \in \Phi$, D lies to the right of $(1, 0)$, whereas $f_\xi(D)$ lies in the left half-plane. Let U denote the intersection of $\overline{Df_\xi(D)}$ with Σ. The right branch of $W^u(Y)$ contains the line segments $\overline{YD}$ and $\overline{Df_\xi(D)}$ and can be 'grown' by iterating $\overline{Df_\xi(D)}$ under f_ξ because this line segment, minus one of its endpoints, is a *fundamental domain* [110] for this branch of the manifold.

As in Chapter 3 let B denote the intersection of $\overline{YD}$ with the line through $f_\xi(D)$ and parallel to the stable subspace $E^s(Y)$, see Fig. 4.4. Recall from Proposition 3.1 that the triangle Ω with vertices D, $f_\xi(D)$, and B is forward invariant under f_ξ for any $\xi \in \Phi_{\text{BYG}}$. In this chapter the geometry of $f_\xi(\Omega)$, see Fig. 4.4, will be particularly important.

The first kink of $W^s(X)$ occurs at the point

$$V = \left(0, \frac{-\lambda_R^u}{\lambda_R^u - 1}\right), \tag{4.7}$$

see again Fig. 4.4. The stable manifold $W^s(X)$ contains $\overline{Vf_\xi^{-1}(V)} \subset E^s(X)$ and can be grown by iterating $\overline{f_\xi(V)f_\xi^{-1}(V)}$ under f_ξ^{-1}. This is because $\overline{f_\xi(V)f_\xi^{-1}(V)}$, minus one of its endpoints, is a fundamental domain for $W^s(X)$.

The next result clarifies how $\overline{Vf_\xi^{-1}(V)}$ intersects the region $f_\xi(\Omega)$ and is used below to prove Lemma 4.8. Specifically Lemma 4.1 implies $f_\xi(V)$ lies to the left of $f_\xi(U)$; consequently $\overline{Vf_\xi^{-1}(V)}$ cuts $f_\xi(\Omega)$ into three pieces.

Lemma 4.1. *Let $\xi \in \Phi$. If $\lambda_L^s + |\lambda_R^s| < 1$ then $U_2 > V_2$.*

Proof. By iterating (4.6) under f_ξ we find that $\overline{Df_\xi(D)}$ has slope $\frac{\delta_R}{\lambda_L^s - \tau_R}$ and consequently

$$U = \left(0, \frac{-\delta_R}{(\lambda_L^s - \tau_R)(1 - \lambda_L^s)}\right). \tag{4.8}$$

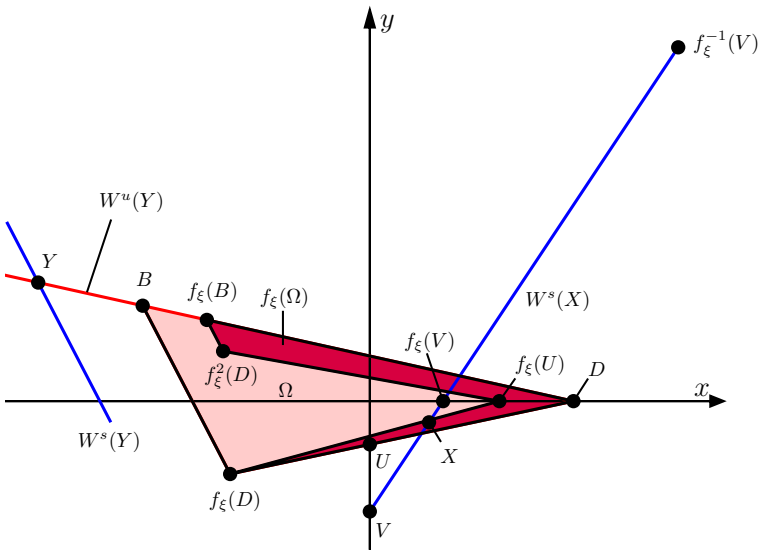

Figure 4.4: A sketch of the forward invariant region Ω that is constructed using kinks of the unstable manifold of Y (red). We also show its image $f_\xi(\Omega)$ and parts of the stable manifolds of X and Y (blue).

By subtracting the second component of (4.7) from that of (4.8) and factorising, we obtain

$$U_2 - V_2 = \frac{|\lambda_R^u|(1-\lambda_L^s+\lambda_R^s)(\lambda_L^s-\lambda_R^u)}{(1-\lambda_L^s)(1-\lambda_R^u)(\lambda_L^s-\tau_R)}. \tag{4.9}$$

If $\lambda_L^s + |\lambda_R^s| < 1$ then each bracketed factor in (4.9) has a positive value, thus $U_2 > V_2$. $\square$

4.4 Invariant expanding cones

In this section we construct invariant expanding cones for the Jacobian matrices A_L and A_R.

Definition 4.1. A nonempty set $C \subset \mathbb{R}^2$ is a *cone* if $tv \in C$ for all $v \in C$ and $t \in \mathbb{R}$.

Definition 4.2. Let A be a real-valued 2×2 matrix.

(i) A cone $C \subset \mathbb{R}^2$ is *invariant* if $Av \in C$ for all $v \in C$.

(ii) The cone is *expanding* if there exists an expansion factor $c > 1$ such that $\|Av\| \geq c\|v\|$ for all $v \in C$.

Given an interval $K \subset \mathbb{R}$, the set

$$\Psi_K = \left\{ t \begin{bmatrix} 1 \\ m \end{bmatrix} \,\middle|\, m \in K, t \in \mathbb{R} \right\}, \tag{4.10}$$

is a cone. The vector $v = \begin{bmatrix} 1 \\ -\lambda_L^s \end{bmatrix}$ is an eigenvector of A_L corresponding to the eigenvalue λ_L^u. Thus

$$\|Av\| = \lambda_L^u \|v\|. \tag{4.11}$$

It is a simple exercise to show that (4.11) holds with $v = \begin{bmatrix} 1 \\ m \end{bmatrix}$ for exactly one other value of $m \in \mathbb{R}$, namely

$$m_{\text{crit}} = \lambda_L^s + \frac{2\tau_L}{\lambda_L^{u^2} - 1}, \tag{4.12}$$

and notice $m_{\text{crit}} > 0$. It is not difficult to show that $\|Av\| \geq \lambda_L^u \|v\|$ for all $v = \begin{bmatrix} 1 \\ m \end{bmatrix}$ with $-\lambda_L^s \leq m \leq m_{\text{crit}}$. The following result generalises this observation.

Lemma 4.2. *Suppose $\tau_L > \delta_L + 1$ and $\delta_L > 0$. Let $K = [-\lambda_L^s, m_{\max}]$ for some $m_{\max} \geq 0$.*

1. *If $m_{\max} \leq m_{\text{crit}}$ then Ψ_K is invariant and expanding for A_L with expansion factor λ_L^u.*

2. *If $m_{\max} \leq 1$ then Ψ_K is invariant and expanding for A_L with expansion factor $c_L = \min\Big\{\lambda_L^u, \frac{\lambda_L^u+1}{\sqrt{2}}\Big\}$.*

Proof. Choose any $v \in \Psi_K$. Then $v = t\begin{bmatrix}1\\ m\end{bmatrix}$ for some $m \in K$ and $t \in \mathbb{R}$. If $t = 0$ then $A_L v \in \Psi_K$ trivially, otherwise the slope of $A_L v$ is $G(m) = \frac{-\delta_L}{\tau_L + m}$. Notice $G(-\lambda_L^s) = -\lambda_L^s$. Also G is increasing and negative-valued on $[0, \infty)$. Therefore $G(m) \in [-\lambda_L^s, 0) \subset K$ and so $A_L v \in \Psi_K$. That is, Ψ_K is invariant for A_L.

For any $c > 1$ and $t \neq 0$,

$$H(m) = \|A_L v\|^2 - c^2\|v\|^2 = t^2\Big(\big(1 - c^2\big)m^2 + 2\tau_L m + \tau_L^2 + \delta_L^2 - c^2\Big), \tag{4.13}$$

is a concave down quadratic function of m. Thus, on K, H achieves its minimum at an endpoint of K. With $m = \lambda_L^s$ or $m = m_{\text{crit}}$ we have

$$\frac{\|A_L v\|^2}{\|v\|^2} = \lambda_L^{u^2}. \tag{4.14}$$

Thus with $m_{\max} \leq m_{\text{crit}}$ and $c = \lambda_L^u$, then $H(m) \geq 0$ for all $m \in K$. That is, Ψ_K is expanding with expansion factor λ_L^u. With instead $m = 1$ we have

$$\frac{\|A_L v\|^2}{\|v\|^2} = \frac{(\tau_L + 1)^2 + \delta_L^2}{2} > \frac{(\lambda_L^u + 1)^2}{2}. \tag{4.15}$$

Thus if $m_{\max} \leq 1$ and c^2 is the minimum of (4.14) and the bound in (4.15) then again $H(m) \geq 0$ for all $m \in K$. That is, Ψ_K is expanding with expansion factor c_L. □

Next we state a result for A_R that is analogous to Lemma 4.22. This can be obtained in the same way so we do not provide a proof.

Lemma 4.3. *Suppose $\tau_R < -\delta_R - 1$ and $\delta_R > 0$. Let $K = [m_{\min}, |\lambda_R^s|]$ for some $m_{\min} \in [-1, 0]$. The cone Ψ_K is invariant and expanding for A_R with expansion factor $c_R = \min\Big\{|\lambda_R^u|, \frac{|\lambda_R^u|+1}{\sqrt{2}}\Big\}$.*

Next we provide a simple lower bound for the value of m_{crit}. We then use this, and Lemmas 4.2 and 4.3, to construct a cone that is invariant and expanding for both A_L and A_R.

Lemma 4.4. *Let $\xi \in \Phi_{\text{BYG}}$. Then $m_{\text{crit}} > 2\delta_R$.*

Proof. Treat m_{crit} as a function of τ_L and δ_L. By directly differentiating (4.12) we obtain

$$\frac{\partial m_{\text{crit}}}{\partial \tau_L} = -\left[\frac{\delta_L}{\lambda_L^{u^2}} + \frac{2\big(\lambda_L^{u^2}+1\big)}{\big(\lambda_L^{u^2}-1\big)^2} + \frac{2\delta_L\big(3\lambda_L^{u^2}-1\big)}{\lambda_L^{u^2}\big(\lambda_L^{u^2}-1\big)^2}\right]\frac{\partial \lambda_L^u}{\partial \tau_L}.$$

By inspection the quantity in square brackets is positive (because $\delta_L > 0$ and $\lambda_L^u > 1$). Also $\frac{\partial \lambda_L^u}{\partial \tau_L} > 0$, therefore, for any fixed $\delta_L > 0$, m_{crit} is a decreasing function of τ_L.

As shown in Chapter 3, in the (τ_L, τ_R)-plane the curve $\phi(\xi) = 0$ intersects $\tau_R = -\delta_R - 1$ at $\tau_L = \lambda^* + \frac{\delta_L}{\lambda^*}$, where λ^* is the larger of the two solutions to

$$-\delta_R\lambda^2 + (1-\delta_L)\lambda + \delta_R = 0, \tag{4.16}$$

as indicated in Fig. 4.2. Since the curve $\phi(\xi) = 0$ has positive slope everywhere (see Proposition 3.4), for any $\xi \in \Phi_{\text{BYG}}$ the value of τ_L is less than $\lambda^* + \frac{\delta_L}{\lambda^*}$. So, since m_{crit} is a decreasing function of τ_L, $m_{\text{crit}} > m^*_{\text{crit}}(\delta_L, \delta_R)$ where

$$m^*_{\text{crit}}(\delta_L, \delta_R) = \frac{\delta_L}{\lambda^*} + \frac{2\big(\lambda^* + \frac{\delta_L}{\lambda^*}\big)}{\lambda^{*2}-1},$$

is obtained by replacing τ_L in (4.12) with $\lambda^* + \frac{\delta_L}{\lambda^*}$.

It remains to show that $m^*_{\text{crit}}(\delta_L, \delta_R) > 2\delta_R$ for all $0 < \delta_L < 1$ and $\delta_R > 0$ because to have $\xi \in \Phi_{\text{BYG}}$ we must have $\delta_L < 1$, see Chapter 3. First observe $m^*_{\text{crit}}(0, \delta_R) = \frac{2\lambda^*}{\lambda^{*2}-1}$ and in view of (4.16) this reduces to $m^*_{\text{crit}}(0, \delta_R) = 2\delta_R$. Also

$$\frac{\partial m^*_{\text{crit}}}{\partial \delta_L} = \frac{1}{\alpha} + \frac{2}{\alpha(\alpha^2-1)} - \frac{\frac{\partial \lambda^*}{\partial \delta_L}}{\lambda^{*2}(\lambda^{*2}-1)^2}\Big[\delta_L\Big(\lambda^{*4} + 4\lambda^{*2} - 1\Big) + 2\lambda^{*2}\Big(\lambda^{*2}+1\Big)\Big].$$

By inspection the quantity in square brackets is positive (because $\delta_L > 0$ and $\lambda^* > 1$). It is a simple exercise to show $\frac{\partial \lambda^*}{\partial \delta_L} < 0$, therefore, for any fixed $\delta_R > 0$, m^*_{crit} is an increasing function of δ_L. Thus $m^*_{\text{crit}}(\delta_L, \delta_R) > m^*_{\text{crit}}(0, \delta_R) = 2\delta_R$, as required. □

Lemma 4.5. *Let $\xi \in \Phi_{\text{BYG}}$. With $K = [-\lambda_L^s, |\lambda_R^s|]$, the cone Ψ_K is invariant for A_L and A_R. Moreover, it is expanding for A_L with expansion factor λ_L^u and expanding for A_R with expansion factor $c_R = \min\Big\{|\lambda_R^u|, \frac{|\lambda_R^u|+1}{\sqrt{2}}\Big\}$.*

Proof. Observe $|\lambda_R^s| < \delta_R < 2\delta_R < m_{\text{crit}}$ using Lemma 4.4. Thus the right end-point of K is bounded above by m_{crit}, hence the result for A_L follows from Lemma 4.21. Also $-1 < -\lambda_L^s$ thus the result for A_R follows from Lemma 4.3. □

4.5 Expanding line segments

In this section we use invariant expanding cones to study how line segments map under f_ξ and to prove Theorem 4.1.

Given points $P, Q \in \mathbb{R}^2$, let $\alpha = \overline{PQ} \subset \mathbb{R}^2$ be the line segment connecting P and Q. Also if $Q = P + v$ then the length of α is $|\alpha| = \|v\|$. We say α *crosses* Σ if it contains points on both sides of Σ. If α does not cross Σ, then all points in α map under the same piece of f_ξ. In this case $f_\xi(\alpha)$ is another line segment and

$$|f_\xi(\alpha)| = \|A_J v\|, \tag{4.17}$$

with $J = L$ or $J = R$ accordingly.

If α crosses Σ, then $f_\xi(\alpha)$ consists of two line segments connected at a point on $f_\xi(\Sigma)$. The next result (inspired by Lemma 2.1 of Veitch and Glendinning [140]) provides a lower bound on the length of the longer of these two segments.

Lemma 4.6. *Let s be the length of the longest line segment in $f_\xi(\alpha)$ and let $c_L, c_R > 0$. If $\|A_L v\| \geq c_L\|v\|$ and $\|A_R v\| \geq c_R\|v\|$, then*

$$s \geq \frac{c_L c_R}{c_L + c_R}\,|\alpha|. \tag{4.18}$$

Proof. Let α_L denote the part of α in the closed left half-plane and α_R denote the part of α in the closed right half-plane. Then $|\alpha_L| = t|\alpha|$ and $|\alpha_R| = (1-t)|\alpha|$ for some $t \in [0,1]$. Observe $|f_\xi(\alpha_L)| = \|A_L(tv)\| \geq tc_L|\alpha|$ and $|f_\xi(\alpha_R)| = \|A_R((1-t)v)\| \geq (1-t)c_R|\alpha|$. Thus $s \geq \max\{tc_L, (1-t)c_R\}|\alpha|$. This length is smallest when $tc_L = (1-t)c_R$. That is, $t = \frac{c_R}{c_L+c_R}$, giving (4.18). □

We are now able to show that the condition $J_1(\xi) > 1$ implies $\xi \in \mathcal{R}_0$ for any $\xi \in \Phi_{\text{BYG}}$. This is because if $\xi \in \Phi_{\text{BYG}}$ then $\phi(\xi) > 0$, so if also $\phi(g(\xi)) < 0$ then $\xi \in \mathcal{R}_0$ by definition, (3.9).

Lemma 4.7. *Let $\xi \in \Phi$. If $J_1(\xi) > 1$ then $\phi(g(\xi)) < 0$.*

Proof. Let $\xi \in \Phi$ and suppose $\phi(g(\xi)) \geq 0$. It remains to show $J_1(\xi) \leq 1$. Let $T \in f_\xi(\Sigma)$ denote the first kink of $W^u(X)$ as we follow it outwards from X, see Fig. 4.5. As shown in Chapter 3, $\phi(g(\xi)) \geq 0$ implies $f_\xi^2(T)$ lies on or to the right of the stable subspace $E^s(X)$. The slope of $E^s(X)$ is $|\lambda_R^u|$, where $|\lambda_R^u| < \frac{1+\sqrt{5}}{2}$ because $\phi(g(\xi)) \geq 0$, see Chapter 3.

The slope of $\overline{Tf_\xi(T)}$ is $|\lambda_R^s|$. This slope belongs to the interval $K = [-\lambda_L^s, |\lambda_R^s|]$ of Lemma 4.5, thus by the invariance of Ψ_K the slope of $\overline{Tf_\xi^2(T)}$ also belongs to this interval. Thus the slope of $\overline{Tf_\xi^2(T)}$ is at least $-\lambda_L^s$, which is greater than -1. Also $f_\xi^2(T)$ lies above $f_\xi(\Sigma)$ (the x-axis) because $f_\xi(T)$ lies to the left of Σ. By putting these observations together we conclude that $f_\xi^2(T)$ must belong to the shaded region of Fig. 4.5. It is then a simple exercise in geometry to show that the distance of any point in this region to T is less than the distance of X to T. Thus $f_\xi^2(T)$ is closer to T than X is.

Now let $\alpha = \overline{Xf_\xi(T)}$. Then $f_\xi(\alpha) = \overline{XT} \cup \overline{Tf_\xi^2(T)}$. We have just shown that the longest line segment in $f_\xi(\alpha)$ is $\overline{XT}$. By Lemma 4.6 this has length

$$s \geq \frac{\lambda_L^u |\lambda_R^u|}{\lambda_L^u + |\lambda_R^u|} |\alpha|, \tag{4.19}$$

using also Lemma 4.5 with $c_R = |\lambda_R^u|$ because $|\lambda_R^u| < \frac{1+\sqrt{5}}{2}$. Since $\overline{XT}$ is aligned with the unstable direction of X, $\left|f_\xi(\overline{XT})\right| = |\lambda_R^u| s$. But $f_\xi(\overline{XT}) = \alpha$, thus (4.19) implies $|\alpha| \geq \frac{\lambda_L^u \left|\lambda_R^u\right|^2}{\lambda_L^u + \left|\lambda_R^u\right|} |\alpha|$. That is, $J_1(\xi) \leq 1$. □

Next we prove that, under certain conditions, when we iterate a line segment under

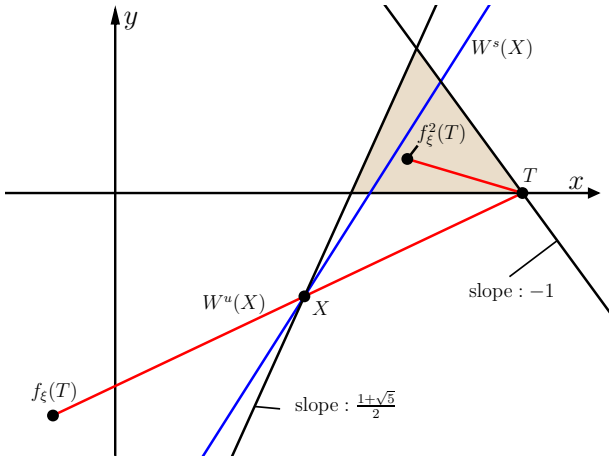

Figure 4.5: A sketch of the phase space of (2.21) with $\xi \in \Phi$ and $\phi(g(\xi)) \geq 0$ to support the proof of Lemma 4.7. The shaded region is bounded by the x-axis, the line through X with slope $\frac{1+\sqrt{5}}{2}$, and the line through T with slope -1.

f_ξ we must eventually intersect $\overline{Vf_\xi^{-1}(V)}$ — the initial linear piece of $W^s(X)$ as it emanates from X. Then only a few more arguments are required to establish the denseness of $W^s(X)$.

Lemma 4.8. *Let $\xi \in \Phi_{\rm BYG}$ and suppose $J_1(\xi) > 1$ and $\lambda_L^s + |\lambda_R^s| < 1$. Let $\alpha \subset \Omega$ be a line segment with slope in $K = [-\lambda_L^s, |\lambda_R^s|]$. Then there exists $n \geq 1$ and points $P \in \Sigma$ and $Q \in f_\xi(\Sigma)$ such that $\overline{PQ} \subset f_\xi^n(\alpha)$. Moreover, $\overline{PQ}$ intersects $\overline{Vf_\xi^{-1}(V)}$ transversally.*

Proof. Let $\alpha_0 = \alpha$. We construct a sequence $\{\alpha_i\}$ of line segments in Ω with slopes in K as follows. If α_i does not cross Σ, let $\alpha_{i+1} = f_\xi(\alpha_i)$. Observe $\alpha_{i+1} \subset \Omega$ because Ω is forward invariant under f_ξ (Proposition 3.1), and α_{i+1} has slope in K because Ψ_K is invariant for both A_L and A_R (Lemma 4.5). Moreover, with c_R as in Lemma 4.5, $|\alpha_{i+1}| \geq d_0|\alpha_i|$ where $d_0 = \min\{\lambda_L^u, c_R\} > 1$.

If α_i crosses Σ, first let β_i be the longer of the two line segments that comprise $f_\xi(\alpha_i)$. If β_i does not cross Σ, let $\alpha_{i+1} = f_\xi(\beta_i)$. Both β_i and α_{i+1} belong to Ω and have slopes in K by the invariance properties. We now show that the situation of β_i not crossing Σ cannot always occur.

The endpoint of β_i that lies on $f_\xi(\Sigma)$ belongs the right half-plane. This is because $\beta_i \subset f_\xi(\Omega)$ and the intersection of $f_\xi(\Omega)$ with $f_\xi(\Sigma)$ is the line segment with endpoints $f_\xi(U)$ and D, see Proposition 3.1. But U lies above V (Lemma 4.1) because we have assumed $\lambda_L^s + |\lambda_R^s| < 1$, thus $f_\xi(U)$ lies to the right of $f_\xi(V)$, which certainly lies to the right of Σ in view of the explicit expression (4.7). So the assumption that β_i does not cross Σ means that β_i lies in the closed right half-plane, thus $|\alpha_{i+1}| \geq c_R|\beta_i|$ by Lemma 4.5. Also $|\beta_i| \geq \frac{\lambda_L^u c_R}{\lambda_L^u + c_R}|\alpha_i|$ by Lemma 4.6, therefore $|\alpha_{i+1}| \geq d_1|\alpha_i|$ where $d_1 = \frac{\lambda_L^u c_R^2}{\lambda_L^u + c_R}$.

If $|\lambda_R^u| > \frac{1+\sqrt{5}}{2}$ then $c_R > \frac{1+\sqrt{5}}{2}$ and so $d_1 > 1$ (because $\lambda_L^u > 1$). Otherwise $c_R = |\lambda_R^u|$ in which case $d_1 = J_1(\xi)$ and so again $d_1 > 1$ (because $J_1(\xi) > 1$ by assumption). Now let $d = \min\{d_0, d_1\}$. Then $|\alpha_n| \geq d^n|\alpha_0| \to \infty$ as $n \to \infty$ because $d > 1$, but Ω is bounded so this is not possible. Thus there must exist $j \geq 0$ such that both α_j and β_j cross Σ. Let $P = \beta_j \cap \Sigma$ and Q be the endpoint of β_j that lies on $f_\xi(\Sigma)$. By construction $\overline{PQ} \subset f_\xi^n(\alpha)$ for some $j + 1 \leq n \leq 2j + 1$.

Finally, $\overline{PQ} \subset f_\xi(\Omega)$ thus P lies on or above U while Q lies on or to the right of $f_\xi(U)$, see Fig. 4.4. We now use Lemma 4.1 to show that $\overline{PQ}$ intersects $\overline{Vf_\xi^{-1}(V)}$ transversally. Since U lies above V, P lies to the left of the stable subspace $E^s(X)$. Since $f_\xi(U)$ lies to the right of $f_\xi(V)$, Q lies to the right of $E^s(X)$. Thus $\overline{PQ}$ intersects $E^s(X)$ transversally at some point $S \in f_\xi(\Omega)$. Finally $S \in \overline{Vf_\xi^{-1}(V)}$ because $f_\xi^{-1}(V)$ lies above the line through $f_\xi^{-1}(D)$ and D (which is the case because V lies below the line through D and $f_\xi(D)$). □

Proof of Theorem 4.1. Since $X \in \Omega$ and Ω is compact and forward invariant under f_ξ, we have $\Lambda \subset \Omega$. Choose any $\tilde{P} \in \Omega$ and $\varepsilon > 0$. Let $\alpha \subset B_\varepsilon(\tilde{P}) \cap \Omega$ be a line segment with slope in $[-\lambda_L^s, |\lambda_R^s|]$. By Lemma 4.8 there exists $n \geq 1$ such that $f_\xi^n(\alpha)$ intersects $W^s(X)$ at some point S. Thus $\tilde{Q} = f_\xi^{-n}(S)$ belongs to $W^s(X)$ and lies within a distance ε of $\tilde{P}$. Since $\tilde{P} \in \Omega$ and $\varepsilon > 0$ are arbitrary, we can conclude that $W^s(X)$ is dense in Ω. □

4.6 Dynamics of the inverse f_ξ^{-1}

In this section we identify invariant expanding cones for A_L^{-1} and A_R^{-1}. Similar calculations have been done to verify uniform hyperbolicity in the Lozi map [99]. The results, Lemmas 4.9 and 4.10, are analogous to the results obtained above in §4.4 for A_L and A_R and can be proved in the same way. We omit such proofs for brevity but instead provide a novel proof of Lemma 4.9 that works by converting A_L^{-1}, via a change of coordinates, to a matrix that has the same companion matrix form as A_L. We also show that the set of points whose backward orbits under f_ξ diverge is dense in $\mathbb{R}^2$, Lemma 4.11. Consequently the attractor Λ cannot contain open sets and this observation is utilised in the next section.

Given an interval K, the set

$$\hat{\Psi}_K = \left\{ t \begin{bmatrix} \hat{m} \\ 1 \end{bmatrix} \,\middle|\, \hat{m} \in K, t \in \mathbb{R} \right\}, \tag{4.20}$$

is a cone.

Lemma 4.9. *Suppose $\tau_L > \delta_L + 1$ and $\delta_L > 0$. Let $K = \left[-\frac{1}{\lambda_L^u}, \hat{m}_{\max}\right]$ for some $\hat{m}_{\max} \in [0,1]$. The cone $\hat{\Psi}_K$ is invariant and expanding for A_L^{-1} with expansion factor $\hat{c}_L = \min\left\{\frac{1}{\lambda_L^s}, \frac{1+\lambda_L^s}{\sqrt{2}\lambda_L^s}\right\}$.*

Proof. Let $P = \begin{bmatrix} 0 & 1 \\ 1 & 0 \end{bmatrix}$ and let

$$B_L = P A_L^{-1} P^{-1} = \begin{bmatrix} \frac{\tau_L}{\delta_L} & 1 \\ -\frac{1}{\delta_L} & 0 \end{bmatrix}.$$

This matrix has the form of A_L with eigenvalues $0 < \frac{1}{\lambda_L^u} < 1 < \frac{1}{\lambda_L^s}$ (the same eigenvalues as A_L^{-1} by similarity). By Lemma 4.22, Ψ_K is invariant and expanding for B_L with expansion factor $\hat{c}_L$. Multiplication by P corresponds to a reflection about the line $y = x$, therefore

$\hat{\Psi}_K$ (the reflection of Ψ_K about $y = x$) is invariant and expanding for A_L^{-1} with same expansion factor. □

Lemma 4.10. *Suppose $\tau_R < -\delta_R - 1$ and $\delta_R > 0$. Let $K = \left[\hat{m}_{\min}, \frac{1}{|\lambda_R^u|}\right]$ for some $\hat{m}_{\min} \in [-1, 0]$. The cone $\hat{\Psi}_K$ is invariant and expanding for A_R^{-1} with expansion factor $\hat{c}_R = \min\left\{\frac{1}{|\lambda_R^s|}, \frac{1+|\lambda_R^s|}{\sqrt{2}|\lambda_R^s|}\right\}$.*

Lemma 4.11. *Let $\xi \in \Phi$ and suppose $J_2(\xi) < 1$. The set*

$$\Xi = \left\{(x, y) \in \mathbb{R}^2 \,\middle|\, \|f_\xi^{-i}(x, y)\| \to \infty \text{ as } i \to \infty\right\}. \tag{4.21}$$

is dense in $\mathbb{R}^2$.

Proof. Choose any $\tilde{P} \in \mathbb{R}^2$ and $\varepsilon > 0$. It remains for us to show $B_\varepsilon(\tilde{P}) \cap \Xi \neq \varnothing$.

Let $\hat{K} = \left[-\frac{1}{\lambda_L^u}, \frac{1}{|\lambda_R^u|}\right]$. By Lemmas 4.9 and 4.10, $\hat{K}$ is invariant for A_L^{-1} and A_R^{-1} with expansion factors $\hat{c}_L$ and $\hat{c}_R$ given above. Notice $J_2(\xi) < 1$ is equivalent to

$$\frac{1}{\hat{c}_L} + \frac{1}{\hat{c}_R} < 1. \tag{4.22}$$

Let $\alpha_0 \subset B_\varepsilon(\tilde{P})$ be a line segment with slope in $\hat{K}$. For each $i \geq 0$, let $\alpha_{i+1} = f_\xi^{-1}(\alpha_i)$ if this is a line segment, otherwise let α_{i+1} be the longest line segment in $f_\xi^{-1}(\alpha_i)$. Each α_i has slope in $\hat{K}$ by invariance. Analogous to (4.18), we have $|\alpha_{i+1}| \geq d|\alpha_i|$ for all $i \geq 0$, where

$$d = \frac{\hat{c}_L \hat{c}_R}{\hat{c}_L + \hat{c}_R}.$$

But $d > 1$ by (4.22), thus $|\alpha_i| \to \infty$ as $i \to \infty$. Thus there exists $\tilde{Q} \in \alpha_0$ with $\|f_\xi^{-i}(\tilde{Q})\| \to \infty$ as $i \to \infty$, so $\tilde{Q} \in B_\varepsilon(\tilde{P}) \cap \Xi$. □

4.7 Devaney chaos

In this section we work towards a proof of Theorem 4.2.

As in the proof of Lemma 4.7, let $T \in f_\xi(\Sigma)$ denote the first kink of $W^u(X)$. But now suppose $f_\xi^2(T)$ lies to the left of the stable subspace $E^s(X)$. This assumption is equivalent to $\phi(g(\xi)) < 0$, see Chapter 3, so by Lemma 4.7 occurs when $J_1(\xi) > 1$. Let Z denote the intersection of $E^s(X)$ with $\overline{Tf_\xi^2(T)}$ and let Δ_0 be the filled triangle with vertices X, T,

and Z, see Fig. 4.6. Also let

$$\Delta = \bigcup_{i=0}^{\infty} f_\xi^i(\Delta_0), \qquad \tilde{\Delta} = \bigcap_{i=0}^{\infty} f_\xi^i(\Delta). \tag{4.23}$$

We first prove the following lemma that extends previous results [58] to a wider range of parameter values.

Lemma 4.12. *Let $\xi \in \Phi_{\mathrm{BYG}}$ and suppose $J_1(\xi) > 1$ and $J_2(\xi) < 1$. Then $\Lambda = \tilde{\Delta}$.*

Proof. Here we write ∂F for the boundary of a set $F \subset \mathbb{R}^2$.

By definition, $\partial\Delta_0 \subset \overline{XZ} \cup W^u(X)$. Consequently $\partial f_\xi^i(\Delta_0) \subset \overline{X f_\xi^i(Z)} \cup W^u(X)$ for all $i \geq 0$. Thus $\partial\Delta \subset \overline{Z f_\xi(Z)} \cup W^u(X)$ and so $\partial f_\xi^i(\Delta) \subset \overline{f_\xi^i(Z) f_\xi^{i+1}(Z)} \cup W^u(X)$ for all $i \geq 0$. Therefore $\partial\tilde{\Delta} \subset \Lambda$ because $f_\xi^i(Z) \to X$. In view of its definition, $\tilde{\Delta}$ is backwards invariant under f_ξ. Thus $\tilde{\Delta} \cap \Xi = \varnothing$, where Ξ is the set (4.21). But Ξ is dense in $\mathbb{R}^2$ (Lemma 4.11), thus $\tilde{\Delta} = \partial\tilde{\Delta}$. Hence $\tilde{\Delta} \subset \Lambda$.

To prove $\Lambda \subset \tilde{\Delta}$, choose any $P \in \Lambda$. Let $\{P^{(k)}\}$ be a sequence of points in $W^u(X)$ with $P^{(k)} \to P$ as $k \to \infty$. For each k we have $f_\xi^i(P^{(k)}) \to X$ as $i \to -\infty$, so there exists $i_k \leq 0$ such that $f_\xi^{i_k}(P^{(k)}) \in \overline{XT} \subset \Delta_0$. Thus $P^{(k)} \in \Delta$ for all k, so $P \in \Delta$. Thus $\Lambda \subset \Delta$. But Λ is forward invariant under f_ξ, thus $\Lambda \subset \tilde{\Delta}$. □

Proof of Theorem 4.2. Observe $W^u(X) = \bigcup_{i\geq 0} f_\xi^i\big(\overline{XT}\big) \setminus \{X\}$. The line segment $\overline{XT}$ has slope $|\lambda_R^s|$ which belongs to the interval $K = [-\lambda_L^s, |\lambda_R^s|]$. By Lemma 4.5 the cone Ψ_K is

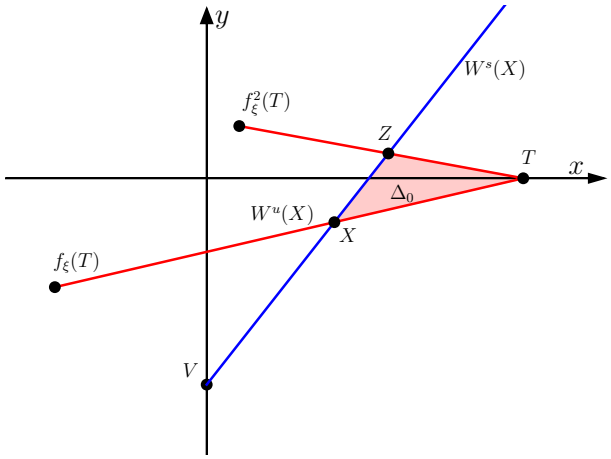

Figure 4.6: A sketch of the phase space of (2.21) with $\xi \in \Phi$ and $\phi(g(\xi)) < 0$ illustrating the definition of Δ_0 (shaded).

invariant for both A_L and A_R, thus each $f_\xi^i\big(\overline{XT}\big)$ is a union of line segments with slopes in K.

Thus for any $\tilde{P} \in \Lambda$ and $\varepsilon > 0$, there exists a line segment $\alpha \subset W^u(X) \cap B_\varepsilon(\tilde{P})$ with slope in K. By Lemma 4.8, there exists $n_1 \geq 1$ such that $f_\xi^{n_1}(\alpha)$ transversally intersects $W^s(X)$ at some point S. Arbitrarily close to S there exists a non-wandering set associated with a Smale horseshoe [132]. In the non-wandering set periodic points of f_ξ are dense. Thus f_ξ has a periodic point $P_{\rm per} \in B_\varepsilon(\tilde{P})$ with $P_{\rm per} \in \Lambda$ because $W^u(X)$ is also dense in the non-wandering set. This shows that periodic points of f_ξ are dense in Λ.

Given any $\tilde{Q} \in \Lambda$, the Lemma [3, 109] implies there exists a point $M \in f_\xi^{n_1}(\alpha)$ such that the forward orbit of M under f_ξ eventually enters $B_\varepsilon(\tilde{Q})$. Since $f_\xi^{-n_1}(M) \in B_\varepsilon(\tilde{P})$, this shows that f_ξ is transitive on Λ. Lastly, f_ξ exhibits sensitive dependence on Λ by the result of [15]. $\square$

Chapter 5

Robust chaos in the orientation-reversing and non-invertible settings.

5.1 Introduction

In Chapter 4 we proved that the attractor for f_ξ satisfies Devaney's definition of chaos for all $\xi \in \Phi_{\mathrm{BYG}}$, i.e, the attractor is transitive, has dense periodic orbits and has sensitive dependence on initial conditions. We have also shown that the chaotic attractor exists beyond Φ_{BYG}, outside $\mathcal{R}_1$.

In this chapter, we extend the construction of [58] to the orientation-reversing and non-invertible cases. We obtain a subset $\Phi_{\mathrm{trap}} \subset \Phi$ in which f_ξ has a trapping region and another subset $\Phi_{\mathrm{cone}} \subset \Phi$ in which f_ξ has an invariant expanding cone. It follows that f_ξ has a chaotic attractor for all $\xi \in \Phi_{\mathrm{trap}} \cap \Phi_{\mathrm{cone}}$. This is an open subset of parameter space, hence the chaos is robust with respect to the family f_ξ. We expect it is also robust to nonlinear perturbations to the pieces of the map, as described by Simpson and Glendinning [131].

Boundaries of $\Phi_{\mathrm{trap}} \cap \Phi_{\mathrm{cone}}$ are where some aspect of the construction fails. As shown below, three of these boundaries correspond to bifurcations where the chaotic attractor is destroyed. Beyond the other boundaries the chaotic attractor appears to persist and we believe robust chaos could be verified on a larger subset of parameter space by using a more complicated construction, e.g. [129], but our aim here is not to optimise the subset, only to obtain a reasonably large subset for both negative and positive values of δ_L and δ_R by using a construction that is both natural and simple.

The remainder of this chapter is organised as follows. We start in §5.2 by calculating the stable and unstable manifolds of the fixed points in the more general setting. Constraints on the geometry of the manifolds as they are extended outwards from the fixed points give rise to our definition of Φ_{trap}. Here we also define Φ_{cone} and state our main result (Theorem

5.1) for the existence of a chaotic attractor. Being four-dimensional the sets Φ_{trap} and Φ_{cone} are difficult to visualise; we show a range of two-dimensional cross-sections to give some impressions of their size and shape.

In §5.3 we use the stable manifold of one of the fixed points to form a region $\Omega \subset \mathbb{R}^2$ and show it is forward invariant under f_ξ for any $\xi \in \Phi_{\text{trap}}$. We then show how Ω can be perturbed into a trapping region for any $\xi \in \Phi_{\text{trap}}$. In §5.4 we identify a cone that is both invariant and expanding for any $\xi \in \Phi_{\text{cone}}$ and prove Theorem 5.1. In §5.5 we further study the extent to which Φ_{trap} and Φ_{cone} cover parameter space. We show a typical cross-section of $\Phi_{\text{trap}} \cap \Phi_{\text{cone}}$ and overlay numerical simulations whereby the presence of robust chaos is estimated from forward orbits. This helps clarify which boundaries of Φ_{trap} and Φ_{cone} correspond to bifurcations and how much of the true robust chaos region is detected by the straight-forward constructions.

5.2 Sufficient conditions for a chaotic attractor

Recall, for any $\xi \in \Phi$ the map f_ξ has saddle fixed points

$$X = \left(\frac{-1}{\tau_R - \delta_R - 1}, \frac{\delta_R}{\tau_R - \delta_R - 1} \right),$$
$$Y = \left(\frac{-1}{\tau_L - \delta_L - 1}, \frac{\delta_L}{\tau_L - \delta_L - 1} \right).$$

The stability multipliers of Y are $\lambda_L^s \in (-1, 1)$ and $\lambda_L^u > 1$, and the stability multipliers of X are $\lambda_R^s \in (-1, 1)$ and $\lambda_R^u < -1$.

5.2.1 The stable and unstable manifolds of the fixed points

As the stable and unstable manifolds of X and Y emanate from these points they do so on lines with directions given by the eigenvectors of A_L and A_R. We will use a subscript 0 to denote the part of each manifold that coincides with the line. These are indicated in Fig. 5.1 for four different combinations of the parameter values.

Next, we describe some points where the stable and unstable manifolds intersect $x = 0$ and $y = 0$ as these are central to our construction in §5.3. As given in Chapter 3, $W_0^s(Y)$ has an endpoint on $x = 0$, call it S. Since $W_0^s(Y)$ has slope $-\lambda_L^u$ from the above formula for Y we obtain

$$S = \left(0, \frac{-\lambda_L^u}{\lambda_L^u - 1} \right), \tag{5.1}$$

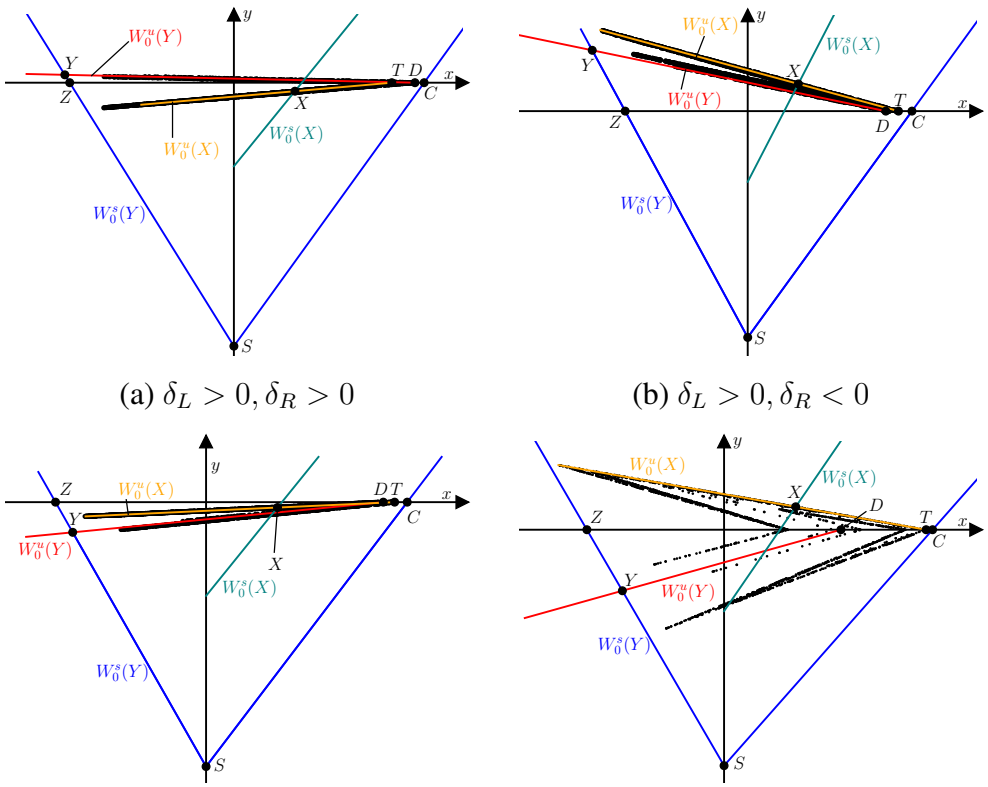

(a) $\delta_L > 0, \delta_R > 0$

(b) $\delta_L > 0, \delta_R < 0$

(c) $\delta_L < 0, \delta_R > 0$

(d) $\delta_L < 0, \delta_R < 0$

Figure 5.1: Phase portraits of f_ξ (2.21) for four different parameter combinations $\xi = (\tau_L, \delta_L, \tau_R, \delta_R) \in \Phi_{\text{trap}} \cap \Phi_{\text{cone}}$; (a) $\xi = (2.1, 0.06, -1.7, 0.18)$; (b) $\xi = (2.1, 0.4, -1.7, -0.55)$; (c) $\xi = (2.2, -0.3, -1.7, 0.1)$; (d) $\xi = (1.8, -0.75, -1.6, -0.4)$. Each plot shows the initial line segments of the stable and unstable manifolds emanating from the fixed points X and Y, as well as an additional segment of the stable manifold of Y. We also show some key points of intersection (S, C, D, T, and Z) of these segments with the coordinate axes, see (5.1), (5.4), (4.6), (3.19), and (5.16) respectively. Note that although point $f_\xi^{-2}(S)$ is relevant, we do not show it in this figure because it lies far away from the rest of the key intersection points. To illustrate the chaotic attractor the black dots show iterates of a typical forward orbit after transient dynamics has decayed.

where $S_2 < -1$. The manifold $W^s(Y)$ continues into the right half-plane but now with slope $\frac{\phi_1(\xi)}{\lambda_L^u}$, where

$$\phi_1(\xi) = \delta_R - \tau_R \lambda_L^u \,. \tag{5.2}$$

Our trapping region construction requires that this linear segment, call it $W_1^s(Y)$, intersects $y = 0$. Certainly this is only possible if $\phi_1(\xi) > 0$. This inequality turns out to be sufficient to ensure $W_1^s(Y)$ intersects $y = 0$ except in the case $\delta_L, \delta_R < 0$ (Fig. 5.1-d). In this case $W_1^s(Y)$ is the line segment connecting S and $f_\xi^{-2}(S)$. So in this case for $W_1^s(Y)$ to intersect $y = 0$ we need $f_\xi^{-2}(S)$ to lie above $y = 0$. A straightforward calculation reveals that the y-component of $f_\xi^{-2}(S)$ is $\frac{\phi_2(\xi)}{\lambda_L^s(\lambda_L^u - 1)\delta_R}$, where

$$\phi_2(\xi) = \delta_R(\lambda_L^s + 1) - \lambda_L^u(\tau_R + (\delta_R + \tau_R)\lambda_L^s). \tag{5.3}$$

Thus we require $\phi_2(\xi) > 0$ (because with $\delta_L, \delta_R < 0$ we have $\lambda_L^s(\lambda_L^u - 1)\delta_R > 0$). In any case, if $W_1^s(Y)$ intersects $y = 0$, it does so at the point

$$C = \left(1 + \frac{\phi_3(\xi)}{(\lambda_L^u - 1)\phi_1(\xi)}, 0\right), \tag{5.4}$$

where

$$\phi_3(\xi) = \delta_R - (\delta_R + \tau_R - (\tau_R + 1)\lambda_L^u)\lambda_L^u. \tag{5.5}$$

Our construction also requires $C_1 > 1$, that is $\phi_3(\xi) > 0$. Note that C_1 is the x-component of the point C.

Now we consider the two unstable manifolds. For all $\xi \in \Phi$, $W_0^u(Y)$ has an endpoint on $y = 0$ at D, see Eq. (4.6), and $W_0^u(X)$ has an endpoint on $y = 0$ at T, see Eq. (3.19). These points are indicated in Fig. 5.1.

5.2.2 Homoclinic and heteroclinic bifurcations

From the above formulas for C and D we obtain

$$C_1 - D_1 = \frac{\phi_4(\xi)}{(\lambda_L^u - 1)(1 - \lambda_L^s)\phi_1(\xi)}, \tag{5.6}$$

where

$$\phi_4(\xi) = \delta_R - (\tau_R + \delta_L + \delta_R - (1 + \tau_R)\lambda_L^u)\lambda_L^u. \tag{5.7}$$

The condition $\phi_4(\xi) > 0$ ensures that C lies to the right of D as in Fig. 5.1-a, and is equivalent to the condition $\phi(\xi) > 0$ of Chapter 3 that $f_\xi(D)$ lies to the right of $W_0^s(Y)$. Recall $\phi(\xi) = 0$ is a homoclinic corner where the attractor is usually destroyed.

In the orientation-reversing case ($\delta_L, \delta_R < 0$) a chaotic attractor can be destroyed when the points C and T collide. Here kinks of the unstable manifold of X lie on the stable manifold of Y (and vice-versa). We have

$$C_1 - T_1 = \frac{\phi_5(\xi)}{(\lambda_L^u - 1)(1 - \lambda_R^s)\phi_1(\xi)}, \tag{5.8}$$

where

$$\phi_5(\xi) = \delta_R - (\delta_R + \tau_R - (1 + \lambda_R^u)\lambda_L^u)\lambda_L^u. \tag{5.9}$$

The condition $\phi_5(\xi) > 0$ ensures that C lies to the right of T as in Fig. 5.1-d. In the special case of the Lozi map, $\phi_5(\xi) > 0$ simplifies (significantly) to equation (3) of Misiurewicz [99].

In view of the above discussion we define

$$\Phi_{\text{trap}} = \{\xi \in \Phi \mid \phi_i(\xi) > 0, i = 1, \ldots, 5\}. \tag{5.10}$$

Fig. 5.2 shows four different cross-sections of Φ_{trap} obtained by fixing τ_L and τ_R. Broadly speaking the size of the cross-section decreases as the values of τ_L and $|\tau_R|$ increase. Notice the topology of the cross-sections is different for different values of τ_L and τ_R. For instance in Fig. 5.2-a the boundary of the cross-section is formed by $\phi_1(\xi) = 0$, $\phi_2(\xi) = 0$, and the boundary of Φ, whereas in Fig. 5.2-d the boundary is formed by $\phi_1(\xi) = 0$, $\phi_3(\xi) = 0$, $\phi_4(\xi) = 0$, $\phi_5(\xi) = 0$, and the boundary of Φ. The figure also includes curves on which $f_\xi(C) = Y$ and $f_\xi(C) = Z$, where $Z = f_\xi(S)$ is the intersection of $W_0^s(Y)$ with $y = 0$. Together with the δ_L and δ_R axes, these curves divide the cross-sections into six parts corresponding to six cases for the vertices of the region Ω that we construct in §5.3.

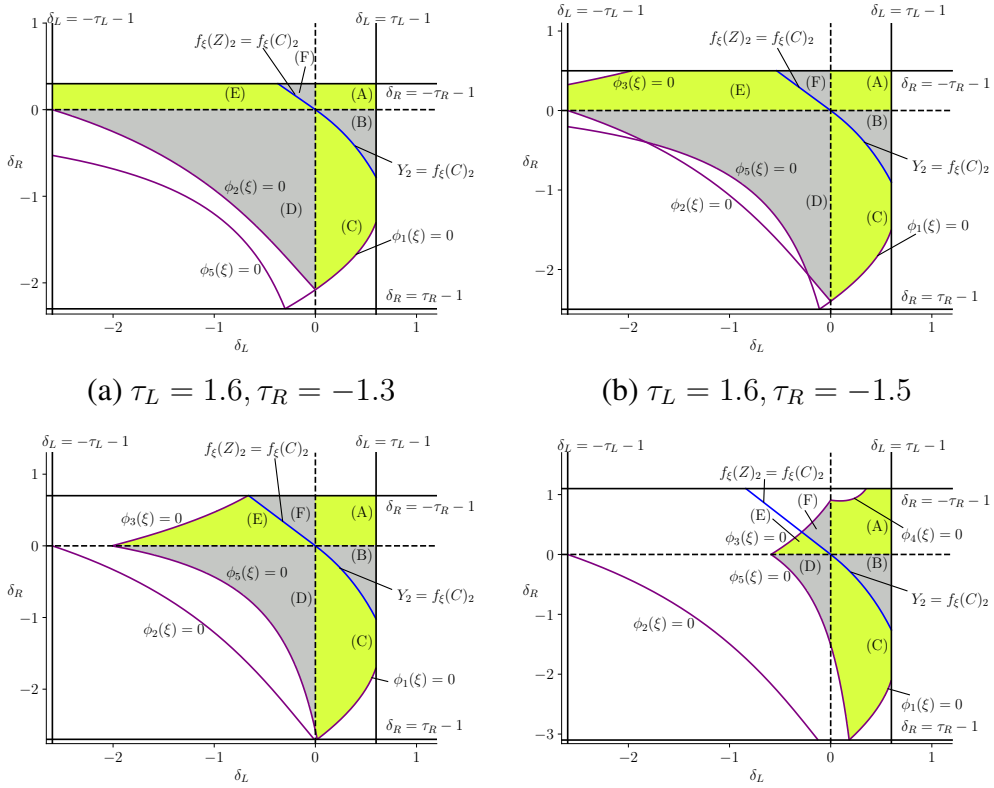

(a) $\tau_L = 1.6, \tau_R = -1.3$

(b) $\tau_L = 1.6, \tau_R = -1.5$

(c) $\tau_L = 1.6, \tau_R = -1.7$

(d) $\tau_L = 1.6, \tau_R = -2.1$

Figure 5.2: Four different two-dimensional cross sections of Φ_{trap}, defined by (5.10). In each plot the cross-section is divided into six parts (A)–(F) where Ω has certain vertices, see §5.3.

5.2.3 Sufficient conditions for robust chaos

Our construction of an invariant expanding cone Ψ_K requires similar constraints on the parameter values to those established above for the trapping region. To this end we define

$$\theta_1(\xi) = (\delta_L + \delta_R - \tau_L\tau_R)^2 - 4\delta_L\delta_R\,, \tag{5.11}$$

$$\theta_2(\xi) = \tau_L^2 + \delta_L^2 - 1 + 2\tau_L \min\Big(0, -\tfrac{\delta_R}{\tau_R}, q_L, \tilde{a}\Big), \tag{5.12}$$

$$\theta_3(\xi) = \tau_R^2 + \delta_R^2 - 1 + 2\tau_R \max\Big(0, -\tfrac{\delta_L}{\tau_L}, q_R, \tilde{b}\Big), \tag{5.13}$$

where

$$q_L = -\tfrac{\tau_L}{2}\Big(1 - \sqrt{1 - \tfrac{4\delta_L}{\tau_L^2}}\Big), \qquad q_R = -\tfrac{\tau_R}{2}\Big(1 - \sqrt{1 - \tfrac{4\delta_R}{\tau_R^2}}\Big),$$

and

$$\tilde{a} = \frac{\delta_L - \delta_R - \tau_L\tau_R - \sqrt{\theta_1(\xi)}}{2\tau_R}, \qquad \tilde{b} = \frac{\delta_R - \delta_L - \tau_L\tau_R - \sqrt{\theta_1(\xi)}}{2\tau_L},$$

assuming $\theta_1(\xi) > 0$. We then define

$$\Phi_{\text{cone}} = \{\xi \in \Phi \,|\, \theta_i(\xi) > 0, i = 1, \ldots, 3\}. \tag{5.14}$$

The condition $\theta_1(\xi) > 0$ ensures $\theta_2(\xi)$ and $\theta_3(\xi)$ are well-defined, and, as explained in §5.4, the conditions $\theta_2(\xi) > 0$ and $\theta_3(\xi) > 0$ ensure that our cone Ψ_K is invariant and expanding.

Fig. 5.3 shows cross-sections of Φ_{cone}. Broadly speaking the size of the cross-section *increases* as the values of τ_L and $|\tau_R|$ increase. Again the topology of the cross-sections is different for different values of τ_L and τ_R. Similar to Fig. 5.2 we have divided the cross-sections into six parts corresponding to six cases for the boundary of Ψ_K (see §5.4). These correspond to different cases for the four quantities in each of (5.12) and (5.13) that attain the minimum (respectively, maximum) value.

Finally, we can state our main result.

Theorem 5.1. *For any $\xi \in \Phi_{\text{trap}} \cap \Phi_{\text{cone}}$ the normal form f_ξ (2.21) has a topological attractor with a positive Lyapunov exponent.*

This is proved at the end of §5.4. We have found that there are many possibilities for the topology of cross-sections of $\Phi_{\text{trap}} \cap \Phi_{\text{cone}}$ defining by fixing τ_L and τ_R, and we do

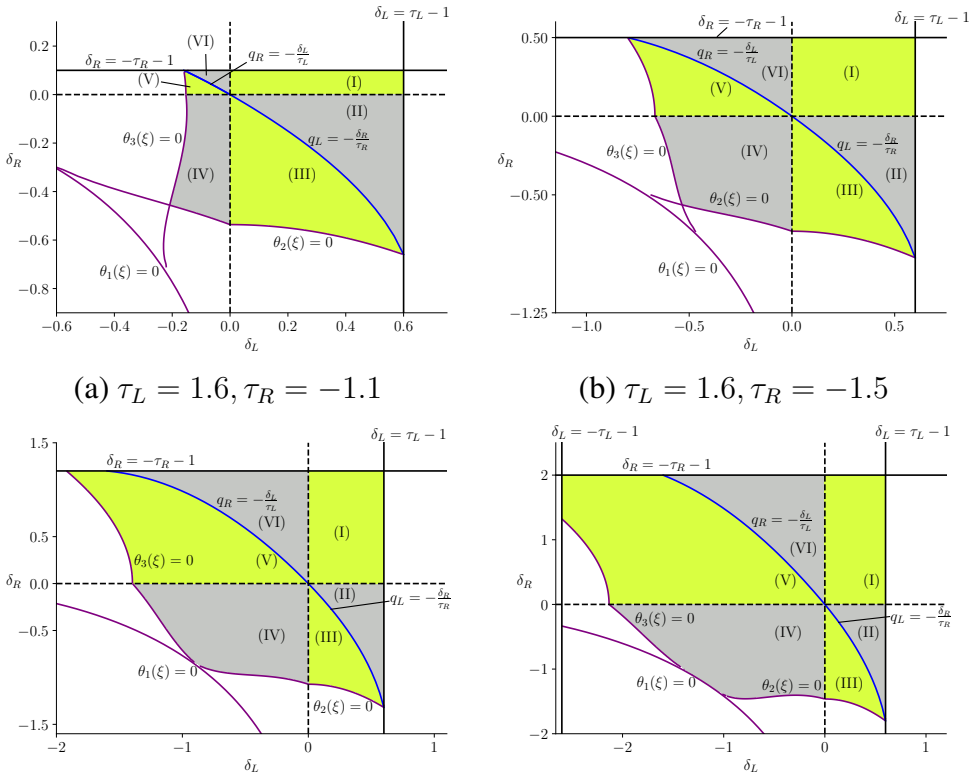

(a) $\tau_L = 1.6, \tau_R = -1.1$

(b) $\tau_L = 1.6, \tau_R = -1.5$

(c) $\tau_L = 1.6, \tau_R = -2.2$

(d) $\tau_L = 1.6, \tau_R = -3$

Figure 5.3: Two-dimensional cross-sections of Φ_{cone}, defined by (5.14). In each plot the cross-section has been divided into six parts (I)–(VI) where the cone Ψ_K has different boundaries, see Fig. 5.6.

not attempt to catagorise these, although in §5.5 we identify critical values of τ_L and τ_R at which the cross-sections of Φ_{trap} and Φ_{cone} vanish entirely.

5.3 A forward invariant region and a trapping region

In this section we construct a triangle Ω and show that for any $\xi \in \Phi_{\text{trap}}$ this region is forward invariant under f (Proposition 5.1). We then show there exists a perturbation of Ω that is a trapping region for f (Proposition 5.2). It is important to stress that the triangle Ω constructed here differs from the triangle constructed in Chapters 3 and 4 for the orientation-preserving case, and by Misiurewicz [99] for the orientation-reversing case, so that the non-invertible cases can be accommodated. For clarity we now suppress the ξ-dependency and write f instead of f_ξ.

The linear segment of the stable manifold of Y that contains Y, denoted $W_0^s(Y)$, was shown in Fig. 5.1 for four different combinations of the parameter values. In any case, this segment lies on the line $y = -\lambda_L^u x + S_2$, where S_2 is the y-component of S, given by (5.1). The point S is the right-most point of $W_0^s(Y)$, and is easy to see that in the other direction $W_0^s(Y)$ extends to infinity if $\delta_L \geq 0$ and to the preimage of S under the left piece of f otherwise:

Lemma 5.1. *Suppose $\delta_L \in \mathbb{R}$ and $\tau_L > |\delta_L + 1|$. Then*

$$W_0^s(Y) = \begin{cases} \left\{(x,y) \,\middle|\, -\frac{S_2}{\delta_L} \leq x \leq 0, y = -\lambda_L^u x + S_2\right\}, & \delta_L < 0, \\ \{(x,y) \,|\, -\infty < x \leq 0, y = -\lambda_L^u x + S_2\}, & \delta_L \geq 0, \end{cases} \tag{5.15}$$

and $f(W_0^s(Y)) \subset W_0^s(Y)$.

In particular $Z = f(S) \in W_0^s(Y)$. This point is the intersection of $W_0^s(Y)$ with $y = 0$ and given by

$$Z = \left(\frac{-1}{\lambda_L^u - 1}, 0\right). \tag{5.16}$$

Now recall if $\phi_1(\xi) > 0$ and $\phi_2(\xi) > 0$ then $C \in W_1^s(Y)$ is given by (5.4).

Lemma 5.2. *Let $\xi \in \Phi$ with $\phi_1(\xi) > 0$ and $\phi_2(\xi) > 0$. Then*

$$Y, Z, f(Z), f(C), f^2(C) \in W_0^s(Y) \setminus \{S\}. \tag{5.17}$$

Proof. Certainly $Y, Z \in W_0^s(Y)\setminus\{S\}$ by construction. Also $f(Z) \in W_0^s(Y)\setminus\{S\}$ because $W_0^s(Y)$ is forward invariant (Lemma 5.1) and $Z = f(S)$ cannot be a preimage of S.

Since $C_1 > 0$ we have $f(C) = (\tau_R C_1 + 1, -\delta_R C_1)$, and it is a simple exercise to use the formula (4.6) to show that $f(C)$ lies on the line $y = -\lambda_L^u x + S_2$. Also $f(C)$ lies to the left of S because $f(C)_1 = \frac{(\tau_R+\delta_R)(\lambda_L^u-1)+\tau_R}{(\lambda_L^u-1)\phi_1(\xi)}$ is negative by inspection, and in the case $\delta_L < 0$ the point $f(C)$ lies to the right of the left-most point of $W_0^s(Y)$ because $f(C)_1 + \frac{S_2}{\delta_L} = \frac{\phi_2(\xi)}{-\lambda_L^s(\lambda_L^u-1)\phi_1(\xi)}$ is positive. Thus $f(C)$ belongs to $W_0^s(Y)$ and is not an endpoint of $W_0^s(Y)$, thus $f(C) \in W_0^s(Y) \setminus \{S\}$ and $f^2(C) \in W_0^s(Y) \setminus \{S\}$ using again Lemma 5.1. □

Given $\xi \in \Phi$ with $\phi_1(\xi) > 0$ and $\phi_2(\xi) > 0$, let Q and R be the upper-most and lower-most points of $\{Y, Z, f(Z), f(C), f^2(C)\}$, respectively. Then let Ω be the compact filled triangle with vertices C, Q, and R (except Ω is a line segment in the special case $\delta_L = \delta_R = 0$). In other words, Ω is the convex hull of Y, Z, $f(Z)$, $f(C)$, $f^2(C)$, and C.

There are six cases for the points that form the vertices of Ω. These are shown in Fig. 5.4 and correspond to the six parts of Φ_{trap} indicated in Fig. 5.2. Fig. 5.4 also shows the set $f(\Omega)$. Notice in each case $f(\Omega)$ has vertices at the images of the points P and V where the boundary of Ω intersects $x = 0$.

Proposition 5.1. *Let $\xi \in \Phi_{\text{trap}}$. Then $f(\Omega) \subset \Omega$.*

Proof. The proof is long so we break it into three steps.

Step 1 — Characterise $f(\Omega)$.

The vertices Q and R lie in the left half-plane, while C lies in the right half-plane. Let P denote the intersection of $\overline{QC}$ (the line segment from Q to C) with $x = 0$, and V denote the intersection of $\overline{RC}$ with $x = 0$, see Fig. 5.4. From the formula (5.4) for C, the y-components of these points are given in terms of Q and R by

$$P_2 = \frac{{\lambda_L^u}^3 Q_2}{{\lambda_L^u}^3 + [\lambda_L^u - Q_2(1-\lambda_L^u)]\phi_1(\xi)}, \tag{5.18}$$

$$V_2 = \frac{{\lambda_L^u}^3 R_2}{{\lambda_L^u}^3 + [\lambda_L^u - R_2(1-\lambda_L^u)]\phi_1(\xi)}. \tag{5.19}$$

So Ω is the union of the quadrilateral Ω_L in the left half-plane with vertices P, Q, R, and V, and the triangle Ω_R in the right half-plane with vertices C, P, and V. Thus $f(\Omega) = f(\Omega_L) \cup f(\Omega_R)$, where $f(\Omega_L)$ and $f(\Omega_R)$ are polygons because each piece of f is affine. Thus since Ω is convex, to prove $f(\Omega) \subset \Omega$ it suffices to show that the vertices of $f(\Omega_L)$ and $f(\Omega_R)$ belong to Ω. These vertices are the points $f(C)$, $f(P)$, $f(Q)$, $f(R)$, and $f(V)$.

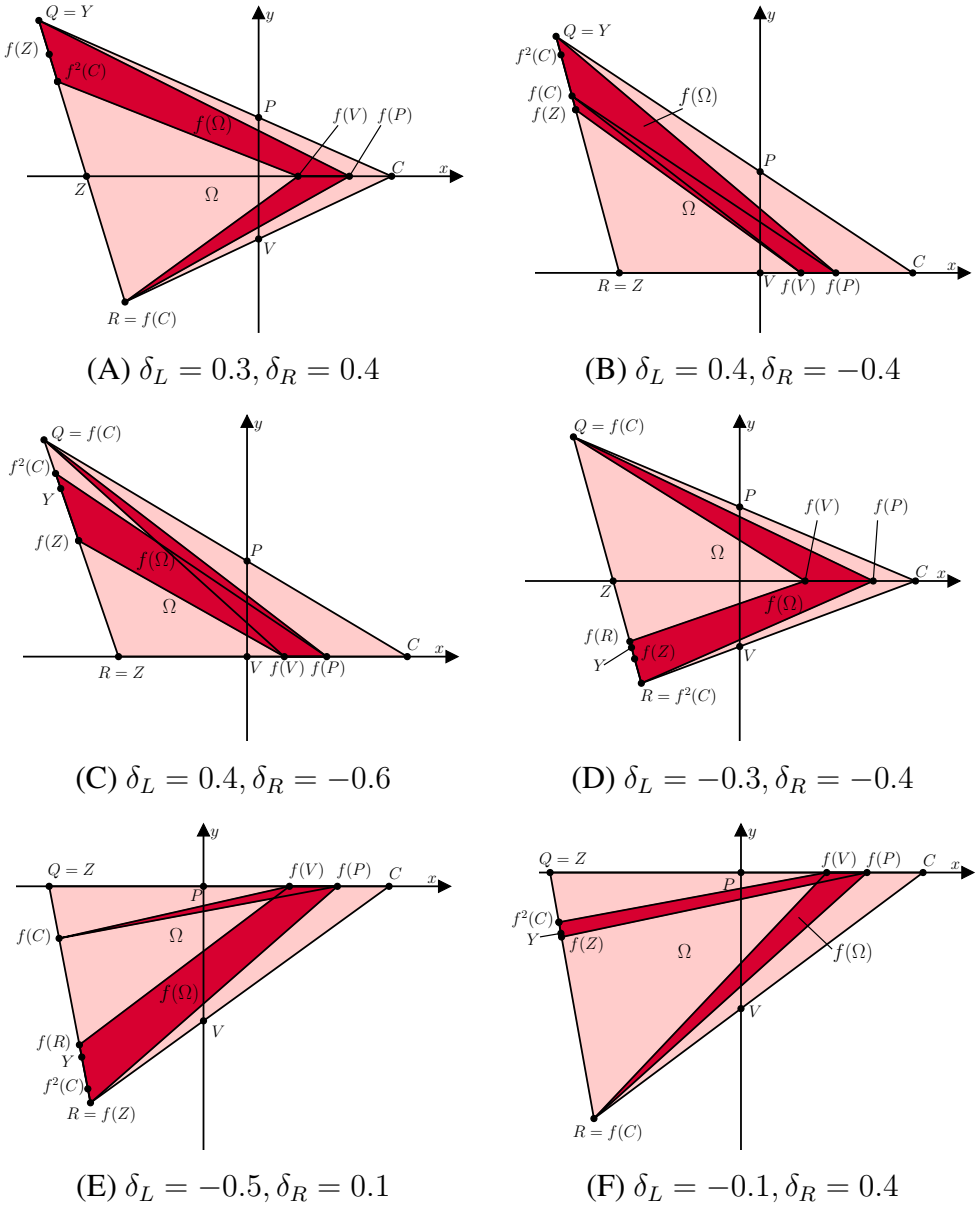

(A) $\delta_L = 0.3, \delta_R = 0.4$ (B) $\delta_L = 0.4, \delta_R = -0.4$

(C) $\delta_L = 0.4, \delta_R = -0.6$ (D) $\delta_L = -0.3, \delta_R = -0.4$

(E) $\delta_L = -0.5, \delta_R = 0.1$ (F) $\delta_L = -0.1, \delta_R = 0.4$

Figure 5.4: The triangle Ω and its image under f with $\tau_L = 1.6$, $\tau_R = -1.5$, and six different values of δ_L and δ_R. These correspond to parts (A)–(F) of Fig. 5.2-b for different cases for the two vertices of Ω in the left half-plane, denoted Q and R (the third vertex is always C). In each case $f(\Omega) \subset \Omega$ by Proposition 5.1 because the parameter combinations belong to Ω_{trap}.

Step 2 — Show C, Q, and R map to Ω.

Certainly $f(C) \in \Omega$ by the definition of Ω. We now show $f(Q), f(R) \in \overline{QR}$ (the left edge of Ω). If $\delta_L > 0$ then $\lambda_L^s > 0$, so $f(Q) \in \overline{QY}$ and $f(R) \in \overline{RY}$ so certainly $f(Q), f(R) \in \overline{QR}$. Also if $\delta_L = 0$, then $f(Q) = f(R) = Y = Z \in \overline{QR}$. Finally if $\delta_L < 0$, then $f(Q)$ and $f(R)$ lie below $y = 0$, so lie below Z, and hence below Q. In this case Q is either $f(C)$ or Z (because Y, $f(Z)$, and $f^2(C)$ lie below $y = 0$), thus $f(Q)$ lies on or above R, by the definition of R. Also $\lambda_L^s < 0$, thus $f(R)$ lies above $f(Q)$, and hence above R. Thus in any case $f(Q), f(R) \in \overline{QR}$.

Step 3 — Show P and V map to Ω.

The points $f(P)$ and $f(V)$ lie on $y = 0$, specifically

$$f(P) = \begin{bmatrix} P_2 + 1 \\ 0 \end{bmatrix}, \qquad f(V) = \begin{bmatrix} V_2 + 1 \\ 0 \end{bmatrix}, \tag{5.20}$$

where P_2 and V_2 are given by (5.18) and (5.19). Also V lies above S, thus $f(V)$ lies to the right of $Z = f(S)$. Hence it remains for us to show that $f(P)$ lies at or to the left of C, that is $C_1 - (P_2 + 1) \geq 0$. To do this we consider the various possibilities for Q in turn. There are three cases: Q is either Y, Z, or $f(C)$. This is because $f(Z)$ cannot lie above Y, while $f^2(C)$ cannot lie above Y if $\delta_L > 0$ and cannot lie above Z if $\delta_L \leq 0$.

Case 1: With $Q = Z$ we have $P_2 = 0$. Thus $C_1 - (P_2 + 1) > 0 = C_1 - 1 > 0$ because $\phi_3(\xi) > 0$.

Case 2: With $Q = Y$, by substituting Y_2, given by (2.27), in place of Q_2 in (5.18) we obtain

$$C_1 - (P_2 + 1) = \left(1 + \frac{\lambda_L^s {\lambda_L^u}^2}{{\lambda_L^u}^2(1 - \lambda_L^s) + \phi_1(\xi)}\right) \frac{\phi_4(\xi)}{\phi_1(\xi)(\lambda_L^u - 1)}.$$

This case requires $\delta_L \geq 0$, thus $\lambda_L^s \geq 0$. Also $C_1 - (P_2 + 1) > 0$ because $\phi_1(\xi) > 0$ and $\phi_4(\xi) > 0$.

Case 3: With $Q = f(C)$ we similarly obtain

$$C_1 - (P_2 + 1) = \left(1 + \frac{\lambda_R^s {\lambda_L^u}^2}{\lambda_L^u(\lambda_L^u - \delta_R)\phi_1(\xi)}\right) \frac{\phi_5(\xi)}{\phi_1(\xi)(\lambda_L^u - 1)}.$$

This case requires $\delta_R \leq 0$ (so that $f(C)_2 \geq 0$), thus $\lambda_R^s \geq 0$. Also $\phi_1(\xi) > 0$ and $\phi_5(\xi) > 0$, thus $C_1 - (P_2 + 1) > 0$. □

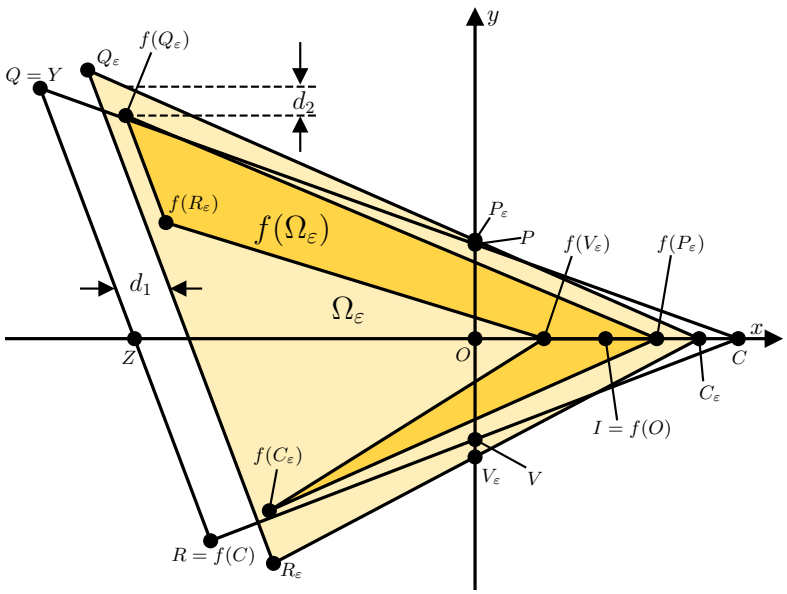

Figure 5.5: The trapping region Ω_ε and its image under f. This figure was produced using $\xi = \{1.6, 0.3, -1.5, 0.4\}$, as in Fig. 5.4-A, and $\varepsilon = 0.3$ which is small enough that $f(\Omega_\varepsilon) \subset \text{int}(\Omega_\varepsilon)$ in accordance with Proposition 5.2.

Proposition 5.2. *Let $\xi \in \Phi_{\text{trap}}$. Given $\varepsilon > 0$ define*

$$\begin{aligned} C_\varepsilon &= C - (\varepsilon, 0), \\ Q_\varepsilon &= Q + \varepsilon^2(C - R), \\ R_\varepsilon &= R + \varepsilon^2(C - Q), \end{aligned}$$

and let Ω_ε be the compact filled triangle with vertices C_ε, Q_ε, and R_ε. Then $f(\Omega_\varepsilon) \subset \text{int}(\Omega_\varepsilon)$, for all sufficiently small $\varepsilon > 0$.

The triangle Ω_ε is shown in Fig. 5.5 for one combination of parameter values. It has been defined so that its left edge lies to the right of $W_0^s(Y)$ and is parallel to $W_0^s(Y)$. Due to the saddle nature of Y, this edge shifts further to the right when iterated under f. Also the left edge is an order ε^2 distance from $W_0^s(Y)$ to ensure $f(C_\varepsilon)$ lies to the right of the image of this edge.

Proof. **Step 1** — Characterise $f(\Omega_\varepsilon)$.
Assume $\varepsilon > 0$ is sufficiently small that Q_ε and R_ε lie to the left of $x = 0$ and C_ε lies to the right of $x = 0$. Then the line segment $\overline{C_\varepsilon Q_\varepsilon}$ intersects $x = 0$ at a unique point P_ε, as does $\overline{C_\varepsilon R_\varepsilon}$ at a point V_ε. Similar to the previous proof, it remains for us to show that C_ε, P_ε, Q_ε,

R_ε, and V_ε map to the interior of Ω_ε.

Step 2 — Show C_ε maps to the interior of Ω_ε.
Let $O = (0,0)$ denote the origin and $I = (1,0)$ be its image under f. Also let $\ell = \overline{CO}$. This line segment maps under the right piece of f to the line segment from $f(C_\varepsilon)$ to I. Since $C_\varepsilon \in \ell$ is an order ε distance from C, its image $f(C_\varepsilon) \in f(\ell)$ is an order ε distance from $f(C)$, which belongs to $\overline{QR}$. Since $\overline{Q_\varepsilon R_\varepsilon}$ is an order ε^2 distance from $\overline{QR}$, $f(C_\varepsilon)$ must lie to the right of $\overline{Q_\varepsilon R_\varepsilon}$ for sufficiently small $\varepsilon > 0$.

Also, $f(\ell)$ lies inside the triangle QRI. Since C_ε lies to the right of I (because $\phi_3(\xi) > 0$ and assuming ε is sufficiently small), this triangle lies below $\overline{Q_\varepsilon C_\varepsilon}$ and above $\overline{R_\varepsilon C_\varepsilon}$. Thus $f(C_\varepsilon)$ lies below $\overline{Q_\varepsilon C_\varepsilon}$ and above $\overline{R_\varepsilon C_\varepsilon}$. Thus $f(C_\varepsilon)$ lies inside all three edges of Ω_ε, hence $f(C_\varepsilon) \in \mathrm{int}(\Omega_\varepsilon)$.

Step 3 — Show P_ε and V_ε map to the interior of Ω_ε.
Let A be any point on $\overline{CZ}$ with $A \neq C, Z$. Then there exists sufficiently small $\varepsilon > 0$ such that $A \in \mathrm{int}(\Omega_\varepsilon)$. We know $f(P)$ and $f(V)$ are located on $\overline{CZ} \setminus \{C, Z\}$, because by construction $Z_1 \leq f(V)_1 < f(P)_1 < C_1$, so belong to $\mathrm{int}(\Omega_\varepsilon)$ for sufficiently small $\varepsilon > 0$. The same is true for $f(P_\varepsilon)$ and $f(V_\varepsilon)$ because $P_\varepsilon \to P$ and $V_\varepsilon \to V$ as $\varepsilon \to 0$.

Step 4 — Show Q_ε and R_ε map to the interior of Ω_ε.
For brevity we just show $f(Q_\varepsilon) \in \mathrm{int}(\Omega_\varepsilon)$ ($f(R_\varepsilon) \in \mathrm{int}(\Omega_\varepsilon)$ can be shown similarly). Let $d_1 > 0$ be the distance that $\overline{Q_\varepsilon R_\varepsilon}$ lies to the right of $\overline{QR}$, see Fig. 5.5. Then $f(Q_\varepsilon)$ lies a distance $\lambda_L^u d_1$ to the right of $\overline{QR}$, as Y is a saddle fixed point with stable direction $\overline{QR}$ and unstable eigenvalue λ_L^u. Since $\lambda_L^u > 1$, the point $f(Q_\varepsilon)$ lies to the right of the line $\overline{Q_\varepsilon R_\varepsilon}$.

If $Q \neq Y$, then $f(Q)$ lies an order 1 distance below $\overline{CQ}$, thus $f(Q_\varepsilon)$ lies below $\overline{C_\varepsilon Q_\varepsilon}$ for sufficiently small $\varepsilon > 0$. Now consider the case $Q = Y$. As shown in Fig. 5.5 let d_2 be the vertical displacement from $f(Q_\varepsilon)$ upwards to the line $\overline{Q_\varepsilon C_\varepsilon}$ (we will show $d_2 > 0$). By direct calculations $d_2 = \beta\varepsilon^2 + O(\varepsilon^3)$ where

$$\beta = \delta_L(C_1 - R_1)(C_1 + (\tau_L - 2)Y_1) - R_2(C_1 + (\delta_L - 1)Y_1).$$

Let $p = C_1 - D_1$ and notice $p > 0$ by (5.6) because $\phi_4(\xi) > 0$. Using also $D_1 = (1 - \lambda_L^u)Y_1$ by (2.27) and (4.6), we obtain

$$\beta = \delta_L(C_1 - R_1)(p - Y_1(1 - \lambda_L^s)) - R_2(p - Y_1\lambda_L^u(1 - \lambda_L^s)),$$

which is positive by inspection (e.g. $Y_1 < 0$). This shows that $d_2 > 0$ for sufficiently small values of ε, that is $f(Q_\varepsilon)$ lies below the upper edge of Ω_ε. By similar calculations one can show that $f(Q_\varepsilon)$ lies above the lower edge of Ω_ε, and therefore $f(Q_\varepsilon) \in \mathrm{int}(\Omega_\varepsilon)$. □

5.4 Invariant expanding cones

We consider cones of the form

$$\Psi_K = \left\{ \alpha \begin{bmatrix} 1 \\ m \end{bmatrix} \,\middle|\, \alpha \in \mathbb{R}, m \in K \right\}, \tag{5.21}$$

where K is an interval. Since $v \mapsto Av$ is a linear map, to verify invariance and expansion of a cone Ψ_K, it suffices to verify properties (i) and (ii) of Definition 4.2 for vectors of the form $v = \begin{bmatrix} 1 \\ m \end{bmatrix}$:

Lemma 5.3. *If $Av \in \Psi_K$ for all $v = \begin{bmatrix} 1 \\ m \end{bmatrix}$ with $m \in K$, then Ψ_K is invariant under A. If there exists $c > 1$ such that $\|Av\| \geq c\|v\|$ for all $v = \begin{bmatrix} 1 \\ m \end{bmatrix}$ with $m \in K$, then Ψ_K is expanding under A.*

Now we focus on the Jacobian matrices

$$A_J = \begin{bmatrix} \tau_J & 1 \\ -\delta_J & 0 \end{bmatrix},$$

where $J \in \{L, R\}$, of the normal form (2.21). The slope of $v = \begin{bmatrix} 1 \\ m \end{bmatrix}$ is m and the slope of $A_J v$ is

$$G_J(m) = -\frac{\delta_J}{\tau_J + m}, \tag{5.22}$$

assuming $m \neq -\tau_J$. Notice

$$\frac{dG_J(m)}{dm} = \frac{\delta_J}{(\tau_J + m)^2}, \tag{5.23}$$

thus $G_J(m)$ is increasing if $\delta_J > 0$, decreasing if $\delta_J < 0$, and flat if $\delta_J = 0$. In any case, $G_J(m)$ is monotone and so in order to verify invariance under A_J it suffices to consider the endpoints of K:

Lemma 5.4. *Let $\tau_J, \delta_J \in \mathbb{R}$ and $K = [a, b]$ be an interval with $-\tau_J \notin K$. If $a \leq G_J(a) \leq b$ and $a \leq G_J(b) \leq b$ then Ψ_K is invariant under A_J.*

Proof. Since $-\tau_J \notin K$, by (5.22) and (5.23) $G_J(m)$ is continuous and monotone on K. Thus for any $m \in K$, $G_J(m)$ is equal to or lies between the values $G_J(a)$ and $G_J(b)$. Thus $a \leq G_J(m) \leq b$. That is, the slope of $A_J \begin{bmatrix} 1 \\ m \end{bmatrix}$ belongs to K, thus $A_J \begin{bmatrix} 1 \\ m \end{bmatrix} \in \Psi_K$. Hence Ψ_K is invariant under A_J by Lemma 5.3. □

Next we introduce the function

$$H_J(m) = \left\| A_J \begin{bmatrix} 1 \\ m \end{bmatrix} \right\|^2 - \left\| \begin{bmatrix} 1 \\ m \end{bmatrix} \right\|^2 = \tau_J^2 + \delta_J^2 - 1 + 2\tau_J m. \tag{5.24}$$

It is easy to show that if $H_J(m) > 0$ for all m in a compact interval K, then Ψ_K is expanding under A_J. Since $H_J(m)$ is a linear function of m it again suffices to consider the endpoints of K:

Lemma 5.5. *Let $\tau_J, \delta_J \in \mathbb{R}$ and $K = [a, b]$ be an interval. If $H_J(a) > 0$ and $H_J(b) > 0$ then Ψ_K is expanding under A_J.*

Proof. Let $h = \min[H_J(a), H_J(b)] > 0$. By (5.24), $H_J(m) \geq h$ for all $m \in K$. Then for any $m \in K$ the vector $v = \begin{bmatrix} 1 \\ m \end{bmatrix}$ satisfies

$$\|A_J v\|^2 = H_J(m) + \|v\|^2 \geq h + \|v\|^2 = \left(\tfrac{h}{\|v\|^2} + 1\right)\|v\|^2 \geq \left(\frac{h}{n} + 1\right)\|v\|^2,$$

where $n = \max_{m \in K}(1 + m^2)$. Thus Ψ_K is expanding under A_J (with expansion factor $c = \sqrt{\frac{h}{n} + 1} > 1$) by Lemma 5.3. □

To prove chaos in (2.21) we need to choose $K = [a, b]$ so that Ψ_K is invariant under A_L and A_R. This favours the interval K being relatively large. However, we want K to be as small as possible in order to maximise the parameter region over which it is expanding under A_L and A_R. This balancing act motivates the following calculations that form the basis of our definition of K given below in Proposition 5.3.

For each $J \in \{L, R\}$, the fixed point equation $G_J(m) = m$ is quadratic in m. If $\delta_J \neq 0$ and $\delta_J < \frac{\tau_J^2}{4}$, then G_J has exactly two fixed points

$$q_J = -\frac{\tau_J}{2}\left(1 - \sqrt{1 - \frac{4\delta_J}{\tau_J^2}}\right), \qquad r_J = -\frac{\tau_J}{2}\left(1 + \sqrt{1 - \frac{4\delta_J}{\tau_J^2}}\right). \tag{5.25}$$

In order for Ψ_K to be invariant under A_L and A_R, we define K so that it contains q_L and

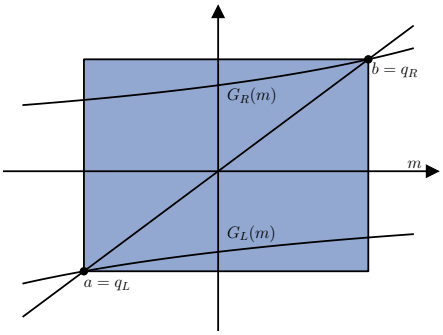

(I) $\delta_L = 0.4$, $\delta_R = 0.4$.

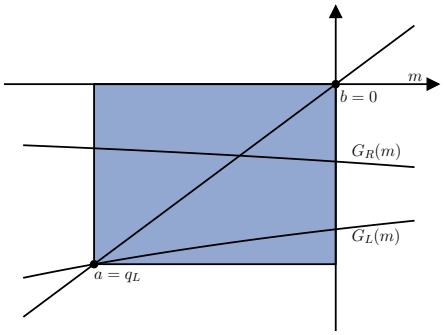

(II) $\delta_L = 0.4$, $\delta_R = -0.2$.

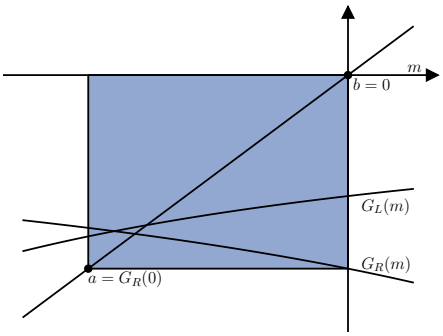

(III) $\delta_L = 0.4$, $\delta_R = -0.6$.

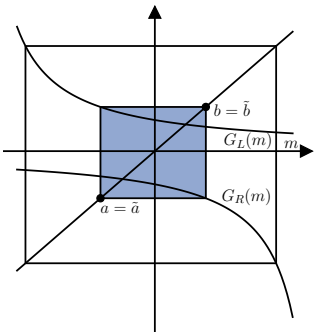

(IV) $\delta_L = -0.5$, $\delta_R = -0.5$.

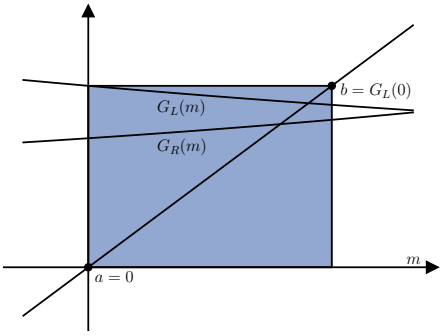

(V) $\delta_L = -0.3$, $\delta_R = 0.2$.

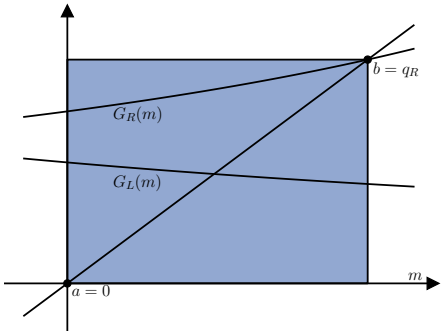

(VI) $\delta_L = -0.3$, $\delta_R = 0.4$.

Figure 5.6: Cobweb diagrams of the slope maps $G_L(m)$ and $G_R(m)$ (5.22) with $\tau_L = 1.6$, $\tau_R = -1.5$, and six different values of δ_L and δ_R. These correspond to parts (I)–(VI) of Fig. 5.3-b. In each case $K = [a, b]$, defined by (5.30) and (5.31), is forward invariant under G_L and G_R as shown. This implies Ψ_K is invariant under A_L and A_R (see Lemma 5.4). In each case K contains the fixed points q_L and q_R; in case (IV) K is defined using one of the two period-two solutions.

q_R, see Fig. 5.6. So the smallest interval we consider is $K = [q_L, q_R]$. In the orientation-preserving case ($\delta_L, \delta_R > 0$), this interval indeed gives invariance, as shown by Glendinning and Simpson [58]. In the orientation-reversing case ($\delta_L, \delta_R < 0$), invariance requires that K contains a period-two solution. The equation $(G_R \circ G_L)(m) = m$ is quadratic in m with discriminant

$$\theta_1(\xi) = (\delta_L + \delta_R - \tau_L\tau_R)^2 - 4\delta_L\delta_R\,,$$

repeating (5.11). So if $\theta_1(\xi) > 0$ there are two period-two solutions, Fig. 5.6-(IV). Of these the inner-most solution is $\{\tilde{a}, \tilde{b}\}$, where

$$\tilde{a} = \frac{\delta_L - \delta_R - \tau_L\tau_R - \sqrt{\theta_1(\xi)}}{2\tau_R}, \qquad \tilde{b} = \frac{\delta_R - \delta_L - \tau_L\tau_R - \sqrt{\theta_1(\xi)}}{2\tau_L}, \tag{5.26}$$

satisfying $G_L(\tilde{a}) = \tilde{b}$ and $G_R(\tilde{b}) = \tilde{a}$. So in this case the smallest interval we can take is $K = [\tilde{a}, \tilde{b}]$, as used by Misiurewicz [99].

In the non-invertible cases the slope maps G_L and G_R are either both non-negative or both non-positive, see again Fig. 5.6. Thus a simple and effective choice for one endpoint of K is $m = 0$. In this case the smallest interval leading to invariance uses also one of q_L, q_R, or the image of $m = 0$ under G_L or G_R:

$$G_L(0) = -\frac{\delta_L}{\tau_L}, \qquad G_R(0) = -\frac{\delta_R}{\tau_R}. \tag{5.27}$$

Proposition 5.3 shows that all cases can be accommodated by simply defining a and b as the minimum and maximum of all points suggested above. Recall Φ_{cone} was defined in §5.2 as the set of all $\xi \in \Phi$ for which $\theta_1(\xi)$, $\theta_2(\xi)$, and $\theta_3(\xi)$ are positive. The condition $\theta_1(\xi) > 0$ ensures $\tilde{a}$ and $\tilde{b}$ are well-defined, while, if a and b are given by (5.30) and (5.31),

$$\theta_2(\xi) = \tau_L^2 + \delta_L^2 - 1 + 2\tau_L a = H_L(a), \tag{5.28}$$

$$\theta_3(\xi) = \tau_R^2 + \delta_R^2 - 1 + 2\tau_R b = H_R(b), \tag{5.29}$$

and $\theta_2(\xi) > 0$ and $\theta_3(\xi) > 0$ ensure Ψ_K is invariant and expanding.

Proposition 5.3. *Let $\xi \in \Phi_{\text{cone}}$ and $K = [a, b]$ where*

$$a = \min\Big[0, -\tfrac{\delta_R}{\tau_R}, q_L, \tilde{a}\Big], \tag{5.30}$$

$$b = \max\Big[0, -\tfrac{\delta_L}{\tau_L}, q_R, \tilde{b}\Big]. \tag{5.31}$$

Then Ψ_K is invariant and expanding under A_L and A_R.

To prove Proposition 5.3 we first establish three lemmas. The first of these provides bounds on the other fixed points, r_L and r_R, of G_L and G_R.

Lemma 5.6. *Let $\xi \in \Phi$. Then $r_L < \frac{1-\delta_L^2-\tau_L^2}{2\tau_L}$ and $r_R > \frac{1-\delta_R^2-\tau_R^2}{2\tau_R}$.*

Proof. We have $\delta_L + 1 < \tau_L$, hence $(\delta_L+1)^2 < \tau_L^2$, and so $(\delta_L-1)^2 < \tau_L^2 - 4\delta_L$. By multiplying the last two inequalities together we obtain $(\delta_L^2-1)^2 < \tau_L^2(\tau_L^2-4\delta_L)$, so $\delta_L^2 - 1 < \tau_L\sqrt{\tau_L^2-4\delta_L}$ which rearranges to $r_L < \frac{1-\delta_L^2-\tau_L^2}{2\tau_L}$ using (5.25). The result for r_R follows similarly. □

Lemma 5.7. *With the assumptions of Proposition 5.3, $a = \tilde{a}$ if and only if $\delta_L \le 0$ and $\delta_R \le 0$; similarly $b = \tilde{b}$ if and only if $\delta_L \le 0$ and $\delta_R \le 0$.*

Proof. First suppose $\delta_L \le 0$ and $\delta_R \le 0$. Then $\tau_L\tau_R\delta_L \ge 0$ (also $\theta_1(\xi) > 0$ by assumption), so we can use (5.26) to obtain

$$2\tau_R(\tilde{a}+\tau_L) = -\sqrt{\theta_1(\xi)} - \sqrt{\theta_1(\xi) + 4\tau_L\tau_R\delta_L} < 0.$$

Thus $\tilde{a} > -\tau_L$ (because $\tau_R < 0$). Also $\tilde{b} < -\tau_R$ by a similar argument.

Notice $\delta_L \le 0$ implies $G_L(m) \ge 0$ for all $m > -\tau_L$, so $q_L \ge 0$, $G_L(0) = -\frac{\delta_L}{\tau_L} \ge 0$, and $G_L(\tilde{a}) = \tilde{b} \ge 0$. Similarly $G_R(m) \le 0$ for all $m < -\tau_R$, so $q_R \le 0$, $G_R(0) = -\frac{\delta_R}{\tau_R} \le 0$, and $G_R(\tilde{b}) = \tilde{a} \le 0$. Also $G_L(m)$ is non-increasing, so $\tilde{a} \le 0$ implies $G_L(\tilde{a}) \ge G_L(0)$. Thus $\tilde{b} \ge -\frac{\delta_L}{\tau_L} \ge 0 \ge q_R$, so $b = \tilde{b}$. Similarly $\tilde{a} \le -\frac{\delta_R}{\tau_R} \le 0 \le q_L$, so $a = \tilde{a}$.

Conversely suppose $a = \tilde{a}$. Then $\tilde{a} = G_R(\tilde{b}) \le 0$, so $\delta_R \le 0$. Thus $G_R(m)$ is non-increasing, so $\tilde{a} = G_R(\tilde{b}) \le G_R(0)$ implies $\tilde{b} \ge 0$. Thus $\tilde{b} = G_L(\tilde{a}) \ge 0$, so $\delta_L \le 0$, as required (also $b = \tilde{b}$ implies $\delta_L \le 0$ and $\delta_R \le 0$ in a similar fashion). □

Lemma 5.8. *With the assumptions of Proposition 5.3, $-\tau_L < a$ and $b < -\tau_R$.*

Proof. For brevity we just show $-\tau_L < a$ ($b < -\tau_R$ can be shown similarly). Using $\theta_2(\xi) > 0$ and Lemma 5.6 we obtain

$$a > \frac{1-\delta_L^2-\tau_L^2}{2\tau_L} > r_L\,. \tag{5.32}$$

Thus if $\delta_L \ge 0$ then

$$r_L + \tau_L = \frac{\tau_L}{2}\left(1 - \sqrt{1 - \frac{4\delta_L}{\tau_L^2}}\right) \ge 0,$$

and so $a > -\tau_L$. Now suppose $\delta_L < 0$. If $\delta_R \geq 0$ then $a = 0 > -\tau_L$, while if $\delta_R < 0$ then $a = \tilde{a}$ (by Lemma 5.7) and $-\tau_L < \tilde{a}$ as shown in the proof of Lemma 5.7. □

Proof of Proposition 5.3. We first show $G_L(a) \geq a$ and $G_L(b) \geq a$. If $\delta_L \leq 0$ then $G_L(m) \geq 0$ for all $m \in K$ (using Lemma 5.8), so certainly $G_L(a) \geq a$ and $G_L(b) \geq a$. Now suppose $\delta_L > 0$. In this case $G_L(m) \geq m$ for all $r_L \leq m \leq q_L$ (i.e. at and between the fixed points of G_L). Observe $r_L < a \leq q_L$ by (5.32) and the definition of a, thus $G_L(a) \geq a$. Also $G_L(m)$ is increasing thus $G_L(b) > G_L(a) \geq a$.

Next we show $G_L(a) \leq b$ and $G_L(b) \leq b$. If $\delta_L \geq 0$ then we have $G_L(m) \leq 0$ for all $m \in K$ (using Lemma 5.8), so certainly $G_L(a) \leq b$ and $G_L(b) \leq b$. Now suppose $\delta_L < 0$. If $\delta_R \leq 0$ then Lemma 5.7 implies $a = \tilde{a}$ and $b = \tilde{b} = G_L(\tilde{a})$, so $b = G_L(a)$, if $\delta_R > 0$ then $a = 0$ and $b \geq G_L(0)$, so $b \geq G_L(a)$. Also $G_L(m)$ is decreasing thus $G_L(b) < G_L(a) \leq b$.

Now from Lemma 5.4 we can conclude that Φ_K is invariant under A_L. Invariance under A_R can be proved in a similar fashion.

Next we prove expansion. By (5.28), $\theta_2(\xi) > 0$ implies $H_L(a) > 0$. Also

$$H_L(b) = \tau_L^2 + \delta_L^2 - 1 + 2\tau_L b = H_L(a) + 2\tau_L(b - a) \tag{5.33}$$

is positive because $\tau_L > 0$ and $b \geq a$. Thus Ψ_K is expanding for A_L by Lemma 5.5. By a similar argument Ψ_K is also expanding for A_R. □

Proof of Theorem 5.1. Choose any $\xi \in \Phi_{\text{trap}} \cap \Phi_{\text{cone}}$. By Proposition 5.2 there exists a trapping region Ω_ε for f. Then $\bigcap_{n\geq 0} f^n(\Omega_\varepsilon)$ is an attracting set and contains a topological attractor Λ. By Proposition 5.3 there exists a non-empty cone Ψ_K that is invariant and expanding for both A_L and A_R with some expansion factor $c > 1$.

Choose any $z \in \Lambda$ and let $v \in \Psi_K$ be non-zero. The Lyapunov exponent $\lambda(z, v)$ for z in the direction v is the limiting rate of separation of the forward orbits of z and $z + \Delta v$ for arbitrarily small $\Delta > 0$ [141]. If the forward orbit of z does not intersect the switching manifold then the derivative of the n^{th} iterate of z under f is well-defined for all $n \geq 1$ and

$$\lambda(z, v) = \limsup_{n\to\infty} \frac{1}{n} \ln(\|\mathrm{D}f^n(x)v\|). \tag{5.34}$$

Observe

$$\mathrm{D}f^n(x) = \mathrm{D}f\big(f^{n-1}(x)\big) \cdots \mathrm{D}f(f(x))\mathrm{D}f(x),$$

where each of the n matrices on the right-hand side is either A_L or A_R. By the invariance and expansion of Ψ_K, $\|\mathrm{D}f^n(x)v\| \geq c^n\|v\|$ for all n, so $\lambda(z, v) \geq \ln(c) > 0$. If instead the

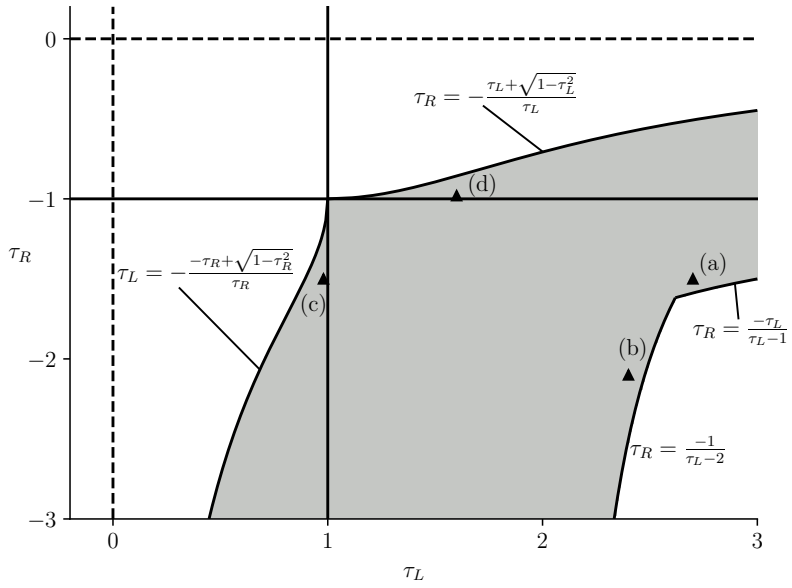

Figure 5.7: The shaded region shows where cross-sections of Φ_{trap} and Φ_{cone}, defined by fixing the values of τ_L and τ_R, are both non-empty. As we exit the shaded region through the lower-right boundaries the cross-section of Φ_{trap} vanishes; as we exit through the upper and left boundaries the cross-section of Φ_{cone} vanishes.

forward orbit of z intersects the switching manifold, $\lambda(z, v)$ can similarly be evaluated and bounded using one-sided directional derivatives because f is piecewise-linear, see [129] for details. □

5.5 Further remarks on the parameter regions Φ_{trap} and Φ_{cone}•

In §5.2 we described two-dimensional cross-sections of Φ_{trap} and Φ_{cone} defined by fixing the values of $\tau_L > 0$ and $\tau_R < 0$. For the most part larger values of τ_L and $|\tau_R|$ yield smaller cross-sections of Φ_{trap} and larger cross-sections of Φ_{cone}, see Fig. 5.2 and Fig. 5.3. This is because with larger values of τ_L and $|\tau_R|$ the map is more strongly expanding, hence less amenable for the existence of a trapping region but more amenable for the existence of an invariant expanding cone.

Fig. 5.7 shows critical curves in the (τ_L, τ_R)-plane where the cross-sections vanish entirely. To explain this figure we treat the critical curves one by one. First consider (τ_L, τ_R) at a point just above the critical curve $\tau_R = \frac{-\tau_L}{\tau_L-1}$. Here the Φ_{trap} cross-section has three vertices, $P^{(1)}$, $P^{(2)}$, and $P^{(3)}$, as shown in Fig. 5.8-a. It is a simple exercise to show

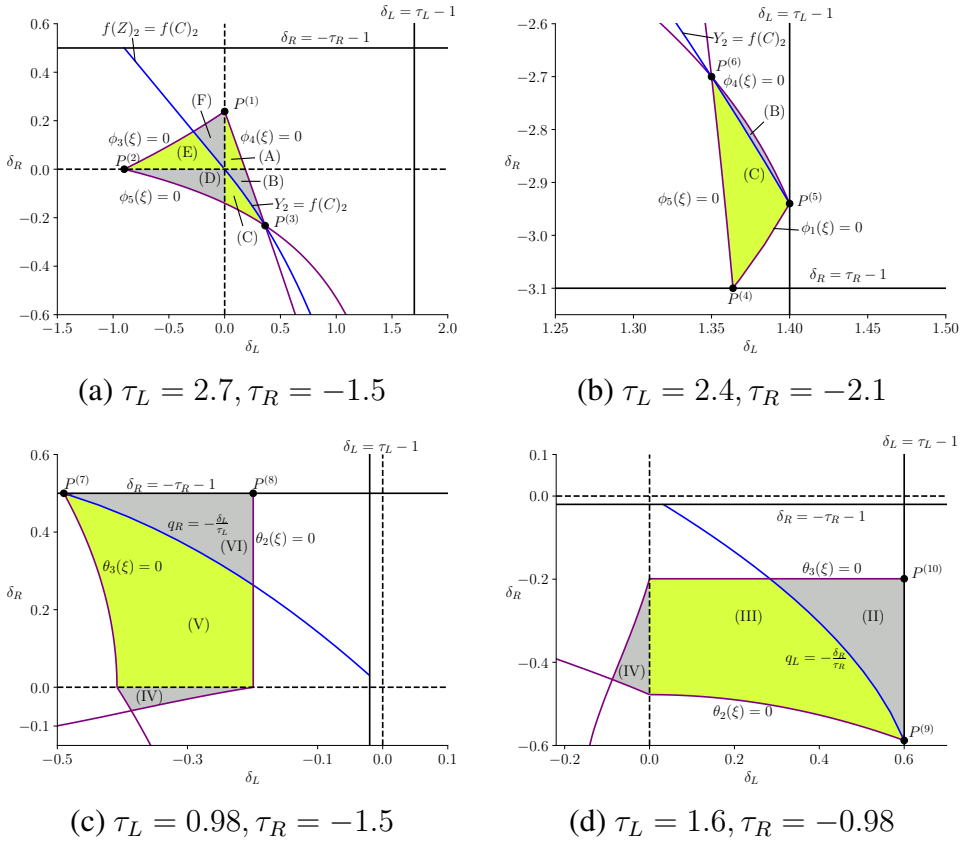

(a) $\tau_L = 2.7, \tau_R = -1.5$ (b) $\tau_L = 2.4, \tau_R = -2.1$

(c) $\tau_L = 0.98, \tau_R = -1.5$ (d) $\tau_L = 1.6, \tau_R = -0.98$

Figure 5.8: Further sample cross-sections of Φ_{trap} (panels (a) and (b)) and Φ_{cone} (panels (c) and (d)). These use the parameter points (τ_L, τ_R) shown in Fig. 5.7.

that as parameters are varied each vertex reaches the origin $(\delta_L, \delta_R) = (0, 0)$ on the critical curve. For instance the upper vertex is where $\phi_3(\xi) = 0$ and $\phi_4(\xi) = 0$ intersect at $P^{(1)} = \left(0, \frac{(\tau_R - (\tau_R+1)\tau_L)\tau_L}{1-\tau_L}\right)$ and solving $P_2^{(1)} = 0$ gives $\tau_R = \frac{-\tau_L}{\tau_L - 1}$. Thus here the Φ_{trap} cross-section contracts to a point and vanishes.

With instead (τ_L, τ_R) at a point just to the left of $\tau_R = \frac{-1}{\tau_L - 2}$, the Φ_{trap} cross-section has three vertices at different points $P^{(4)}$, $P^{(5)}$, and $P^{(6)}$, as shown in Fig. 5.8-b. Explicit calculations reveal that each vertex reaches the corner $(\delta_L, \delta_R) = (\tau_L + 1, \tau_R - 1)$ when $\tau_R = \frac{-1}{\tau_R - 2}$. For instance, $P^{(4)} = \left(\frac{(\tau_L\tau_R - \tau_R + 1)(\tau_R - 1)}{\tau_R^2}, \tau_R - 1\right)$, and solving $P_1^{(4)} = \tau_L + 1$ gives $\tau_R = \frac{-1}{\tau_R - 2}$. Thus here the Φ_{trap} cross-section again vanishes.

With τ_L just less than 1 and $\tau_R < -1$ the Φ_{cone} cross-section appears as in Fig. 5.8-c. As parameters are varied the Φ_{cone} cross-section vanishes when the vertices $P^{(7)} = \big(\tau_L(\tau_R+1), -(\tau_R+1)\big)$ and $P^{(8)} = \big(-\sqrt{1-\tau_L^2}, -(\tau_R+1)\big)$ coincide. Solving $P_1^{(7)} = P_1^{(8)}$ yields the critical curve $\tau_R = -\frac{\tau_L + \sqrt{1-\tau_L^2}}{\tau_L}$ of Fig. 5.7. Similarly with $\tau_L > 1$ and τ_R just

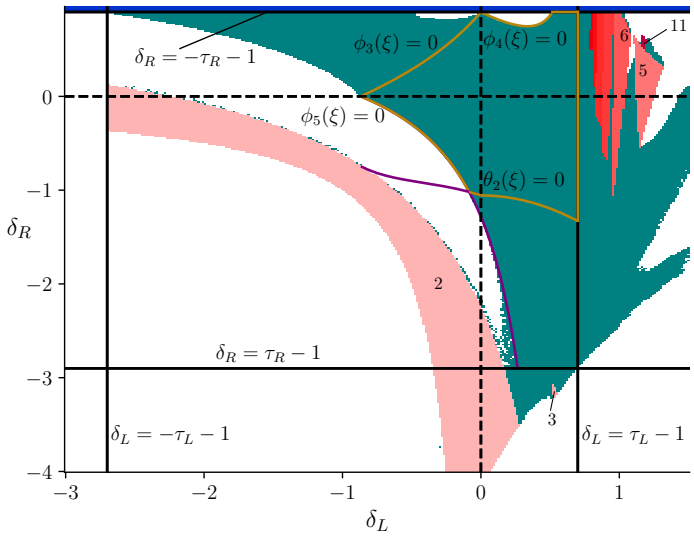

Figure 5.9: A two-parameter bifurcation diagram of (1) with $\tau_L = 1.7$ and $\tau_R = -1.9$. The boundary of $\Phi_{\text{trap}} \cap \Phi_{\text{cone}}$ is shown in yellow. The curves $\phi_5(\xi) = 0$ and $\theta_2(\xi) = 0$ are illustrated in purple. The coloured regions show the result of a numerical simulation (white: no attractor; green: chaotic attractor; other colours: periodic attractor). Some periods are indicated (e.g. in the large pink region the map has a stable period-2 solution. In the blue strip at the top the fixed point X is stable.

greater than -1 the Φ_{cone} cross-section appears as in Fig. 5.8-d. The cross-section vanishes when $P^{(9)}$ and $P^{(10)}$ coincide on $\tau_L = -\frac{-\tau_R + \sqrt{1-\tau_R^2}}{\tau_R}$.

The geometry and topology of cross-sections of $\Phi_{\text{trap}} \cap \Phi_{\text{cone}}$ admit many possibilities and a complete analysis is beyond the scope of this chapter. Here we examine one example, Fig. 5.9. The cross-section of $\Phi_{\text{trap}} \cap \Phi_{\text{cone}}$ is bounded by the following curves (going anticlockwise): $\delta_L = \tau_L - 1$, $\delta_R = -\tau_R - 1$, $\phi_4(\xi) = 0$, $\phi_3(\xi) = 0$, $\phi_5(\xi) = 0$, and $\theta_2(\xi) = 0$ (which has a kink at $\delta_L = 0$). The first two of these curves are boundaries of our overall parameter region Φ, the next three curves are boundaries of Φ_{trap}, and the last curve is a boundary of Φ_{cone}.

Fig. 5.9 also shows the result of a simple numerical simulation to investigate the nature of the attractor. For each point in a 300×300 equispaced grid of (δ_L, δ_R) values, we computed 10^7 iterates of the forward orbit using a random initial condition. Green points are where an estimate of the maximal Lyapunov exponent was positive, white points are where the orbit appeared to diverge (its norm exceeded 10^4), and other points are where there exists a stable periodic solution (determined by solving for periodic solutions exactly).

Note the numerical simulation gives an imperfect picture. For example, we believe no attractor exists immediately to the left of the heteroclinic bifurcation $\phi_5(\xi) = 0$, yet some green points are present here (with small $\delta_L > 0$ and $-3 < \delta_R < -2$) because orbits often experience a long transient before diverging and 10^7 iterations are insufficient to detect this.

Nevertheless, the numerics effectively highlights the fact that three of the boundaries of $\Phi_{\text{trap}} \cap \Phi_{\text{cone}}$ are bifurcations where the chaotic attractor is destroyed, so these boundaries cannot be improved upon. As we cross $\delta_R = -\tau_R - 1$ the fixed point X becomes stable, $\phi_4(\xi) = 0$ is a homoclinic bifurcation where the attractor is destroyed [14], and $\phi_5(\xi) = 0$ is a heteroclinic bifurcation where the attractor is destroyed. Elsewhere the attractor is destroyed in a variety of other global bifurcations. Above $\phi_3(\xi) = 0$ and to the right of $\delta_L = \tau_L - 1$ the trapping region construction of §5.3 fails. An alternate construction that partially deals with this is described by Simpson [129]. Below $\theta_2(\xi) = 0$ the cone Ψ_K of §5.4 fails to be expanding. For some parameter combinations below $\theta_2(\xi) = 0$ it is possible to construct an invariant expanding cone, and hence verify the presence of chaos, by using an induced map [59]. In the next chapter we study how renormalisation could be used to explain some of the bifurcation structure within the robust chaos regions identified here.

Chapter 6

Renormalisation in the orientation-reversing and non-invertible settings.

6.1 Introduction

In Chapter 3 we used renormalisation to identify an infinite sequence of bifurcations where the number of connected components of a chaotic attractor changes. However, this was only achieved for parameter values for which the map is orientation-preserving. The purpose of this chapter to treat the orientation-reversing and non-invertible scenarios. Again we use renormalisation to find bifurcations, but now this approach misses some bifurcations. For this reason we combine the analytical framework with brute-force numerical simulations that estimate the number of connected components from the behaviour of forward orbits.

This chapter is organised as follows. We start in §6.2 by briefly reminding the reader about the geometry of the stable and unstable manifolds of the fixed points X and Y. In §6.3 we reintroduce the renormalisation scheme and describe some basic aspects of this scheme that hold for all values of δ_L and δ_R. Then in §6.4 we summarise the results of Chapter 3 for the orientation-preserving setting.

Next in §6.5 we describe an algorithm for numerically determining the number of connected components of attractor. The algorithm outputs the greatest common divisor of a set of iteration numbers required for an orbit to return close to its starting point. The algorithm is effective when the components of attractor are not too close and the dynamics on the attractor is ergodic. Applied to the orientation-preserving setting it reproduces the bifurcation structure obtained by renormalisation.

In §6.6, §6.7, and §6.8 we study the orientation-reversing and non-invertible cases and explain why the same renormalisation scheme should be expected to work in these settings. Formal proofs are beyond the scope of this thesis because, as evident from Chapter 3, these

require a detailed analysis of the four-dimensional nonlinear renormalisation operator, plus will involve additional complexities because now stable period-two and period-four solutions are possible. Also if $\delta_L < 0$ and $\delta_R > 0$ the bifurcations that destroy the attractor are different and more difficult to characterise. In §6.9 we describe a special case unique to the non-invertible settings where the dynamics reduces to one dimension.

6.2 Two-dimensional piecewise-linear maps with two saddle fixed points

Throughout the parameter region Φ, (2.25), the map (2.21) has two saddle fixed points X and Y. Fig.6.1 shows these and parts of their stable and unstable manifolds in four phase portraits, one for each of the four cases for the signs of δ_L and δ_R. Notice if $\delta_L > 0$ (upper plots) the left half-plane maps to the upper half-plane, while if $\delta_L < 0$ (lower plots) the left half-plane maps to the lower half-plane. Similarly if $\delta_R > 0$ (left plots) the right half-plane maps to the lower half-plane, while if $\delta_R < 0$ (right plots) the right half-plane maps to the upper half-plane. Each plot indicates the important points T, D, and C, where some of the manifolds intersect $y = 0$.

6.3 Renormalisation in two dimensions

We first identify the subset of Φ where (2.21) has a stable LR-cycle. Generalising (2.17) we have that the matrix $A_L A_R$ (whose eigenvalues are the stability multipliers of the LR-cycle) has an eigenvalue -1 when $\alpha(\xi) = 0$, where

$$\alpha(\xi) = \tau_L \tau_R + (\delta_L - 1)(\delta_R - 1). \tag{6.1}$$

If $\alpha(\xi) > 0$ this eigenvalue is greater than -1. For the LR-cycle to be stable we also need $\det(A_L A_R) < 1$, where $\det(A_L A_R) = \delta_L \delta_R$, so we define

$$\mathcal{P}_2 = \{\xi \in \Phi \,|\, \delta_L \delta_R < 1,\ \alpha(\xi) > 0\}. \tag{6.2}$$

Proposition 6.1. *If $\xi \in \mathcal{P}_2$ then f_ξ has an asymptotically stable LR-cycle.*

Proof. Let $\tilde{\tau}_R = \tau_L \tau_R - \delta_L - \delta_R$ and $\tilde{\delta}_R = \delta_L \delta_R$ be the trace and determinant of $A_L A_R$. All eigenvalues of $A_L A_R$ have modulus less than 1 if and only if $\tilde{\delta}_R < 1$ and $-\tilde{\delta}_R - 1 <$

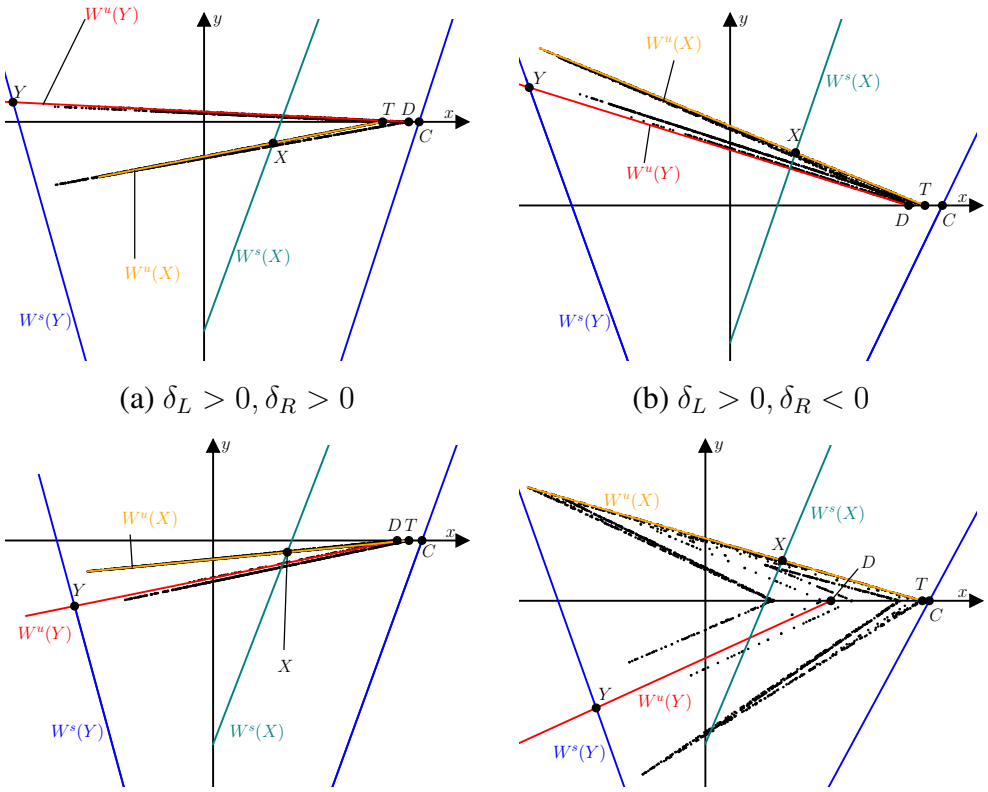

(a) $\delta_L > 0, \delta_R > 0$ (b) $\delta_L > 0, \delta_R < 0$

(c) $\delta_L < 0, \delta_R > 0$ (d) $\delta_L < 0, \delta_R < 0$

Figure 6.1: Phase portraits of the two-dimensional border-collision normal form (2.21) for four different parameter combinations: (a) $\xi = (2.1, 0.06, -1.7, 0.18)$; (b) $\xi = (2.1, 0.4, -1.7, -0.55)$; (c) $\xi = (2.2, -0.3, -1.7, 0.1)$; (d) $\xi = (1.8, -0.75, -1.6, -0.4)$. Each plot shows the linear segments of the stable and unstable manifolds emanating from the fixed points X and Y, as well as an adjoining segment of the stable manifold of Y. We also indicate some of their intersections with $y = 0$: T, D, and C; formulas for these are given by (3.19), (4.6), and (5.4). To illustrate the chaotic attractor the black dots show 2000 iterates of a typical forward orbit after transient dynamics has decayed.

$\tilde{\tau}_R < \tilde{\delta}_R + 1$. Certainly $\tilde{\delta}_R < 1$ by assumption, and $-\tilde{\delta}_R - 1 < \tilde{\tau}_R$ by the definition of α; also

$$\tilde{\tau}_R - \tilde{\delta}_R - 1 = \tau_L\tau_R - (\delta_L + 1)(\delta_R + 1) < -|(\delta_L + 1)(\delta_R + 1)| - (\delta_L + 1)(\delta_R + 1) \leq 0$$

by the definition of Φ.

The composed map $f_R \circ f_L$ is an affine map with unique fixed point

$$P = \frac{-1}{\tilde{\tau}_R - \tilde{\delta}_R - 1}\big(\tau_R + \delta_R + 1, -\delta_R(\tau_L + \delta_L + 1)\big).$$

Let

$$Q = f_L(P) = \frac{-1}{\tilde{\tau}_R - \tilde{\delta}_R - 1}\big(\tau_L + \delta_L + 1, -\delta_L(\tau_R + \delta_R + 1)\big).$$

Notice the first component of P is negative while the first component of Q is positive, thus $\{P, Q\}$ is a periodic solution of f_ξ. Above we showed all eigenvalues of A_LA_R have modulus less than 1, hence $\{P, Q\}$ is asymptotically stable. □

If $\alpha(\xi) < 0$ the LR-cycle is unstable. This is always the case if $\delta_L + \delta_R \geq 0$:

Proposition 6.2. *If $\xi \in \Phi$ with $\delta_L + \delta_R \geq 0$ then $\alpha(\xi) < 0$.*

Proof. Suppose $\xi \in \Phi$ with $\delta_L + \delta_R \geq 0$. If $\delta_L, \delta_R \geq -1$ then

$$\alpha(\xi) < -(\delta_L + 1)(\delta_R + 1) + (\delta_L - 1)(\delta_R - 1) = -2(\delta_L + \delta_R) \leq 0,$$

using the definition of Φ in the first inequality. If instead $\delta_L < -1$ or $\delta_R < -1$ then $\delta_L\delta_R < -1$ because $\delta_L + \delta_R > 0$, so

$$\alpha(\xi) < (\delta_L + 1)(\delta_R + 1) + (\delta_L - 1)(\delta_R - 1) = 2(\delta_L\delta_R + 1) < 0.$$

□

Now we show that if $\alpha(\xi) < 0$ then the renormalisation operator g produces another instance of (2.21) in Φ.

Proposition 6.3. *If $\xi \in \Phi$ and $\alpha(\xi) < 0$ then $g(\xi) \in \Phi$.*

Proof. Let $\tilde{\tau}_L = \tau_R^2 - 2\delta_R$, let $\tilde{\delta}_L = \delta_R^2$, and let $\tilde{\tau}_R$ and $\tilde{\delta}_R$ be as in the proof of Proposition 6.1; then $g(\xi) = \big(\tilde{\tau}_L, \tilde{\delta}_L, \tilde{\tau}_R, \tilde{\delta}_R\big)$. Observe $\tilde{\tau}_L - \tilde{\delta}_L - 1 = \tau_R^2 - (\delta_R + 1)^2 > 0$ because $\tau_R < -(\delta_R + 1)$, and $\tilde{\tau}_L + \tilde{\delta}_L + 1 = \tau_R^2 + (\delta_R + 1)^2 > 0$ because $\tau_R < 0$, thus $\tilde{\tau}_L > |\tilde{\delta}_L + 1|$.

Also $\tilde{\tau}_R - \tilde{\delta}_R - 1 = \tau_L\tau_R - (\delta_L + 1)(\delta_R + 1) < 0$ because $\tau_L > \delta_L + 1$ and $\tau_R < \delta_R + 1$, and $\tilde{\tau}_R + \tilde{\delta}_R + 1 = \alpha(\xi) < 0$, by assumption, thus $\tilde{\tau}_R < -|\tilde{\delta}_R + 1|$. □

As in Chapter 3, let

$$\Pi_\xi = \big\{ f_\xi^{-1}(x, y) \,\big|\, x \geq 0 \big\}, \tag{6.3}$$

be the set of all points that map to the right half-plane. On Π_ξ the second iterate f_ξ^2 has only two pieces:

$$f_\xi^2(x, y) = \begin{cases} (f_{R,\xi} \circ f_{L,\xi})(x, y), & x \leq 0, \\ f_{R,\xi}^2(x, y), & x \geq 0. \end{cases} \tag{6.4}$$

For any $\xi \in \Phi$ (6.4) is affinely conjugate to $f_{g(\xi)}$. Specifically $f_\xi^2 = h_\xi^{-1} \circ f_{g(\xi)} \circ h_\xi$ on Π_ξ, where h_ξ 3.21 is the necessary change of coordinates. As another orientation-preserving example, Fig. 6.2-a shows Π_ξ (in the phase space of f_ξ) at the parameter point

$$\xi_{\text{ex}}^{(1)} = (1.5, 0.4, -1.5, 0.4), \tag{6.5}$$

while Fig. 6.2-b shows $h_\xi(\Pi_\xi)$ (in the phase space of $f_{g(\xi)}$). The map $f_{g(\xi)}$ has an invariant set $\Lambda \subset h_\xi(\Pi_\xi)$, so by the results of Chapter 3 $h_\xi^{-1}(\Lambda) \subset \Pi_\xi$ is an invariant set of f_ξ^2. Moreover, the union of $h_\xi^{-1}(\Lambda)$ and its image under f_ξ is an invariant set of f_ξ. It is easy to infer the number of connected components in this set from the number of connected components of Λ. The following results formalises this in a way that incorporates the orientation-reversing and non-invertible settings.

Proposition 6.4. *Suppose $\Lambda \subset h_\xi(\Pi_\xi)$ is an invariant set of $f_{g(\xi)}$. Then $\tilde{\Lambda} = h_\xi^{-1}(\Lambda) \cup f_\xi\big(h_\xi^{-1}(\Lambda)\big)$ is an invariant set of f_ξ. Moreover, if $h_\xi^{-1}(\Lambda) \cap f_\xi\big(h_\xi^{-1}(\Lambda)\big) = \varnothing$ then the number of connected components of $\tilde{\Lambda}$ is twice the number of connected components of Λ.*

Proof. Let $S = h_\xi^{-1}(\Lambda)$. Since $S \subset \Pi_\xi$,

$$f_\xi^2(S) = h_\xi^{-1}\big(f_{g(\xi)}(h_\xi(S))\big). \tag{6.6}$$

But $h_\xi(S) = \Lambda$ and $f_{g(\xi)}(\Lambda) = \Lambda$, so the right-hand side of (6.6) is $h_\xi^{-1}(\Lambda) = S$. Thus S is invariant under f_ξ^2, so $S \cup f_\xi(S)$ is invariant under f_ξ. Since h_ξ is invertible the number of components of S is the same as the number of components of Λ. If $S \cap f_\xi(S) = \varnothing$ then $f_\xi(S)$ also has this many components (for otherwise $f_\xi^2(S) = S$ would not be possible because f_ξ is continuous). □

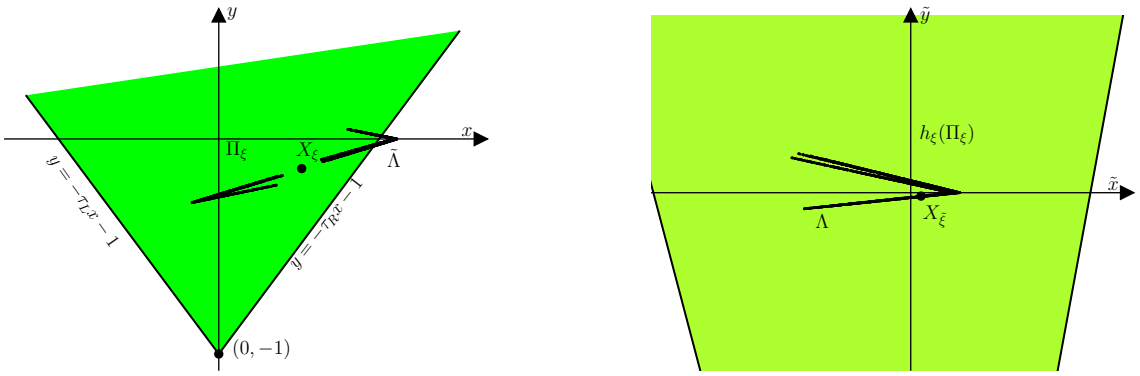

(a) $\xi = \xi_{\text{ex}}^{(1)} \in \mathcal{R}_1^{(1)}$ (b) $\xi = g\big(\xi_{\text{ex}}^{(1)}\big) \in \mathcal{R}_0^{(1)}$

Figure 6.2: Phase portraits of (2.21). Panel (a) uses the example parameter point $\xi_{\text{ex}}^{(1)}$ given by (6.5) where the attractor $\tilde{\Lambda}$ has two connected components, one of which lies entirely in Π_ξ (shaded). Panel (b) uses the parameter point $g\big(\xi_{\text{ex}}^{(1)}\big)$ where the attractor Λ has one connected component in $h_\xi(\Pi_\xi)$ (shaded).

6.4 The orientation-preserving case

Here we briefly summarise the results of Chapter 3 in a way that we attempt to mimic for the orientation-reversing and non-invertible settings. Let

$$\Phi^{(1)} = \{\xi \in \Phi \mid \delta_L > 0, \delta_R > 0\}, \tag{6.7}$$

be the subset of Φ for which (2.21) is orientation-preserving. In a large part of $\Phi^{(1)}$ an attractor is destroyed when the points C and D coincide, and straight-forward algebra gives

$$C_1 - D_1 = \frac{\phi^+(\xi)}{(\lambda_L^u - 1)(1 - \lambda_L^s)(\delta_R - \tau_R \lambda_L^u)}, \tag{6.8}$$

where

$$\phi^+(\xi) = \delta_R - (\tau_R + \delta_L + \delta_R - (1 + \tau_R)\lambda_L^u)\lambda_L^u. \tag{6.9}$$

Note, the function in (6.9) was denoted ϕ in Chapter 3; here we have embellished it with a plus to distinguish it from a similar function (given below) that arises in the orientation-reversing setting.

Fig. 6.3 shows an example. In panel (a) the closure of the unstable manifold of X,

$$\Lambda = \mathrm{cl}(W^u(X)), \tag{6.10}$$

is a chaotic attractor. As the value of τ_L is increased the attractor approaches the point D and is destroyed at $\tau_L \approx 1.9083$ when $\phi^+(\xi) = 0$, panel (b). At larger values of τ_L almost all forward orbits diverge, panel (c).

Repeating (3.9) (but now with superscript (1)), we define

$$\mathcal{R}_n^{(1)} = \left\{\xi \in \Phi^{(1)} \,\middle|\, \phi^+(g^n(\xi)) > 0,\ \phi^+(g^{n+1}(\xi)) \le 0\right\}, \tag{6.11}$$

for all $n \ge 0$. Notice that none of these regions contain points in the period-two region $\mathcal{P}_2$ because by Proposition 6.2, if $\xi \in \Phi^{(1)}$ then automatically $\alpha(\xi) < 0$. As shown in Chapter 3 the regions $\mathcal{R}_n^{(1)}$ are disjoint and cover the subset of $\Phi^{(1)}$ for which $\phi^+(\xi) > 0$. Fig. 6.4 shows two-dimensional slices of parameter space defined by fixing $\delta_L > 0$ and $\delta_R > 0$. The following results explain the nature of the attractor in $\mathcal{R}_0^{(1)}$ and repeat Theorem 3.2.

Theorem 6.1. *For any $\xi \in \mathcal{R}_0^{(1)}$,*

(i) Λ is bounded, connected, and invariant under f_ξ,

(ii) has a positive Lyapunov exponent, and

(iii) if $\delta_R < 1$ there exists a forward invariant set $\Delta \subset \mathbb{R}^2$ with non-empty interior such that

$$\bigcap_{n=0}^{\infty} f_\xi^n(\Delta) = \Lambda. \tag{6.12}$$

The next result is a special case of Lemma 3.8 that we will replicate below for the orientation-reversing and non-invertible settings.

Proposition 6.5. *If $\xi \in \mathcal{R}_n^{(1)}$ with $n \ge 1$, then $g(\xi) \in \mathcal{R}_{n-1}^{(1)}$.*

So if $\xi \in \mathcal{R}_n^{(1)}$ then $g^n(\xi) \in \mathcal{R}_0^{(1)}$ where the attractor is connected. Then by n applications of Proposition 6.4, f_ξ has an attractor with 2^n connected components as long as the assumptions of Proposition 6.4 are satisfied in each application. Theorem 3.3 shows that this is indeed the case. This result can be expressed briefly as follows.

Theorem 6.2. *For any $\xi \in \mathcal{R}_n^{(1)}$ with $n \ge 0$, f_ξ has a chaotic Milnor attractor with exactly 2^n connected components.*

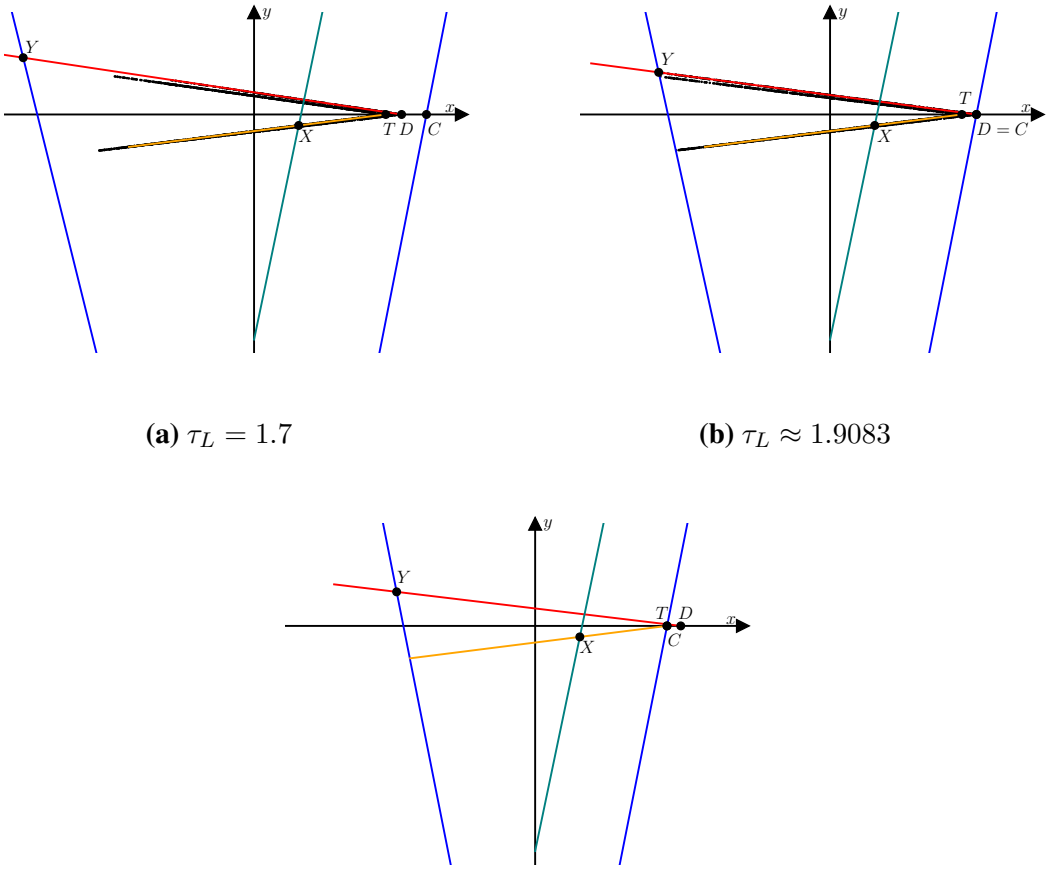

(a) $\tau_L = 1.7$

(b) $\tau_L \approx 1.9083$

(c) $\tau_L = 2.1$

Figure 6.3: Phase portraits of (2.21) with $\delta_L = 0.1$, $\delta_R = 0.1$, $\tau_R = -2$ and three different values of τ_L. These parameter values correspond to the black triangles in Fig. 6.4-a. Panel (b) uses τ_L such that $\phi^+(\xi) = 0$ to ten decimal places. In (a) $\mathrm{cl}(W^u(X))$ is a chaotic attractor; in (b) $W^s(Y)$ and $W^u(Y)$ form a homoclinic corner by intersecting at $D = C$; in (c) there is no attractor. The coloured lines illustrate the stable and the unstable manifolds of the fixed points coloured following the scheme in Fig. 6.1.

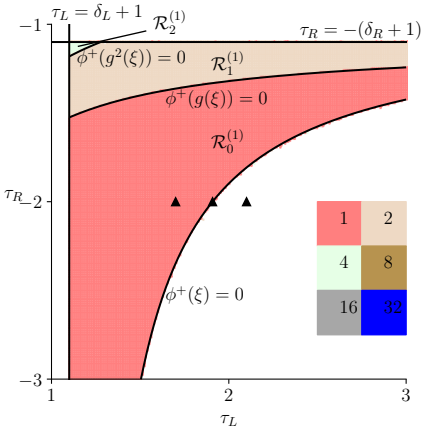

(a) $\delta_L = 0.1, \delta_R = 0.1$.

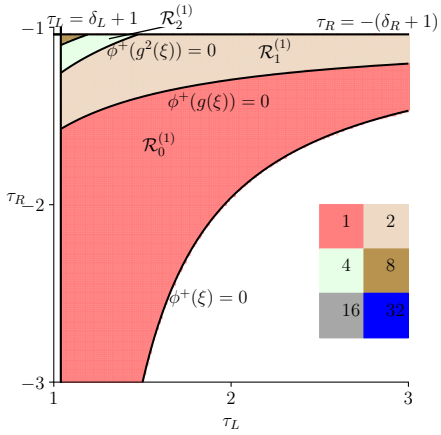

(b) $\delta_L = 0.04, \delta_R = 0.04$.

Figure 6.4: Two-dimensional slices of the orientation-preserving parameter region $\Phi^{(1)}$ showing the curves $\phi(g^n(\xi)) = 0$, for low values of n, overlaid upon the numerical results of Eckstein's greatest common divisor algorithm, explained in §6.5. Each point in a 200×200 grid is coloured by the greatest common divisor of a set of close return iteration numbers J according to the colour bar on the right. Also points are coloured white if iterates appeared to diverge. The values $\varepsilon = 0.001$ and $M = 10^6$ where used in the algorithm. The black triangles correspond to the parameter values of Fig. 6.3.

6.5 A component counting algorithm.

To support an extension of the theoretical results of §6.4 to the orientation-reversing and non-invertible settings, we perform numerical simulations to count the number of connected components of the attractors. There are many methods for estimating the number of connected components of a set Ψ from a finite collection F of points in Ψ. For example Robins *et al.* [116] connect all pairs of points in F with line segments to form a complete graph, then base their estimation from a minimal spanning tree. In our setting Ψ is generated by a map, so it is more effective to use a method that utilises the dynamics. For this reason we compute the number of components as the greatest common divisor of a certain set of computed values. This method originates with Eckstein [44] and is described by Avrutin *et al.* [7]. As explained at the end of this section, the effectiveness of the method relies on the following result.

Lemma 6.1. *Suppose a compact invariant set Ψ of a continuous map f has $k \geq 2$ connected components, and f has an orbit that visits all components. Then the components can be labelled as $\Psi_1, \Psi_2, \ldots, \Psi_k$ such that $f(\Psi_1) = \Psi_2, f(\Psi_2) = \Psi_3, \ldots, f(\Psi_{k-1}) = \Psi_k$, and $f(\Psi_k) = \Psi_1$.*

Thus the components of Ψ are ordered cyclically, each has one 'predecessor' and one 'successor'. The following proof is adapted from [7,44]. It uses a small quantity ε to avoid reference to path-connectedness.

Proof of Lemma. 6.1. By assumption there exists $P \in \Psi$ whose forward orbit enters all components. Let Ψ_1 be the component containing P. Suppose for a contradiction $f(\Psi_1)$ contains points in two different components, T and U. Since Ψ is compact there exists $d > 0$ such that any point in T and any point in U are at least a distance d apart. Since Ψ_1 is connected, for any $\varepsilon > 0$ there exist $Q, R \in \Psi_1$ with $\|Q - R\| < \varepsilon$ such that $f(Q) \in T$ and $f(R) \in U$. But $\|f(Q) - f(R)\| > d$ so this is not possible because f is continuous, hence $f(\Psi_1)$ is a subset of one component of Ψ. This component is not Ψ_1 (because then Ψ_1 would be forward invariant and the forward orbit of P could not reach the other components), let us call it Ψ_2. So $f(\Psi_1) \subset \Psi_2$.

By a similar argument $f(\Psi_2)$ is a subset of one component, and if $k > 2$ this component is neither Ψ_1 nor Ψ_2, call it Ψ_3. Inductively we obtain $\Psi_1, \Psi_2, \ldots, \Psi_k$ with $f(\Psi_1) \subset \Psi_2, f(\Psi_2) \subset \Psi_3, \ldots, f(\Psi_{k-1}) \subset \Psi_k$. Also $f(\Psi_k)$ is a subset of one component.

But Ψ is invariant, meaning $f(\Psi) = \Psi$. Thus $f(\Psi_k) \subset \Psi_1$, and further $f(\Psi_1) = \Psi_2, f(\Psi_2) = \Psi_3, \ldots, f(\Psi_{k-1}) = \Psi_k$, and $f(\Psi_k) = \Psi_1$ as required. □

Now fix ξ and suppose f_ξ has an attractor Λ with $k \geq 1$ connected components. To compute the value k, which is assumed to be unknown to us *a priori*, the algorithm proceeds as follows. Fix $\varepsilon > 0$ (we used $\varepsilon = 0.001$ or $\varepsilon = 0.0001$) and $M > 0$ (we used $M = 10^6$) and let $J = \varnothing$. Choose some initial point assumed to be in the basin of attraction of Λ and iterate it under f_ξ a reasonably large number of times (we used 10^4 iterations) to remove transient dynamics and obtain a point in Λ, or extremely close to Λ, call it (x_0, y_0). Iterate further, and for all $i = 1, 2, \ldots, M$ evaluate the distance (Euclidean norm in $\mathbb{R}^2$) between $f_\xi^i(x_0, y_0)$ and (x_0, y_0). If this distance is less than ε, append the number i to the set J. Finally evaluate the greatest common divisor of the elements in J — this is our estimate for the value of k.

For example using $\xi = \xi_{\text{ex}}^{(1)}$, as in Fig. 6.2-a, the algorithm generated a set of 1249 numbers

$$J = \{1292, 3170, 3778, \ldots, 999930\},$$

whose elements have greatest common divisor 2 (and indeed at this parameter point the attractor has two components).

Fig. 6.4 shows the output of this algorithm over a 200×200 grid of parameter points. The results show excellent agreement to the theory described in §6.4. For example pa-

rameter points where the greatest common divisor of the numbers in J is two are coloured light red, and the boundary of the light red region indeed appears indistinguishable from the bifurcation boundaries $\phi(g(\xi)) = 0$ and $\phi(g^2(\xi)) = 0$.

Two principles underlie the effectiveness of the algorithm. First, if the distance between any two components of Λ is greater than ε, then $\left\| f_\xi^i(x_0, y_0) - (x_0, y_0) \right\| < \varepsilon$ implies that $f_\xi^i(x_0, y_0)$ and (x_0, y_0) belong to the same component of Λ (assuming $(x_0, y_0) \in \Lambda$). By Lemma 6.1 this is only possible if i is a multiple of k. Thus the elements of J are all multiples of k.

Second, assuming f_ξ is ergodic on Λ, the set of all $i > 0$ giving $\left\| f_\xi^i(x_0, y_0) - (x_0, y_0) \right\| < \varepsilon$ will not be expected to share a multiple larger than k. This is because ergodicity implies the dynamics of f_ξ^k on any component are well mixed (see Haydn *et al.* [67] and references within for theory on the probability distribution of the values of i when ε is small). In our setting $M = 10^6$ seems to generate large enough sets J to ensure the greatest common divisor of the numbers in J is k, instead a multiple of k. One can also modify the algorithm, as described by Avrutin *et al.* [7] and Eckstein [44], to search for a close return to several reference points, instead of the single point (x_0, y_0).

6.6 The orientation-reversing case

Let

$$\Phi^{(2)} = \{\xi \in \Phi \mid \delta_L < 0, \delta_R < 0\}, \tag{6.13}$$

be the subset of Φ for which (2.21) is orientation-reversing. As shown originally by Misiurewicz [99], the closure of the unstable manifold of the fixed point X can be a chaotic attractor. This attractor contains the point T, as shown in Fig. 6.1-d, so under parameter variation is destroyed when $T = C$. This is a heteroclinic bifurcation beyond which the unstable manifold of X is unbounded. From the formulas (3.19) and (5.4) we obtain

$$C_1 - T_1 = \frac{\phi^-(\xi)}{(\lambda_L^u - 1)(1 - \lambda_R^s)(\delta_R - \tau_R \lambda_L^u)}, \tag{6.14}$$

where

$$\phi^-(\xi) = \delta_R - (\delta_R + \tau_R - (1 + \lambda_R^u)\lambda_L^u)\lambda_L^u\,, \tag{6.15}$$

which was given in Chapter 5 as (5.9). An example illustrating the destruction of the attractor is shown in Fig. 6.5. As the value of τ_L is increased the attractor is destroyed when $T = C$ at $\tau_L \approx 2.0104$.

We are now ready to subdivide $\Phi^{(2)}$ into regions based upon the renormalisation operator g, (3.6). But $\xi \in \Phi^{(2)}$ implies $g(\xi) \in \Phi^{(1)}$, so we again use the preimages of $\phi^+(\xi) = 0$ under g to define the region boundaries. Specifically we let

$$\mathcal{R}_0^{(2)} = \left\{\xi \in \Phi^{(2)} \,\middle|\, \phi^-(\xi) > 0, \phi^+(g(\xi)) \leq 0, \alpha(\xi) < 0\right\}, \tag{6.16}$$

$$\mathcal{R}_n^{(2)} = \left\{\xi \in \Phi^{(2)} \,\middle|\, \phi^+(g^n(\xi)) > 0, \phi^+\big(g^{n+1}(\xi)\big) \leq 0, \alpha(\xi) < 0\right\}, \qquad \text{for all } n \geq 1. \tag{6.17}$$

Fig. 6.6 shows these regions in two typical two-dimensional slices of parameter space. Unlike in the orientation-preserving setting we need to impose $\alpha(\xi) < 0$ in these regions so that they don't overlap $\mathcal{P}_2$ where a stable LR-cycle exists.

We conjecture that throughout $\mathcal{R}_0^{(2)}$ the map has a unique chaotic attractor with one connected component equal to the closure of the unstable manifold of X, as in Fig. 6.5-a. In Chapter 5 we proved this to be true on a subset of $\mathcal{R}_0^{(2)}$. In the special case $\tau_L = -\tau_R$ and $\delta_L = \delta_R$ of the Lozi family of maps, the constraint $\phi^-(\xi) > 0$ reduces to equation (3) of Misiurewicz [99].

The following result is a simple consequence of Propositions 6.2 and 6.3 and (6.17).

Proposition 6.6. *If $\xi \in \mathcal{R}_n^{(2)}$ with $n \geq 1$, then $g(\xi) \in \mathcal{R}_{n-1}^{(1)}$.*

This suggests that for any $\xi \in \mathcal{R}_n^{(2)}$ (2.21) has an attractor with 2^n connected components. For example

$$\xi_{\text{ex}}^{(2)} = (2.5, -0.1, -1.1, -0.2) \tag{6.18}$$

belongs to $\mathcal{R}_1^{(2)}$ and indeed the attractor shown in Fig. 6.7-a appears to have two connected components. One component belongs to Π_ξ so Proposition 6.4 applies. Hence this component is an affine transformation of the attractor of (2.21) at the parameter point $g\big(\xi_{\text{ex}}^{(2)}\big)$ that belongs to $\mathcal{R}_0^{(1)}$. We know its attractor has one component by Theorem 6.1.

Fig. 6.6 shows that our conjecture is supported by the output of the greatest common divisor algorithm. The boundaries of the $\mathcal{R}_n^{(2)}$ closely approximate the places with the value of the greatest common divisor changes. This value changes slightly above $\phi^+(g(\xi)) = 0$ because here the two components of the attractor are very close and $\varepsilon = 0.0001$ is insufficient to detect this difference. Also the reader might notice $\mathcal{R}_0^{(2)}$ has some pixels erro-

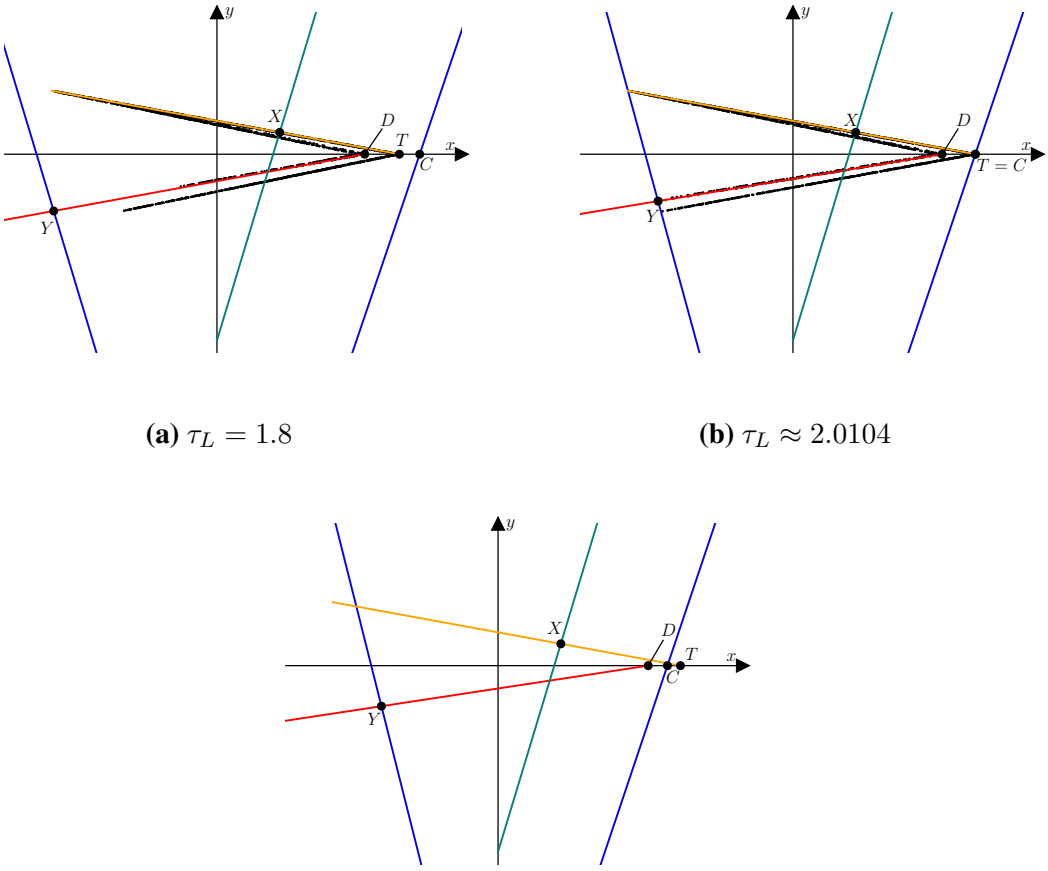

(a) $\tau_L = 1.8$

(b) $\tau_L \approx 2.0104$

(c) $\tau_L = 2.2$

Figure 6.5: Phase portraits of (2.21) with $\delta_L = -0.2$, $\delta_R = -0.2$, $\tau_R = -1.8$, and three different values of τ_L corresponding to the black triangles in Fig. 6.6-b. Panel (b) uses τ_L such that $\phi^-(\xi) = 0$ to ten decimal places. In (a) $\mathrm{cl}(W^u(X))$ is a chaotic attractor; in (b) $W^u(X)$ and $W^s(Y)$ have corner intersections; in (c) there is no attractor. The coloured lines illustrate the stable and the unstable manifolds of the fixed points coloured following the scheme in Fig. 6.1.

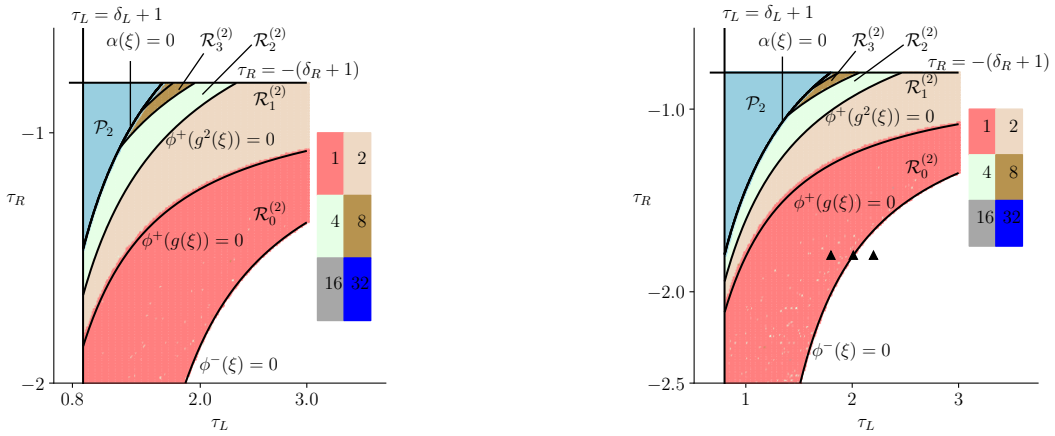

(a) $\delta_L = -0.1, \delta_R = -0.2$. (b) $\delta_L = -0.2, \delta_R = -0.2$.

Figure 6.6: Two-dimensional slices of the orientation-reversing parameter region $\Phi^{(2)}$ showing the bifurcation curves overlaid upon numerical results obtained using $\varepsilon = 0.0001$ and $M = 10^6$. The black triangles correspond to the parameter values of Fig. 6.5.

neously corresponding to more than one component because here the attractor is relatively large and $M = 10^6$ iterations is insufficiently many for the algorithm to consistently obtain a greatest common divisor of 1.

6.7 The non-invertible case $\delta_L > 0$, $\delta_R < 0$.

Here we study the parameter region

$$\Phi^{(3)} = \{\xi \in \Phi \mid \delta_L > 0, \delta_R < 0\}, \tag{6.19}$$

where (2.21) is non-invertible. In this region an attractor of (2.21) can be destroyed by crossing either the homoclinic bifurcation $\phi^+(\xi) = 0$ or the heteroclinic bifurcation $\phi^-(\xi) = 0$. This is because near these boundaries the attractor contains the point T and is close to the point D so is destroyed when one of these points collides with C. For example in Fig. 6.8 T lies to the left of D, so the attractor is destroyed when $D = C$, i.e. when $\phi^+(\xi) = 0$. In contrast in Fig. 6.9 T lies to the right of D, so the attractor is destroyed when $T = C$, i.e. when $\phi^-(\xi) = 0$. For this reason we define

$$\phi_{\min}(\xi) = \min[\phi^+(\xi), \phi^-(\xi)]. \tag{6.20}$$

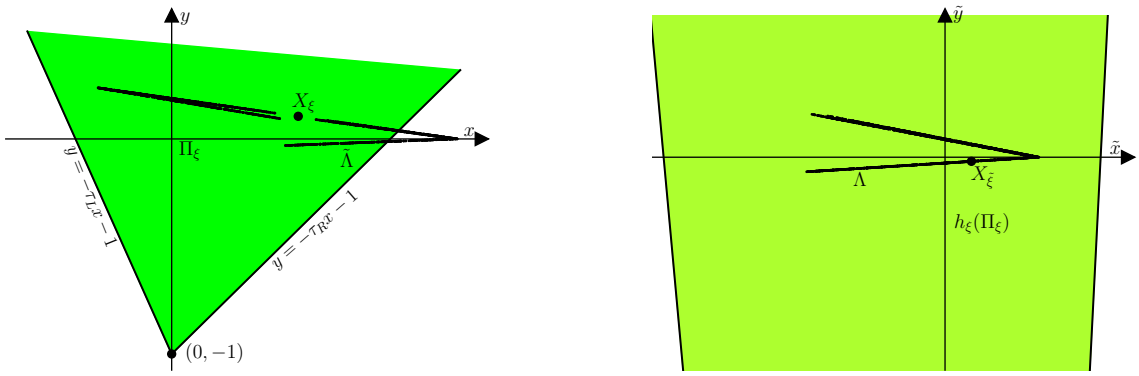

(a) $\xi = \xi_{\text{ex}}^{(2)} \in \mathcal{R}_1^{(2)}$ (b) $\xi = g\big(\xi_{\text{ex}}^{(2)}\big) \in \mathcal{R}_0^{(1)}$

Figure 6.7: Panel (a) is a phase portrait of (2.21) at the parameter point $\xi_{\text{ex}}^{(2)}$ (6.18) where the attractor has two connected components in the orientation-reversing case. Panel (b) uses instead $g\big(\xi_{\text{ex}}^{(2)}\big)$.

and

$$\mathcal{R}_n^{(3)} = \big\{\xi \in \Phi^{(3)} \,\big|\, \phi_{\min}(g^n(\xi)) > 0,\ \phi_{\min}\big(g^{n+1}(\xi)\big) \le 0,\ \alpha(\xi) < 0\big\}, \tag{6.21}$$

for all $n \ge 0$. Two-dimensional slices of these regions are shown in Fig. 6.10. We conjecture that throughout the first region $\mathcal{R}_0^{(3)}$ the map (2.21) has a unique chaotic attractor with one connected component, and this is supported by the numerical results shown in Fig. 6.10. To explain the dynamics in the remaining regions we use the following analogy to Propositions 6.5 and 6.6. Here, however, the result is not trivial, so we provide a proof.

Proposition 6.7. *If $\xi \in \mathcal{R}_n^{(3)}$ with $n \ge 1$, then $g(\xi) \in \mathcal{R}_{n-1}^{(3)}$.*

Proof. Choose any $\xi \in \mathcal{R}_n^{(3)}$ with $n \ge 1$ and write $g(\xi) = \big(\tilde{\tau}_L, \tilde{\delta}_L, \tilde{\tau}_R, \tilde{\delta}_R\big)$ as in the proof of Proposition 6.3. By Proposition 6.3 we have $g(\xi) \in \Phi$. Further, $g(\xi) \in \Phi^{(3)}$ because $\tilde{\delta}_L = \delta_R^2 > 0$ and $\tilde{\delta}_R = \delta_L\delta_R < 0$. Also $\phi_{\min}\big(g^{n-1}(g(\xi))\big) > 0$ and $\phi_{\min}\big(g^n(g(\xi))\big) \le 0$. Finally $\alpha(g(\xi)) = \tilde{\tau}_L\tilde{\tau}_R + (\tilde{\delta}_L - 1)(\tilde{\delta}_R - 1)$ where $\tilde{\tau}_L = \tau_R^2 - 2\delta_R$, $\tilde{\delta}_L = \delta_R^2$, $\tilde{\tau}_R = \tau_L\tau_R - \delta_L - \delta_R$, and $\tilde{\delta}_R = \delta_L\delta_R$. By substituting $\tau_L > \delta_L + 1$ and $\tau_R < -(\delta_R + 1)$ (true because $\xi \in \Phi$) we obtain (after simplification)

$$\alpha(g(\xi)) < -2\big(1 + \delta_R + \delta_R^2\big)(\delta_L + \delta_R).$$

So if $\delta_L + \delta_R > 0$ then $\alpha(g(\xi)) < 0$ (because $1 + \delta_R + \delta_R^2 \ge \frac{3}{4} > 0$). If instead $\delta_L + \delta_R \le 0$

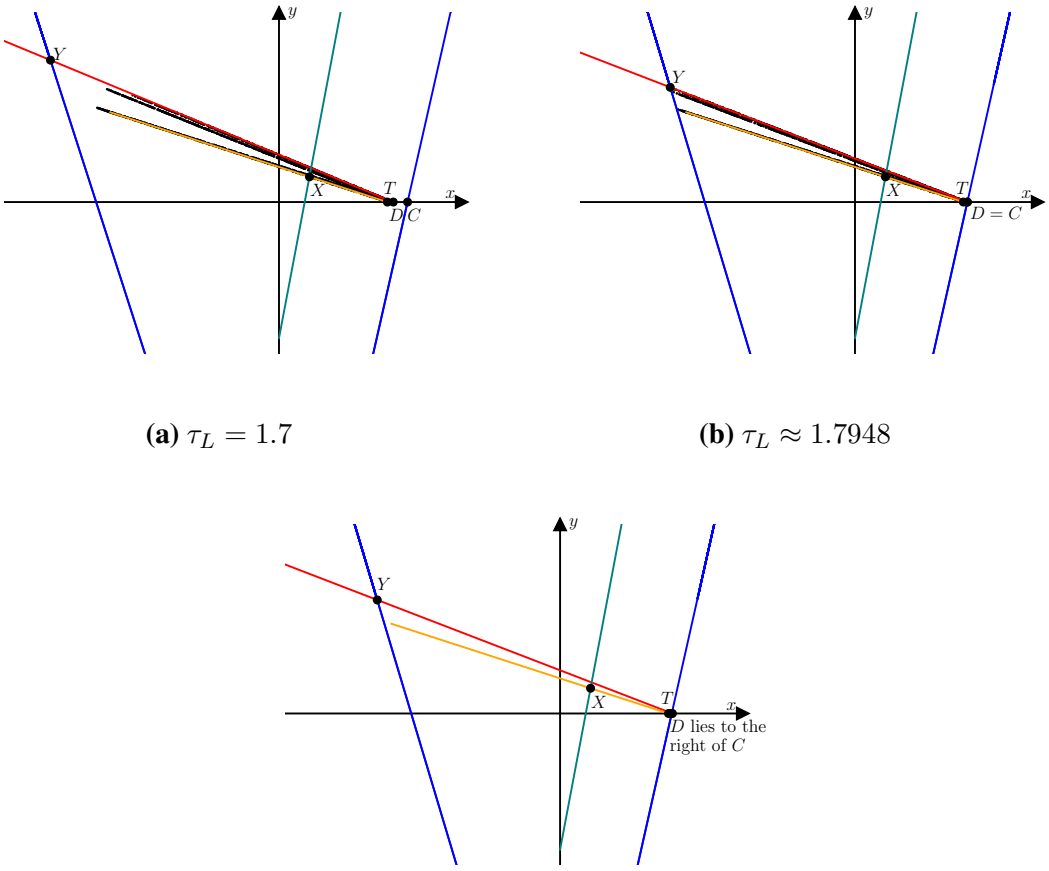

(a) $\tau_L = 1.7$

(b) $\tau_L \approx 1.7948$

(c) $\tau_L = 1.8$

Figure 6.8: Phase portraits of (2.21) with $\delta_L = 0.3$, $\delta_R = -0.4$, $\tau_R = -2.4$ and three different values of τ_L corresponding to the blue triangles in Fig. 6.10-b. The coloured lines illustrate the stable and the unstable manifolds of the fixed points coloured following the scheme in Fig. 6.1.

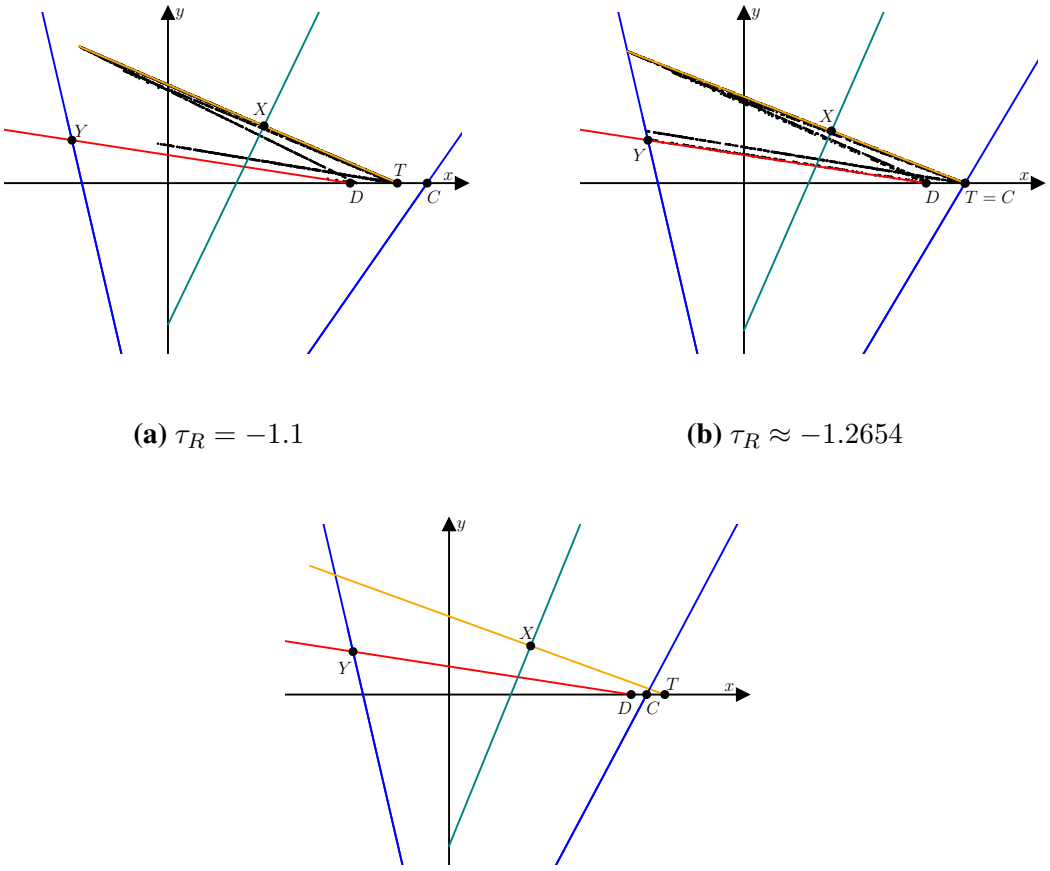

(a) $\tau_R = -1.1$

(b) $\tau_R \approx -1.2654$

(c) $\tau_R = -1.4$

Figure 6.9: Phase portraits of (2.21) with $\delta_L = 0.3$, $\delta_R = -0.4$, $\tau_L = 3$, and three different values of τ_R corresponding to the black triangles in Fig. 6.10-b. The coloured lines illustrate the stable and the unstable manifolds of the fixed points coloured following the scheme in Fig. 6.1.

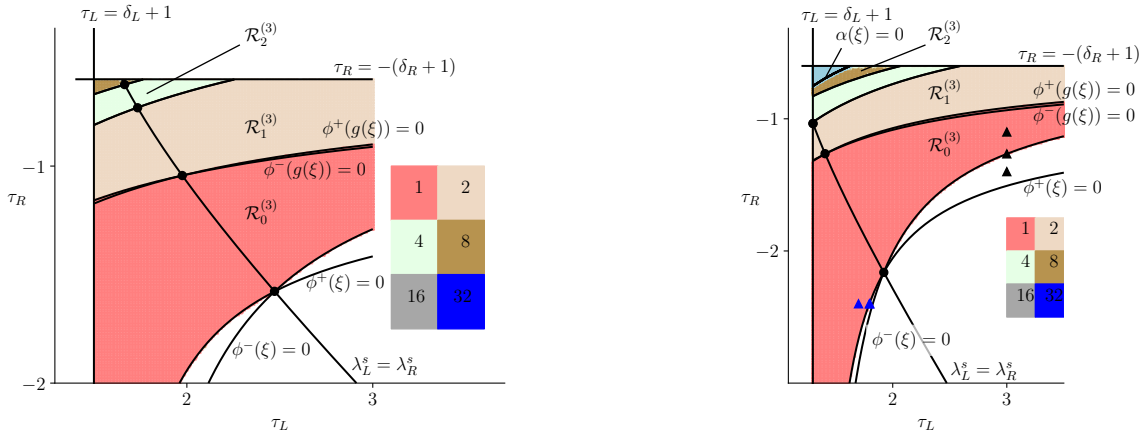

(a) $\delta_L = 0.5, \delta_R = -0.4$.

(b) $\delta_L = 0.3, \delta_R = -0.4$.

Figure 6.10: Two-dimensional slices of the non-invertible parameter region $\Phi^{(3)}$ showing the bifurcation curves overlaid upon numerical results obtained using $\varepsilon = 0.001$ and $M = 10^6$. The blue [black] triangles correspond to the parameter values of Fig. 6.8 [Fig. 6.9].

then $\tilde{\delta}_L + \tilde{\delta}_R = \delta_R(\delta_L + \delta_R) \geq 0$ because $\delta_R < 0$, so again $\alpha(g(\xi)) < 0$ by Proposition 6.2 applied to the parameter point $g(\xi)$. □

Proposition 6.7 suggests that throughout each $\mathcal{R}_n^{(3)}$ with $n \geq 1$ (2.21) has an attractor with exactly 2^n connected components, and Fig. 6.10 supports this conjecture. Fig. 6.11-a provides an example using the parameter point

$$\xi_{\text{ex}}^{(3)} = (3, 0.3, -.9, -0.4), \tag{6.22}$$

which belongs to $\mathcal{R}_1^{(3)}$. The attractor has two pieces, one of which belongs to Π_ξ, so as above this piece is an affine transformation of the attractor of $g\big(\xi_{\text{ex}}^{(3)}\big) \in \mathcal{R}_0^{(3)}$ shown in Fig. 6.11-b.

6.8 The non-invertible case $\delta_L < 0$, $\delta_R > 0$

It remains for us to consider

$$\Phi^{(4)} = \{\xi \in \Phi \mid \delta_L < 0, \delta_R > 0\}, \tag{6.23}$$

where (2.21) is non-invertible. In this region the attractor is usually destroyed before the boundaries $\phi^+(\xi) = 0$ and $\phi^-(\xi) = 0$ in a heteroclinic bifurcation that cannot be char-

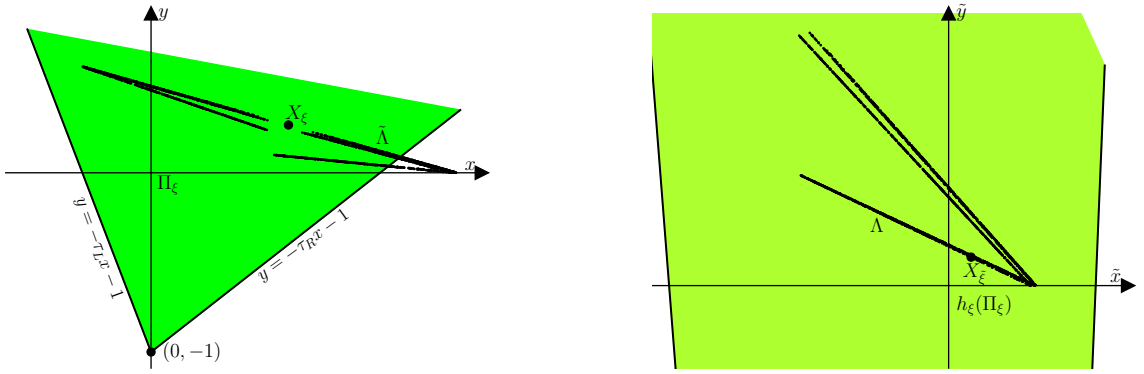

(a) $\xi = \xi_{\text{ex}}^{(3)} \in \mathcal{R}_1^{(3)}$ (b) $\xi = g\big(\xi_{\text{ex}}^{(3)}\big) \in \mathcal{R}_0^{(3)}$

Figure 6.11: Panel (a) is a phase portrait of (2.21) at the parameter point $\xi_{\text{ex}}^{(3)}$ (6.22) where the attractor has two connected components in the $\delta_L > 0$ non-invertible case. Panel (b) uses instead $g\big(\xi_{\text{ex}}^{(3)}\big)$.

acterised by an explicit condition on the parameter values. This occurs when the attractor contains points on $y = 0$ that lie to the right of D and T and is destroyed when its right-most point collides with C.

Fig. 6.12 shows an example. In panel (a) the attractor is the closure of the unstable manifold of X. As we grow the unstable manifold outwards from X it develops points on $y = 0$ that lie further and further to the right, but not beyond C. This occurs as a consequence of the geometric configuration afforded by f_R being orientation-preserving and f_L being orientation-reversing. As the value of τ_L is increased the attractor is destroyed when its right-most point collides with C, panel (b). With a slightly larger value of τ_L, panel (c), typical forward orbits diverge even though D and T still lie to the left of C. Fig. 6.13 provides a second example. Here the parameter values are such that D and T are switched around but the attractor is destroyed in the same way.

Fig. 6.14 shows the results of numerical simulations applied to two slices of $\Phi^{(4)}$. The white areas just to the left of $\phi^+(\xi) = 0$ and $\phi^-(\xi) = 0$ correspond to the phenomenon that we have just described. These areas are bounded on the left by a curve of heteroclinic bifurcations. Since we cannot identify this curve with hand calculations, it is natural to attempt to compute the curve numerically with numerical continuation methods. However, we do not show the result of such a computation because from the results of Osinga [105] we suspect that this curve is highly irregular, e.g. non-differentiable at infinitely many points.

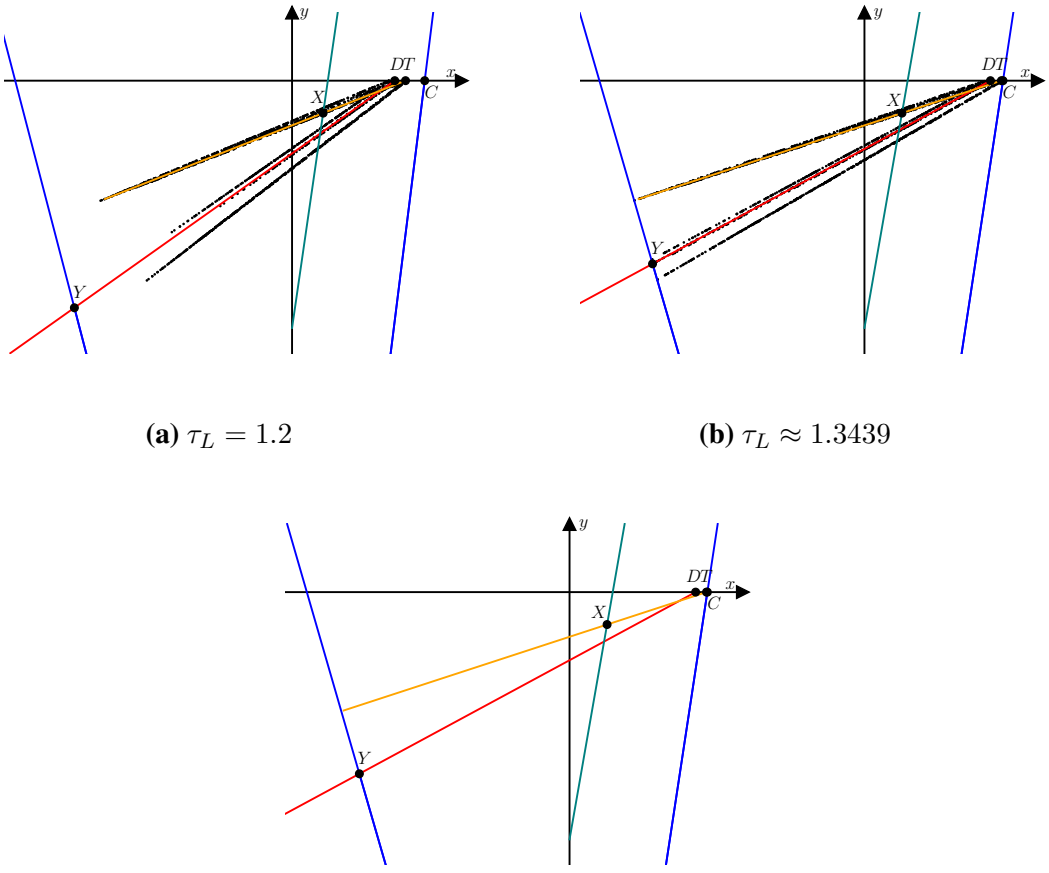

(a) $\tau_L = 1.2$

(b) $\tau_L \approx 1.3439$

(c) $\tau_L = 1.35$

Figure 6.12: Phase portraits of (2.21) with $\delta_L = -0.4$, $\delta_R = 0.4$, $\tau_R = -2.8$, and three different values of τ_L corresponding to the blue triangles in Fig. 6.14-a. The parameter value used in panel (b) is approximately where the attractor is destroyed. In all three panels D lies to the left of T which lies to the left of C. The coloured lines illustrate the stable and the unstable manifolds of the fixed points coloured following the scheme in Fig. 6.1.

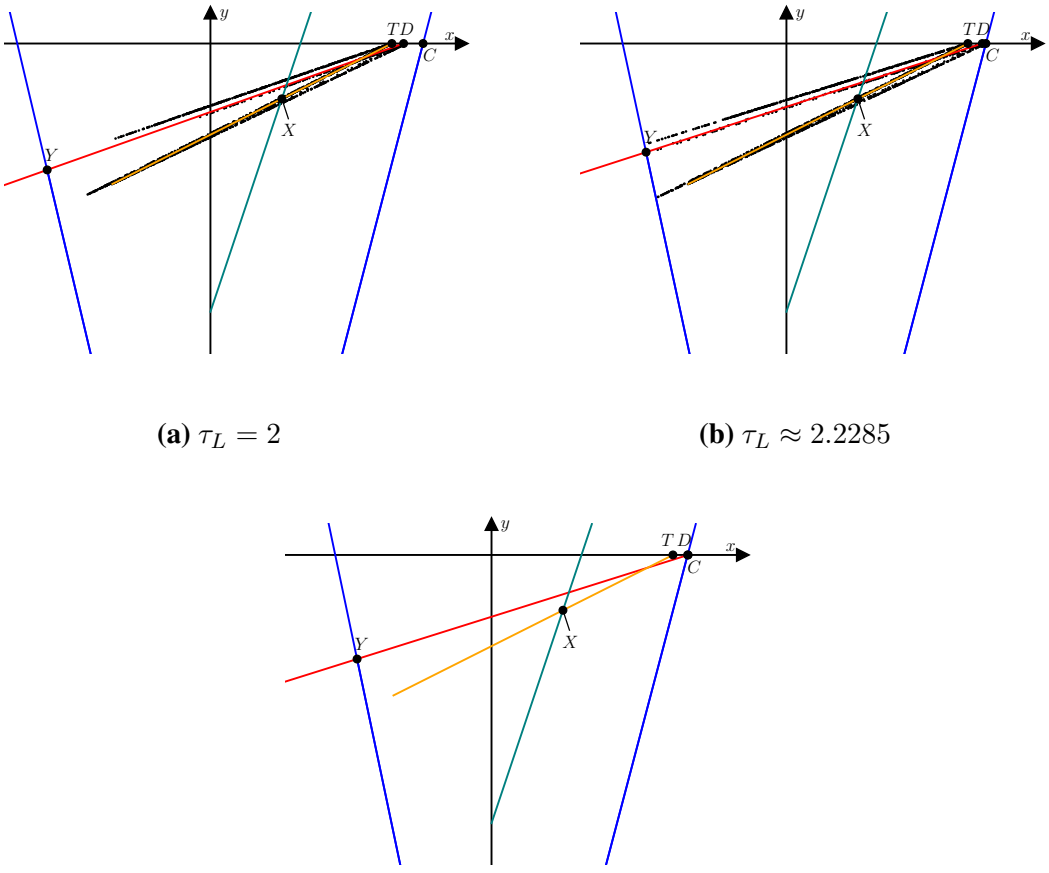

(a) $\tau_L = 2$

(b) $\tau_L \approx 2.2285$

(c) $\tau_L = 2.3$

Figure 6.13: Phase portraits of (2.21) with $\delta_L = -0.4$, $\delta_R = 0.4$, $\tau_R = -1.8$, and three different values of τ_L corresponding to the black triangles in Fig. 6.14-a. The parameter value used in panel (b) is approximately where the attractor is destroyed. In all three panels T lies to the left of D which lies to the left of C. The coloured lines illustrate the stable and the unstable manifolds of the fixed points coloured following the scheme in Fig. 6.1.

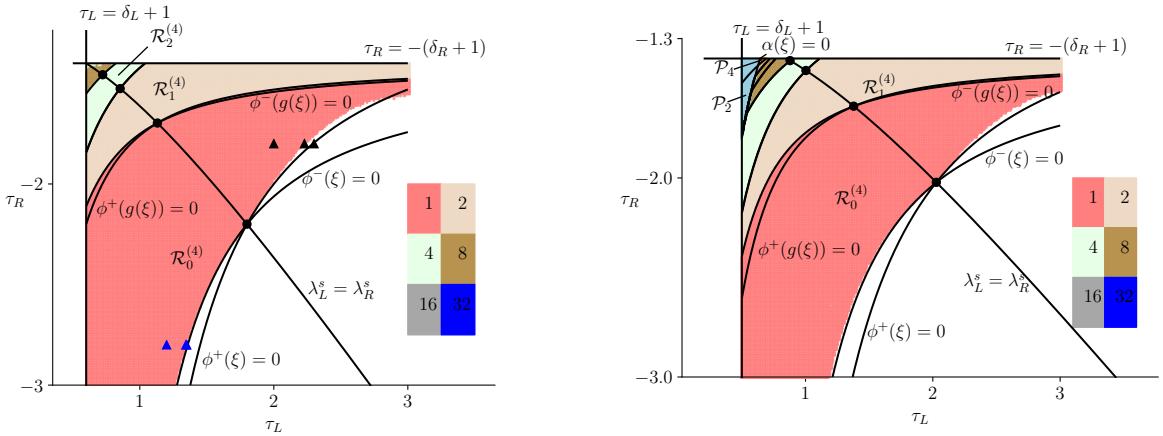

(a) $\delta_L = -0.4, \delta_R = 0.4$.

(b) $\delta_L = -0.5, \delta_R = 0.4$.

Figure 6.14: Two-dimensional slices of the non-invertible parameter region $\Phi^{(4)}$ showing the bifurcation curves overlaid upon numerical results obtained using $\varepsilon = 0.001$ and $M = 10^6$. The blue [black] triangles correspond to the parameter values of Fig. 6.12 [Fig. 6.13].

In each plot in Fig. 6.14 the attractor does in fact persist up to where the boundaries $\phi^+(\xi) = 0$ and $\phi^-(\xi) = 0$ meet. This is because on the curve $\lambda_L^s = \lambda_R^s$ the right-most point of the attractor is D and T, which are equal. Also near the plot of panel Fig. 6.14-a the attractor persists slightly beyond $\phi^+(\xi) = 0$ because here the attractor fails to approach D so is not destroyed when $D = C$ at $\phi^+(\xi) = 0$.

Despite the extra complexities in $\Phi^{(4)}$ it still appears that renormalisation is helpful for explaining the bifurcation structure. Let

$$\mathcal{R}_0^{(4)} = \left\{ \xi \in \Phi^{(4)} \middle| \, \phi_{\min}(\xi) > 0, \, \phi_{\min}(g(\xi)) \leq 0, \, \alpha(\xi) < 0 \right\}. \tag{6.24}$$

Based on Fig. 6.14 we conjecture that for any $\xi \in \mathcal{R}_0^{(4)}$, if (2.21) has an attractor then this attractor is chaotic with one connected component. Now let

$$\mathcal{R}_n^{(4)} = \left\{ \xi \in \Phi^{(4)} \middle| \, \phi_{\min}(g^n(\xi)) > 0, \, \phi_{\min}(g^{n+1}(\xi)) \leq 0, \, \alpha(\xi) < 0, \alpha(g(\xi)) < 0 \right\}. \tag{6.25}$$

Unlike in previous sections here we have included the extra constraint $\alpha(g(\xi)) < 0$ so that the $\mathcal{R}_n^{(4)}$ do not include the region $\mathcal{P}_4$, defined to be where (2.21) has a stable period-four solution with symbolic itinerary $LRRR$. This region is visible in Fig. 6.14-b and shown more clearly in the magnification, Fig. 6.15. Note that here we do not show the result of the numerics because the component counting algorithm does not work efficiently close to

the curve $\alpha(g(\xi)) = 0$. The following result is a trivial consequence of our definitions.

Proposition 6.8. *If* $\xi \in \mathcal{R}_n^{(4)}$ *with* $n \geq 1$, *then* $g(\xi) \in \mathcal{R}_{n-1}^{(3)}$.

Based on this we conjecture that for any $\xi \in \mathcal{R}_n^{(4)}$ with $n \geq 1$ the map (2.21) has a chaotic attractor with exactly 2^n connected components, and this is supported by the numerics in Fig. 6.14. Fig. 6.16-a shows the attractor of (2.21) for a typical parameter point in $\mathcal{R}_1^{(4)}$, specifically

$$\xi_{\text{ex}}^{(4)} = (2.2, -0.4, -1.5, 0.4). \tag{6.26}$$

As expected it has two connected components, one of which is contained in Π_ξ, and both of which are affine transformations of the single-component attractor of (1.1) with $g\big(\xi_{\text{ex}}^{(4)}\big) \in \mathcal{R}_0^{(3)}$ shown in Fig. 6.16-b.

6.9 Reduction to one dimension

Finally we address a novelty of the non-invertible settings. In these settings the stable eigenvalues λ_L^s and λ_R^s have the same sign (they are both positive if $\delta_L > 0$ and $\delta_R < 0$,

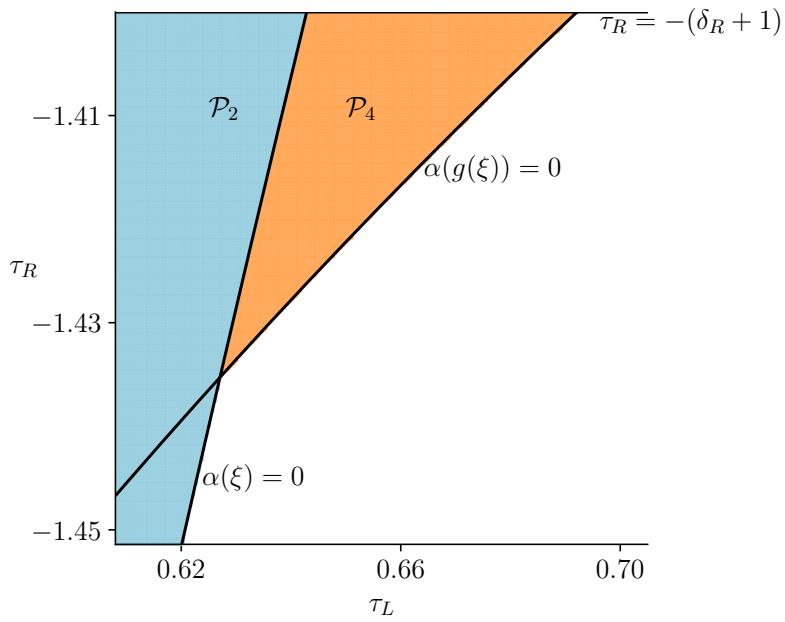

Figure 6.15: A magnified version of Fig. 6.14-b showing the regions having a stable LR-cycle (period-two solution) $\mathcal{P}_2$ and a stable $LRRR$-cycle (period-four solution) $\mathcal{P}_4$.

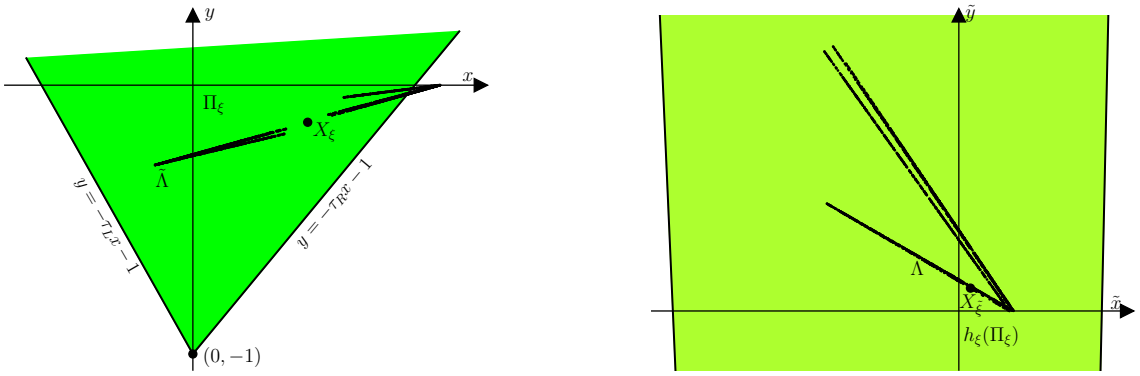

(a) $\xi = \xi_{\text{ex}}^{(4)} \in \mathcal{R}_1^{(4)}$ (b) $\xi = g\big(\xi_{\text{ex}}^{(4)}\big) \in \mathcal{R}_0^{(3)}$

Figure 6.16: Panel (a) is a phase portrait of (2.21) at the parameter point $\xi_{\text{ex}}^{(4)}$ (6.26) where the attractor has two connected components in the $\delta_L < 0$ non-invertible case. Panel (b) uses instead $g\big(\xi_{\text{ex}}^{(4)}\big)$.

and both negative if $\delta_L < 0$ and $\delta_R > 0$), so it is possible for them to be equal. From the formulas (3.19) and (4.6) for the points D and T we have

$$D_1 - T_1 = \frac{\lambda_L^s - \lambda_R^s}{(1 - \lambda_L^s)(1 - \lambda_R^s)}. \tag{6.27}$$

Thus D and T coincide when the stable eigenvalues are equal. Thus the boundaries $\phi^+(\xi) = 0$ and $\phi^-(\xi) = 0$, where $C = D$ and $C = T$ respectively, intersect where $\lambda_L^s = \lambda_R^s$, and this is evident in Figs. 6.10 and 6.14. Also for each $n \geq 1$ the boundaries $\phi^+(g^n(\xi)) = 0$ and $\phi^-(g^n(\xi)) = 0$ intersect where $\lambda_L^s = \lambda_R^s$.

We now show that if $\lambda_L^s = \lambda_R^s$ then the pertinent dynamics reduces to one dimension, as in Fig. 6.17.

Proposition 6.9. *If $\xi \in \Phi$ with $\phi_{\min}(\xi) > 0$ and $\lambda_L^s = \lambda_R^s$, then f_ξ is forward invariant on the line segment from T to $f_\xi(T)$. Moreover, on this segment f_ξ is conjugate to the skew tent map*

$$z \mapsto \begin{cases} \lambda_L^u z + 1, & z \leq 0, \\ \lambda_R^u z + 1, & z \geq 0, \end{cases} \tag{6.28}$$

on $[\lambda_R^u + 1, 1]$.

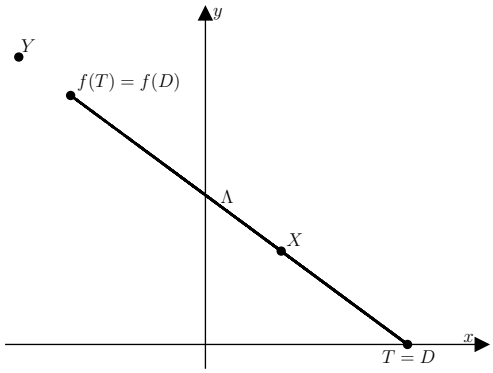

(a) $\xi = (2.323, 0.5, -1.427, -0.4)$

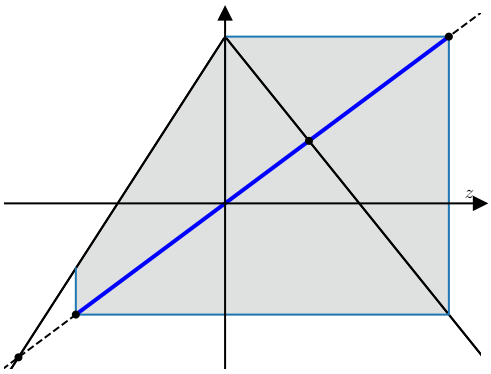

(b) corresponding cobweb diagram

Figure 6.17: Panel (a) shows the attractor of (2.21) at the given parameter point which belongs to $\mathcal{R}_0^{(3)}$. This attractor is the line segment from T to $f_\xi(T)$. The restriction of f_ξ to the attractor is the one-dimensional map (6.28) indicated in panel (b).

Proof. The line segment from T to $f_\xi(T)$ is

$$\Gamma = \left\{\gamma(z) \,\middle|\, z \in \left[\lambda_R^u + 1, 1\right]\right\}, \text{ where } \gamma(z) = \left(\frac{z}{1-\lambda_R^s}, \frac{(1-z)\lambda_R^s}{1-\lambda_R^s}\right),$$

because putting $z = 1$ gives $(x, y) = \left(\frac{1}{1-\lambda_R^s}, 0\right) = T$ by (3.19), while putting $z = \lambda_R^u + 1$ gives $(x, y) = \left(\frac{1+\lambda_R^u}{1-\lambda_R^s}, \frac{-\lambda_R^s\lambda_R^u}{1-\lambda_R^s}\right)$ which is identical to $f_\xi(T) = (\tau_R T_1 + 1, -\delta_R T_1)$ (since $\tau_R = \lambda_R^s + \lambda_R^u$ and $\delta_R = \lambda_R^s\lambda_R^u$). If $z \in [0, 1]$ then

$$f_\xi(\gamma(z)) = (\tau_R x + y + 1, -\delta_R x) = \left(\frac{1+\lambda_R^u z}{1-\lambda_R^s}, \frac{-\lambda_R^s\lambda_R^u z}{1-\lambda_R^s}\right) = \gamma(\lambda_R^u z + 1),$$

while if $z \in [\lambda_R^u + 1, 1]$ then

$$f_\xi(\gamma(z)) = (\tau_L x + y + 1, -\delta_L x) = \left(\frac{1+\lambda_L^u z}{1-\lambda_R^s}, \frac{-\lambda_R^s\lambda_L^u z}{1-\lambda_R^s}\right) = \gamma(\lambda_L^u z + 1),$$

and the result follows. □

The map (6.28) has $\lambda_L^u > 1$ and $\lambda_R^u < -1$, which corresponds in Fig. 2.3 to a point in some $\mathcal{R}_n$, with $n \geq 0$. Thus, with this value of n, the attractor of the skew tent map (6.28) is comprised of 2^n disjoint intervals. Consequently the attractor of f_ξ is comprised of 2^n disjoint line segments. Places where the value of n changes can be computed by solving

for where $\phi_0 \circ g^n = 0$ in Fig. 2.3. We computed these points numerically and have plotted them in Figs. 6.10 and 6.14 from which we see that, as expected, these points are where $\phi^+ \circ g^n = 0$ and $\phi^- \circ g^n = 0$. In this way the conjectures in §6.7 and §6.8 on the number of connected components of the attractors are confirmed in the special codimension-one scenario that the stable stability multipliers associated with X and Y are equal.

Chapter 7

Extension to higher-dimensional maps.

7.1 Introduction

In this chapter we extend the trapping region construction described in §5.3 from the two-dimensional border-collision normal form to the N-dimensional border-collision normal form, for any $N \geq 2$. This paves a way towards understanding the conditions that govern robust chaos in higher dimensional maps.

To obtain useful results we require some restrictions on the parameters of the N-dimensional border-collision normal form (1.8). These parameters are coefficients of the characteristic polynomials of the left and right Jacobian matrices A_L and A_R (in (1.8) these are denoted C_L and C_R), so it is equivalent to place restrictions on the eigenvalues of these matrices. In two dimensions we considered the parameter set Φ (2.25) which can be interpreted as follows. It is where A_L has exactly one unstable eigenvalue, and this eigenvalue is greater than 1, while A_R also has exactly one unstable eigenvalue, but this eigenvalue is less than -1. In this chapter we use this constraint and allow any number of dimensions.

7.2 The N-dimensional border-collision normal form

In N dimensions the left and right Jacobian matrices of the normal form are

$$A_L = \begin{bmatrix} -a_L^1 & 1 & 0 & \dots & 0 \\ -a_L^2 & 0 & 1 & \dots & 0 \\ -a_L^3 & 0 & 0 & \dots & 0 \\ \vdots & \vdots & \vdots & \ddots & \vdots \\ -a_L^{N-1} & 0 & 0 & \dots & 1 \\ -a_L^N & 0 & 0 & \dots & 0 \end{bmatrix}, \tag{7.1}$$

and

$$A_R = \begin{bmatrix} -a_R^1 & 1 & 0 & \dots & 0 \\ -a_R^2 & 0 & 1 & \dots & 0 \\ -a_R^3 & 0 & 0 & \dots & 0 \\ \vdots & \vdots & \vdots & \ddots & \vdots \\ -a_R^{N-1} & 0 & 0 & \dots & 1 \\ -a_R^N & 0 & 0 & \dots & 0 \end{bmatrix}, \tag{7.2}$$

with

$$b = \begin{bmatrix} 1 \\ 0 \\ 0 \\ \vdots \\ 0 \\ 0 \end{bmatrix}. \tag{7.3}$$

We will assume A_L has an eigenvalue $\lambda_L^1 > 1$, and A_R has an eigenvalue $\lambda_R^1 < -1$. We will also assume all other eigenvalues of A_L and A_R have modulus less than 1. This ensures, for instance, that the left piece of the map has a unique fixed point. This point is *admissible* (i.e. it is a fixed point of (1.8)), and straight-forward calculations give us the following

explicit formula for the fixed point:

$$Y = \left(\frac{1}{1+\sum_{i=1}^{N} a_L^i}, -\frac{\sum_{j=2}^{N} a_L^j}{1+\sum_{i=1}^{N} a_L^i}, -\frac{\sum_{j=3}^{N} a_L^j}{1+\sum_{i=1}^{N} a_L^i}, \ldots, -\frac{(a_L^{N-1}+a_L^N)}{1+\sum_{i=1}^{N} a_L^i}, -\frac{a_L^N}{1+\sum_{i=1}^{N} a_L^i} \right). \tag{7.4}$$

The stable manifold of Y has dimension $N-1$. As it emanates from Y it is coincident to the stable subspace

$$E^s(Y) = \{x \in \mathbb{R}^N | u^T(x-Y) = 0\}, \tag{7.5}$$

where u is the following left eigenvector of A_L corresponding to λ_L^1

$$u = \left((\lambda_L^1)^{N-1}, (\lambda_L^1)^{N-2}, \ldots, (\lambda_L^1)^3, (\lambda_L^1)^2, \lambda_L^1\right). \tag{7.6}$$

Recall that the two-dimensional formula for C (5.4) was obtained by finding the point where the stable manifold of Y intersects the x_1-axis after experiencing one kink. In fact this is the unique point on the x_1-axis that maps to the stable subspace of Y. Similarly, in the N-dimensional case, there exists a point C on the x_1-axis

$$C = (C_1, 0, 0, \ldots, 0), \tag{7.7}$$

whose image $f_\xi(C)$ lies on the stable subspace of Y (7.5). Assuming C_1 the point C maps under the right piece of the map, so

$$f_\xi(C) = \left(-a_R^1 C_1 + 1, -a_R^2 C_1, -a_R^3 C_1, \ldots, -a_R^{N-1} C_1, -a_R^N C_1\right). \tag{7.8}$$

Note that C_1 is the x_1 component of the point C. By using (7.5) to solve $f_\xi(C) \in E^s(Y)$ we obtain

$$C_1 = \frac{(\lambda_L^1)^{N-1} \sum_{i=1}^{N} a_L^i + \sum_{k=2}^{N} (\lambda_L^1)^{N-k} \sum_{j=k}^{N} a_L^j}{(\sum_{m=1}^{N} (\lambda_L^1)^{N-m} a_R^m)(1+\sum_{i=1}^{N} a_L^i)}. \tag{7.9}$$

7.3 Asymptotic calculations

Let us write the stable eigenvalues of A_L and A_R as $\lambda_J^i = r\eta_J^i, i = 2, 3, \ldots, N$, with $r = \max\{|\lambda_L^i|, |\lambda_R^i|\} < 1$. Our idea is to construct a region that is forward invariant under (1.8)

assuming r is sufficiently small. In two dimensions this is equivalent to taking small values of δ_L and δ_R which in Chapter 5 we showed could effectively be accommodated. In the limit $r \to 0$ the map (1.8) reduces to the one-dimensional skew tent map with slopes $\lambda_L^1 > 1$ and $\lambda_R^1 < -1$. Recall from §2.9.1 that this one-dimensional map has an attractor if $\phi_0(\lambda_L^1, \lambda_R^1) > 0$ where $\phi_0 = \lambda_L^1 \lambda_R^1 + \lambda_L^1 - \lambda_R^1$.

Since the numbers in the first column of A_L are the coefficients of the characteristic polynomial of A_L, they can be written in terms of λ_L^1 and η_L^i by

$$\begin{aligned}
a_L^1 &= -\sum_{i=1}^{N} \lambda_L^i = -(\lambda_L^1 + r\sum_{i=2}^{N} \eta_L^i) \\
a_L^2 &= \sum_{i \neq j} \lambda_L^i \lambda_L^j = r\lambda_L^1 \sum_{i=2}^{N} \eta_L^i + \mathcal{O}(r^2) \\
a_L^3 &= -r^2 \lambda_L^1 \sum_{i=2}^{N-1} \sum_{j=i+1}^{N} \eta_L^i \eta_L^j + \mathcal{O}(r^3) \\
&\vdots \\
a_L^N &= (-1)^N \lambda_L^1 \lambda_L^2 \ldots \lambda_L^N.
\end{aligned} \tag{7.10}$$

This enables us to write Y as

$$\begin{aligned}
Y = \frac{1}{1 - \lambda_L^1 + \mathcal{O}(r)} \Bigg(& 1, -r\lambda_L^1 \sum_{i=2}^{N} \eta_L^i + \mathcal{O}(r^2), \\
& r^2 \lambda_L^1 \sum_{i=2}^{N-1} \sum_{j=i+1}^{N} \eta_L^i \eta_L^j + \mathcal{O}(r^3), \ldots, (-1)^{N-1} \lambda_L^1 \lambda_L^2 \ldots \lambda_L^N \Bigg),
\end{aligned} \tag{7.11}$$

Notice $Y_2 \leq r\frac{\lambda_L^1}{\lambda_L^1 - 1}(N-1) + \mathcal{O}(r^2)$, $Y_3 \leq -r^2 \frac{\lambda_L^1}{\lambda_L^1 - 1} \frac{(N-1)(N-2)}{2!} + \mathcal{O}(r^3)$, …, $Y_k \leq (-1)^k r^{k-1} \frac{\lambda_L^1}{\lambda_L^1 - 1} \frac{(N-1)(N-2)\ldots(N-k+1)}{(k-1)!} + \mathcal{O}(r^k)$, …, $Y_N \leq (-1)^N r^{N-1} \frac{\lambda_L^1}{\lambda_L^1 - 1}$. This motivates

us to define the quantities

$$\begin{aligned} R_2 &= \alpha \frac{\lambda_L^1}{\lambda_L^1 - 1}(N-1) \\ R_3 &= \alpha \frac{\lambda_L^1}{\lambda_L^1 - 1}\frac{(N-1)(N-2)}{2!} \\ &\vdots \\ R_N &= \alpha \frac{\lambda_L^1}{\lambda_L^1 - 1}. \end{aligned} \tag{7.12}$$

Now let

$$H = \left\{ x \in \mathbb{R}^N \,\middle|\, |x_2| \le R_2 r,\, |x_3| \le R_3 r^2,\, \ldots, |x_N| \le R_N r^{N-1} \right\}$$

be the set of all points $x \in \mathbb{R}^N$ whose i^{th} component has a value between $-R_i r^{i-1}$ and $R_i r^{i-1}$, for all $i = 2, 3, \ldots, N$. Next let K be the part of $E^s(Y)$ that belongs to H. Finally let Ω be the convex hull of K and C.

Conjecture 7.1. *Let $\lambda_L^1 > 1$ and $\lambda_R^1 < -1$ be such that $\phi_0(\lambda_L^1, \lambda_R^1) > 0$. Let $\eta_J^i \in \mathbb{C}$ with $|\eta_J^i| \le 1$ for all $i = 2, 3, \ldots, N$ and $J \in \{L, R\}$. For all sufficiently small $r > 0$, if A_L has eigenvalues λ_L^1 and $\lambda_L^i = r\eta_L^i$ and A_R has eigenvalues λ_R^1 and $\lambda_R^i = r\eta_R^i$ then Ω is forward invariant under* (1.8)*.*

In the remainder of this section we perform some calculations that form the first step towards proving Conjecture 7.1. The set K is a convex polytope with 2^{N-1} vertices

$$\begin{aligned} P^{(i)} &= \left(P_1^{(i)}, P_2^{(i)}, \ldots, P_{N-1}^{(i)}, P_N^{(i)} \right) \\ &= \left(P_1^{(i)}, \sigma_2^{(i)} R_2 r, \sigma_3^{(i)} R_3 r^2, \ldots, \sigma_{N-1}^{(i)} R_{N-1} r^{N-2}, \sigma_N^{(i)} R_N r^{N-1} \right), \end{aligned} \tag{7.13}$$

where $\sigma^{(i)} = \pm 1$ for each $i = 2, 3, \ldots, N$ and the first component $P_1^{(i)}$ is determined by

the requirement that $P^{(i)}$ belongs to $E^s(Y)$. For example, for $N = 4$,

$$\begin{aligned}
P^{(1)} &= (P_1^{(1)}, R_2 r, R_3 r^2, R_4 r^3),\\
P^{(2)} &= (P_1^{(2)}, -R_2 r, R_3 r^2, R_4 r^3),\\
P^{(3)} &= (P_1^{(3)}, R_2 r, -R_3 r^2, R_4 r^3),\\
P^{(4)} &= (P_1^{(4)}, -R_2 r, -R_3 r^2, R_4 r^3),\\
P^{(5)} &= (P_1^{(5)}, R_2 r, R_3 r^2, -R_4 r^3),\\
P^{(6)} &= (P_1^{(6)}, -R_2 r, R_3 r^2, -R_4 r^3),\\
P^{(7)} &= (P_1^{(7)}, R_2 r, -R_3 r^2, -R_4 r^3),\\
P^{(8)} &= (P_1^{(8)}, -R_2 r, -R_3 r^2, -R_4 r^3).
\end{aligned} \tag{7.14}$$

By using the expression (7.5) for $E^s(Y)$, we obtain the following formula for $P_1^{(i)}$:

$$P_1^{(i)} = \frac{1}{1 + \sum_{m=1}^{N} a_L^m} \left[1 - \sum_{k=1}^{N-1} \frac{\sum_{j=k+1}^{N} a_L^j}{(\lambda_L^1)^k} \right] - \sum_{l=1}^{N-1} \frac{\sigma_{l+1}^{(i)} R_{l+1} r^l}{(\lambda_L^1)^l}. \tag{7.15}$$

Also $f_\xi\big(P^{(i)}\big)$ is given by

$$\begin{aligned}
f_\xi(P^{(i)}) = \Big(& -a_L^1 P_1^{(i)} + \sigma_2^{(i)} R_2 r + 1, -a_L^2 P_1^{(i)} + \sigma_3^{(i)} R_3 r^2,\\
& -a_L^3 P_1^{(i)} + \sigma_4^{(i)} R_4 r^2, \ldots,\\
& -a_L^{N-1} P_1^{(i)} + \sigma_N^{(i)} R_N r^{N-1}, -a_L^N P_1^{(i)} \Big).
\end{aligned} \tag{7.16}$$

To facilitate further calculations we introduce the quantities $\xi_0 = 1$, $\xi_1 = \sum_{i=2}^{N} \eta_L^i$, $\xi_2 = \sum_{i=2}^{N} \sum_{j=i+1}^{N} \eta_L^i \eta_L^j$, …, $\xi_k = \underbrace{\sum_{i=1}^{N-k+1} \cdots \sum_{l=j+1}^{N}}_{k \text{ terms}} \underbrace{\eta_L^i \eta_L^j \ldots \eta_L^l}_{k \text{ terms}}$, …, $\xi_{N-1} = \underbrace{\eta_L^2 \eta_L^3 \ldots \eta_L^N}_{N-1 \text{ terms}}$,

and $\xi_N = 0$. Then (7.10) can be re-written as

$$\begin{aligned}
a_L^1 &= -(\lambda_L^1 + \xi_1 r) \\
a_L^2 &= \lambda_L^1 \xi_1 r + \xi_2 r^2 \\
a_L^3 &= -(\lambda_L^1 \xi_2 r^2 + \xi_3 r^3) \\
&\vdots \\
a_L^k &= (-1)^k (\lambda_L^1 \xi_{k-1} r^{k-1} + \xi_k r^k) \\
&\vdots \\
a_L^{N-1} &= (-1)^{N-1} (\lambda_L^1 \xi_{N-2} r^{N-2} + \xi_{N-1} r^{N-1}) \\
a_L^N &= (-1)^N \xi_{N-1} r^{N-1}.
\end{aligned} \tag{7.17}$$

The intersection of Ω with the switching manifold $x_1 = 0$ is a convex polytope with 2^{N-1} vertices. Each vertex is a point $S^{(i)}$ given by where the line through $P^{(i)}$ (a point in K) and C intersects the switching manifold, thus is given by

$$\begin{aligned}
S^{(i)} = \Bigg(0, \frac{C_1}{C_1 - P_1^{(i)}} \sigma_2^{(i)} R_2 r, \frac{C_1}{C_1 - P_1^{(i)}} \sigma_3^{(i)} R_3 r^2, \\
\ldots, \frac{C_1}{C_1 - P_1^{(i)}} \sigma_{N-1}^{(i)} R_{N-1} r^{N-2}, \frac{C_1}{C_1 - P_1^{(i)}} \sigma_N^{(i)} R_N r^{N-1} \Bigg).
\end{aligned} \tag{7.18}$$

The images of these points are given simply by

$$f_\xi\big(S^{(i)}\big) = \begin{bmatrix} S_2^{(i)} + 1 \\ S_3^{(i)} \\ \vdots \\ S_N^{(i)} \\ 0 \end{bmatrix}. \tag{7.19}$$

To show that Ω is forward invariant under f, it remains to show that $f_\xi(C)$ and each point (7.16) and (7.19) lies inside Ω. This requires us to consider every face (side) of Ω which is daunting task, and left for future work. But preliminary calculations are promising: by defining H so that the bounds on the components accumulate powers of the small quantity r, we expect the vertices of Ω to map inside Ω because the action of the f shifts components up one place, as evident, for instance, in (7.19). In fact it appears we can obtain an explicit value r_{critical} such that Conjecture 7.1 holds for all $r < r_{\text{critical}}$. Our formula for

$r_{\rm critical}$ is a minimum of nine quantities. Often only three of these quantities are relevant, in which case $r_{\rm critical}$ has the form

$$r_{\rm critical} = \min\Bigg(\frac{1-\frac{1}{\beta}}{2^{N-1}(N-3)+(2^{N-1}-1)\{\alpha\lambda_L^1 2^{N-1}-\left(1-\frac{1}{\beta}\right)\}},$$
$$(\lambda_L^1)^N\left(1-\frac{1}{\gamma}\right)\frac{1}{\Gamma_1-\Gamma_2-\Gamma_3},$$
$$\frac{|\lambda_R^1|}{\gamma\lambda_L^1 R_2}\left[\frac{\lambda_L^1}{\gamma|\lambda_R^1|}+\frac{1}{\beta}\right]\Bigg), \tag{7.20}$$

where α, β, and γ are parameters satisfying

$$1 \le \beta < \alpha,$$
$$1 \le \gamma \le \frac{\lambda_L^1}{(\lambda_L^1-1)|\lambda_R^1|}, \tag{7.21}$$

and

$$\Gamma_1 = (\lambda_L^1)^{N-1}(\lambda_L^1+1)(2^{N-1}-1)+(\lambda_L^1)^N[(\lambda_L^1(N-1)+N-3)2^{N-2}+1],$$
$$\Gamma_2 = \frac{(\lambda_L^1)^N}{|\lambda_R^1|}(2^{N-1}-1)[|\lambda_R^1|+(\lambda_L^1-\lambda_R^1)2^{N-1}],$$
$$\Gamma_3 = \frac{(\lambda_L^1)^N\gamma}{|\lambda_R^1|}\left(1-\frac{1}{\gamma}\right)(\lambda_L^1-\lambda_R^1)(2^{N-1}-1)2^{N-1}. \tag{7.22}$$

The value $r_{\rm critical}$ is plotted in Fig. 7.1 for $N = 3$. Here we have used $\lambda_L^2 = 0.07$, $\lambda_L^3 = 0.087$, $\lambda_R^2 = -0.04$, and $\lambda_R^3 = -0.05$, and set the three parameter values as $\gamma = \frac{1}{2}\left(1+\frac{\lambda_L^1}{(\lambda_L^1-1)|\lambda_R^1|}\right)$, $\beta = \gamma$, and $\alpha = \gamma^2$. Notice $r_{\rm critical}$ tends to zero at the boundary $\phi_0(\lambda_L^1, \lambda_R^1) = 0$. Thus our bound is positive over the largest possible range for the values of the unstable eigenvalues because, as mentioned above, beyond this boundary there is no attractor in the limit $r \to 0$.

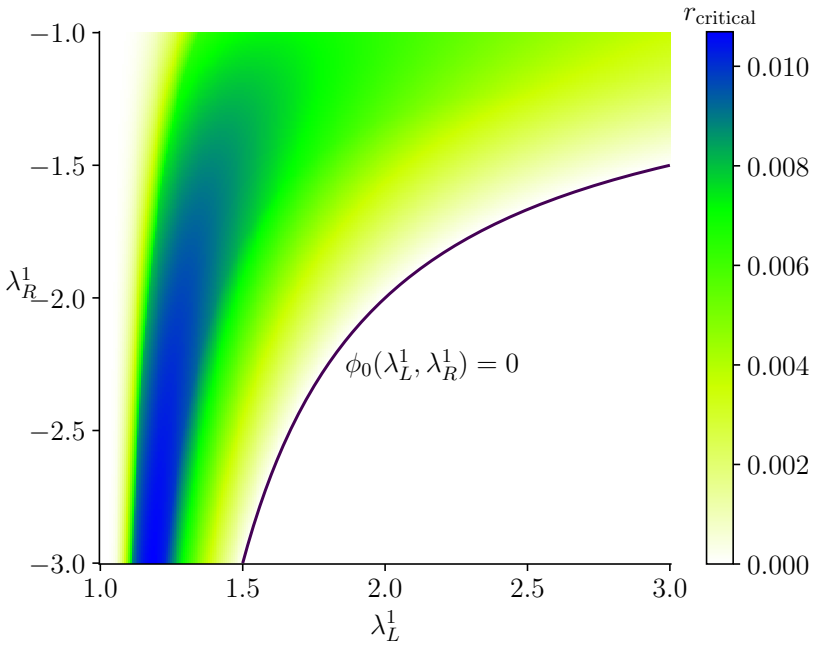

Figure 7.1: A heat map showing the value of r_{critical} (7.20).

Chapter 8

Conclusions

This thesis has relied mainly on three techniques for understanding the dynamics of piecewise-linear maps: trapping regions, invariant expanding cones and renormalisation. Trapping regions are a relatively elementary tool that provide a way for us to prove the map has an attractor. Invariant expanding cones allow us to show an attractor is chaotic; they are more niche but have been applied to diverse types of dynamical systems at least since the work of Alekseev [2]. Renormalisation is used to identify bifurcations and common dynamics in different parameter regions. This also is fairly specialised but has been applied to many problems in dynamical systems, perhaps most famously by Feigenbaum in regards to period-doubling cascades.

While many papers have studied the dynamics of multi-dimensional piecewise-linear maps, it seems that few have applied the above techniques. This thesis shows they are highly effective for piecewise-linear maps. For trapping regions is often suffices to consider simple polygons. For invariant expanding cones the expansion condition only needs to hold for each piece of the map, which is far easier to check than for smooth maps where the Jacobian matrix varies throughout phase space. Indeed in Chapter 5 a suitable cone was constructed by using eigenvectors of the two Jacobian matrices. Finally for renormalisation in our setting the dimension of the renormalisation operator is finite.

Specifically for the two-dimensional border-collision normal form (2.21) in the orientation-preserving setting we applied renormalisation in Chapter 3. This enabled us to partition the parameter space into regions $\mathcal{R}_n$ where (2.21) has an attractor with 2^n connected components. It is also interesting to consider the analogy of Feigenbaum's constant in our setting. The regions $\mathcal{R}_n$ converge to ξ, and the 4×4 Jacobian matrix $\mathrm{D}g(\xi^*)$ has exactly one unstable eigenvalue: 2. It follows that the diameter of $\mathcal{R}_n$ divided by the diameter of $\mathcal{R}_{n+1}$ tends, as $n \to \infty$, to the constant 2. In contrast, as discussed in §2.8, Feigenbaum's constant for the rate of convergence of consecutive period-doubling bifurcations is

approximately 4.6692.

In Chapter 4 we strengthened Theorem 3.2 by proving that in a subregion of $\mathcal{R}_0$, the attractor satisfies Devaney's definition of chaos. In particular we used the condition $J_1(\xi) > 1$ to show that line segments grow sufficiently quickly when iterated under the map. It remains to identify different and presumably more powerful methods to verify the conjecture that $J_1(\xi) > 1$ can in fact be replaced by the weaker condition $\phi(g(\xi)) < 0$.

Furthermore we extended the construction from the orientation-preserving setting to the orientation-reversing and non-invertible settings in Chapter 5. Specifically we identified an open parameter region $\Phi_{\rm trap}$, where the map has a trapping region, and an open parameter region $\Phi_{\rm cone}$, where it has an invariant expanding cone, see Figs. 5.2 and 5.3. Throughout $\Phi_{\rm trap} \cap \Phi_{\rm cone}$ the map has an attractor with a positive Lyapunov exponent, Theorem 5.1. At some boundaries of $\Phi_{\rm trap} \cap \Phi_{\rm cone}$ the attractor is destroyed, see Fig. 5.9, in which case our construction is optimal in that it identifies bifurcations where the attractor is destroyed. Past other boundaries the chaotic attractor persists. We expect our construction could be adapted to verify robust chaos beyond these boundaries, and already this has been achieved in some cases [59, 129]. Within $\Phi_{\rm trap} \cap \Phi_{\rm cone}$ the attractor appears to undergo bifurcations like in the orientation-preserving case where the number of connected components changes. In Chapter 6 we explored this numerically and showed how renormalisation appears to remain effective in this more general setting, but there are some unique complications such as stable period-2 and period-4 solutions and the presence of other possibly fractal bifurcation curves. It remains to verify the conjectures in §6.6–§6.8 which we believe should be managable by employing the ideas used in Chapter 3. But we feel this would likely be a major undertaking because it is necessary to understand in detail the dynamics of the renormalisation operator by extending the extensive calculations performed in §3.6. Also it remains to see if renormalisation schemes based on other symbolic substitution rules can be used to explain parameter regimes where (2.21) has attractors with other numbers of components, e.g. three components, as described in [57].

We stress that in Fig. 5.9 the cross-section of $\Phi_{\rm trap} \cap \Phi_{\rm cone}$ includes a neighbourhood of $(\delta_L, \delta_R) = (0, 0)$. This is the case for many values of τ_L and τ_R and is a significant achievement because it shows robust chaos is not lost as we cross from the orientation-preserving setting to the orientation-reversing and non-invertible settings. Thus the presence of robust chaos is not dependent on the overall topological properties of the map. Moreover, this provides a path for robust chaos to be demonstrated in higher dimensional maps. This was explored in Chapter 7 where we considered the N-dimensional border-collision normal form with two saddle fixed points: X with an eigenvalue $\lambda_R^u < -1$, and Y with an

eigenvalue $\lambda_L^u > 1$. If all other eigenvalues associated with X and Y have modulus at most r, where $r > 0$ is small (which in two dimensions means (δ_L, δ_R) is sufficiently close to $(0, 0)$), and with appropriate constraints on the values of λ_R^u and λ_L^u, we believe the map must have a chaotic attractor. We expect this can be proved by again constructing a trapping region and an invariant expanding cone. Conjecture 7.1 suggests how the trapping region can be constructed for the N-dimensional setting by choosing vertices $P^{(i)}$ whose j^{th} component is proportional to r^{j-1}. For the cone we expect it will be too difficult to use eigenvectors of the Jacobian matrices as in Chapter 5. Instead we envisage a weaker construction that again utilises powers of r. As one application, it is hoped that this could be used as the key space for an encryption scheme [79].

The main motivation for studying two-piece piecewise-linear maps is that they approximate the dynamics near border-collision bifurcations arising in diverse physical systems. As explained in Chapter 1 the piecewise-linear form arises from dropping higher order terms. Naturally we would like assurance that the dynamics we have described for the piecewise-linear map is retained in the full map. In general the dynamics does appear to retained typically, but for chaotic attractors this is difficult to prove. Recently Simpson and Glendinning [131] showed that trapping regions and invariant expanding cones are robust to higher order terms so in case the chaotic attractor persists.

A tantalising avenue of future research would be to apply our methods to maps having more than two pieces. Such maps have been used as mathematical models in areas such as neuronal dynamics [71] and economics [24]. Also our methods should apply well to discontinuous piecewise-linear maps, indeed Li *et al.* [87] have achieved this for a family of two-dimensional discontinuous maps.

In regards to higher dimensions as a first step we have focussed on the case that the map has one direction of instability for each piece of the map. But maps with multiple directions of instability should be just as relevant, giving the possibility of so-called wild chaos [69, 75], and it remains to treat these scenarios. Already Glendinning [53] has considered the case that all directions are unstable in any number of dimensions and rigorously proven the existence of a chaotic attractor.

Overall the dynamics of piecewise-smooth maps is extraodinarily rich because they have an extreme form of nonlinearity. Many open problems remain, as described above, another example being the uniqueness of the attractor, which seems to be an exciting and important direction to look into. Remarkably it is still unknown whether or not the normal form can exhibit more than one attractor throughout the robust chaos parameter region of Banerjee *et al.* [14], and the more generalised parameter seetings where the normal form is

orientation-reversing and non-invertible.

Bibliography

[1] R.H. Abraham, L. Gardini, and C. Mira. *Chaos in Discrete Dynamical Systems: A Visual Introduction in 2 Dimensions*. Springer New York, NY, 1997.

[2] V.M. Alekseev. Quasirandom dynamical systems. I. Quasirandom diffeomorphisms. *Math. USSR Sb.*, 5:73–128, 1968.

[3] K. T. Alligood, T. D. Sauer, and J. A. Yorke. *Chaos: an introduction to dynamical systems*. Springer New York, NY, 1997.

[4] G. Alvarez, F. Montoya, M. Romera, and G. Pastor. Cryptanalysis of a discrete chaotic cryptosystem using external key. *Phys. Lett. A*, 319(3-4):334–339, 2003.

[5] J. Alves, A. Pumariño, and E. Vigil. Statistical stability for multidimensional piecewise expanding maps. *Proc. Amer. Math. Soc.*, 145(7):3057–3068, 2017.

[6] J.A. Amador, G. Olivar, and F. Angulo. Smooth and Filippov models of sustainable development: Bifurcations and numerical computations. *Differ. Equ. Dyn.*, 21:173–184, 2013.

[7] V. Avrutin, B. Eckstein, and M. Schanz. On detection of multi-band chaotic attractors. *Proc. R. Soc. A*, 463(2081):1339–1358, 2007.

[8] J. Awrejcewicz and C. Lamarque. *Bifurcation and chaos in nonsmooth mechanical systems*. World Scientific, 2003.

[9] M. Babaei. A novel text and image encryption method based on chaos theory and DNA computing. *Nat. Comput.*, 12(1):101–107, 2013.

[10] S. Banerjee and C. Grebogi. Border collision bifurcations in two-dimensional piecewise smooth maps. *Phys. Rev. E*, 59(4):4052–4061, 1999.

[11] S. Banerjee, M.S. Karthik, G. Yuan, and J.A. Yorke. Bifurcations in one-dimensional piecewise smooth maps-theory and applications in switching circuits. *IEEE Trans. Circuits Systems I: Fund. Theory Appl.*, 47(3):389–394, 2000.

[12] S. Banerjee and G.C. Verghese. *Nonlinear phenomena in power electronics*. IEEE Piscataway Township, NJ, USA, 1999.

[13] S. Banerjee and G.C. Verghese, editors. *Nonlinear Phenomena in Power Electronics*. IEEE Press, New York, 2001.

[14] S. Banerjee, J.A. Yorke, and C. Grebogi. Robust chaos. *Phys. Rev. Lett.*, 80(14):3049–3052, 1998.

[15] J. Banks, J. Brooks, G. Cairns, G. Davis, and P. Stacey. On Devaney's definition of chaos. *Amer. Math. Monthly*, 99(4):332–334, 1992.

[16] S. Behnia, A. Akhshani, H. Mahmodi, and A. Akhavan. A novel algorithm for image encryption based on mixture of chaotic maps. *Chaos Solit.*, 35(2):408–419, 2008.

[17] M.V. Berry. Quantum chaology (the Bakerian lecture). In *A Half-Century of Physical Asymptotics and Other Diversions: Selected Works by Michael Berry*, pages 307–322. World Scientific, 1987.

[18] B. Blazejczyk-Okolewska. *Chaotic mechanics in systems with impacts and friction*. World Scientific, 1999.

[19] C. Bonatti, L. J. Díaz, and M. Viana. *Dynamics beyond uniform hyperbolicity: A global geometric and probabilistic perspective*. Springer, 2005.

[20] B. Brogliato and B. Brogliato. *Nonsmooth mechanics*. Springer, 1999.

[21] C. Brooks. Chaos in foreign exchange markets: a sceptical view. *Comput. Econ.*, 11:265–281, 1998.

[22] V.A. Brousin, Yu.I. Neimark, and M.I. Feigin. On some cases of dependence of periodic motions of relay system upon parameters. *Izv. Vyssh. Uch. Zav. Radiofizika*, 4:785–800, 1963. In Russian.

[23] J. Caballé, X. Jarque, and E. Michetti. Chaotic dynamics in credit constrained emerging economies. *J. Econ. Dyn. Control*, 30(8):1261–1275, 2006.

[24] G. Campisi, A. Panchuk, and F. Tramontana. A discontinuous model of exchange rate dynamics with sentiment traders. To appear *Ann. Operat. Res.*, 2023.

[25] A. Colombo. Boundary intersection crossing bifurcation in the presence of sliding. *Phys. D*, 237(22):2900–2912, 2008.

[26] F.B. Cunha, D.J. Pagano, and U.F. Moreno. Sliding bifurcations of equilibria in planar variable structure systems. *IEEE Trans. Circuits Systems I: Fund. Theory Appl.*, 50(8):1129–1134, 2003.

[27] J.H.B. Deane. Chaos in a current-mode controlled boost DC-DC converter. *IEEE Trans. Circuits Systems I: Fund. Theory Appl.*, 39(8):680–683, 1992.

[28] J.H.B. Deane and D.C. Hamill. Improvement of power supply EMC by chaos. *Electron. Lett.*, 32(12):1045, 1996.

[29] O. Decroly and A. Goldbeter. From simple to complex oscillatory behaviour: analysis of bursting in a multiply regulated biochemical system. *J. Theor. Biol.*, 124(2):219–250, 1987.

[30] F. Dercole, A. Gragnani, Yu.A. Kuznetsov, and S. Rinaldi. Numerical sliding bifurcation analysis: An application to a relay control system. *IEEE Trans. Circuits Systems I: Fund. Theory Appl.*, 50(8):1058–1063, 2003.

[31] F. Dercole, A. Gragnani, and S. Rinaldi. Bifurcation analysis of piecewise smooth ecological models. *Theor. Popul. Biol.*, 72(2):197–213, 2007.

[32] R. Devaney. *An introduction to chaotic dynamical systems*. Addison-Wesley, 2nd edition, 1989.

[33] M. di Bernardo. Normal forms of border collisions in high-dimensional nonsmooth maps. In *Proceedings of the 2003 International Symposium on Circuits and Systems, 2003. ISCAS'03.*, volume 3, pages III–III. IEEE, 2003.

[34] M. di Bernardo, C. Budd, and A. Champneys. Grazing, skipping and sliding: analysis of the non-smooth dynamics of the DC/DC buck converter. *Nonlinearity*, 11(4):859, 1998.

[35] M. di Bernardo, C. Budd, A.R. Champneys, and P. Kowalczyk. *Piecewise-smooth dynamical systems: theory and applications*. Springer-Verlag, New York, 2008.

[36] M. di Bernardo, C.J. Budd, and A.R. Champneys. Corner collision implies border-collision bifurcation. *Phys. D*, 154(3-4):171–194, 2001.

[37] M. di Bernardo, K.H. Johansson, and F. Vasca. Self-oscillations and sliding in relay feedback systems: Symmetry and bifurcations. *Int. J. Bifurcation Chaos*, 11(04):1121–1140, 2001.

[38] M. di Bernardo, P. Kowalczyk, and A. Nordmark. Bifurcations of dynamical systems with sliding: Derivation of normal-form mappings. *Phys. D*, 170:175–205, 2002.

[39] M. di Bernardo, P. Kowalczyk, and A. Nordmark. Sliding bifurcations: a novel mechanism for the sudden onset of chaos in dry friction oscillators. *Int. J. Bifurcation Chaos*, 13(10):2935–2948, 2003.

[40] M. di Bernardo, P. Kowalczyk, and A. Nordmark. Sliding Bifurcations: A novel mechanism for the Sudden Onset of Chaos in Dry Friction Oscillators. *Int. J. Bifurcation Chaos*, 13(10):2935–2948, 2003.

[41] M. di Bernardo and C.K. Tse. Chaos in power electronics: An overview. *Chaos in circuits and systems*, pages 317–340, 2002.

[42] R. Dilão and T. Domingos. Periodic and quasi-periodic behavior in resource-dependent age structured population models. *Bull. Math. Biol.*, 63(2):207–230, 2001.

[43] R.W. Easton. *Geometric methods for discrete dynamical systems*. Number 50. Oxford University Press, USA, 1998.

[44] B. Eckstein. *Bandcounter: counting bands of multiband chaotic attractors*. Universitätsbibliothek der Universität Stuttgart, 2006.

[45] R. Edwards and L. Glass. Dynamics in genetic networks. *Amer. Math. Monthly*, 121(9):793–809, 2014.

[46] H.O. Fatoyinbo and D.J.W. Simpson. A synopsis of the non-invertible, two-dimensional, border-collision normal form with applications to power converters. *Int. J. Bifurcation Chaos*, 33(8):2330019, 2023.

[47] M.I. Feigin. Doubling of the oscillation period with C-bifurcations in piecewise continuous systems. *J. Appl. Math. Mech.*, 34(5):822–830, 1970. Translation of *Prikl. Mat. Mekh.*, 34(5):861-869, 1970.

[48] M.I. Feigin. On the structure of C-bifurcation boundaries of piecewise-continuous systems. *J. Appl. Math. Mech.*, 42(5):885–895, 1978. Translation of *Prikl. Mat. Mekh.*, 42(5):820-829, 1978.

[49] A.F. Filippov. Differential equations with discontinuous right-hand side. *Mat. Sb.*, 93(1):99–128, 1960.

[50] M. Gallegati, L. Gardini, T. Puu, and I. Sushko. Hicks' trade cycle revisited: cycles and bifurcations. *Math. Comput. Simul.*, 63(6):505–527, 2003.

[51] O. Galor. *Discrete dynamical systems*. Springer Science & Business Media, 2007.

[52] P. Glendinning. *Stability, instability and chaos: an introduction to the theory of nonlinear differential equations*. Cambridge university press, 1994.

[53] P. Glendinning. Bifurcation from stable fixed point to N-dimensional attractor in the border collision normal form. *Nonlinearity*, 28:3457–3464, 2015.

[54] P. Glendinning. Bifurcation from stable fixed point to 2D attractor in the border collision normal form. *IMA J. Appl. Math.*, 81(4):699–710, 2016.

[55] P. Glendinning. Robust chaos revisited. *Eur. Phys. J. Special Topics*, 226(9):1721–1738, 2017.

[56] P. Glendinning and C.H. Wong. Two dimensional attractors in the border-collision normal form. *Nonlinearity*, 24(4):995–1010, 2011.

[57] P. A. Glendinning and D. J. W. Simpson. Robust chaos and the continuity of attractors. *Trans. Math. Appl.*, 4(1):tnaa002, 2020.

[58] P. A Glendinning and D.J.W. Simpson. A constructive approach to robust chaos using invariant manifolds and expanding cones. *Discrete Contin. Dyn. Syst.*, 41(7):3367–3387, 2021.

[59] P.A. Glendinning and D.J.W. Simpson. Chaos in the border-collision normal form: A computer-assisted proof using induced maps and invariant expanding cones. *Appl. Math. Comput.*, 434:127357, 2022.

[60] A. S. Gonchenko, S. V. Gonchenko, A. O. Kazakov, and A. D. Kozlov. Elements of contemporary theory of dynamical chaos: A tutorial. Part I. Pseudohyperbolic attractors. *Int. J. Bifurcation Chaos*, 28(11):1830036, 2018.

[61] S. Gonchenko, A. Kazakov, and D. Turaev. Wild pseudohyperbolic attractor in a four-dimensional Lorenz system. *Nonlinearity*, 34(4):2018–2047, 2021.

[62] C. Grebogi, E. Ott, and J.A. Yorke. Crises, sudden changes in chaotic attractors, and transient chaos. *Phys. D*, 7(1-3):181–200, 1983.

[63] J. Guckenheimer and P. Holmes. *Nonlinear oscillations, dynamical systems, and bifurcations of vector fields*. Springer Science & Business Media, 2013.

[64] J. Guckenheimer and R. F. Williams. Structural stability of Lorenz attractors. *Publ. Math. IHES*, 50:59–72, 1979.

[65] F. Haake. *Quantum signatures of chaos*. Springer, 1991.

[66] P. Hartman. On local homeomorphisms of Euclidean spaces. *Bol. Soc. Mat. Mexicana*, 5(2):220–241, 1960.

[67] N. Haydn, Y. Lacroix, and S. Vaienti. Hitting and return times in ergodic dynamical systems. *Ann. Probab.*, 33(5):2043–2050, 2005.

[68] S. Hittmeyer, B. Krauskopf, H. M. Osinga, and K. Shinohara. Existence of blenders in a Hénon-like family: Geometric insights from invariant manifold computations. *Nonlinearity*, 31(10):R239–R267, 2018.

[69] S. Hittmeyer, B. Krauskopf, and H.M. Osinga. Interacting global invariant sets in a planar map model of wild chaos. *SIAM J. Appl. Dyn. Sys.*, 12(3):1280–1329, 2013.

[70] C.H. Hommes, H.E. Nusse, and A. Simonovits. Cycles and chaos in a socialist economy. *J. Econ. Dyn. Control*, 19(1-2):155–179, 1995.

[71] B. Ibarz, J.M. Casado, and M.A.F. Sanjuán. Map-based models in neuronal dynamics. *Phys. Rep.*, 501:1–74, 2011.

[72] S. Ito, H. Nakada, and S. Tanaka. On Unimodal Linear Transformations and Chaos II. *Tokyo J. Math.*, 2(2):241–259, 1979.

[73] S. Ito, S. Tanaka, and H. Nakada. On unimodal linear transformations and chaos. *Proc. Japan Acad. Ser. A*, 55:231–236, 1979.

[74] M.R. Jeffrey and S.J. Hogan. The geometry of generic sliding bifurcations. *SIAM Rev.*, 53(3):505–525, 2011.

[75] H. Jelleyman and H.M. Osinga. Matching geometric and expansion characteristics of wild chaotic attractors. *Eur. Phys. J. Spec. Top.*, 231(3):403–412, 2022.

[76] M. Johansson. *Piecewise linear control systems*. PhD thesis, Lund Institute of Technology, Sweden, 1999.

[77] F. Juárez. Applying the theory of chaos and a complex model of health to establish relations among financial indicators. *Procedia Comput. Sci.*, 3:982–986, 2011.

[78] E. Karatetskaia, A. Shykhmamedov, and A. Kazakov. Shilnikov attractors in three-dimensional orientation-reversing maps. *Chaos*, 31:011102, 2021.

[79] L. Kocarev and S. Lian, editors. *Chaos-Based Cryptography: Theory, Algorithms and Applications*. Springer, New York, 2011.

[80] P. Kowalczyk. Robust chaos and border-collision bifurcations in non-invertible piecewise-linear maps. *Nonlinearity*, 18(2):485, 2005.

[81] P. Kucharski. Strange attractors for the family of orientation preserving Lozi maps. *arXiv:2211.10296*, 2022.

[82] A. Kumar, S.F. Ali, and A. Arockiarajan. Enhanced energy harvesting from nonlinear oscillators via chaos control. *IFAC-PapersOnLine*, 49(1), 2016.

[83] Y.A. Kuznetsov. *Elements of applied bifurcation theory*. Springer, 2004.

[84] C. Kyrtsou and W.C. Labys. Evidence for chaotic dependence between US inflation and commodity prices. *J. Macroecon.*, 28(1):256–266, 2006.

[85] A. Lasota and J.A. Yorke. On the existence of invariant measures for piecewise monotonic transformations. *Trans. Amer. Math. Soc.*, 186:481–488, 1973.

[86] J. Laugesen and E. Mosekilde. Border-collision bifurcations in a dynamic management game. *Comput. Oper. Res.*, 33(2):464–478, 2006.

[87] D. Li, P. Miao, J. Xie, and C. Grebogi. Hausdorff dimension of chaotic attractors in a class of nonsmooth systems. *Chaos Solit.*, 151:111218, 2021.

[88] T. Li and J.A. Yorke. Ergodic transformations from an interval into itself. *Trans. Amer. Math. Soc.*, 235(1):183–192, 1978.

[89] C. Liu, A. Di Falco, D. Molinari, Y. Khan, B.S. Ooi, T.F. Krauss, and A. Fratalocchi. Enhanced energy storage in chaotic optical resonators. *Nature Photon.*, 7:473–478, 2013.

[90] E. Liz and A. Ruiz-Herrera. Chaos in discrete structured population models. *SIAM J. Appl. Dyn. Sys.*, 11(4):1200–1214, 2012.

[91] E. Lorenz. Predictability: Does the flap of a butterfly's wing in Brazil set off a tornado in Texas? 1972.

[92] R. Lozi. Un attracteur étrange (?) du type attracteur de Hénon. *J. Phys. (Paris)*, 39(C5):9–10, 1978. In French.

[93] R. MacKay. *Renormalisation in Area-preserving maps*. World Scientific, Singapore, 1993.

[94] Yu.L. Maistrenko, V.L. Maistrenko, and L.O. Chua. Cycles of chaotic intervals in a time-delayed Chua's circuit. *Int. J. Bifurcation Chaos.*, 3(6):1557–1572, 1993.

[95] F.R. Marotto. Snap-back repellers imply chaos in $\mathbb{R}^n$. *J. Math. Anal. Appl.*, 63(1):199–223, 1978.

[96] F.R. Marotto. On redefining a snap-back repeller. *Chaos Solit.*, 25(1):25–28, 2005.

[97] P. Miao, D. Li, Y. Yue, J. Xie, and C. Grebogi. Chaotic attractor of the normal form map for grazing bifurcations of impact oscillators. *Phys. D*, 398:164–170, 2019.

[98] J. Milnor. On the concept of attractor. *Commun. Math. Phys.*, 99:177–195, 1985.

[99] M. Misiurewicz. Strange attractors for the Lozi mappings. *Nonlinear dynamics, Annals of the New York Academy of Sciences*, 357(1):348–358, 1980.

[100] A. Morbidelli. Chaotic diffusion in celestial mechanics. *Regul. Chaotic Dyn.*, 6(4):339–353, 2001.

[101] P.J. Myrberg. Iteration von quadratwurzeloperationen. *Ann. Acad. Sci. Fenn.*, 259:2–16, 1958. In German.

[102] H.E. Nusse and J.A. Yorke. Border-collision bifurcations including "period two to period three" for piecewise smooth systems. *Phys. D*, 57(1-2):39–57, 1992.

[103] H.E. Nusse and J.A. Yorke. Border-collision bifurcations for piecewise-smooth one-dimensional maps. *Int. J. Bifurcation Chaos.*, 5(1):189–207, 1995.

[104] P.J. Olver and C. Shakiban. *Applied linear algebra*. Springer, 2006.

[105] H. M. Osinga. Boundary crisis bifurcation in two parameters. *J. Diff. Eq. Appl.*, 12(10):997–1008, 2006.

[106] G. Osorio, M. di Bernardo, and S. Santini. Corner-impact bifurcations: a novel class of discontinuity-induced bifurcations in cam-follower systems. *SIAM J. Appl. Dyn. Sys.*, 7(1):18–38, 2008.

[107] G. Ostrovski. Dynamics of a continuous piecewise affine map of the square. *Phys. D*, 271:1–9, 2014.

[108] D. Ou. Critical points in higher dimensions, I: Reverse order of periodic orbit creations in the Lozi family. *arXiv preprint arXiv:2203.02326*, 2022.

[109] J. Palis and W. de Melo. *Geometric theory of dynamical systems. An introduction*. Springer-Verlag, 1982.

[110] J. Palis and F. Takens. *Hyperbolicity and sensitive chaotic dynamics at homoclinic bifurcations*. Cambridge University Press, New York, 1993.

[111] S.H. Piltz, M.A. Porter, and P.K. Maini. Prey switching with a linear preference trade-off. *SIAM J. Appl. Dyn. Sys.*, 13(2):658–682, 2014.

[112] A. Pumariño, J. Á. Rodríguez, and E. Vigil. Renormalization of two-dimensional piecewise linear maps: Abundance of 2-D strange attractors. *Discrete Contin. Dyn. Syst.*, 38:941–966, 2018.

[113] A. Pumariño, J. Á. Rodríguez, and E. Vigil. Persistent two-dimensional strange attractors for a two-parameter family of expanding Baker maps. *Discrete Contin. Dyn. Syst. Ser. B*, 24(2):657–670, 2019.

[114] T. Puu and I. Sushko. *Business Cycle Dynamics: Models and Tools.* Springer-Verlag, New York, 2006.

[115] M.G. Roberts, R.I. Hickson, J.M. McCaw, and L. Talarmain. A simple influenza model with complicated dynamics. *J. Math. Bio.*, 78(3):607–624, 2019.

[116] V. Robins, J.D. Meiss, and E. Bradley. Computing connectedness: Disconnectedness and discreteness. *Phys. D*, 139(3–4):276–300, 2000.

[117] R. Robinson. *An introduction to dynamical systems: continuous and discrete*. Prentice Hall, Upper Saddle River, NJ, 2004.

[118] N.F. Rulkov. Modeling of spiking-bursting neural behavior using two-dimensional map. *Phys. Rev. E*, 65(4):041922, 2002.

[119] J.T. Sandefur. *Discrete dynamical systems: Theory and applications*. Clarendon Press, 1990.

[120] E. Sander and J.A. Yorke. Chaos and its manifestations. *SIAM News.*, 48(7), 2015.

[121] E. Sataev. Ergodic properties of the Belykh map. *J. Math. Sci.*, 95(5):2564–2575, 1999.

[122] A. Sfondrini. An introduction to universality and renormalization group techniques. *arXiv preprint arXiv:1210.2262*, 2012.

[123] J. Sieber. Dynamics of delayed relay systems. *Nonlinearity*, 19(11):2489, 2006.

[124] J. Sieber and P. Kowalczyk. Event collisions in systems with delayed switches. *IFAC Proceedings Volumes*, 39(10):66–71, 2006.

[125] D.J.W. Simpson. Sequences of periodic solutions and infinitely many coexisting attractors in the border-collision normal form. *Int. J. Bifurcation Chaos*, 24(06):1430018, 2014.

[126] D.J.W Simpson. Border-collision bifurcations in $\mathbb{R}^n$. *SIAM Rev.*, 58(2):177–226, 2016.

[127] D.J.W. Simpson. Unfolding homoclinic connections formed by corner intersections in piecewise-smooth maps. *Chaos*, 26(7):073105, 2016.

[128] D.J.W. Simpson. The structure of mode-locking regions of piecewise-linear continuous maps: I. Nearby mode-locking regions and shrinking points. *Nonlinearity*, 30(1):382–444, 2017.

[129] D.J.W. Simpson. Detecting invariant expanding cones for generating word sets to identify chaos in piecewise-linear maps. *J. Difference Eq. Appl.*, pages 1–33, 2022.

[130] D.J.W. Simpson. Border-collision bifurcations from stable fixed points to any number of coexisting chaotic attractors. *J. Difference Eq. Appl.*, pages 1–21, 2023.

[131] D.J.W. Simpson and P.A. Glendinning. Inclusion of higher-order terms in the border-collision normal form: Persistence of chaos and applications to power converters. *arXiv preprint arXiv:2111.12222*, 2021.

[132] S. Smale. Differentiable dynamical systems. *Bull. Amer. Math. Soc.*, 73(6):747–817, 1967.

[133] S. Strogatz. *Nonlinear Dynamics and Chaos: With Applications to Physics, Biology, Chemistry, and Engineering, Second Edition*. 2014.

[134] I. Sushko, V. Avrutin, and L. Gardini. Bifurcation structure in the skew tent map and its application as a border collision normal form. *J. Diff. Eq. Appl.*, 22(8):1040–1087, 2016.

[135] R. Szalai and H. M. Osinga. Invariant polygons in systems with grazing-sliding. *Chaos*, 18(2):023121, 2008.

[136] D. Towers, D. Edwards, and M. Hamson. *Guide to mathematical modelling*. Macmillan Education, UK, 2001.

[137] W. Tucker. The Lorenz attractor exists. *C. R. Acad. Sci. Paris*, 328(12):1197–1202, 1999.

[138] V.I. Utkin. *Sliding modes in control and optimization*. Springer Science & Business Media, 2013.

[139] S. van Strien. One-parameter families of smooth interval maps: Density of hyperbolicity and robust chaos. *Proc. Amer. Math. Soc.*, 138(12):4443–4446, 2010.

[140] D. Veitch and P. Glendinning. Explicit renormalisation in piecewise linear bimodal maps. *Phys. D*, 44(1-2):149–167, 1990.

[141] M. Viana. *Lectures on Lyapunov Exponents.* Cambridge studies in advanced mathematics. Cambridge University Press, Cambridge, 2014.

[142] S. Wiggins. *Global Bifurcations and Chaos: Analytical Methods*. Springer, New York, 1988.

[143] E. Zeraoulia and J. Sprott. *Robust chaos and its applications*. World Scientific, 2012.

[144] Z.T. Zhusubaliyev and E. Mosekilde. *Bifurcations and Chaos in Piecewise-Smooth Dynamical Systems*. World Scientific, Singapore, 2003.

MASSEY UNIVERSITY
TE KUNENGA KI PŪREHUROA
UNIVERSITY OF NEW ZEALAND

GRADUATE RESEARCH SCHOOL

STATEMENT OF CONTRIBUTION
DOCTORATE WITH PUBLICATIONS/MANUSCRIPTS

We, the student and the student's main supervisor, certify that all co-authors have consented to their work being included in the thesis and they have accepted the student's contribution as indicated below in the Statement of Originality.

Student name:	Indranil Ghosh
Name and title of main supervisor:	Dr. David J.W. Simpson

In which chapter is the manuscript/published work?	Chapter 3
What percentage of the manuscript/published work was contributed by the student?	80%

Describe the contribution that the student has made to the manuscript/published work:

The candidate has been involved with the conceptualisation, investigation, calculation, computation, visualisation, writing, reviewing, and editing.

Please select one of the following three options:

- (●) **The manuscript/published work is published or in press**

  Please provide the full reference of the research output:

  I. Ghosh and D.J.W. Simpson, "Renormalisation of the two-dimensional border-collision normal form" in Int. J. Bifurcation Chaos, 32(12):2250181, 2022.

- ( ) **The manuscript is currently under review for publication**

  Please provide the name of the journal:

- ( ) **It is intended that the manuscript will be published, but it has not yet been submitted to a journal**

Student's signature:	Indranil Ghosh — Digitally signed by Indranil Ghosh Date: 2024.05.30 13:28:15 +12'00'	Main supervisor's signature:	David Simpson — Digitally signed by David Simpson Date: 2024.05.30 20:38:44 +12'00'

This form should appear at the end of each thesis chapter/section/appendix submitted as a manuscript/ publication or collected as an appendix at the end of the thesis.

MASSEY UNIVERSITY
TE KUNENGA KI PŪREHUROA
UNIVERSITY OF NEW ZEALAND

GRADUATE RESEARCH SCHOOL

STATEMENT OF CONTRIBUTION
DOCTORATE WITH PUBLICATIONS/MANUSCRIPTS

We, the student and the student's main supervisor, certify that all co-authors have consented to their work being included in the thesis and they have accepted the student's contribution as indicated below in the Statement of Originality.

Student name:	Indranil Ghosh
Name and title of main supervisor:	Dr. David J.W. Simpson
In which chapter is the manuscript/published work?	Chapter 4
What percentage of the manuscript/published work was contributed by the student?	80%

Describe the contribution that the student has made to the manuscript/published work:

The candidate has been involved with the conceptualisation, investigation, calculation, computation, visualisation, writing, reviewing, and editing.

Please select one of the following three options:

- (●) **The manuscript/published work is published or in press**

  Please provide the full reference of the research output:

  I. Ghosh and D.J.W. Simpson, "Robust Devaney chaos in the two-dimensional border-collision normal form." in Chaos, 32:043120, 2022

- ( ) **The manuscript is currently under review for publication**

  Please provide the name of the journal:

- ( ) **It is intended that the manuscript will be published, but it has not yet been submitted to a journal**

Student's signature:	Indranil Ghosh — Digitally signed by Indranil Ghosh Date: 2024.05.30 13:30:10 +12'00'	Main supervisor's signature:	David Simpson — Digitally signed by David Simpson Date: 2024.05.30 20:38:22 +12'00'

This form should appear at the end of each thesis chapter/section/appendix submitted as a manuscript/ publication or collected as an appendix at the end of the thesis.

MASSEY UNIVERSITY
TE KUNENGA KI PŪREHUROA
UNIVERSITY OF NEW ZEALAND

GRADUATE RESEARCH SCHOOL

STATEMENT OF CONTRIBUTION
DOCTORATE WITH PUBLICATIONS/MANUSCRIPTS

We, the student and the student's main supervisor, certify that all co-authors have consented to their work being included in the thesis and they have accepted the student's contribution as indicated below in the Statement of Originality.

Student name:	Indranil Ghosh
Name and title of main supervisor:	Dr. David J.W. Simpson

In which chapter is the manuscript/published work?	Chapter 5
What percentage of the manuscript/published work was contributed by the student?	80%

Describe the contribution that the student has made to the manuscript/published work:

The candidate has been involved with the conceptualisation, investigation, calculation, computation, visualisation, writing, reviewing, and editing.

Please select one of the following three options:

- ○ **The manuscript/published work is published or in press**
  Please provide the full reference of the research output:
- ◉ **The manuscript is currently under review for publication**
  Please provide the name of the journal:
  I. Ghosh, R.I. McLachlan, and D.J.W. Simpson, "Robust chaos in orientation-reversing and non-invertible two-dimensional piecewise-linear maps." Submitted to: J. Nonlinear Sci.
- ○ **It is intended that the manuscript will be published, but it has not yet been submitted to a journal**

Student's signature:	Indranil Ghosh Digitally signed by Indranil Ghosh Date: 2024.05.30 13:38:24 +12'00'	Main supervisor's signature:	David Simpson Digitally signed by David Simpson Date: 2024.05.30 20:38:05 +12'00'

This form should appear at the end of each thesis chapter/section/appendix submitted as a manuscript/ publication or collected as an appendix at the end of the thesis.

MASSEY UNIVERSITY
TE KUNENGA KI PŪREHUROA
UNIVERSITY OF NEW ZEALAND

GRADUATE RESEARCH SCHOOL

STATEMENT OF CONTRIBUTION
DOCTORATE WITH PUBLICATIONS/MANUSCRIPTS

We, the student and the student's main supervisor, certify that all co-authors have consented to their work being included in the thesis and they have accepted the student's contribution as indicated below in the Statement of Originality.

Student name:	Indranil Ghosh
Name and title of main supervisor:	Dr. David J.W. Simpson
In which chapter is the manuscript/published work?	Chapter 6
What percentage of the manuscript/published work was contributed by the student?	80%

Describe the contribution that the student has made to the manuscript/published work:

The candidate has been involved with the conceptualisation, investigation, calculation, computation, visualisation, writing, reviewing, and editing.

Please select one of the following three options:

- (●) **The manuscript/published work is published or in press**

  Please provide the full reference of the research output:

  I. Ghosh, R.I. McLachlan, and D.J.W. Simpson, "The bifurcation structure within robust chaos for two-dimensional piecewise-linear maps." in Commun. Nonlinear Sci. Numer. Simul., 134, 2024

- ( ) **The manuscript is currently under review for publication**

  Please provide the name of the journal:

- ( ) **It is intended that the manuscript will be published, but it has not yet been submitted to a journal**

Student's signature:	Indranil Ghosh — Digitally signed by Indranil Ghosh Date: 2024.05.30 13:41:26 +12'00'	Main supervisor's signature:	David Simpson — Digitally signed by David Simpson Date: 2024.05.30 20:37:17 +12'00'

This form should appear at the end of each thesis chapter/section/appendix submitted as a manuscript/ publication or collected as an appendix at the end of the thesis.